TECHNO-ECONOMIC ANALYSIS AND LIFE CYCLE ASSESSMENT FOR PRODUCTION OF BIOFUELS FROM SPENT COFFEE GROUNDS

Submitted in fulfillment of the requirements for the degree of Master of Engineering in the Department of Chemical Engineering, Faculty of Engineering and the Built Environment at the Durban University of Technology

Green Engineering Research Group

By

Wilberforce Kisiga (22175215)

2023

SUPERVISOR: _____ Date: _____
Prof. M. Chetty

CO-SUPERVISOR: _____ Date: _____
Prof. S. Rathilal

DECLARATION

I, **Wilberforce Kisiga**, student number **22175215** declare that:

i. The research presented in this thesis is my own work, unless where stated otherwise.
ii. This thesis has never been submitted for examination to any University before.
iii. Any data, pictures or information of other persons that has been used in this thesis was specifically acknowledged as being sourced from other persons and referenced accordingly.
iv. This thesis has been written in my own words and in case other persons' words have been used, these words have been put in quotes and referenced accordingly.
v. This thesis does not contain texts, graphs, pictures or tables from internet, except when categorically stated and properly referenced.

Signed: Date: 14/08/2023

W. Kisiga

ABSTRACT

Spent Coffee Grounds (SCGs) are one of the most abundant agro-industrial residues generated from the coffee brewing industry and coffee espresso machines in restaurants, cafeterias, cafes and homes. It is believed that for every ton of coffee beans processed, 650 kg of SCG is left as solid residues. Coffee being the second traded commodity after petroleum, means that a lot of SCGs are generated annually and end up into landfills. Efforts are being made to turn this valuable waste into biofuels, however, most of these efforts end up at laboratory benches and few studies have focused on industrial scale production of biofuels from SCG.

Six biomass-to-energy conversion technologies were compared from technical, economic and environmental perspectives: Fast pyrolysis, Hydrothermal Liquefaction (HTL), gasification, Anaerobic Digestion (AD), fermentation and biodiesel production. The processing technologies were selected because they are the most researched biomass-to-fuel conversion routes. Each of the processing routes was simulated in Aspen plus V11 using input data from literature. The mass and energy balances obtained from simulations were used to conduct Techno-Economic Analyses (TEAs) and Life Cycle Assessments (LCAs). TEA was conducted with help of Aspen Process Economic Analyzer (APEA) and Microsoft Excel spreadsheets whereas OpenLCA V1.11.0 software was employed for LCA.

After the processing routes were successfully simulated, APEA was used to estimate the installed Cost of all Equipment (COE). The Capital Expenditure (CAPEX) required to build the biorefineries was then estimated basing on COE for each biorefinery. Then the Operating Expenses (OPEX) required for running the day-to-day operations of the plant were estimated as the sum of Variable Operating Expenses (VOC) and Fixed Operating Expenses (FOC). The revenues from the sales of finished products were estimated and used to calculate the gross profit. For the plant life of 25 years; using straight-line depreciation of 10% per year, discount rate of 12% and tax rate of 28%, the Discounted Cash Flow Analysis (DCFA) was used to calculate the economic indicators i.e. the Net Present Value (NPV), Profitability Index (PI), Internal Rate of Return (IRR) and Discounted Payback Period (DPBP).

For LCA, the methodology outlined by the ISO 14040/44 framework was used. The method outlines four steps followed to conduct LCA i.e. goal and cope definition, Life Cycle Inventory

(LCI), Life Cycle Impact Assessment (LCIA) and interpretation of results. The goal of this study was to identify the processing route with least environmental impacts and the cradle-to-gate system boundary was selected. LCI was conducted using the mass and energy balances obtained from Aspen plus simulation and the flows present in the Agribalyse Version 3 database, downloaded from OpenLCA nexus. LCIA was conducted using the ReCiPe 2016 Midpoint (H) and was also downloaded from OpenLCA nexus. Eight impact categories namely, global warming, fossil resource scarcity, particulate matter formation, terrestrial acidification, freshwater eutrophication, marine eutrophication, mineral resource scarcity and water consumption were selected. The results were analysed to identify the conversion route with less environmental effects.

Results from the economic analysis showed that fast pyrolysis was the most economically profitable processing route with a NPV, PI, DPBP and IRR of 6.3 million USD, 1.85, 5.4 years and 37%, respectively. In the second position was biogas production with a NPV, PI, DPBP and IRR of 3.4 million USD, 1.65, 5.7 years and 34%, respectively. Gasification was in the third position with a NPV, PI, DPBP and IRR of 5.4 million USD, 1.48, 6.0 years and 32%, respectively. In the fourth position was biodiesel production with a NPV, PI, DPBP and IRR of 3.9 million USD, 0.86, 8.0 years and 24%, respectively. HTL was in the fifth position with a NPV, PI, DPBP and IRR of 0.68 million USD, 0.29, 13.0 years and 16%, respectively. Bioethanol production was not economically profitable as the revenues generated from sales of finished products were smaller than the operating expenses, thus no profit could be generated.

Results from environmental impact assessment showed that fast pyrolysis was the most environmentally friendly processing route, followed by biogas production, biodiesel production, gasification, and bioethanol production, whereas HTL had the highest environmental impacts. Electricity consumption was the biggest contributor to the environmental impacts, making HTL, which was the highest electricity consuming processing route, to be the worst environmentally. However, biogas production was the least electricity consuming processing route but not the best environmentally due to large production of carbon dioxide and methane (biogas) from anaerobic digestion. The large production of carbon dioxide can be mitigated through using it to grow algae or in supercritical carbon dioxide extraction of lipids. However, the cost associated with additional unit processes can escalate the biogas production costs. These greenhouse gases were the biggest contributors of global warming, pushing biogas production to the second position after pyrolysis.

Fast pyrolysis was proposed to be the best environmentally and economically feasible processing route for the production of biofuels from SCG.

DEDICATION

Firstly, I dedicate this work to my beloved mother Ms. Namiiro Fransiska Namukasa and granny Mrs. Nantale Imelda Lutaaya who have been supportive in my journey to achieve academic excellence. For you two ladies, words alone are not enough to describe who you are to me.

Secondly, I dedicate this work to my dear brother Mr. Enoka Ssemmanda for always showing me a way to go with the dynamics of life's challenges.

ACKNOWLEDGEMENT

In the first place I would like to thank ALLAH, the most Gracious, and the most Merciful for the providence of good health, wisdom, the opportunity to be admitted to this institution and the financial blessings.

Secondly, I would to love extend my sincere gratitude to my Supervisor Prof. Manimagalay Chetty and co-supervisor Prof. Sudesh Rathilal for their academic and parental guidance throughout the process of conducting my research and preparation of this thesis. It is their advice and counseling that has enabled me complete this research work successfully.

Thirdly, I would like to thank the grants management department of Durban University of Technology for the DUT Bursary Scheme that has been my major source of income during my studies. This financial support has created a conducive environment for me to concentrate on research work.

I am also greatly indebted to the team of Green Engineering research group for their encouragement, positive criticism and emotional support that I believe has been instrumental throughout the course of this research. To Dr. EK Tetteh, my sister Nikita Singh, my brothers Boldwin Mutsvene, Dr. Olusegun Olagunju and Stephen Okiemute Akpasi, words alone cannot express the joy that I have at heart for all the academic support you have rendered to me.

I cannot forget to make mention of NRF-BRICS for financially sponsoring me to attend academic retreats and conferences. This has exposed me to the world of research and enabled me to interact with fellow researchers. Thank you Prof. YM Isa.

To my dear mother and granny, I thank you so much for being there for me in narrow and thin. It is because of you that I decided to work hard and make you proud.

Lastly, I would like to thank whoever has helped me through the course of my studies. I can confidently say that I have grown into a strong person who is more focused and determined to climb more heights to achieve academic excellence.

TABLE OF CONTENTS

LIST OF FIGURES

LIST OF TABLES

KEYWORDS

Aspen plus simulation

Biofuels

Biomass

Biomass-to-fuel conversion technologies

Life cycle impact assessment

Techno-economic analysis

NOMENCLATURE

AD: Anaerobic Digestion

APEA: Aspen Process Economic Analyzer

CAPEX: Capital Expenditure

CC: Contingency Costs

CCE: Carbon Conversion Efficiency

CDCF: Cumulative Discounted Cash Flow

CEPCI: Chemical Engineering Plant Cost Index

CGE: Cold Gas Efficiency

CHP: Combined Heat and Power

COE: Cost of all major Equipment

COL: Cost of Operating Labor

DCF: Discounted Cash Flow

DCFA: Discounted Cash Flow Analysis

DPBP: Discounted Payback Period

DSCG: Defatted Spent Coffee Grounds

EC: Engineering Costs

ER: Equivalence Ratio

FC: Fixed Carbon

FCI: Fixed Carbon Investment

FFA: Free Fatty Acids

FOC: Fixed Operating Costs

GGE: Gasoline-Gallon Equivalence

GHG: Greenhouse Gases

HHV: Higher Heating Value

HTC: Hydrothermal Carbonization

HTG: Hydrothermal Gasification

HTL: Hydrothermal Liquefaction

IRR: Internal Rate of Return

ISBL: Inside Battery Limit Investment

LB: Lignocellulosic Biomass

LCA: Life Cycle Assessment

LCI: Life Cycle Inventory

LCIA: Life Cycle Impact Assessment

LHV: Lower Heating Value

NCG: Non-Condensable Gases

NPV: Net Present Value

OPEX: Operating Expenses

OSBL: Off-Site Plant Costs

PI: Profitability Index

S/B: Steam-to-Biomass ratio

SCG: Spent Coffee Grounds

SSF: Simultaneous Saccharification and Fermentation

SUC: Startup Costs

TEA: Techno-Economic Analysis

USD: United States Dollar

VFA: Volatile Fatty Acids

VM: Volatile Matter

VOC: Variable Operating Costs

WC: Working Capital

PREFACE

Research outputs

Conference participation:

Kisiga, W., Singh, N. and Chetty, M. 2022. Valorization of spent coffee grounds. 2nd sustainable bioenergy and processes conference, 12th – 14th December 2022, Cape Town, South Africa.

Journal articles:

Kisiga, W., Chetty, M. and Rathilal, S. 2023. Techno-economic analysis of alternative technologies for production of biofuels from spent coffee grounds. *Chemical Engineering Journal*, **under peer review**.

Kisiga, W., Chetty, M. and Rathilal, S. 2023. Environmental impact assessment of alternative technologies for production of biofuels from spent coffee grounds. *Journal of Cleaner Production*, **under peer review**.

Kisiga, W., Chetty, M. and Rathilal, S. 2023. Biomass-to-biofuel conversion technologies. A comprehensive review. *Sustainable Energy Technologies and Assessments*, **in progress**.

1. INTRODUCTION

1.1. Background of study

The rapidly increasing human population has resulted in increased energy consumption in the production and transport sectors. In the same sense, there is a subsequent increase in energy consumed in homesteads for cooking, heating, refrigeration, and other home appliance operations. However, the predominant energy source available today is fossil fuels, with about 80% of world's energy demands currently being met by fossil fuels, and yet these fuels are finite and are associated with emissions of greenhouse gases (Sahoo *et al.* 2021; Feng *et al.* 2022). The need for sustainable supply of energy to meet the current demand together with strict environmental protection strategies across the world have posed a pressing desire to venture into renewable, greener sources of energy (Li *et al.* 2022; Mumtaz *et al.* 2022).

Biomass is a promising feedstock for production of biofuels, chemicals and energy (Gonzalez-Arias *et al.* 2021). Biomass includes different kinds of biological matter: wood, agricultural waste, energy crops, algae, animal waste, organic matter of municipal waste and others (de Caprariis *et al.* 2017; Li *et al.* 2022). Wood or the forestry sectors constitutes the most abundant biomass sources with about 85% of all used feedstock for bio-energy sources (Tezer *et al.* 2022). The renewable energy sources include biodiesel, bioethanol, biogas, bio-char, bio-oil, bio-syngas, bio-hydrogen (Sharma, Singh and Arya 2020; Mumtaz *et al.* 2022). According to Tezer *et al.* (2022), biomass in 2017 contributed about 56 EJ to the primary energy supply and is about 9.5% of the world's total energy consumption with Africa consuming 96% of energy from biomass, whereas America, Asia and Europe consume 59%, 65% and 59%, respectively.

Waste biomass is the perfect feedstock for synthesis of biofuels since it doesn't compete with food production (Khounani *et al.* 2019). Also, use of waste biomass for synthesis of useful products helps to relieve the environment on waste generation since most of these wastes are always disposed into landfills (Sharma, Singh and Arya 2020). Disposing of these wastes into the landfills is dangerous since most organic matter require a lot of oxygen to be completely degraded (Atabani *et al.* 2019), so recycling and reuse of these organic wastes for generation of valuable products like biofuels does not only generate income from sales of new products but also helps to relieve the environment of these wastes. Waste biomass includes rice husks, corn stover, the organic fraction

of municipal solid wastes, wastewater sludge, coffee husks, fruit peels, corncobs, cornhusks, Spent Coffee Grounds (SCG), waste woods and many others. Waste valorization has become a strategy of increasing resource efficiency as well as reducing the negative impacts these wastes pose to the environment. A circular economy (Rajesh Banu *et al.* 2020) as advocated by the United Nations, the World Economic Forum and the European Union is a model that helps to keep resources longer into the systems thereby reducing waste accumulation and environmental impacts and in turn create jobs and promote sustainable development. In this context different technologies have been developed and promoted to convert these wastes into valuable products like energy, food and animal feed (Schmidt Rivera *et al.* 2020).

SCG is chosen for this study since it is readily available, has a higher bulk density and thus lower transportation costs, and doesn't require aggressive pretreatment operations like size reduction which consume a lot of energy. Also, unlike other lignocellulosic waste biomass, SCG contains lipids which can be extracted and transformed into a myriad of useful products including liquid fuels like biodiesel. SCG is a rich biomass which is more than a waste and can be used to extract and/or synthesize a variety of useful products including biodiesel, renewable diesel, bio-ethanol, bio-char, fuel pellets, biopolymers, bio-ethers, biogas, bio-catalysts, antioxidants and so on (Araujo *et al.* 2022).

SCG is a promising feedstock for bio-refinery since it is readily available at almost no cost, does not compete with food production and above all supports a bio-refinery concept. A bio-refinery is a group of conversion routes that are sustainably used to transform biomass into fuel, energy or other valuable chemicals (Araujo *et al.* 2022).

Several processing routes for production of biofuels from SCG and other lignocellulosic biomass have been extensively researched and are classified as physical, chemical, biochemical and thermochemical conversions (Mahapatra *et al.* 2021). The physical conversion involves the mechanical compression of biomass to form briquette fuel. Chemical conversion results in biodiesel production through transesterification of lipids extracted from biomass; biochemical conversion involves technologies like fermentation and anaerobic digestion produces bioethanol and biogas. The thermochemical conversion is a broad route involving different technologies like combustion, carbonization, gasification, pyrolysis and liquefaction producing a range of biofuels

like smock, active carbon, bio-syngas, bio-oil, bio-char and non-condensable gases (Zabaniotou and Kamaterou 2019; Mahapatra *et al.* 2021; Zhang *et al.* 2021b; Li *et al.* 2022).

1.2. Problem statement

With increased human population, generation of wastes has also increased in the same direction because of increased consumption. This has led to rapid accumulation of agro-industrial wastes which is currently being incinerated or deposited into landfills. Inappropriate disposal of these wastes has led to environmental pollution. The decomposition of these solid wastes emits a great deal of greenhouse gases like methane which cause global warming, their leachates end up in water bodies and cause eutrophication, acidification and toxicity. Also the decomposition of waste biomass requires a lot of oxygen causing a higher carbon oxygen demand (COD).

Also, the world is largely depending on fossil fuels, which accounts for about 80% of the world's energy needs (Afolabi, Sohail and Cheng 2020). These fuels are finite and are anticipated to be depleted in the years to come. The process of mining, transportation, refining and combustion of these fuels emit large amounts of greenhouse gases (CO_2, methane, water vapor, sulfur and nitrous oxides), hence increased environmental pollution (Shahbeik *et al.* 2022). The excessive reliance on fossil fuels has not only resulted in negative environmental impacts but also has led to increased fuel prices. The fuel prices have risen due to increase in production costs of fossil fuels as sweet crude oils are dwindling and the available heavy crude needs sophisticated technologies which are expensive. Higher costs of production are reflected in fluctuating and increased prices of fossil-based fuels. The dividends of using waste biomass as feedstock for biofuels production are two fold; the environment will be relieved of rapid accumulation of wastes and alternative renewable clean sources of fuel will be provided. This will also help to reduce on escalating fuel prices caused as a result of limited quantities of fossil resources.

Among the most traded commodities worldwide, coffee is in the second position after petroleum (Brachi, Santes and Torres-Garcia 2021; Kibret *et al.* 2021). It is the second most consumed beverage after tea and for every kilogram of soluble coffee prepared; about 2 kg of wet SCG is left as a solid residue (Rajesh Banu *et al.* 2020; Schmidt Rivera *et al.* 2020). This means that SCG is an abundant waste whose economic potentials have to be exploited. SCG is mainly from two sources; instant coffee industries; and catering and outlet shops (cafeterias and cafes). This

valuable waste contains a large amount of natural compounds that can be converted into useful products.

Several studies at laboratory scale have been done to investigate the possibility of producing biofuels from SCG but there are gaps that need to be filled on the economic feasibility and environmental impact assessment of industrial production of these biofuels. Most of the studies conducted before focus on one or two processing routes and this does not give room for examination of full potential of SCG as feedstock for biorefineries. Hence, the need for a more robust study that compared six processing routes for production of biofuels from SCG. The studied processing routes were hydrothermal liquefaction, fast pyrolysis, anaerobic digestion, fermentation, gasification and biodiesel production.

1.3. Aims and objectives of this study

1.3.1. Aim

To identify the most economically profitable and eco-friendly processing route for production of biofuels from SCG.

1.3.2. Specific objectives

i. To simulate the various conversion routes to biofuels from SCG using ASPEN Plus process simulator
ii. To perform a techno-economic analysis for production of biofuels from SCG
iii. To perform a life cycle assessment for production of biofuels from SCG

1.4. Importance and significance of study

Since most of the studies on valorisation of SCG to biofuels end at laboratory benches, performing the economic evaluation of large-scale production of the biofuels will help potential investors and governments identify areas of investment. Producing biofuels from biomass will help to reduce the current prices of biofuels that are predominantly produced from edible feedstock like the sweet corn, edible oils, sorghum and sugar cane. Use of waste biomass as feedstock for production of value products at commercial scale will help relieve the environment of the current rapid accumulation of solid waste which is largely deposited into landfills or incinerated. Due to the exhaustion of sweet crude oils, the available heavy crude oils contain a lot of impurities like transition metals, sulfur and nitrogen which end up in the environment. Thus, producing cleaner

fuels from waste biomass will help to reduce the world's dependence on fossil fuels which contain a lot of impurities. Conducting the LCA for biofuels production will help during decision making. Potential investors will be able to choose the best environmentally friendly processing among alternatives. Industrial production of biofuels from SCG will help to create jobs especially from the youth who are languishing is pathetic poverty. The life cycle of biofuels production will create jobs during feedstock collection, production process, biofuels distribution and marketing. For South Africa's case, commercializing biofuels production will help to reduce the over dependence on coal for electricity generation, hence attenuating the problem of load shedding.

1.5. Structure of thesis

Chapter 1: Gives details about the background of the study. States problem that the study aims to address and outlines the importance and significance of the study.

Chapter 2: Presents the detailed review of literature on the SCG availability and chemical composition, biofuels and biorefineries. Current literature on techno-economic assessment and life cycle assessment of biofuels from waste biomass is also reviewed in this chapter.

Chapter 3: Presents the detailed methodology that was followed in this study. It is divided into four sections: Section 3.1 outlines the overview of the general structure of this chapter; section 3.2 presents the methodology used to simulate the six processing routes in Aspen plus software whereas section 3.3 and section 3.4 contains the economic evaluation and environmental assessment, respectively.

Chapter 4: Outlined the results obtained from simulation, economic evaluation and life cycle assessment of biofuels from SCG. The discussion of these results are also presented in this chapter.

Chapter 5: Outlines the conclusions and recommendations drawn from this study.

Bibliography: Presents the list of references that were consulted during the whole process of conducting this study.

Appendices: Presents important data and materials used in conducting this study.

2. LITERATURE REVIEW

2.1. Introduction

This chapter presents a comprehensive review of available literature on biomass-to-energy conversion technologies. The chapter begins with presenting the classification of biomass, coffee production and availability. The chemical composition and valorisation of spent coffee grounds, a by-product of coffee brewing process is also presented in this chapter. Also the classification of biofuels and the process parameters affecting the yields and quality of biofuels obtained from different conversion technologies are presented in this chapter. The chapter ends with an in-depth review of the techno-economic analysis and life cycle assessment for production of biofuels from waste biomass.

2.2. Biomass

Biomass is the fourth most abundant source of energy after coal, petroleum and natural gas (Glushkov *et al.* 2021; Zhang *et al.* 2021a). Currently, a lot of research is being focused on the derivation of energy from biomass because it is readily available, regarded as carbon neutral and contains less sulfur and nitrogen. Biomass doesn't contain transition metals like fossil fuels which makes the fuels clean and less polluting. Biomass is the broad term used to refer to terrestrial plants and their residues, waterweed and algae (Rodionova *et al.* 2022). Terrestrial plants are the most abundant category of biomass and are classified as starch, sugar-based and lignocellulosic biomass (LB). Starch and sugar-based biomass are the primary sources of food and with increased food shortage worldwide, deriving biofuels from such feedstock is no longer sustainable. The most abundant and ideal feedstock for bioenergy production is the LB for it does not compete with food production as it is nonedible and mostly ends up in landfills. Examples of LB include crop residues, forestry residues, food industry wastes and the organic fraction of solid municipal waste. LB are mainly composed of cellulose, hemicellulose and lignin.

2.2.1. Coffee production

It is believed that coffee was first discovered in Ethiopia about a thousand years ago and is of the family Rubiaceae (Atabani *et al.* 2019). Coffee is the second most traded commodity after petroleum (Atabani *et al.* 2019; Rajesh Banu *et al.* 2020; Araujo *et al.* 2022), and its consumption is on the rise worldwide with about 10 million tons consumed annually. Coffee production has

increased in the last 20 years by around 60%, from around 6 million metric tons in 2000 to over 10 million metric tons in 2020 (Tian *et al.* 2021). Coffee *Arabica* and coffee *Canephora* also known as Robusta coffee are two major species of coffee commercially produced worldwide, with *Arabica* coffee representing about 75% of the world's total coffee production (Rajesh Banu *et al.* 2020; Araujo *et al.* 2022). According to Atabani *et al.* (2019), *Arabica* coffee represents 75 to 80% of the world's total coffee production.

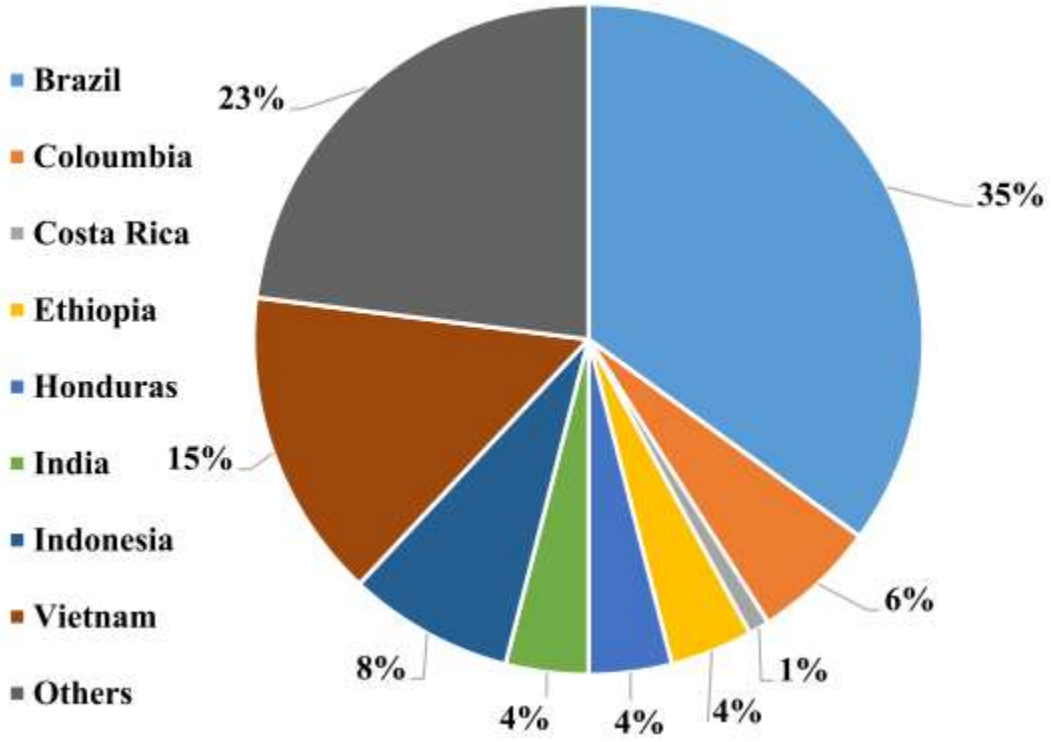

Figure 2. 1: Breakdown of the total world coffee production (Atabani *et al.* 2019)

It can be seen from Figure 2.1 that Brazil is the largest producer of coffee (35%) followed by Vietnam (15%), Indonesia (8%), and Colombia (6%) whereas Ethiopia (4%), India (4%) and Honduras (4%) have equal coffee production capacity. The same hierarchy was reported by Rajesh Banu *et al.* (2020) putting Brazil in first position with 53 million bags of coffee produced per year, followed by Vietnam, Columbia, Indonesia and Ethiopia with 28, 14, 12 and 7 million bags of coffee, respectively. Coffee growing in Brazil is being favored by the tropical rain forests that are responsible for adequate rainfall received in Brazil throughout the year. In Africa, Ethiopia and

Uganda are the leading coffee producers and exporters because of the availability of tropical fertile lands and adequate rains received in two seasons of the year.

2.2.2. Spent Coffee Grounds

Spent Coffee Grounds (SCG) are sold residues of fine particles obtained as the end product of coffee brewing. It contains a higher moisture content, higher concentration of organics and acid content and it estimated that 40 to 45 wt.% of the dry coffee bean remains as SCG after brewing (Araujo *et al.* 2022). It has been reported that SCG comprise of over 1000 different species of organic materials including carbohydrates, fibers, proteins, caffeine, holocellulose, lignin, fatty acids, amino acids, tannins, polyphenols among others (Atabani *et al.* 2019). According to Rajesh Banu *et al.* (2020), about 2 kilograms of wet SCG are produced for every one kilogram of instant coffee made. As a result, approximately 6 million tons of wet SCG are produced annually across the globe (Brachi, Santes and Torres-Garcia 2021). This shows that SCG is an abundant waste and a readily available feedstock for a biorefinery. Different methods have been proposed to valorize SCG into valuable products. These include hydrolysis of SCG with sulfuric acid to form sugars followed by fermentation to obtain bioethanol. The coffee oil could be obtained from the residue after hydrolysis and converted into biodiesel and glycerin through transesterification. The defatted SCG could either be used as fuel pellets (Thoppil and Zein 2021) or soil amendment. Bio-hydrogen can produced from glycerin formed as by-product during biodiesel production (Atabani *et al.* 2019). Biofuels, biopolymers, antioxidants, bio-composites can also be prepared from SCG (Karmee 2018; Dattatraya Saratale *et al.* 2020). Apart from the production of biodiesel as a green fuel, other fuels like bio-oil, bio-char, syngas, biogas, fuel pellets, bioethanol can be obtained from SCG through a range of conversion processes as shown in Figure 2.2. Other than biofuels, valuable compounds like caffeine, tannins, glycerin, compost, polyhydroxyalkanoates, phenolic compounds, bio-active compounds etc. can also be recovered from SCG (Rajesh Banu *et al.* 2020). SCG support a bio-refinery concept because of the possibility to obtain more than one valuable product from a single feedstock.

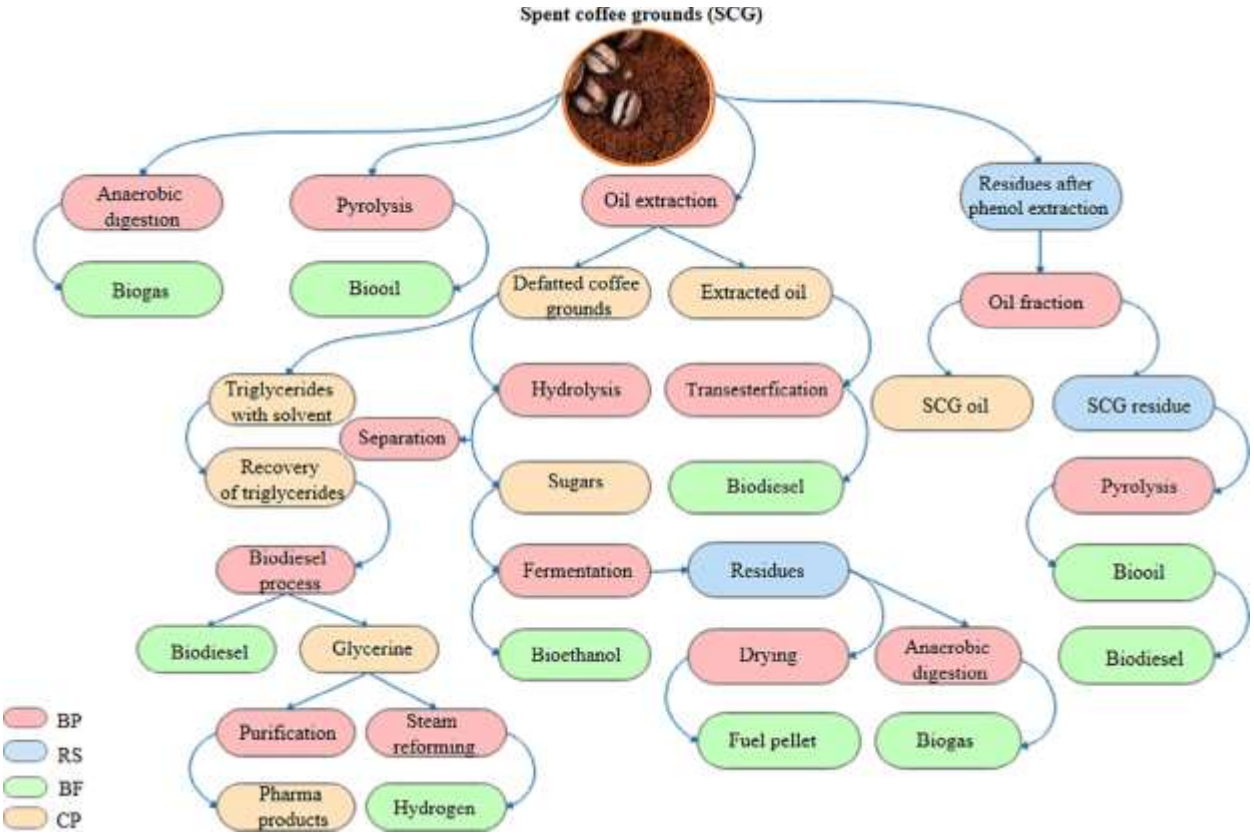

Figure 2. 2: Integrated biorefineries for biofuel production (Rajesh Banu et al. 2020)

where BP- Biorefinery process, RS – Solid residues, BF- Biofuel produced and CP- Co-products

However, in most parts of the world, this valuable waste ends up into landfills. This is wastage of resources in addition to potential environmental threats as a result of excessive accumulation of solid wastes into landfills. Coffee brewing uses a lot of water and the process leaves SCG with a higher moisture content (Tian *et al.* 2021). When left to decompose, SCG results in greenhouse gas (GHG) emissions. Therefore, valorisation of this valuable waste does not only support a circular economy as advocated by UNESCO-UNEVOC but also helps to save the environment.

2.2.2.1.Chemical composition of SCG

The proximate and ultimate analysis of SCG on a dry basis is reported in Table 2.1. It contains high volatile matter (VM) with Mukherjee *et al.* (2022) reporting VM to be 81.2 wt.%, fixed carbon (FC) as 14.6 wt.% and ash content to be 0.9 wt.%. There is a big disparity in the ash content reported in literature and this can be attributed to the difference in coffee composition because of different coffee species grown in different places of the world. SCG contains a high content of

carbon (over 50 wt.%) and this enables a myriad of carbon-based compounds to be recovered from this valuable resource that is currently being incinerated or disposed into landfills.

Table 2. 1: Proximate and ultimate analysis of SCG

Proximate analysis (wt. %)				Ultimate analysis (wt. %)					Reference
Moisture	**VM**	**FC**	**Ash**	**C**	**O**	**H**	**N**	**S**	
3.3	81.2	14.6	0.9	50.0	39.0	6.7	2.5	0.9	Mukherjee *et al.* (2022)
4.3	76.6	16.9	2.6	53.8	30.9	5.8	2.5	0.3	Fu *et al.* (2023)
7.0	64.9	21.3	7.1	56.1	34.0	7.2	2.4	0.14	Tian *et al.* (2021)
	77.9	20.5	1.6	53.9	36.7	7.1	2.3		Afolabi, Sohail and Cheng (2020)
2.98	76.22	20.33	0.47	49.37	39.47	7.37	2.26	0.09	Kibret *et al.* (2021)

Many researchers report different figures for elemental composition of SCG and this is attributed to different coffee bean types, geographical location and coffee brewing methods. The biochemical composition (cellulose, hemicellulose, lignin and lipids) of SCG reported in literature also varies. Taleb *et al.* (2020) performed thermogravimetry to quantify the amount of cellulose, hemicellulose, linin and oils present in SCG. It was reported that on a dry basis, moisture was 2.7%, oils and hemicellulose combined were 38.18%, cellulose was 17.20% and lignin was 18.4%. Leow *et al.* (2021) reported that cellulose and hemicellulose account for 50 wt.% of SCG on a dry basis and coffee oil ranging between 7 to 15%. According to Pereira *et al.* (2019), SCG was reported to contain up to 55% w/w carbohydrates, 25% w/w lignin, 24% w/w lipids and about 2% w/w ash. Rijo *et al.* (2021) gave the average composition (wt.%) of hemicellulose, cellulose, lignin, lipids and proteins as 44.1, 12.4, 20.6, 10.0 and 12.9, respectively.

2.2.2.2.Lipids

There are several techniques used to extract the lipids from SCG but the most commonly used ones are solid-liquid extraction using organic liquids, microwave-assisted extractions, ultrasound-assisted extractions, supercritical fluid extraction and pressurized fluid extraction (Araujo *et al.* 2022). Solid-liquid extraction using organic solvents like hexane is by far the most commonly used method of extracting coffee oil from SCG. However, according to Atabani *et al.* (2019), solid-

liquid has got drawbacks in that it requires longer durations, large amounts of solvent, large quantities of energy in the form of heat and moreover achieves lower yields of oil. The same authors report that SFE is suitable for feedstock with relatively low moisture content and requires extremely high pressure and temperature which makes it expensive. Also, use of some organic solvents such as hexane leads to air pollution and are hazardous to human health. Conversely, ultrasound-assisted extractions give higher oil yield from feedstock with higher moisture content while requiring minimal amounts of energy.

2.2.3. Biofuels

In the European Union, the 2009/28/EC directive categorises biofuels into first generation and advanced (second and subsequent generations) biofuels whereas the advanced generation biofuels are the truly sustainable biofuels. This is because the first generation biofuels (bioethanol and biodiesel) are commonly derived from edible biomass feedstock like soybean, rapeseed, sweet corn, sorghum, sugarcane, wheat etc., and this makes bioenergy production compete with food production (Scarsella *et al.* 2020; Rodionova *et al.* 2022). To overcome this challenge, nonedible waste biomass feedstock which are less expensive and readily available are utilised in bio-refineries. Among them is the largest portion of Lignocellulose Biomass (LB) i.e. forestry and agricultural residues, waste papers, sawmill dust and animal manure. The biofuels produced from LB are termed as second generation biofuels (Rodionova *et al.* 2022). However, LB is associated with a more recalcitrant molecular structure which is more resistant to pretreatment operations like size reduction, and has low bulk density which increases transportation costs from source to bio-refineries when compared to first generation biomass feedstock (Scarsella *et al.* 2020).

Another category of biofuels called the third generation biofuels is derived from algal biomass and waterweed, of which biodiesel is the most produced biofuel from this category. Third generation biofuels have advantage over the first classes of biofuels. They don't compete for arable land with food production because of their ability to grow in sewage and wastewaters. They don't need aggressive pre-treatment steps and also guarantees a reliable feedstock supply due to their higher growth rates. However, algal biomass is associated with lower lipid content which depends on a number of growth parameters that must be closely monitored for optimal growth. Such factors include light intensity, temperature, pH of culture medium, nutrient concentration among others (Rodionova *et al.* 2022). The fourth generation biofuels are derived from Genetically Modified

Organisms (GMOs). These include microalgae and cyanobacteria (Rodionova *et al.* 2022). With the use of genetic engineering, growth conditions can be altered enabling these organisms to replicate rapidly and with fewer steps, biofuels can be derived from these organisms. However, there are still questions on the sustainability of GMOs in relation to human health and the environment as a whole.

2.2.4. Bio-refineries

There are four categories of techniques used to convert biomass into fuels and energy namely, thermochemical and biochemical (Gonzalez-Arias *et al.* 2021; Lachos-Perez *et al.* 2022; Rodionova *et al.* 2022; Shahbeik *et al.* 2022), physicochemical, and mechanical or physical means. Thermochemical conversion technologies are faster and easy to operate and produce biofuels with favourable qualities unlike the biochemical means which produce fuels with low energy density, high water content and low viscosity. The physical means are not broadly employed to produce fuels due to their extremely low yields. With thermochemical conversions, the most superior techniques are gasification, pyrolysis and Hydrothermal Liquefaction (HTL) since biomass and waste plastics can be converted to liquid fuels (Mishra *et al.* 2022). Due to the highly-crystalline nature of cellulose entangled within the lignin the matrix, biochemical conversion technologies are technically less feasible compared to thermochemical means (gasification, pyrolysis, carbonization and liquefaction) which are associated with the use of coarse and severe operating conditions like catalysts, higher temperatures and pressure (Scarsella *et al.* 2020). Table 2.2 and Figure 2.3 show different bio-refinery technologies and primary products. In general biochemical conversion technologies require lower energy inputs, lower capital investment and operating costs, require milder operating conditions but are associated with low biofuel yields, longer reaction durations and require pre-treatment processes like biomass hydrolysis. On the other hand thermochemical processes can handle a wide range of feedstock, higher biomass conversion rates, not greatly disrupted with variations in feedstock composition and have well-established technologies, however, they require a lot of energy inputs, and require sophisticated equipment which raises initial investment costs and operating expenses (Shahbeik *et al.* 2022).

Table 2. 2: Biorefinery technologies, products and their uses

Route	Technology	Products	Use	Reference
Physical conversion	Compression	Briquette fuel	Heat/Chemicals	Fehse, Kummich and Schröder 2021
Thermochemical	Combustion	Heat	Heat/Electric power	Glushkov *et al.* 2021
	Carbonization	Active carbon	Heat/Adsorbent	Akbari, Oyedun and Kumar 2019
	Gasification	Syngas	Fuel/Electric power	Tezer *et al.* 2022
	Pyrolysis	Bio-oil/Bio-char	Fuel/Chemicals	Schroeder *et al.* 2017
	Liquefaction	Bio-oil/Bio-char	Fuel/Chemicals	Zhang *et al.* 2021a
Physicochemical	Transesterification	Biodiesel	Fuel/Chemicals	Nguyen *et al.* 2020
Biochemical	Fermentation	Bioethanol	Fuel/Chemicals	Rajesh Banu *et al.* 2021
	Anaerobic digestion	Biogas	Fuel/Chemicals	Bahadur Pal *et al.* 2022

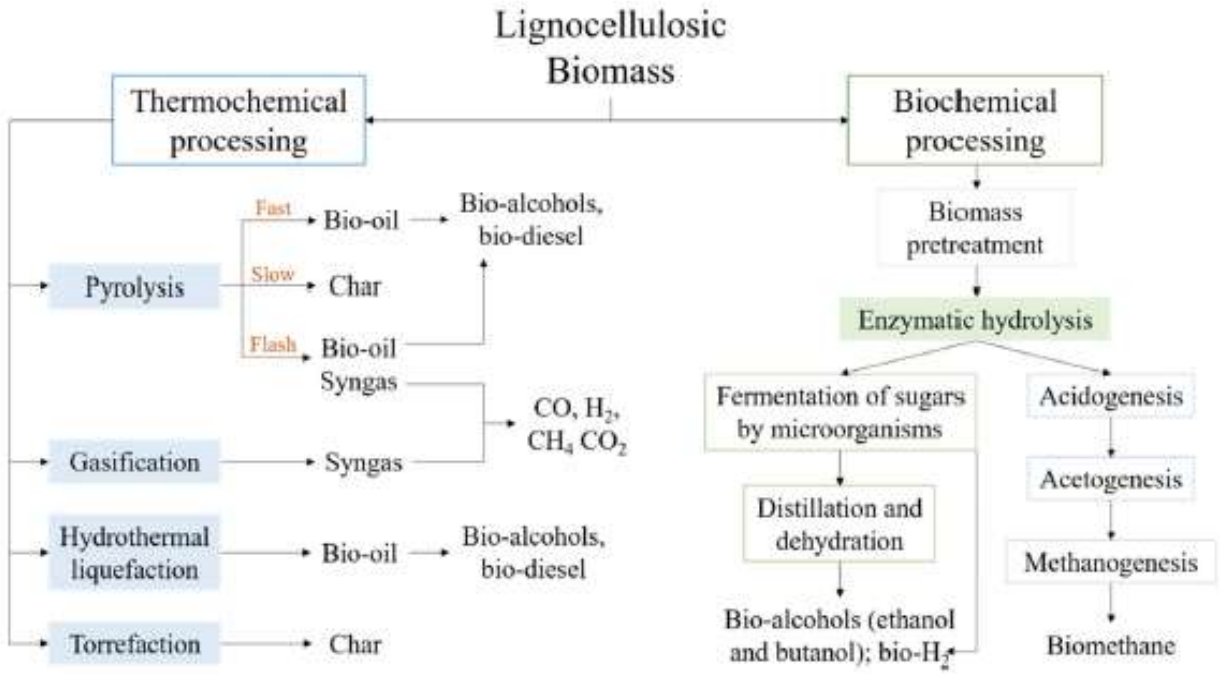

Figure 2. 3: Bio-refinery technologies for conversion of LB into biofuels (Rodionova *et al.* 2022)

2.3. Thermochemical conversion

Thermochemical conversion of biomass into biofuels is the thermal treatment of biomass in the presence or absence of oxygen and/or water to produce biofuels. The fuels typically produced by thermochemical means include syngas, bio-oil, bio-coal (bio-char and hydro-char) and heat. This is the broadest category of biomass to energy conversion technologies which include pyrolysis, gasification, carbonisation, liquefaction and combustion (Lachos-Perez *et al.* 2022; Shahbeik *et al.* 2022). Thermochemical processes are suitable for handling LB since they employ heat which can break down the recalcitrant structure of lignocellulose. Each of the thermochemical processing routes is explained in detail in the following sub-sections.

2.3.1. Pyrolysis

It is a physiochemical conversion that involves thermal breakdown of organic compounds, under oxygen-free medium at elevated temperatures usually in the range between 500 – 1000 ^{0}C to form a liquid product (bio-oil), solid product (bio-char) and non-condensable gas commonly referred to as syngas (Atabani *et al.* 2019). There are different techniques of pyrolysis classified according to reaction temperature, heating rate and vapor residence time (Jaroenkhasemmeesuk *et al.* 2022); i.e., slow, fast, intermediate, vacuum ablative or flash pyrolysis (Patel, Zhang and Kumar 2016) .In all four techniques, the product stream is composed of all the three products, i.e., bio-oil, syngas and bio-char),but their proportions and product distribution differ. Slow pyrolysis enhances the production of bio-char; flash pyrolysis maximises the production of syngas whereas fast pyrolysis maximises bio-oil production.

Both SCG and DSCG have a higher potential for bio-oil production via pyrolysis compared to other organic wastes, especially woody biomass with relatively low energy content. However, bio-oil obtained from SCG has a higher HHV than that recovered from DSCG, and this is attributed to the loss of carbon and hydrogen to extracted coffee oil (lipids) and the relatively higher oxygen content in DSCG bio-oil. Also DSCG bio-oil has a higher nitrogen content than SCG bio-oil and thus its combustion may cause more nitrogen oxide emissions (Atabani *et al.* 2019).

Table 2. 3: Pyrolysis type, process parameters and product distribution (Rijo *et al.* 2022)

Process parameter		Slow pyrolysis	Fast pyrolysis	Flash pyrolysis
Feedstock size (mm)		5 – 50	3	0.2
Temperature (^{0}C)		300 – 700	400 – 800	800 – 1000
Heating rate (^{0}C/s)		0.1 – 1	10 – 200	1000
Vapor residence time		10 – 100 min	0.5 – 5 min	0.5 s
Yield (wt. %)	Gases	35	30	13
	Bio-char	35	20	12
	Bio-oil	30	50	75

It can be seen from Table 2.3 that slow pyrolysis requires milder conditions (lower temperature), longer residence time and process biomass with larger particle size with bio-char being the dominant product. Fast pyrolysis requires slightly higher temperature than that of slow pyrolysis, shorter residence time (less than 5 min) and requires biomass with relatively smaller particle size (3 mm) to form bio-oil as the main product. Flash pyrolysis requires extremely harsh conditions (higher temperatures above 800 ^{0}C), very short residence time (less than 0.5 s), biomass particle size of 0.2 mm and a higher heating rate (1000 ^{0}C/s) to give non-condensable gases as the main product. This means that pyrolysis is a robust conversion route that can yield of any of the three products, i.e., bio-oil, bio-char or syngas, under optimised operating conditions.

Pyrolysis bio-oil has the potential of replacing fossil fuels for heat and power generation, as a drop-in fuel upon upgrading and as a precursor for synthesis of a wide range of chemicals. The drawback of bio-oil as opposed to fossil fuels is that it contains a higher oxygen content which makes it acidic and unstable, thus it cannot be used directly in combustion engines without engine modification or bio-oil upgrading. Both engine modification and bio-oil upgrading make the use of pyrolysis derived biofuel less economically competitive. The quality and yield of pyrolysis products depend upon a number of process parameters that include presence of catalyst, temperature, pressure, residence time, feedstock type, heating rate, particle size, moisture content of feedstock, etc. These factors are explained in detail in the sub-sections below.

2.3.1.1. Effect of catalyst on product distribution

Bio-oil produced from biomass pyrolysis is of low quality because it contains higher oxygen content and cannot be directly used in combustion engines without a need for engine modification or bio-oil upgrading. Quality of bio-oil can be improved by use of catalysts in the pyrolysis process

which helps to reduce the oxygen content. Oxygen is removed in the form of CO_2, CO and water in the presence of suitable catalyst (Ly *et al.* 2022).

Rijo *et al.* (2022) carried out a study simulation to investigate the effect of different catalysts (CaO, marble powder, bauxite, zeolite and Na_2CO_3) on the pyrolysis of Portuguese forest residues (maritime pine and eucalyptus globulus). It was observed that addition of catalysts resulted in the decrease in bio-oil yield while increasing the yield of gaseous products except for bauxite and marble powder which gave the highest bio-oil yield of 36% and 39%, respectively. The decrease in bio-oil yield and increase in gaseous product yield with the use of other catalysts was due to the increase in gasification reactions boosted by such catalysts. However, catalysts produced bio-oil with a lower oxygen content compared to that obtained without the use of catalysts. This means that extra care is needed in choosing the appropriate type of catalyst that will improve the quality of bio-oil produced without greatly reducing the yield.

In the study conducted by Ly *et al.* (2022) on pyrolysis of spent coffee waste in the presence of a catalyst, it was observed that the use of catalyst resulted in lower bio-oil yields and higher gaseous product yield, and this is attributed to the catalytic cracking of pyrolysis vapors into low molecular weight compounds (gases.) However, the use of catalysts resulted in an increase in bio-oil quality because the presence of catalysts enhanced the deoxygenation reactions like dehydration, decarboxylation and decarbonylation resulting in lighter fractions and non-condensable gases. It can therefore be concluded that the presence of a catalyst during biomass pyrolysis decreases bio-oil yield and enhances syngas yield. The bio-oil yield decreases but its quality increases and this means that a tradeoff exists between increased bio-oil quality and decreased yield when a catalyst is used.

2.3.1.2. Effect of temperature on product yield

Temperature is one of the most important parameters that must be properly controlled and monitored for maximum bio-yield from fast pyrolysis. The yield of bio-oil increases with increasing temperature until a maximum point is reached where any further increase in temperature results in a drop in bio-oil yield. In the study conducted by Ly *et al.* (2022) on fast pyrolysis of spent coffee waste (SCW), it was observed that increasing temperature from 673 K to 733 K increased bio-oil yield from 55 wt.% to 59 wt.% while bio-char yield decreased from 28 wt.% to 26 wt.% and gaseous product yield increased from to 16 wt.% to 26 wt.%. However, further rise

in temperature to 772 K decreased bio-oil yield to 52 wt.%. This is due to thermal decomposition of bio-oil fractions into lighter organic compounds releasing gases at elevated temperatures. The conclusion from Ly *et al.* (2022) is in agreement with the findings made by Hasan *et al.* (2022) on product yield and bio-oil composition of waste macadamia nutshell (WMNS) using Aspen plus modeling. In their study, they reported that increasing the temperature from 350 ^{0}C to 500 ^{0}C increased bio-oil yield which then dropped as temperature was increased beyond 500 ^{0}C, while syngas yield increased and bio-char yield decreased even further. Again, this observation is attributed to thermal decomposition of heavy pyrolysis components as temperature increases forming lighter fractions with low molecular mass. In the study conducted by Liu *et al.* (2022a) on preparation of bio-char from biomass pyrolysis using Aspen plus modeling, it was observed that increasing the temperature from 300 ^{0}C to 500 ^{0}C caused a slight decrease in bio-char yield. The drop in bio-char yield became more rapid when the temperature was increased beyond 500 ^{0}C. This is explained by secondary cracking of bio-char fractions at elevated temperatures. It can be inferred that temperature is a sensitive parameter that must be closely monitored and can used to manipulate the selectivity of the three (bio-oil, bio-char and syngas) pyrolysis products.

2.3.1.3. Effect of pressure on biomass pyrolysis

Pressure is not a highly significant factor affecting both the yield and product distribution of biomass pyrolysis (Jaroenkhasemmeesuk *et al.* 2022). Most researchers on biomass pyrolysis have used atmospheric pressure (1 bar) for both lab-scale experiments and computer simulations.

2.3.1.4. Effect of residence time on biomass pyrolysis

Residence time is not an independent factor and largely depends on temperature used (Jaroenkhasemmeesuk *et al.* 2022). It can be seen from Figure 2.4 that at 450 ^{0}C, increasing residence time increases syngas and bio-oil yield at the expense of decreasing bio-char yield. It can be deduced from Figure 2.4 that for optimal bio-oil yield, a temperature of 500 ^{0}C and 5 seconds residence time should be used. Together with variation in temperature and heating rate, residence time defines the type of pyrolysis and the variations in the yields of bio-char, bio-oil and syngas. For residence time between 10 – 100 minutes and temperature range of 300 – 700 ^{0}C, the pyrolysis type is slow pyrolysis and bio-char is the dominant product. For residence time between 0.5 – 5 minutes and temperature range of 400 – 800 ^{0}C, the pyrolysis type is fast pyrolysis and bio-oil is the dominant product. For residence time less than 0.5 minutes and temperature range of 800

– 1000 ^{0}C, the pyrolysis type is flash pyrolysis and syngas is the dominant product (Rijo *et al.* 2022).

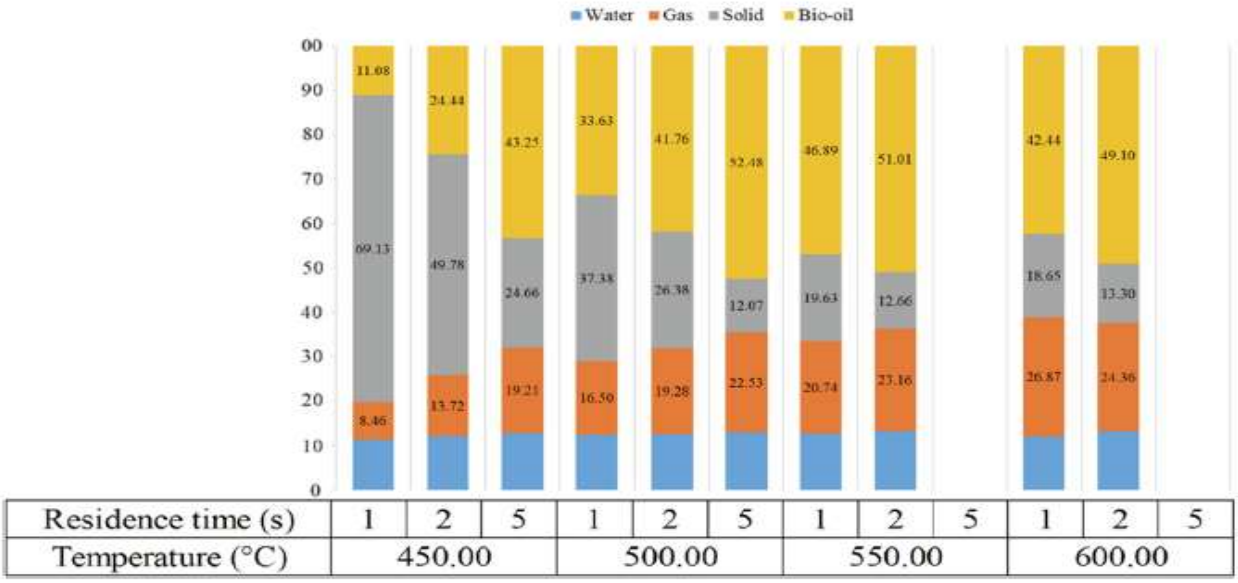

Figure 2. 4: Variation of pyrolysis product yields with temperature and residence time (Jaroenkhasemmeesuk et al. 2022)

2.3.1.5. Effect of feedstock type on product distribution

The type of feedstock used also determines the product distribution of biomass pyrolysis. In the study conducted by AlNouss *et al.* (2021) on five different types of fruit wastes namely orange peel, banana peel, mango endocarp, apricot kernel shell, and date pits; it was observed that the highest char yield (50.9 wt.%) was obtained from date pits whereas the mango endocarp gave the highest syngas yield (54.2 wt.%). The highest char yield from date pits is attributed to its highest carbon content of all the fruit waste samples used, and the highest syngas yield from mango endocarp is because of its highest volatile matter content. Therefore, it can be concluded that high carbon content favors char yield whereas high volatile matter content enhances syngas yield.

2.3.1.6. Effect of feedstock particle size on biomass pyrolysis

Particle size is so crucial during biomass pyrolysis since lignocellulose biomass is a non-conducting material (Patel, Zhang and Kumar 2016). In the study conducted by Hasan *et al.* (2022), it was observed that high bio-char yield was obtained from feedstock with larger particle size whereas bio-oil yield was not favored by larger particles of feedstock. This observation is

explained by uneven heat distribution with larger particles which leads to low carbon conversion efficiency, hence lower bio-oil yield but higher bio-char yield. Syngas yield showed the same trend as bio-oil with its yield increasing with decreasing biomass particle size.

2.3.1.7. Effect of biomass moisture content on product distribution

The presence of moisture in biomass greatly affects the yield and distribution of pyrolysis products. In the study conducted by Hasan *et al.* (2022), it was observed that an increase of moisture in biomass increased bio-oil yield at the expense of both bio-char and syngas yields as illustrated in Figure 2.5. This was attributed to steam cracking of larger molecules into bio-oil vapors at high moisture content. Also, the amount of carbon in bio-oil decreased whereas oxygen content increased as shown in Figure 2.6. This is brought about as a result of char gasification while water is dissociated into hydrogen and oxygen. This means that for good bio-oil quality, moisture content should be kept as low as possible in order to reduce oxygen content in the resulting oil.

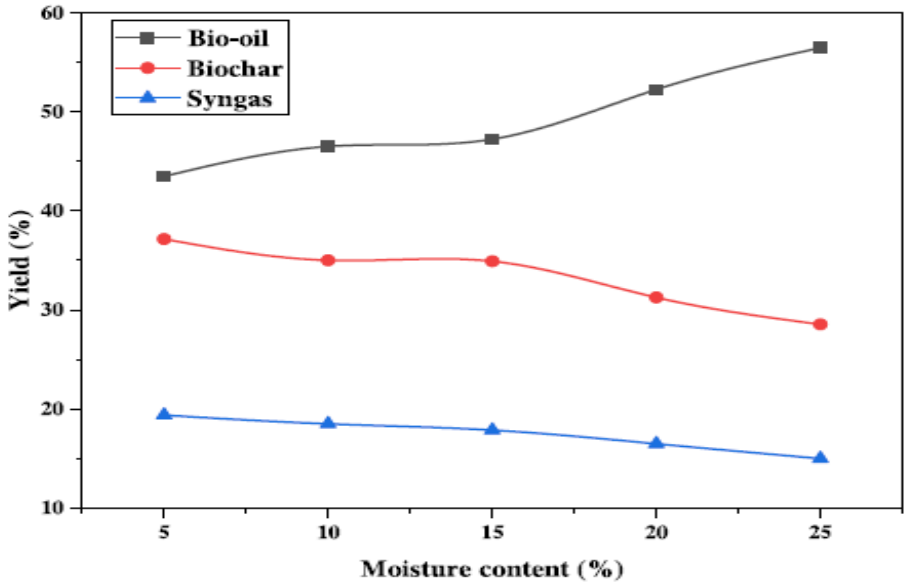

Figure 2. 5: Effect of moisture content on pyrolysis product distribution (Hasan *et al.* (2022)

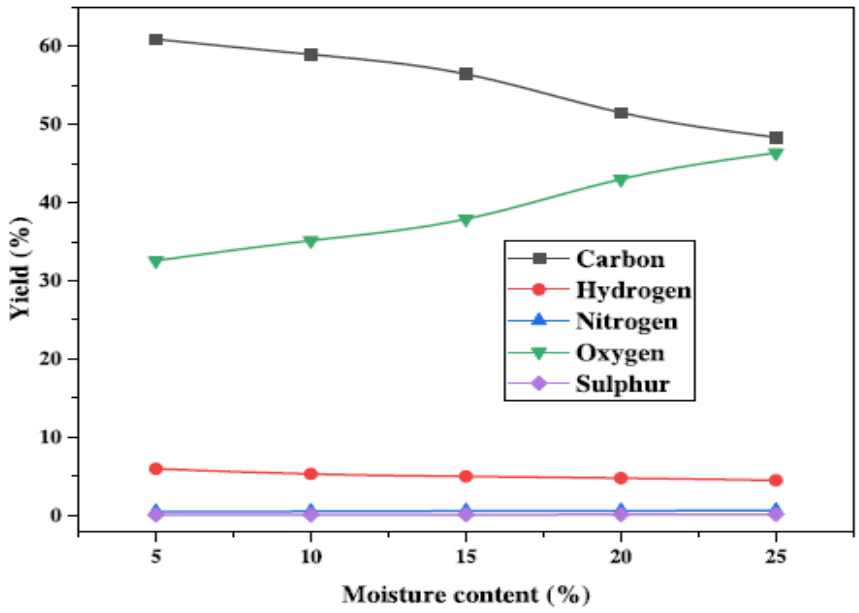

Figure 2. 6: Effect of moisture content on bio-oil elemental composition (Hasan *et al.* (2022)

2.3.2. Hydrothermal liquefaction

This is a thermochemical conversion route that involves the conversion of biomass into four phases; the bio-oil phase, NCG, bio-char and the aqueous phase containing organics, at high pressure in the presence of water. Hydrothermal liquefaction (HTL) differs from traditional processes like pyrolysis and gasification in the sense that it handles wet biomass with high moisture content and no pre-drying required, hence saves energy that would otherwise be consumed in the drying process (de Caprariis *et al.* 2017; Biswas *et al.* 2022; Forero *et al.* 2022; Li *et al.* 2022). HTL is a promising thermochemical conversion route to bioenergy, bio-crude has asphalt-like properties and hydro-char can work as an adsorbent of dyes and help in soil amendment as fertilizer (Zhou *et al.* 2022). The possible disadvantage of HTL is the use of high pressure which may lead to high equipment cost required for large scale production (de Caprariis *et al.* 2017). HTL gives higher yield of bio-oil with a higher quality, lower oxygen and water amounts and higher HHV compared to the bio-oil obtained from pyrolysis. Also the polar organics produced dissolve in the aqueous phase and not in the bio-oil phase as it is the case with pyrolysis (de Caprariis *et al.* 2017).

Bio-crude has a lower oxygen content compared to bio-oil obtained by conventional pyrolysis hence HTL bio-crude has a higher HHV (Scarsella *et al.* 2020). However, bio-crude cannot be

directly used as a drop-in liquid fuel due to relatively higher oxygen content and needs upgrading technologies like hydro-treatment or catalytic cracking. Both of these upgrading technologies require large amounts of hydrogen gas which makes them expensive and hence influencing the profitability of the production process. A lot of research is being conducted to valorize the production of hydrogen gas from biomass but nevertheless, the predominant method of its production is by natural gas steam reforming which makes the bio-crude upgrading process still dependent on fossil fuels (Scarsella *et al.* 2020). The properties of bio-crude obtained by biomass HTL are largely dependent on feedstock characteristics and operating conditions like temperature, residence time, pressure, nature of solvent and catalyst used (Alherbawi *et al.* 2021). These process conditions are explained in detail in the following sub-sections.

2.3.2.1. Effect of temperature on HTL

The temperature range (250 – 400 ^{0}C) used in HTL is relatively lower than that used in conventional pyrolysis and this helps to save on the energy input of the process. Figure 2.7 shows the variation of reaction temperature with bio-crude and bio-char yield. Bio-crude yield increases with temperature until a threshold is reached where any further increase in temperature lowers bio-crude yield and this is mainly because of the two reactions; hydrolysis and re-polymerisation. Zhang *et al.* (2021a) conducted a study on co-liquefaction rice straws (RS) and waste cooking oil (WCO), and observed that increasing the temperature from 250 ^{0}C to 300 ^{0}C increased the bio-crude yield from 65% to 66%. However, further increase of temperature to 350 ^{0}C decreased the yield of bio-crude to 62.4%. This is due to secondary decomposition and Boudouard reactions at higher temperatures which converts bio-crude into the gaseous products and water-soluble compounds. They observed a decrease in bio-crude and solid residue whereas the yield of aqueous and gaseous phase increased at higher temperatures. This agrees with the study conducted by Alper *et al.* (2021) who observed that bio-crude yield increased with increasing temperatures from 250 ^{0}C to 300 ^{0}C, and a further increase of temperature to 350 ^{0}C reduced the yield of bio-crude. Again, this is attributed to the gasification reactions of bio-crude at elevated temperatures, increasing the gas yield at the expense of bio-crude yield. It was further observed that the solid residue yield decreased when the temperature was increased further to 350 ^{0}C.

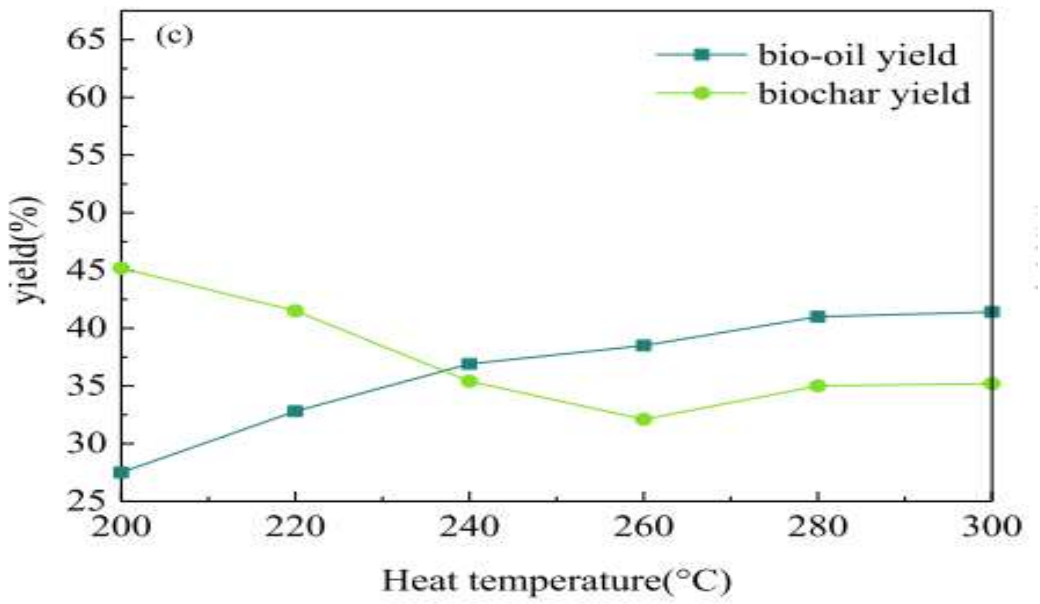

Figure 2. 7: Effect of temperature on HTL product yield (Zhou *et al.* (2022)

2.3.2.2. Effect of biomass particle size on HTL

Unlike with pyrolysis, for hydrothermal liquefaction, biomass particle size has been found to have a less significant effect on bio-crude yield and quality, and this is due to the use of supercritical or subcritical water which improves the mass transfer limitations (Mishra *et al.* 2022).

2.3.2.3. Effect of catalyst on HTL

Like all chemical reactions, the use of catalysts in HTL of biomass has numerous advantages ranging from reduction of activation energy of reaction, lowering the optimal temperature, increasing bio-crude yield, improving the HHV of bio-crude, improving flow properties ,lowering heteroatom content of bio-crude to enhancing biomass conversion efficiency (Nagappan *et al.* 2021). Use of catalysts also helps to improve the bio-oil yield and its properties by reducing the condensation and re-polymerisation of intermediate products.

Different catalysts have been used and these include acid catalysts, basic catalysts and heterogeneous catalysts. Homogeneous acidic and alkaline catalysts (HCl, H_3PO_4, Na_2CO_3, K_2CO_3, KOH, NaOH, and Ca $(OH)_2$) have been largely researched. They are inexpensive and their use has been reported to enhance the quality and yield of bio-crude. However, their homogeneity nature makes the whole process expensive due to additional costs associated with separation

processes and also corrosive resistant materials of construction are required when using these catalysts. Another challenge with homogeneous catalysis is recovery of the catalyst. During HTL, the catalyst is discharged with the aqueous phase which complicates waste management operations like the addition of acid or base to neutralise the catalyst which eventually increases waste management costs (Scarsella *et al.* 2020; Nagappan *et al.* 2021).

On the other hand, heterogeneous catalysts (alkaline metal oxides, transition metals, lanthanide oxides and zeolites) have a higher catalytic activity and can easily be recovered from the liquid mixture making reusability possible. Also heterogeneous catalysts are not corrosive and have a higher thermal stability. However, homogeneous catalysts are not extensively used when compared to heterogeneous catalysts owing to the external and internal mass transfer limitations associated with heterogeneous (solid-liquid and gas-solid) reactions (Scarsella *et al.* 2020).

In the study conducted by Zhang *et al.* (2021a) on the co-liquefaction of rice straw and waste cooking oil, the effect of K_2CO_3 as a catalyst was investigated and it was observed to have a negative effect on bio-crude yield. The addition of a catalyst enhanced the formation of aqueous and gaseous phases, and reduced the solids and bio-crude yield. Alper *et al.* (2021) conducted a study to investigate the catalytic effect of a Lewis acid ($Mg(ClO4)_2$), Bronsted acid (HClO4) and their combined effect ($HClO4/Mg(ClO4)_2$) on bio-crude yield. It was observed that at optimum conditions (temperature of 300 ^{0}C and residence time of 30 minutes), HTL of teak wood showed the highest bio-crude yield in the absence of a catalyst. In other words, all the three forms of catalysts had a negative effect on bio-crude yield which greatly decreased with increasing catalyst loading.

The use of alkali catalysts like KOH, Na_2CO_3 and K_2CO_3 help to reduce the solid residue yield and enhances bio-crude yield from woody biomass because of their ability to liquefy lignin and also facilitate the hydrolytic decomposition of holocelulose. Acid catalysts help to improve the flow properties of bio-crude through lowering its viscosity and high boiling components. However, their use increases the yield of the gaseous phase and are also not effective in reducing the heteroatom content of bio-crude (Nagappan *et al.* 2021).

Figure 2.8 shows the effect of three catalysts namely; KOH, HCL and H_2SO_4 on bio-crude and hydro-char yield. It can been observed that acid catalysts enhance the yield of solid residue at the

expense of reducing the bio-crude yield with sulfuric acid showing the lowest bio-crude yield. On the other hand, alkali catalysts enhance bio-crude yield and are regarded as inhibitors for bio-char yield. This means that alkali catalysts are suitable when the desired product is bio-crude.

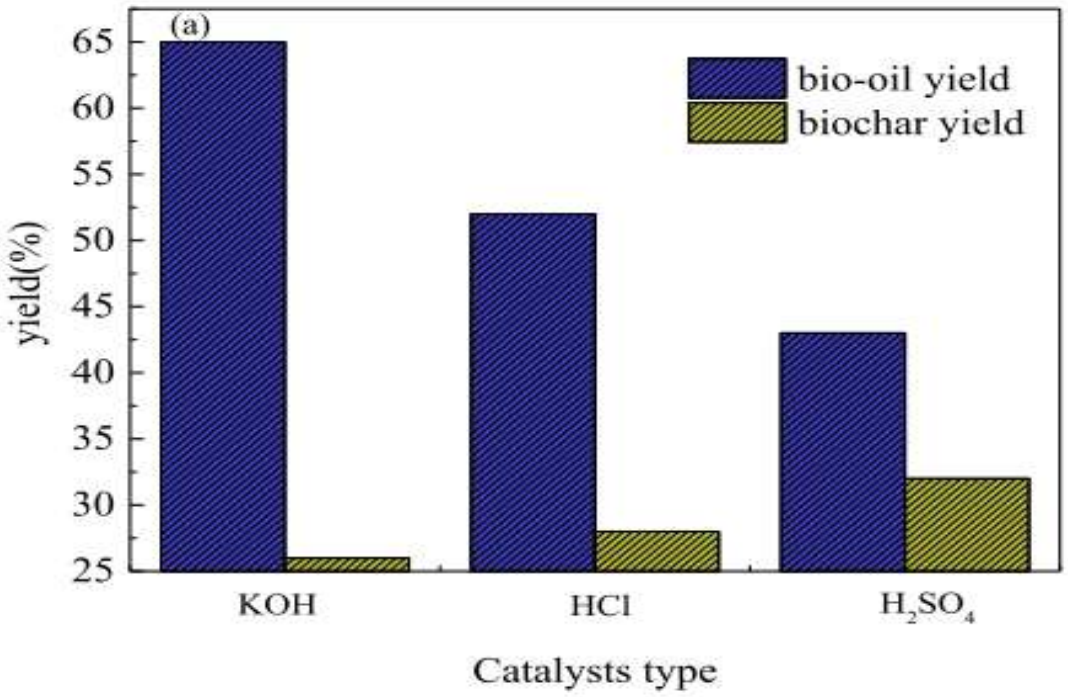

Figure 2. 8: Effect of catalyst on bio-crude and solid residue yield (Zhou *et al.* 2022)

2.3.2.4. Residence time

Increasing residence time enhances bio-crude yield until a threshold above which bio-crude yield decreases as shown in Figure 2.9. This is due to the cracking and re-polymerization of bio-crude and its intermediates. Residence time is always monitored with temperature and there is no optimal residence time for different types of feedstock and different temperatures. In the study conducted by Zhang *et al.* (2021a) on the co-liquefaction of rice straw and waste cooking oil, it was observed that increasing residence time from 10 to 30 minutes decreased bio-crude yield while increasing the yield of aqueous phase, solid and gaseous phases. In fact, a further increase in residence time to 60 minutes sharply decreased the yield of bio-crude. This is due to decomposition of bio-crude into gaseous products and water soluble compounds and re-polymerization of bio-crude intermediates into hydro-char at longer residence time. This concurs with observations made by

Alper *et al.* (2021) on the study conducted on HTL of teak wood. There was no significant change in bio-crude and solid residue yield between 15 to 30 minutes, however, increasing residence time to 60 minutes gave the lowest bio-crude yield.

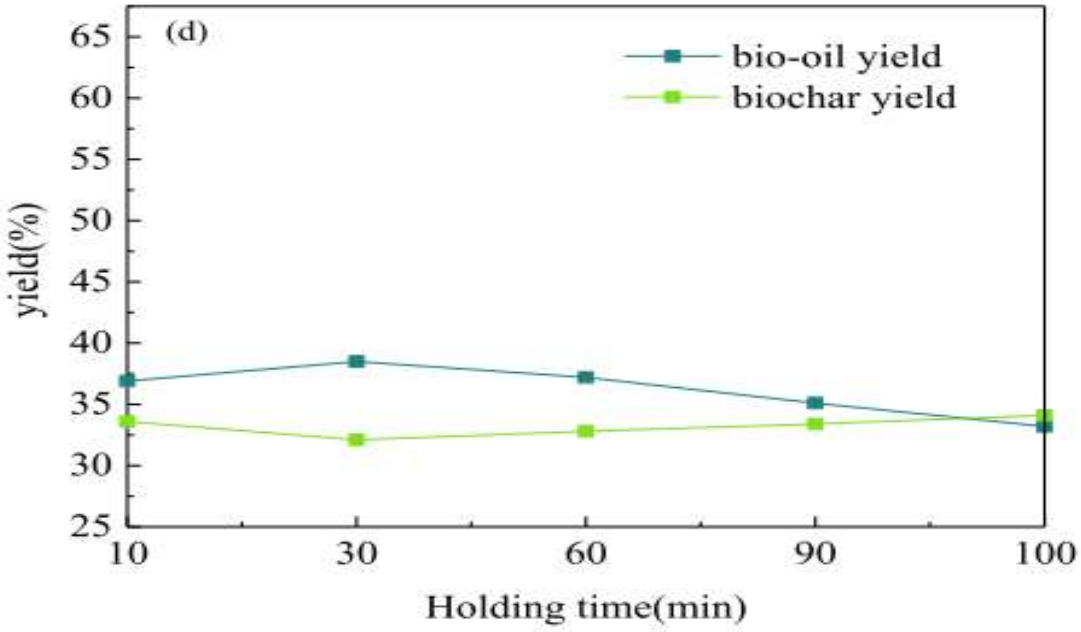

Figure 2. 9: Effect of residence time on HTL product yield (Zhou *et al.* 2022)

2.3.2.5. Effect of solvent

Different solvents have been used during HTL and these include water and organic solvents like methanol, ethanol and acetone, with water being the most commonly used due to its availability at low cost (Mishra *et al.* 2022). Another advantage of using water as a solvent is that it is environmentally friendly. Also near the critical point of water (374 ^{0}C, 22.064 MPa), its Viscosity and dielectric constant decrease allowing for solubility of hydrophobic organic compounds while its ionic product increases making it act as a catalyst for acid-base reactions (Scarsella *et al.* 2020). The drawback of using water as a solvent is its higher boiling point, higher dielectric constant and higher critical point than that of organic solvents like methanol (239.45 ^{0}C, 8.09 MPa) and ethanol (240.75 ^{0}C, 6.14 MPa). This means that the use of organic solvents employs moderate temperature and pressure compared to water with a higher critical point. Also, higher molecular mass compounds can easily dissolve in organic solvents owing to their low dielectric constant. However, water is still the most commonly used solvent for HTL (Mishra *et al.* 2022).

2.3.3. Hydrothermal gasification

Hydrothermal gasification (HTG) is analogous to conventional gasification in a way that both processes aim at syngas (H_2, CO, CO_2) production in an oxidant-free environment. The remarkable difference is that HTG handles wet biomass at the supercritical point of water i.e., at 374 ^{0}C and 22.1 MPa (Okolie *et al.* 2021; Shahbeik *et al.* 2022), whereas gasification handles dry biomass at temperatures around 1000 ^{0}C and atmospheric pressure. The ability of HTG to handle wet biomass helps to remove the pre-drying step which consumes a lot of energy (Elias Bamaca Saquic *et al.* 2021). Another advantage of HTG is that there is no tar formation since supercritical water solubilises all tar intermediates. Tar formation is a major challenge during conventional gasification (Hoang *et al.* 2022). There is relatively lower energy consumption with HTG since its reactions take place at relatively lower temperatures (about 374 ^{0}C) as compared to about 700 - 1000 ^{0}C for conventional gasification. However, HTG is not fully developed and most gasification plants employ the conventional technology. This is because HTG requires special equipment of construction due to the use of high pressure. This leads to high capital investment needed to set up an HTG plant. Corrosion resistant equipment must be used since there is salt precipitation during HTG. Corrosion resistant materials are made of special alloys that are expensive which also raises the initial capital investment.

2.3.4. Hydrothermal Carbonisation

Hydrothermal carbonization (HTC) is the thermochemical conversion of wet biomass into a coal-like sold, bio-oil and NCG in an oxygen-free environment at moderate temperatures, between 180 ^{0}C – 300 ^{0}C (Akbari, Oyedun and Kumar 2019, 2020) and pressure between 2 – 10 MPa (Gonzalez-Arias *et al.* 2021). HTC differs from conventional pyrolysis in the sense that it handles wet biomass at moderate temperatures and aims to maximize the solid yield. The solid product from torrefaction has several names namely bio-coal, bio-char, charcoal, hydro-char, torrefied wood and green coal (Akbari, Oyedun and Kumar 2019, 2020). Although these names are often used interchangeably, these products don't necessarily have the same properties. For example, the names hydro-char and bio-char are used to refer to solid product formed during wet torrefaction (or HTC) and dry torrefaction (or simply torrefaction), respectively (Akbari, Oyedun and Kumar 2020), and they have different properties. Hydro-char contains less ash compared to bio-char because most of the organic compounds dissolve in the aqueous phase during wet torrefaction which is not the case for bio-char since no water is present to serve as a solvent for organics during dry torrefaction.

HTC is different from torrefaction or slow pyrolysis since it is capable of handling wet biomass and this helps to remove the necessity of biomass pre-drying (Gonzalez-Arias *et al.* 2021). The process of moisture removal consumes a lot of energy in the form of heat which makes torrefaction more expensive than HTC. Hydro-char has several advantages namely it has lower oxygen-to-carbon ratio as volatiles are released during HTC making it less susceptible to self-ignition during size reduction. It is durable and can be stored outside over a long period of time, thereby removing costs of building storage facilities (Akbari, Oyedun and Kumar 2020). Bio-coal has a higher heating value, higher energy density and is more hydrophobic (Gonzalez-Arias *et al.* 2021).

Hydro-char is similar to conventional coal (Akbari, Oyedun and Kumar 2020) and thus can be co-fired with coal or used as a perfect substitution for coal. Co-firing with bio-coal has several advantages over wet biomass as the latter has a higher moisture content which lowers its calorific value. It has a lower biomass-to-coal ratio, high transport costs due to its low bulk density and loss of mass upon storage caused by fungal activity due to its moisture content.

Due to increased environmental concerns worldwide, attempts are being made to completely abandon coal firing energy plants and replace them with biomass derived feedstock or renewable energy solutions. Wet torrefaction is the possible substitute for conventional coal and its ability to handle heterogeneous biomass feedstock makes a perfect solution (Akbari, Oyedun and Kumar 2020).

2.3.5. Gasification

Gasification is a thermochemical conversion route that transforms biomass into gaseous fuels at high temperatures between 700 – 1200 ^{0}C (Hoang *et al.* 2022). The gaseous product is a mixture of CO, H_2, and CH_4, undesired components like N_2, CO_2, and hydrocarbons. The desired product (CO, H_2) is called synthetic gas or commonly known as syngas and is a precursor for synthesis of many useful substances like methanol, bio-hydrogen and liquid hydrocarbons through the Fischer-Tropsch synthesis (Yong and Abdul Rasid 2021; Kushwah, Reina and Short 2022). Gasification involves mainly four stages, namely drying, pyrolysis, oxidation and reduction. Drying involves the expulsion of water from wet biomass at temperatures less than 150 ^{0}C. Pyrolysis occurs between 150 – 700 ^{0}C and involves the breakdown of biomass into volatile fractions including CO, CO_2, hydrocarbons, tar, and pyrolysis oil in the absence of air (oxygen). Oxidation occurs between 700 – 1200 ^{0}C where the products of pyrolysis react with the gasifying agent to generate

heat needed by the endothermic reactions in the gasification process. Reduction occurs between 800 – 1100 ^{0}C where char reacts with hot gas to form syngas. Gasification is carried out in the presence of a gasifying agent which is usually air, steam or pure oxygen, all of which steam gasification has received more attention because it enhances the concentration of hydrogen in the gaseous product and also gives a higher Cold Gas Efficiency (CGE) (Yong and Abdul Rasid 2021; Tezer *et al.* 2022).

2.3.5.1.Types of gasifiers

There are two types of gasifiers, namely fixed-bed and fluidized-bed gasifiers (Hoang *et al.* 2022). The fixed-bed gasifiers are classified according to the direction of flow of the gasifying agent and are further divided into cross-draft, updraft and downdraft gasifiers. Figure 2.10 shows the design of two main fixed-bed gasifiers (updraft and downdraft). In updraft gasifiers (Figure 2.10b), the gasifying agent enters through the bottom whereas biomass enters through the top of the gasifier creating a countercurrent flow between the gasifying agent and biomass. This configuration of gasifiers is easy to use and has a higher thermal efficiency, however, it is prone to tar formation and only effective for small scale operations (Hoang *et al.* 2022). With downdraft gasifiers, both biomass and gasifying agent flow in a co-current direction as shown in Figure 2.10 (b). The advantage of this design over the updraft gasifier is its capacity to reduce tar formation. Approximately 75% of world's commercial gasification plants use fixed-bed downdraft gasifiers (Chen *et al.* 2020). Another type of gasifier is the fluidised-bed gasifier which is also classified as circulating fluidised-bed gasifiers, bubbling fluidised-bed gasifiers, dual fluidised-bed gasifiers and entrained-bed gasifiers (Hoang *et al.* 2022). In fluidised-bed gasifiers, an oxygen-rich gas suspends feedstock particles within the gasifier and the resulting bed acts a fluid. To maintain fluidisation within the gasifier, feedstock of small particle size usually less than 6 mm is normally used (NETL 2024).

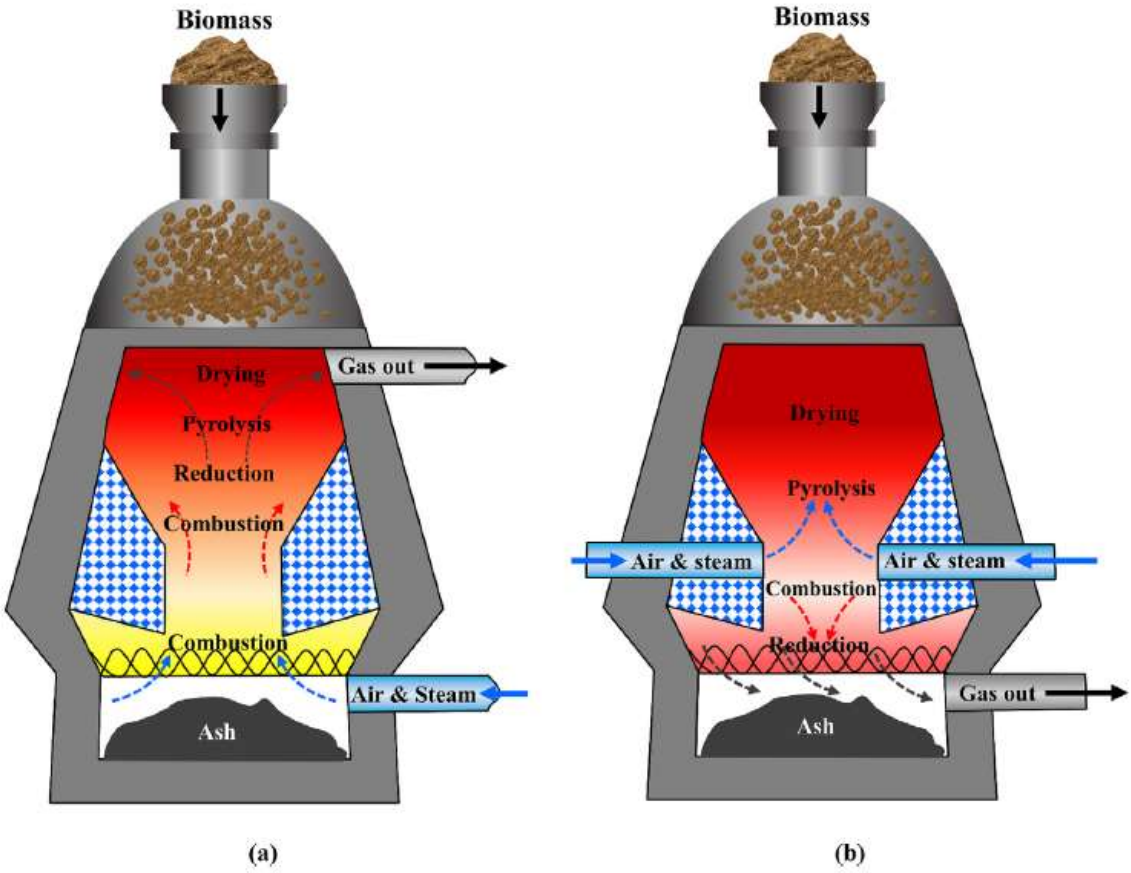

Figure 2. 10: Fixed-bed gasifiers, (a) updraft gasifier and (b) downdraft gasifier (Hoang *et al.* 2022)

There are a number of process parameters that affect both syngas yield and its composition. These parameters include temperature, pressure, moisture content, biomass particle size, equivalence ratio if air is used as the gasifying agent, or steam-to-biomass ratio, if steam is used as the gasifying agent, and nature of gasifying agent. Each of these factors is explained in the following sections.

2.3.5.2. Effect of temperature

As temperature increases, CO and H_2 content increases, whereas CO_2, char and CH_4 content decrease. According to Le Chatelier's principle, an increase in temperature shifts the equilibrium to the right favouring products if the reaction is endothermic, and the equilibrium is shifted more to the left favouring reactants if the reaction is exothermic (Liu *et al.* 2022b). CO and H_2 content increase because increasing temperature favours the endothermic reactions (Boudouard, water-gas and methane reforming reactions) as shown in Table 2.4. Since the Boudouard reaction is endothermic, an increase in temperature shifts the equilibrium to the right favouring the formation

of CO while consuming more char. The water-gas shift reaction is exothermic and therefore an increase in temperature shifts the equilibrium to the left causing products CO_2 and H_2 to react to form more CO. This explains the decrease of CO_2 as temperature increases. It can be seen from Figure 2.11 that at 600 ^{0}C, CO_2 yield is 40% but its yield decreases to 30% at 800 ^{0}C, and further decreases to 20% at 900 ^{0}C. The methane reforming reaction is endothermic and thus an increase in temperature favours the forward reaction causing more CH_4 to react forming 1 mole of CO and 3 moles of H_2. This explains the decrease of CH_4 content and increase of H_2 at elevated temperatures. Also, the thermal cracking of hydrocarbons increases with increasing temperature, and this increases the carbon conversion efficiency.

Table 2. 4: Reactions taking place during biomass gasification (Kibret et al. 2021; Kumar et al. 2022)

Reaction equation	Name of reaction	Heat of reaction
$C + \frac{1}{2}O_2 \rightarrow CO$	Incomplete combustion	$-110.5\ kJ/mol$
$C + O_2 \rightarrow CO_2$	Complete combustion	$-394\ kJ/mol$
$C + H_2O \rightarrow H_2 + CO$	Water-gas	$+131.5\ kJ/mol$
$C + CO_2 \rightarrow 2CO$	Boudouard	$+173\ kJ/mol$
$CO + H_2O \rightarrow CO_2 + H_2$	Water-gas shift	$-41\ kJ/mol$
$CH_4 + H_2O \rightarrow CO + 3H_2$	Methane reforming	$+206\ kJ/mol$
$C + 2H_2 \rightarrow CH_4$	Methanation	$-75\ kJ/mol$

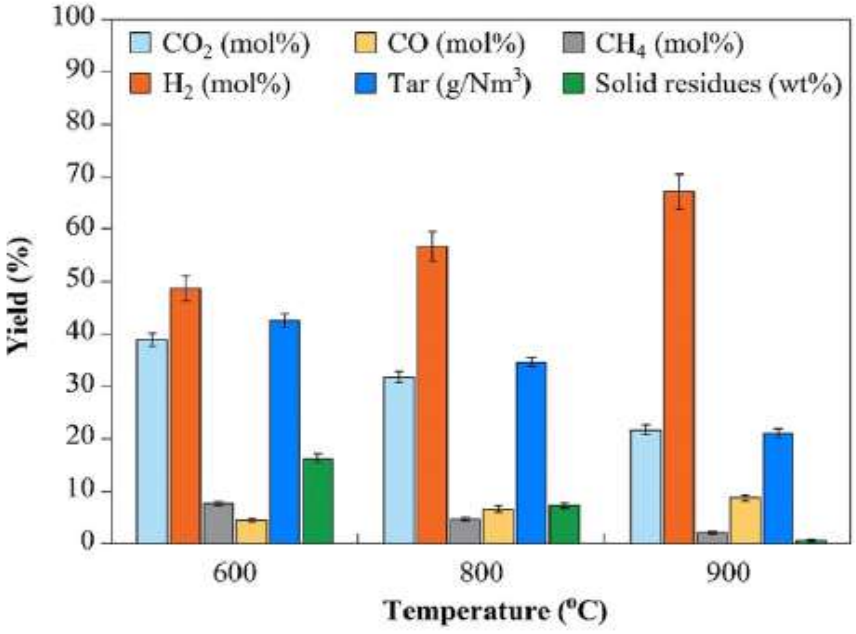

Figure 2. 11: Effect of temperature on gasification product yield (Hoang *et al.* 2022)

2.3.5.3. Effect of gasification temperature on LHV

The LHV of the producer gas increases with increasing content of CO and H_2 in the gas mixture. This therefore means that increasing temperatures increases the LHV of syngas since high temperature favors endothermic reactions (Boudouard reaction, water-gas reaction, water-gas shift reaction and methane reforming) which in turn favours the production of the main combustible gases, i.e., CO, and H_2. (Chen *et al.* 2019).

2.3.5.4. Effect of gasifying agent on biomass gasification

There are mainly four gasifying agents, namely air, oxygen, steam and carbon dioxide which can be used independently or as a mixture of two gasifying agents. However, steam and air are the most superior and commonly used gasifying agents in biomass gasification. Several studies have been carried out to investigate the effect of equivalence ratio (air-to-biomass ratio) and steam-to-biomass ratio on hydrogen concentration, syngas ratio (H_2-to-CO ratio), carbon conversion efficiency (CCE) and the high heating value (HHV) of syngas. According to the study made by Yong and Abdul Rasid (2021) to investigate the effect of equivalence ratio (ER) and steam-to-

biomass ratio (S/B) on the gasification of an empty fruit bunch, it was observed that an increase in ER from 0.2 to 0.4 caused the hydrogen concentration in syngas to decrease. This is because as air concentration increases, oxidation is more enhanced than cracking, boosting the formation of more CO_2 at the expense of decreasing H_2 concentration. Consequently, HHV and syngas ratio also decreased with the maximum syngas ratio of 1.03 obtained at ER of 0.2. The same study observed a boost in hydrogen concentration when air, as a gasifying agent, was replaced by steam. The maximum syngas ratio of 2.5 was achieved at S/B of 0.3. Increase in S/B ratio boosted hydrogen concentration because of the three reactions: water-gas reaction, water-gas shift reaction and methane reforming reaction whose equilibrium is shifted to the right with an increase in steam concentration producing more hydrogen (Yong and Abdul Rasid 2021). An increase in S/B ratio causes a decrease in CH_4, CO and char content in syngas due to the boost of methane reforming reaction, water-gas shift and water-gas reaction, respectively, at higher steam concentration.

2.3.5.5. Effect of pressure on biomass gasification

According to Le Chatelier's principle (Liu *et al.* 2022b), if a dynamic equilibrium is perturbed by altering the conditions, the equilibrium position shifts so as to annul the change to regain an equilibrium. For gaseous reactions, high pressure shifts the equilibrium to the side of fewer moles of gas in order to reduce the pressure (Singh *et al.* 2022). In the methane reforming reaction, 1 mole of methane reacts with 1 mole of steam to form 1 mole of carbon monoxide and 3 moles of hydrogen. This means that an increase in pressure shifts the equilibrium to the left causing more hydrogen and carbon monoxide to combine forming methane and water. Consequently, the concentration of CO and H_2 decreases as that of CH_4 is boosted. Syngas ratio (H_2/CO) moderately increases with increasing pressure since the decrease of CO is more rapid than that of H_2 (Singh *et al.* 2022). HHV of syngas increases with increase in pressure due the increase in methane concentration. Although the concentrations of CO and H_2 decrease with increasing pressure, that of methane increases and yet methane is the largest contributor to the HHV of syngas as shown in equation 2.1.

$$HHV\left(\frac{MJ}{Nm^3}\right) = \frac{12.76\,(vol\%\ H_2) + 12.63\,(vol\%\ CO) + 39.76\,(vol\%\ CH_4)}{100} \qquad 2.1$$

2.3.5.6.Nature of gasifying agent

Steam, air, oxygen or a mixture of the two are used as gasifying agents during biomass gasification (Hoang *et al.* 2022). Of all the gasifying agents, steam is superior resulting in syngas with higher hydrogen content and higher heating value.

2.4. Biochemical conversion

Biochemical conversion is the conversion of biomass to biofuels with the help of biocatalysts and microorganisms (Rodionova *et al.* 2022). Broadly, anaerobic digestion (AD) and fermentation are the two methods of biomass biological conversion producing bio-methane and bioethanol, respectively. Fermentation involves enzyme hydrolysis of biomass to form fermentable sugars which are fermented to bioethanol by microorganisms called yeast. On the other hand, AD involves four steps, namely hydrolysis, acidogenesis, acetogenesis and methanogesis producing methane and carbon dioxide (Rodionova *et al.* 2022). Biochemical methods are relatively cheaper and do not require sophisticated materials of construction and generally require mesosphilic conditions (25 – 40 ^{0}C). However, they are associated with low biofuel yields and longer reaction durations which is usually in days (Lachos-Perez *et al.* 2022). Each of the processing routes is explained in the following sections.

2.4.1. Anaerobic digestion

Anaerobic digestion (AD) is the biological decomposition of biomass in an oxygen-free environment to produce a mixture of gases composed of mainly methane (50 – 75% by volume), carbon dioxide (25 – 45% by volume) and small traces of ammonia, hydrogen and hydrogen sulfide (Lombardi and Francini 2020). The undigested biomass and water, known as digestate, is commonly used as compost f when excess water is removed. The mixture of gases is commonly called biogas. Anaerobic digestion is a competitive biomass to energy conversion since it has a higher feedstock flexibility, and does not require aggressive pretreatment processes like moisture removal which consumes a great deal of energy. Common feedstock for AD are food waste, wastewater sludge, animal refuse and agricultural wastes (Naqi, Kuhn and Joseph 2019; Anaya Menacho, Mazid and Das 2022).

The process of AD occurs in four consecutive stages: hydrolysis, acidogenesis, acetogenesis and methanation (Mayer, Bhandari and Gath 2019). Figure 2.12 depicts a simple block flow diagram for anaerobic digestion. During the hydrolysis stage, solid biomass is solubilised and converted into constituent monomers like sugars, amino acids and fatty acids. Acidogenesis is the biological conversion of soluble organic molecules (monomers) to form volatile fatty acids. The volatile fatty acids are converted into acetic acid, carbon dioxide and hydrogen in a biological reaction known

as acetogenesis. Methanogenesis is the biological reaction in which acetic acid and hydrogen are consumed to yield methane and carbon dioxide.

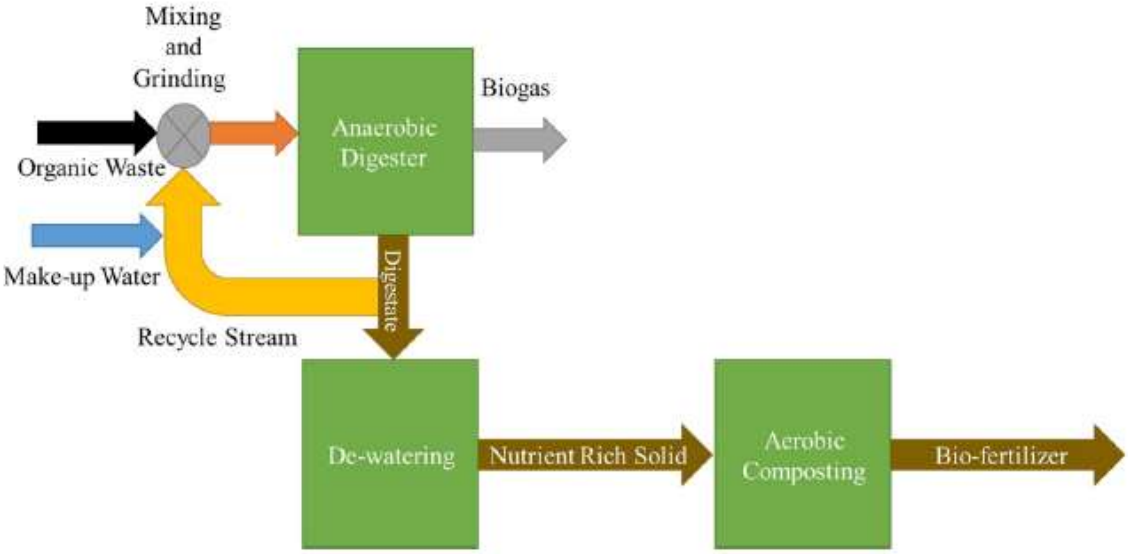

Figure 2. 12: Simple block flow diagram of anaerobic digestion process (Naqi, Kuhn and Joseph (2019)

Biogas yield and composition depends upon a number of factors which include nature of feedstock, feedstock particle size, pH, carbon-to-nitrogen ratio of biomass, hydraulic retention time, temperature of the digester, organic loading rates, among others (Anaya Menacho, Mazid and Das 2022). Also the concentrations of volatile fatty acids (VFAs), ammonia and hydrogen sulfide in the bio-reactor determine the effectiveness of the AD process. VFAs are intermediates of AD but at concentrations above 10 g/l tend to hinder the growth of bacteria responsible for methanogesis reactions (Anaya Menacho, Mazid and Das 2022).

AD being a natural process has several advantages. It is used in livestock to remove odors and growth of pathogens during the storage of animal manure. These pathogens are harmful to humans and animals. The digestate left after AD contains almost the same nutrients as the original manure (Moreira *et al.* 2022). Also, unlike other biomass to energy conversion technologies, AD occurs at mesosphilic (25 – 40 ^{0}C) or thermophilic (45 – 60 ^{0}C) conditions (Anaya Menacho, Mazid and Das 2022). These conditions require moderate heating, hence less energy is required and also it

doesn’t require expensive materials of construction like metal alloys which resist high temperatures.

Biogas is predominantly used for heating, power generation and in combined heat and power (CHP) systems (Barbera *et al.* 2019; Naqi, Kuhn and Joseph 2019; Lombardi and Francini 2020), however, downstream processing and upgrading is necessary to remove impurities like hydrogen sulfide and ammonia, and to reduce the concentration of carbon dioxide in the gas. Recent research has seen high purity bio-methane used as a transportation fuel (Barbera *et al.* 2019; Ravendran, Abdulrazik and Zailan 2019). The upgrading process is necessary to improve its calorific value and the resulting bio-methane resembles natural gas, and can be used directly in combustion engines without blending or engine modifications (Barbera *et al.* 2019). Several technologies have been employed for biogas upgrading: pressure water scrubbing, chemical scrubbing with amines or hot potassium carbonate, pressure swing adsorption (Barbera *et al.* 2019; Naqi, Kuhn and Joseph 2019) and membrane permeation (Lombardi and Francini 2020).

2.4.2. Fermentation

Bioethanol is the most produced among biofuels contributing to about 65% of world’s total biofuel production, with Brazil taking the highest share (about 25%) of the total global bioethanol production (Sadhukhan *et al.* 2019). Bioethanol is classified into first generation, second generation and third generation bioethanol according to the type of feedstock used in its production. First generation bioethanol is prepared from feedstock such as sugarcane, sweet corn, cassava, rice, wheat and sorghum (Daylan and Ciliz 2016; Sadhukhan *et al.* 2019). Second generation bioethanol is prepared from lignocellulosic biomass like agricultural, forestry and agro-processing industrial residues. On the other hand third generation bioethanol is prepared from algal biomass. Over the years first generation bioethanol has dominated the bioethanol market globally, but with the advancement in research and technology, second generation bioethanol production is on the rise since it doesn’t compete with food production (Daylan and Ciliz 2016). Also, production of bioethanol from biomass wastes promotes resource utilisation hence reducing the burden posed to landfills. The drawback of second generation bioethanol production is the recalcitrant structure of LB which requires aggressive pretreatment methods which incurs high production costs. However, valorisation of co-products helps to boost revenues and on-site

production helps to reduce feedstock transportation costs, hence improving the economic feasibility of lignocellulosic bioethanol (Sadhukhan *et al.* 2019).

Ethanol production from LB mainly involves 4 stages: pretreatment, enzyme hydrolysis, fermentation and distillation. Figure 2.13 shows a typical bioethanol scheme from LB.

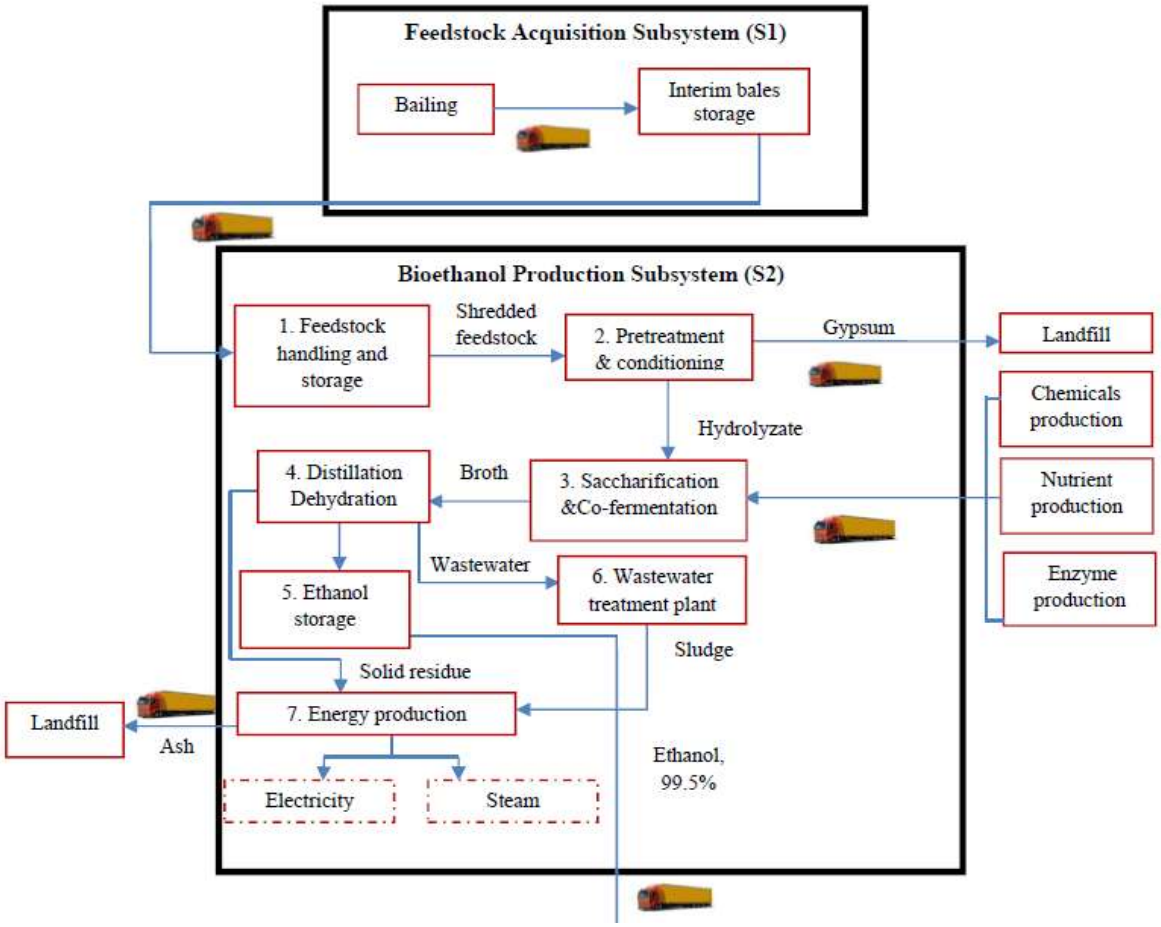

Figure 2. 13: Typical bioethanol production scheme from LB (Daylan and Ciliz 2016)

Pretreatment is necessary to dismantle the crystalline structure of LB into cellulose, hemicellulose and lignin releasing C5 and C6 sugars for fermentation into bioethanol. Pretreatment contributes about 20% of the total cost of cellulosic ethanol production and enzyme production and hydrolysis contributes to another 20% (Mupondwa *et al.* 2017), and this is attributed to the recalcitrance of lignocellulosic biomass which requires aggressive operations. Pretreatment methods include physical, chemical, biological and physical-chemical means. Physical means like hammer milling is used to reduce the crystalline structure of cellulose and increase the surface area for enzyme

hydrolysis. Chemical pretreatment employs acids, alkalis, oxidizing agents, ionic liquids or organic solvents to dismantle the crystalline structure of biomass cellulose. Biological pretreatment is accomplished by use of microorganisms (fungi and bacteria) having enzymes capable of breaking down the crystalline arrangement of biomass. Physical-chemical pretreatment methods combine both physical and chemical processes such as catalyzed steam explosion (e.g. CO_2 and SO_2 explosion), liquid hot water and ammonium fiber expansion. Physical pretreatment methods are effective but require high capital investment purchasing equipment such as hammer mills and also associated with high energy consumption which possesses challenges at a commercial level (Mupondwa *et al.* 2017).

The C5 and C6 sugars then undergo fermentation in the presence of fermenting yeast to produce ethanol. The common fermenting yeast are saccharomyces serevisae and zymomonas mobilis (Khounani *et al.* 2019).

2.5. Physicochemical conversion

This technology is primarily used to produce biodiesel from plant oils. Biodiesel can be substituted for or blended with conventional diesel with no or minimal modifications to the existing combustion engines. It has lower net carbon emissions, is less toxic, biodegradable, contains low sulfur and particulates, helps to reduce engine wear because of its high lubricity and contains high oxygen content which enhances complete combustion. However, the many merits of biodiesel notwithstanding, its production costs are still very high and also its combustion emits considerably high NO_x due to high oxygen content (Gebremariam and Marchetti 2021).

Coffee oil extraction, hydrolysis of the extracted oil into free fatty acids and glycerol, and esterification of free fatty acids (FFAs) to form biodiesel form the three major unit operations involved in the process of making biodiesel from SCG (Thoppil and Zein 2021). Since coffee oil extraction is the first step, its optimization is paramount to the overall efficiency of the biodiesel production process. There are several techniques used in coffee oil extraction but the Soxhlet extraction (SE) is by far the most used solid-liquid extraction method (Thoppil and Zein 2021). However, the SE faces several drawbacks such as longer extraction durations, considerable loss of extraction solvent, large energy consumption and use of low boiling organic solvents whose vapors escape into the atmosphere and pose a potential threat to human health and the environment as a whole.

Other techniques such as microwave-assisted extraction (MAE), ultrasonic-assisted extraction (USE), accelerated solvent extraction (ASE) and the known supercritical fluid extraction (SFE) can overcome the challenges of SE (Thoppil and Zein 2021). The SFE technique uses carbon dioxide or methanol as green solvents but stringent operating conditions (high temperature and pressure) requires highly specialised equipment which makes the technique very expensive. The USE, MAE and ASE techniques require short extraction durations and are more feasible at laboratory scale but there are major challenges in scale up (Thoppil and Zein 2021). The challenges associated with all the coffee oil extraction techniques prompted researchers to use in-situ transesterification methods for biodiesel production from SCG (Schmidt Rivera *et al.* 2020). In this method, no drying of SCG is required and all the stages (extraction, hydrolysis and esterification) occur in a single step (Thoppil and Zein 2021), however, the difficulty of solvent

recovery and separation of biodiesel from the resultant mixture is the major drawback of this technique.

The most commonly used method for biodiesel production is through the single phase based-catalysed transesterification (Gebremariam and Marchetti 2021), where glycerol is produced as a by-product. Glycerol must be removed from biodiesel and this is the main drawback of this method because it involves many unit operations which make it expensive. Another challenge with the single step transesterification is the formation of soap due to the presence of the hydroxide from the catalyst, especially for oil with a free fatty acid content greater than 0.5 wt.% (Gebremariam and Marchetti 2021; Pacheco *et al.* 2022). Saponification does not only consume the catalyst but also makes its separation from biodiesel more problematic. Consequently, the product mixture has to be washed with a lot of water. The catalyst and glycerol leave in the aqueous layer and biodiesel is decanted. This operation leaves a great amount of wastewater which increases waste treatment costs and in turn makes the whole process expensive and less profitable.

Different alternative biodiesel production routes have been studied and used to overcome the challenges associated with the single-step transesterification. These include homogeneous and heterogeneous acid catalysts (Gebremariam and Marchetti 2021), solid base catalysed transesterification, use of enzymes or ionic liquids as catalyst and supercritical transesterification (Gebremariam and Marchetti 2021; Feng *et al.* 2022; Pacheco *et al.* 2022).

Use of homogeneous acid catalysts is associated with separation problems and the corrosive nature of acids requires highly sophisticated materials of construction. Solid acid catalysts like the sulfated carbon have been used at ethanol-to-oil molar ratio of 30:1, temperature of 180 ^{0}C, catalyst load of 7.5% of the oil mass and residence time of 4 hours to achieve a conversion of 99% (Gebremariam and Marchetti 2021). However, this method requires construction materials that can withstand high temperatures and also the large amount of alcohol used makes it expensive which affects its economic viability. The use of solid base catalysts solves the separation and reusability problems, are not corrosive, non-toxic, cheaper, readily available and most importantly has a higher catalytic activity (Gebremariam and Marchetti 2021). For example, calcium oxide as a basic solid catalyst, can be prepared by the calcination of animal wastes like the chicken eggshells (Gebremariam and Marchetti 2021), snail shells and animal bones.

Supercritical transesterification employs alcohols, viz. methanol, ethanol and propanol at their supercritical conditions (Gebremariam and Marchetti 2021; Feng *et al.* 2022),. Three reactions take place, namely transesterification of triglycerides into biodiesel, hydrolysis of triglycerides into FFAs in presence of large amounts of water and esterification of FFAs to form biodiesel (Pacheco *et al.* 2022). Therefore, unlike in conventional methods, the presence of high water content and FFAs in oil is feasible when this method is used. Thus supercritical transesterification requires minimal feedstock pretreatment, like removal of water from the oil and requires fewer unit operations. Also, higher yields of biodiesel are achieved in a very short time with no need of a catalyst (Gebremariam and Marchetti 2021). Supercritical transesterification occurs at a temperature of 350 ^{0}C, a pressure of 20 MPa and methanol-to-oil molar ratio of 42:1 (Pacheco *et al.* 2022). These three conditions show that this process requires sophisticated material of construction which can withstand high temperatures and pressures. These three conditions show that this process requires sophisticated material of construction which can bear high temperatures and pressures. Such materials are expensive, high temperatures used can cause biodiesel to decompose and the process requires large amount of alcohol. Severe process conditions can be attenuated (reduce temperature and pressure) by use of co-solvents and/or use of two-step supercritical transesterification, however, both alternatives make the whole process expensive because of added solvents and the addition of more unit operations (Pacheco *et al.* 2022).

2.6. Mechanical conversion

During mechanical conversion of biomass to energy, there is no change in the chemical nature of biomass. Mechanical energy in the form of pressure is exerted to produce briquette fuel with a higher bulk density than that of raw biomass. Briquetting can overcome the problems associated with raw biomass. Unprocessed biomass has a lower calorific value, higher ash content, higher moisture content, non-uniform particle size and shape, and low bulk density. The poor quality of raw biomass makes transportation and storage difficult, necessitating biomass processing. Briquetting is a simpler processing which does not need sophisticated equipment and produces briquettes with homogeneous shape and size, and high bulk density. According to research conducted by Ferronato *et al.* (2022) on wood sawdust and cardboard-based biomass, it was observed that briquettes had increased thermal efficiency, decreased fuel consumption rate, decreased energy consumption rate, lower carbon dioxide and fine particulate emissions compared to raw biomass.

Figure 2.14 shows the equipment used during briquetting and the produced briquettes. Briquettes have an average diameter and height of 5 cm and 5.2 cm, respectively. The density of briquetted biomass ranges from 800 to 1200 kg/m^3 and this largely depends on the biomass type and the compaction pressure used (Ferronato *et al.* 2022). Figure 2.14 (a) shows the shredding machine where biomass is torn into pieces of smaller sizes using mechanical energy before being sent to the briquetting machine in Figure 2.14 (b). The briquetting machine uses compaction pressure usually between 50 to 250 bars to compress biomass into a homogenized solid in Figure 2.14 (c).

The process of briquette production varies according to biomass type. For woody biomass, it is an easy and simple process but more complicated for agricultural residues and agro-processing wastes. The process involves biomass pre-drying, carbonisation, grinding, addition of binders, pressing and drying of briquettes (Bot *et al.* 2022). This is because agro-processing residues like the SCG contain a lot of moisture and high volatile matter which must be reduced before briquettes are produced. Also, for such biomass feedstock, special additives which serve as binders are necessary additions during the briquetting processing.

(a) (b) (c)

Figure 2. 14: Machines used for briquetting and briquettes produced: (a) shredding machine (b) briquetting machine (c) produced briquettes (Ferronato *et al.* 2022)

2.7. Techno-economic analysis

Techno-economic analysis (TEA) is used to study the economic feasibility of new technologies or for optimising the old ones. TEA studies are used to predict whether the proposed process will be profitable given the assumptions made, thus saving companies from pursuing dead-ends. TEA helps during research and development when doing economic sensitivity analysis. Economic parameters that are highly sensitive to the economic viability of a new proposed project can be identified through conducting the TEA. Typically, any TEA model follows the six steps, namely designing of the process, developing process model, sizing of equipment used in the model, estimation of fixed capital costs, estimation of operating expenses and conducting a cash flow analysis (Iglesias *et al.* 2021). Broadly, TEA studies are conducted with the help of spreadsheets software like Microsoft Excel or process simulators like Aspen plus, HYSYS, SuperPro Designer, etc.

Many studies have been conducted to evaluate the economic feasibility of producing biofuels from waste biomass. These studies aimed at comparing proposed processing routes, feedstock types, plant sizes, co-production, feedstock blends, reactor configurations, etc. Table 2.5 outlines some of TEA studies conducted on biofuel production from waste biomass in the last five years.

Table 2. 5: TEA studies conducted on biofuels production from waste biomass

Feedstock type	Scope of study	Observations	Reference
SCG	Industrial production of biodiesel via fat hydrolysis and esterification	The plant with biodiesel throughput of 2600 tons/year needed a capital investment of USD 123 million. After 15 years, the NPV was USD - 44 million. Thus under the assumptions made, the project was not profitable	Thoppil and Zein (2021)
SCG	Co-production of biodiesel and active carbon	The minimum selling prices of biodiesel and active carbon were found to be CNY 1.8/kg and 4.4/kg, respectively. It was concluded that these prices are well below the current market prices of these products, hence under the set of assumptions made, the project was profitable.	Tian *et al.* (2021)
Nonedible oil	Three biodiesel production alternative technologies, namely the use of sulfated carbon as a catalyst, use of glycerol-enriched calcium oxide as a catalyst and supercritical ethanol process were studied.	All the three technologies were found to be technically feasible although only the glycerol-enriched calcium oxide process was economically feasible.	Gebremariam and Marchetti (2021)
Waste cooking oil (WCO)	Two biodiesel production routes, namely one-step supercritical methanol and two-step supercritical methanol were compared.	The plant processing 15000 tons of WCO per year needed a capital investment of 6.1 million EUR and 5.8 million EUR for one-step and two-step supercritical methanol, respectively. It was also observed that large plant capacities have lower operating and capital expenditures per unit of biodiesel produced.	Martinovic *et al.* (2018)
Safflower seed and safflower straw	Two bioethanol scenarios were compared. Scenario A used *Zymomonas mobilis* produced on site as a fermenting yeast whereas scenario B used *Saccharomyces cerevisiae* purchased from yeast suppliers.	The profitability index for scenario A was 1.14, whereas that of scenario B was 0.81. Hence, scenario A was economically feasible while scenario B was not. This means that the use of *Zymomonas mobilis* instead of *Saccharomyces cerevisiae* boosts the economic potential of bioethanol production.	Khounani *et al.* (2019)
Crude glycerol obtained from biodiesel industry	Three scenarios i.e. Scenario 1 included hydrothermal gasification (HTG) and syngas fermentation, scenario 2 involved HTG, syngas fermentation and carbon dioxide capture, whereas scenario 3 involved HTG, syngas fermentation and biomethanation.	The minimum selling prices of one liter of bioethanol for scenario 1, 2 and 3 were USD 1.32, 1.40 and 0.32, respectively. This implies that scenario three is the most economically feasible alternative. It was deduced that co-production of biofuels boosts the economic feasibility of biorefineries.	Okolie *et al.* (2021)
Sugarcane bagasse	Two hydrothermal liquefaction (HTL) scenarios were studied. Scenario 1 was a stand-alone HTL while scenario 2 was a HTL plant integrated in the sugar distillery.	It was observed that integrating HTL in the sugar distillery increased the internal rate of return of the plant to 12.6% per year from 8.1% for the stand-alone facility.	Deuber *et al.* (2021)

Eucalyptus forest residue	Industrial production of bio-oil, bio-char, syngas through fast pyrolysis.	The proposed plant required a fixed capital investment and operating expenditure of 6 million USD and 3 million USD per year. The sales from co-products (bio-char, syngas and acid extract) lowered the operating costs by 22%.	Iglesias *et al.* (2021)
Corncob	A comparative study of three thermochemical biomass-to-energy conversion routes were studied i.e. methanol production from gasification, bio-oil from pyrolysis and electricity from direct combustion.	All processes were profitable as long as the feedstock cost does not exceed 75 USD per ton. The minimum selling prices for methanol, bio-oil and electricity were 305 USD/ton, 1.47 USD/GGE and 80.1 USD/MWh, respectively. Gasification had the highest NPV, followed by combustion and then pyrolysis.	Brigagãoa *et al.* (2019)
Wastewater sludge from olive mills	Two pyrolysis vapor condensation schemes were studied: Scheme-1 used a vapor compression refrigeration machine, whereas scheme-2 used a vapor absorption refrigeration machine	For the plant capacity of 100 ton of wet biomass per day, scheme-2 had the lowest minimum bio-oil selling price. The capital expenditures for scheme-1 and 2 where 22.1 million and 17.5 million pound sterling, respectively	Khan *et al.* (2022)
Pine biomass, bio-char and pyrolysis bio-oil	Bio-methanol production through gasification of three different feedstocks, namely pine, bio-char and bio-oil.	For the plant capable of processing 1000 tons of feedstock per day, the internal rate of return (IRR) when using bio-char was the highest of all three feedstock types, followed by pine biomass and bio-oil showed the lowest IRR.	Zhang *et al.* (2021c)
Microalgae and wood	Two HTL scenarios were studied. Scenario 1 used microalgae only as feedstock while scenario 2 used a feedstock mix of microalgae and wood. The produced bio-crude for each scenario was upgraded into naphtha and diesel blends.	Blending of feedstock reduced the minimum fuel selling price by 21%. Also the production costs with exclusion of feedstock cost were reduced by 13% when microalgae was blended with wood biomass.	Zhu *et al.* (2020)

2.7.1. Plant costs

The Capital Expenditure (CAPEX), also known as the total capital investment, and the Operating Expenses (OPEX) are the two main costs that have to be incurred for construction, erection and running of any chemical engineering plant (Mukherjee *et al.* 2022). CAPEX encompass such costs as total equipment costs, buildings elevation and improvements, computers, vehicles, office furniture and all other costs associated with construction and elevation of the plant. On the other hand, OPEX are costs incurred on a daily basis throughout the project life (Iglesias *et al.* 2021; Mukherjee *et al.* 2022). OPEX involve costs like rent and utilities, taxes, interest rates, accounting and legal fees, salaries and wages, overhead costs and others. The CAPEX is calculated as the sum of fixed capital investment, working capital and Startup Costs (SUC) (Sinnott and Towler 2009; Thoppil and Zein 2021; Mukherjee *et al.* 2022).

2.7.1.1. Fixed Capital Investment

The fixed Capital Investment (FCI) is the cost of the plant itself, including land acquisition, putting up structures, equipment procurement and all other physical items that run the chemical manufacturing plant. It is calculated as the sum of Inside Battery Limits (ISBL) plant costs, Off-Site Battery Limits Investment (OSBL), Engineering Costs (EC) and Contingency Costs (CC). ISBL investment is the total cost of procuring all major equipment and all installations necessary to erect a new plant. This is the baseline of economic analysis and all other plant costs are factored into the total Cost of all major Equipment (COE). This implies that the accuracy of economic analysis of a project depends upon COE and must be estimated as accurately as possible. The accuracy of COE depends upon what stage project planning and design has reached at the time of economic assessment (Sinnott and Towler 2009). COE is more accurate during later stages of design as information about equipment size, materials of construction and number of equipment required is available unlike in the early stages of design when the equipment flow sheet is not even available.

In addition to COE, other direct costs incurred during plant installation and thus their contribution to FCI must be computed. This is done by the correlations proposed by Lang (1948) and Hand (1958) which give different factors depending on process type; whether there are fluids only, fluids and gas or gas only as shown in Table 2.6 (Sinnott and Towler 2009). These costs include plant foundations, any structural works and equipment installation, all costs related to piping like

insulation materials and painting, electricity connections, wiring and lighting requirements, process control units, other buildings like offices, laboratories, canteens and workshops, storage facilities for products and raw materials (Sinnott and Towler 2009).

Table 2. 6: Correlation factors proposed by Lang (1948) and Hand (1958) (Sinnott and Towler (2009)

Item	Process type		
	Fluids only	**Fluid and gas**	**Solids only**
Equipment erection (a)	0.3	0.5	0.6
Piping (b)	0.8	0.6	0.2
Instrumentation and control (c)	0.3	0.3	0.2
Electricals (d)	0.2	0.2	0.15
Civil (e)	0.3	0.3	0.2
Structures and buildings (f)	0.2	0.2	0.1
Lagging and paint (g)	0.1	0.1	0.05

Then ISBL is calculated using the equation below

$$\mathrm{ISBL} = \mathrm{COE} \times (1 + a + b + c + d + e + f + g) \quad 2.2$$

where;

$$\mathrm{COE} = \sum_{i=1}^{i=M} \mathrm{Ce} \quad 2.3$$

$\mathrm{COE} = \text{total cost of all equipment}$

$\mathrm{Ce} = \text{purchase cost of equipment i}$

$\mathrm{M} = \text{total number of equipment}$

Equation 2.2 is true for carbon steel material of construction and other correlations for special alloys can be found in Sinnott and Towler (2009). This method was used by Medina-Martos *et al.* (2020) to evaluate the economic potentials of combining HTC and AD in wastewater treatment.

Sometimes COE is not available especially during early stages of design or when the purpose of economic analysis is to compare the profitability of proposed alternatives. In this case ISBL plant costs can be estimated using equations 2.4 and 2.5 (Sinnott and Towler 2009; Thoppil and Zein 2021).

$$C = 280000N\left(\frac{Q}{s}\right)^{0.3} \quad \text{for } Q < 60{,}000 \qquad 2.4$$

$$C = 3200N\left(\frac{Q}{s}\right)^{0.675} \quad \text{for } Q > 60{,}000 \qquad 2.5$$

where;

$C = \text{ISBL on a US Gulf coast, 2000 basis}$

$Q = \text{Plant capacity in metric tons/year}$

$N = \text{Number of processing units}$

$s = \text{Reactor conversion, which is ratio of mass of product to mass of feed to reactor}$

The results of equations 2.4 and 2.5 are on a US Gulf coast, 2000 basis, therefore cost escalation index and location factor are required to update the ISBL plant cost to the base year of cost analysis and proposed plant location. Sinnott and Towler (2009) outlined different location factors for different locations on the globe, but Africa was not mentioned.

Another common method of estimating the cost of equipment is by using the scaling exponent method (Okolie *et al.* 2021). The method gives the relationship between known cost of a base equipment of a plant that used the same technology and that of the plant under consideration (Sinnott and Towler 2009), as shown in equation 2.6.

$$C = C_O\left(\frac{S}{S_O}\right)^n \qquad 2.6$$

where;

$C = \text{required equipment cost}$

$C_O = \text{known cost of base equipment}$

$S = \text{capacity of equipment whose cost is reqired}$

$S_O = \text{capacity of equipment whose cost is known}$

$n = \text{scaling factor}$

For the method described by equation 2.6 to be used to estimate the cost of equipment, the cost of similar equipment used in similar technology should be known. The exponent, n usually ranges

between 0.4 to 0.9, but on average, 0.6 is used as the exponent and this is the reason why this method is commonly referred to as the six-tenths rule (Sinnott and Towler 2009).

Sometimes it is practically difficult for engineers to collect cost data from recent projects and accurately use it to estimate the cost of the plant under consideration (Sinnott and Towler 2009). Also, because of technological advancements, newer proposed plants will use a slightly different technology from that of old projects which makes it difficult to use the six-tenths rule explained above. Recently engineers have resorted to use commercial software tools to make preliminary cost estimates in industry (Sinnott and Towler 2009). A number of software tools are available but by far Aspen Process Economic Analyzer (APEA) is the most commonly used. APEA is quick, reliable and give cost estimates without needing a large amount of design information. To use APEA, a process simulation must be run in Aspen plus or HYSYS without errors. The simulation blocks are mapped to real plant equipment and if any dummy items are selected, they must be excluded during this stage. Then the software sizes all mapped equipment according to mass and energy balances and give cost estimates.

OSBL involves all costs related to site infrastructure to cater for plant modifications or expansion (Sinnott and Towler 2009; Thoppil and Zein 2021). OSBL is always estimated as a percentage of ISBL, usually between 10 to 100%. For example, in cases where adequate information about site conditions and modifications is not readily available, a bigger percentage of about 40% should be assumed (Thoppil and Zein 2021). EC are the costs paid to contractors whose expertise is needed during project design, civil engineering works, equipment procurement and requisitions, supervision of construction process, etc. These costs are always estimated as a percentage of the sum of ISBL and OSBL costs. Sinnott and Towler (2009) gave EC as 10% of (ISBL+OSBL) for bigger projects and 30% for smaller ones. On the other hand, CC is costs included during project planning to cater for unforeseen circumstances like changes in prices adopted during the budgeting process. Above all the actual prices of major equipment is not known especially at earlier stages of design, hence the need to prepare the budget as flexible as possible. These costs are always estimated as 10% of the sum of ISBL and OSBL for projects with conventional technologies and a higher percentage (about 50%) is assumed for novel projects as uncertainties are higher in such cases (Thoppil and Zein 2021).

2.7.1.2. Working Capital

After the construction, installation and commissioning of the chemical plant, money is required to finance the day-to-day operations until it starts generating profit. This is called Working Capital (WC). Due to uncertainties, it may take a long time for a new plant to start generating profits therefore, WC should be big enough to push the new project from start to the point in time when revenues generated from sales of finished products can shoulder the operations of the plant. For simple manufacturing plants, WC can be assumed to be 5% of sum of ISBL and OSBL, and 30% for large and sophisticated chemical plants. Nevertheless, WC is usually taken to be 15% of the sum of ISBL and OSBL for petrochemicals (Sinnott and Towler 2009; Thoppil and Zein 2021).

2.7.1.3. Startup Costs

Startup Costs (SUC) are the expenses any new project incurs during the process of its conceptualization. SUC involves such costs needed for budget planning, research work, advertising, borrowing expenses if own capital is not available, license and insurance charges among others. SUC are always assumed to be 10% of direct costs (sum of ISBL plus OSBL) (Thoppil and Zein 2021).

2.7.1.4. Operating Expenditure

The Operating Expenditures (OPEX) are costs incurred on a daily basis to run the project from the start until the end of its life. The OPEX are classified into the fixed and variable operating costs (Mukherjee *et al.* 2022). The variable operating costs depend on production rate whereas fixed operating costs don't usually change with changes in plant throughput (Sinnott and Towler 2009; Thoppil and Zein 2021). The variable operating costs involve all costs of buying feedstock for the plant, utilities like electricity, cooling water, steam and all other consumables like catalysts, solvents, drying agents, etc. Conversely, fixed costs are constant even if the plant is not operating at full capacity. These include labor costs, supervision costs, rent, insurance and tax expenses, maintenance costs, costs to cover research and development, costs to pay fringe benefits of workers, their insurance and many others (Sinnott and Towler 2009). Since it is always difficult to generate revenues in early years of project execution, it is necessary to estimate the operating costs high enough to run the operations of the project until the sales of finished products are high enough to shoulder plant day-to-day activities.

2.7.1.5. Sales revenue

The cash inflow realized from sales of major products and by-products is known as sales revenue. The profitability of any manufacturing process largely depends on revenues, and thus revenues should be maximized. Companies do this by supplementing sales of main products with those of by-products. By-products are inevitable in any manufacturing as they are generated either in reaction stoichiometry, side reactions or through decomposition of final products (Sinnott and Towler 2009). Selling of by-products also helps companies to reduce on waste treatment costs which would otherwise be escalated if these products needed waste disposal. Thoppil and Zein (2021) proposed that biodiesel production from SCG can generate more revenue if the defatted SCG are converted into coffee pellets and sold together with wet glycerol.

2.7.1.6. Margin

The gross margin is obtained by subtracting feedstock costs from revenues. Since the cost of raw materials is the largest component of production costs, margins can be used to predict the prices products should be sold for a plant to make profits (Sinnott and Towler 2009). In cases where the cost of raw materials is negligible, e.g. when the feedstock is a waste stream from another processing plant, the gross margin can be assumed to be equal to revenues (Thoppil and Zein 2021).

2.7.1.7. Profit

Profit is the driving force for setting up any project and investors will maintain funding or running the business which generates income from its operations. The product revenues should be large enough to surpass production costs if profit is to be realized. Profit is estimated based on the Cash Cost of Production (CCOP) (Sinnott and Towler 2009). CCOP is the sum of fixed and variable operating costs minus revenues from sales of by-products. The gross profit is then estimated by subtracting CCOP from main product revenues. The incomes generated are subject to corporate taxes and must be deducted from gross profit to obtain the net profit. This is the return on capital invested.

2.7.1.8. Depreciation

As fixed assets are used over a long period of time, they are susceptible to wear and tear, deterioration or obsolescence, and thus an allowance for this must be given before tax is levied. Depreciation is a non-charge expense which reduces the income before taxes are deducted. In other

words, it is a tax allowance that governments use as incentives for investment (Sinnott and Towler 2009). In order to get the net cash flow, depreciation is always added to the net income after taxes are deducted. Broadly, straight-line depreciation, declining-balance depreciation and the Modified Accelerated Recovery System (MARCS) are the three different methods that companies and economists use to calculate depreciation expenses (Sinnott and Towler 2009; Iglesias *et al.* 2021; Thoppil and Zein 2021). Of all, straight-line depreciation is the simplest way of calculating depreciation expenses (Sinnott and Towler 2009). The method considers a uniform amount of depreciation over a given period of time, until the salvage value of an asset. Salvage value is the book value of an asset at the end of depreciable life. For chemical plants, salvage value is always zero since the plant may remain in use for a long period of time even after its depreciable life (Sinnott and Towler 2009). Equation 2.7 is used to calculate depreciation using the straight-line method. Useful life of an asset is the time in years an asset remains in use for revenue generation.

$$\text{Depreciation} = \frac{\text{cost of an asset} - \text{salvage value}}{\text{useful life}} \qquad 2.7$$

Conversely, with the declining balance method, higher charges are allowed in early years, and this allows for higher cash flows in early stages of the project. The value charged as depreciation goes on declining until the salvage value of an asset is reached (Sinnott and Towler 2009). On the other hand, MARCS as introduced by the US Tax Reform Act of 1986 is essentially a merger of both the straight-line and the declining-balance methods (Sinnott and Towler 2009). Thoppil and Zein (2021) used this method during their study about the economic feasibility of biodiesel production from SCG.

2.7.1.9. Taxes

The main source of income for governments globally is the tax levied on every incoming generating activity. Chemical manufacturing plants are not exonerated from paying corporate taxes since the main aim of starting such plants is to generate profit. After depreciation, expense is deducted from gross profit; tax income is then deducted to obtain the net income. Because taxes are subtracted after depreciation has been subtracted from gross profit, depreciation is commonly referred to as tax allowance. Tax rate always expressed as a percentage is used to compute the amount of tax payable and it differs from country to country depending on size and nature of business. For example, in the UK, corporate taxes stood at 28% for companies with profits greater

than 1.5 million pounds in the year 2009 (Sinnott and Towler 2009). Thoppil and Zein (2021) assumed 11% for a plant to be located in the US West coast whereas Iglesias *et al.* (2021) used 34% for a plant proposed to be established in Sao Paul, Brazil.

2.7.2. Economic feasibility indicators

As the primary motive to venture into any investment is to generate profit, it is necessary to compare the economic performance of different projects before execution is done. This allows the management to choose, among alternatives, the best project that is worthy being ventured into (Sinnott and Towler 2009). There are different economic indicators used by engineers, researchers and economists to compare and assess the economic viability of different projects before a decision is made to start spending capital investment. These include but are not limited to net present value, internal rate of return, return on investment, pay-back period, time value of money, profitability index and the product minimum selling price (Sinnott and Towler 2009; Thoppil and Zein 2021; Mukherjee *et al.* 2022).

2.7.2.1. Payback Period

The simplest of all methods for economic analysis is the Payback Period (PBP) also known as the pay-back time. This is the time in years it takes the investment to recover the initial capital i.e. fixed capital plus working capital. An investment with a shorter PBP is more desirable and every investor would want to venture into a project that would return the capital invested in as short a time as possible. In other words, an economically feasible project is one with a PBP smaller than the project life (Mukherjee *et al.* 2022). It is simply calculated by dividing total investment by the average annual cash flow. PBP is calculated using equation 2.8.

$$\text{PBP} = \frac{\text{total investment}}{\text{average annual cash flow}} \qquad 2.8$$

The disadvantage of PBP is that it assumes that revenue is generated immediately after kick starting of the project and that all the capital is invested in year zero. In practice this is not true as most projects spend year one in designing, year two during construction and plant installation, and operations usually begin in year three but still not at full production capacity. Also PBP doesn't take into account taxation and depreciation (Sinnott and Towler 2009). A more realistic way to measure the profitability potential of a project using payback time is by calculating the Discounted

Payback Period (DPBP) (Zhang *et al.* 2021c; Gonzalez-Arias, Sanchez and Cara-Jimenez 2022). DPBP is the amount of time in years it takes for the cumulative cash flows to be equal to zero. It can be conveniently obtained from the graph of net present value against time. Many researches have compared the PBP of different alternatives to make decisions. Mukherjee *et al.* (2022) compared the economic feasibility of producing active carbon from SCG looking at three scenarios. The calculated PBP for scenario 1, 2 and 3 were 2.6, 3.1 and 4.1 years, respectively. If the decision was to be made based on only the results of PBP, scenario 1 is more economically feasible than the other two scenarios since it requires the shortest time for the cash flows to be equal to the initial investment. However, other economic indicators must be considered for an informed decision to be made.

2.7.2.2.Rate of Return on Investment

Another simple indicator of economic performance of a project is the Return on Investment (ROI). It is calculated using equation 2.9.

$$\text{ROI} = \frac{\text{net annual profit}}{\text{total investment}} \times 100\% \qquad 2.9$$

It can be clearly seen from equation 2.9 that a project with a bigger return on investment is desirable as it shows the potential for generating large profit on a smaller investment made. It is always difficult to calculate ROI with inclusion of depreciation and tax charges. This is the reason why the pre-tax ROI is often used. When pre-tax ROI is used, the net annual profit in equation 2.9 is replaced with pre-tax cash flow (Sinnott and Towler 2009).

2.7.2.3. Net present value

Another useful economic indicator is the Net Present Value (NPV), which is the total of all the present values of future cash flows. NPV is more realistic than PBP as it considers the time value of money and the dynamics in revenues and expenditures (Sinnott and Towler 2009). Calculation of NPV may give either a positive or negative value or simply a zero. A project with positive NPV is more desirable as it indicates the possibility of recovering the initial investment and realizes profit at the end of its life (Gonzalez-Arias, Sanchez and Cara-Jimenez 2022). When NPV is zero, it means that the project can only recover the total capital investment with no profits or losses made at the end of its life. Conversely, a negative NPV indicates that the project is not

economically feasible as it is not able to recover the cost of capital invested at the end of its life. NPV is calculated using equation 2.10.

$$\mathrm{NPV} = \sum_{n=1}^{n=t} \frac{\mathrm{CF_n}}{(1+\mathrm{i})^n} \qquad 2.10$$

where;

$\mathrm{CF_n} = \text{cash flow of year n}$

$\mathrm{t} = \text{project life in years}$

$\mathrm{i} = \text{discount/interst rate}$

2.7.2.4. Internal Rate of Return

A more realistic and meaningful economic indicator that is often used when comparing project alternatives is the Internal Rate of Return (IRR) which is also known as the Discounted Cash Flow Rate of Return (DCFROR) (Sinnott and Towler 2009). It gives the measure of how much of interest a project can pay and still be able to recover the total capital investment at the end of its life. In other words, IRR is the interest rate for which the NPV at the end of the project life is zero (Gonzalez-Arias, Sanchez and Cara-Jimenez 2022). IRR is calculated as shown by equation 2.11.

$$\text{If} \sum_{n=1}^{n=t} \frac{\mathrm{CF_n}}{(1+\mathrm{i})^n} = 0, \qquad \text{then } \mathrm{i} = \mathrm{IRR} \qquad 2.11$$

where;

$\mathrm{CF_n} = \text{cash flow of year n}$

$\mathrm{t} = \text{project life in years}$

$\mathrm{i} = \text{discount or interst rate}$

The value of i in equation 2.11 is the IRR. It is always calculated by try-and-error or with the help of spreadsheet like Microsoft Excel (Sinnott and Towler 2009). An investment with the highest IRR is more desirable and investors usually expect IRR to be greater than the interest rate (Sinnott and Towler 2009; Gonzalez-Arias, Sanchez and Cara-Jimenez 2022). IRR is more desired than

NPV as it is able to compare the economic feasibility of projects of varying sizes, doesn't depend on amount of capital, project's life or interest rate, as it is the case for the NPV (Sinnott and Towler 2009). Bigger projects always have larger values of NPV but again require large amounts of capital, which doesn't give an informed comparison if projects compared are of different sizes. Therefore, it can be stated that IRR is the most superior of all the project economic indicators and that good projects are those that are capable of paying the highest interest rate regardless of their size or initial capital investment.

2.7.2.5. Profitability Index

Profitability Index (PI) is the ratio of NPV and CAPEX (Gonzalez-Arias *et al.* 2021; Gonzalez-Arias, Sanchez and Cara-Jimenez 2022) as shown in equation 2.12. A more profitable project is one with the highest PI. It is a measure of money accumulated per dollar invested (Gonzalez-Arias *et al.* 2021).

$$\mathrm{PI} = \frac{\mathrm{NPV}}{\mathrm{CAPEX}} \qquad 2.12$$

Profitability index is a perfect replacement for the ROI (equation 2.9) since it is always difficult to determine the net annual profit when depreciation and taxation are included. A bigger PI implies that bigger net cash flows are generated at the end of project life in relation to initial capital invested.

2.7.3. Discounted Cash Flow Analysis

It is the climax of economic evaluation as it determines whether or not an investment is worthy. It is analyzed throughout the entire life of a project and puts into account the tax allowance which is often regarded as depreciation, and the discount rate. The discount rate or the interest rate tells how much return on capital invested a project can generate at the end of its life. The NPV, DPBT and IRR are the most common economic indicators calculated by the discounted cash flow analysis. During the cash flow analysis, project's life in years is clearly defined including preliminary stages like project designing, construction and startup to full capacity operation until the last year of its operation. Discounted flow analysis is always done using spreadsheets and reported in tabular form (Sinnott and Towler 2009). For a project life of 5 years for example, discounted cash flow analysis can be arranged as shown in the Table 2.7.

Table 2. 7: Illustration of discounted cash flow analysis (Sinnott and Towler 2009; Thoppil and Zein 2021)

Year of project	Gross profit	Depreciation expense	Taxable income	Taxes paid	Cash flow	Discount factor	Discounted cash flow
0							
1							
2							
3							
4							
5							

Almost every study on the techno-economic analysis has employed the discounted cash flow analysis to calculate the NPV, PBP and IRR (Gonzalez-Arias, Sanchez and Cara-Jimenez 2022). Thoppil and Zein (2021) used the cash flow analysis to determine the economic feasibility of producing biodiesel from SCG with the biorefinery proposed to be located in Seattle, United States with production capacity of 2.6 kiloton per year. In their study, the NPV and IRR were found to be -$44 million and 2%, respectively. With negative NPV and IRR being smaller than the discount rate (11% used in the study), it was concluded that the proposed project is not economically feasible as it was not able to generate profit at the end of 15 years which was its proposed plant life.

2.8. Life Cycle Assessment

Life Cycle Assessment (LCA) is a common tool used to examine the environmental impacts of a product over its entire life (Daylan and Ciliz 2016). The aim of LCA can be to quantify the environmental impacts of a product or process, identify the areas for improvement or choose among alternatives the most environmentally friendly processing route or product.

Generally, the most commonly used methodology of conducting LCA is outlined by the ISO 14040/44 framework (Demichelis *et al.* 2020; Lombardi and Francini 2020; Liu *et al.* 2021). The methodology outlines a typical LCA study in four steps; goal and scope definition, life cycle inventory, life cycle impact assessment and interpretation of results. Each of these steps is explained in detail in the following sections.

2.8.1.1. Goal and scope definition

This stage involves defining the aim of conducting LCA, selecting the functional unit and the scope or system boundary. The aim defines the goal that LCA study wants to achieve. Broadly, LCA studies are being conducted to aid in decision making during project design and planning. The governments nowadays require that minimum environmental guidelines be followed before any chemical plant starts its operations and monitoring is done to ensure that these guidelines are adhered to during the plant operations. This has in turn made LCA studies more relevant today. The aim of LCA can be to compare different raw materials (Demichelis *et al.* 2020; Vilen, Laurell and Vahala 2022), compare different products (Daylan and Ciliz 2016) or to investigate the contribution of each manufacturing step to the total environmental impacts of the whole production process (Liu *et al.* 2021). A functional unit is a reference flow used to give a fair comparison during the LCA study. It can be the mass of feedstock processed, distance travelled or the amount of energy produced. In the study conducted by Medina-Martos *et al.* (2020) to compare the environmental performance of a stand-alone AD and a combined HTC and AD in wastewater treatment, 1000 kg of sewage sludge processed was used as a functional unit. Schmidt Rivera *et al.* (2020) used one ton of SCG as the functional unit. Generally, if the main aim of an LCA study is to compare environmental footprints of different processing routes, a mass flow of feedstock is chosen as a functional unit.

2.8.1.2. System boundaries

There are four system boundaries that a typical LCA study can be based on and these include cradle-to-gate, gate-to-gate, gate-to-grave and cradle-to-grave. Cradle-to-gate encompasses such stages as raw material extraction, raw material transportation to the bio-refinery and the manufacturing process. Gate-to-gate considers only the manufacturing process. Gate-to-grave includes transportation of finished products to customers, customer use, transportation of wastes to disposal units and the waste disposal process. Cradle-to-grave encompasses all stages from material extraction to waste disposal.

The choice of system boundaries depends upon the aim of conducting such an LCA study. If the main aim of the study is to choose among alternatives the best processing routes, investigate the contribution of each processing unit to the environmental impacts or select the best feedstock, a cradle-to-gate system boundary is always selected. For example, in the study conducted by Demichelis *et al.* (2020) in which the environmental and economic benefits of producing bioethanol from three categories of biomass i.e. starch, sugar-based and lignocellulosic, a cradle-to-gate system boundary was selected. It comprised of feedstock transportation to plant facility, biomass preparation and biomass conversion to bioethanol. Vilen, Laurell and Vahala (2022) chose a cradle-to-gate system boundary in their study to compare the environmental impacts of activated carbon production from different feedstock with the aim of determining the raw material with reduced environmental impacts.

If the aim of an LCA study is to compare the environmental benefits of using different products for the same purpose, a cradle-to-grave system boundary is always selected. For example in the study conducted by Daylan and Ciliz (2016) to compare the environmental benefits of using bioethanol blends (E10 and E85) with conventional gasoline, a cradle-to-grave system boundary was selected. It included feedstock collection, raw material and final product transportation, the manufacturing process and combustion of these fuels in a medium-sized car for a distance of 1 km. A cradle-to-grave system boundary can also be used in case of comparing process alternatives. For example, Schmidt Rivera *et al.* (2020) compared the environmental sustainability of biodiesel production from SCG with other valorization routes, namely incineration, landfilling, compositing, anaerobic digestion and direct use for soil amendment. The scope of their study was from cradle-

to-grave and it was observed that for all the selected impact categories, incineration showed the lowest negative impacts whereas biodiesel production was the worst of all.

2.8.1.3. Life cycle impact assessment

There's different software tools currently used for measuring environmental impacts. These include IPCC, TRACI, GABI and ReCiPe. IPCC measures only the global warming potential (kg CO_2 eq.) and it translates all the GHGs (CH_4, NO_x, HCFCs, etc.) into CO_2 equivalents. TRACI (by the US Environmental Protection Agency) measures the following impacts. For resource depletion it measures fossil fuels depletion, for ecosystem quality it measures climate change, acid rain, Eco-toxicity, water eutrophication, ionizing radiation, stratospheric ozone and habitat destruction and for human health, carcinogens and human toxicity, smog and particulates. The impacts measured by ReCiPe (by Pre) include resource depletion, ecosystem quality and human health. For resource depletion it measures fossil fuels and minerals depletion. For ecosystem quality it measures freshwater eutrophication, marine eutrophication, marine eco-toxicity, terrestrial eco-toxicity, freshwater eco-toxicity, terrestrial acidification, natural land transformation, urban land occupation and agricultural land occupation. For human health it measures human toxicity, photochemical oxidants, particulate matter, climate change, ozone depletion and ionizing radiation. In the study made by Daylan and Ciliz (2016) to compare the environmental advantages of blending bioethanol with conventional gasoline, the selected environmental impact indicators used were global warming, photochemical ozone layer depletion, acidification potential and eutrophication.

3. METHODOLOGY

3.1. Introduction

This chapter covers the methods, tools and materials used in the present study. The general methodology followed is illustrated in Figure 3.1. Available literature was reviewed to obtain input data for Aspen plus simulations. All the process parameters like moisture content, pressure, temperature, type of catalyst etc. were obtained from the works of other researchers. Biomass-to-energy conversion technologies were simulated in Aspen plus V11 to obtain the mass and energy balances that served as the basis for economic analysis and life cycle assessment.

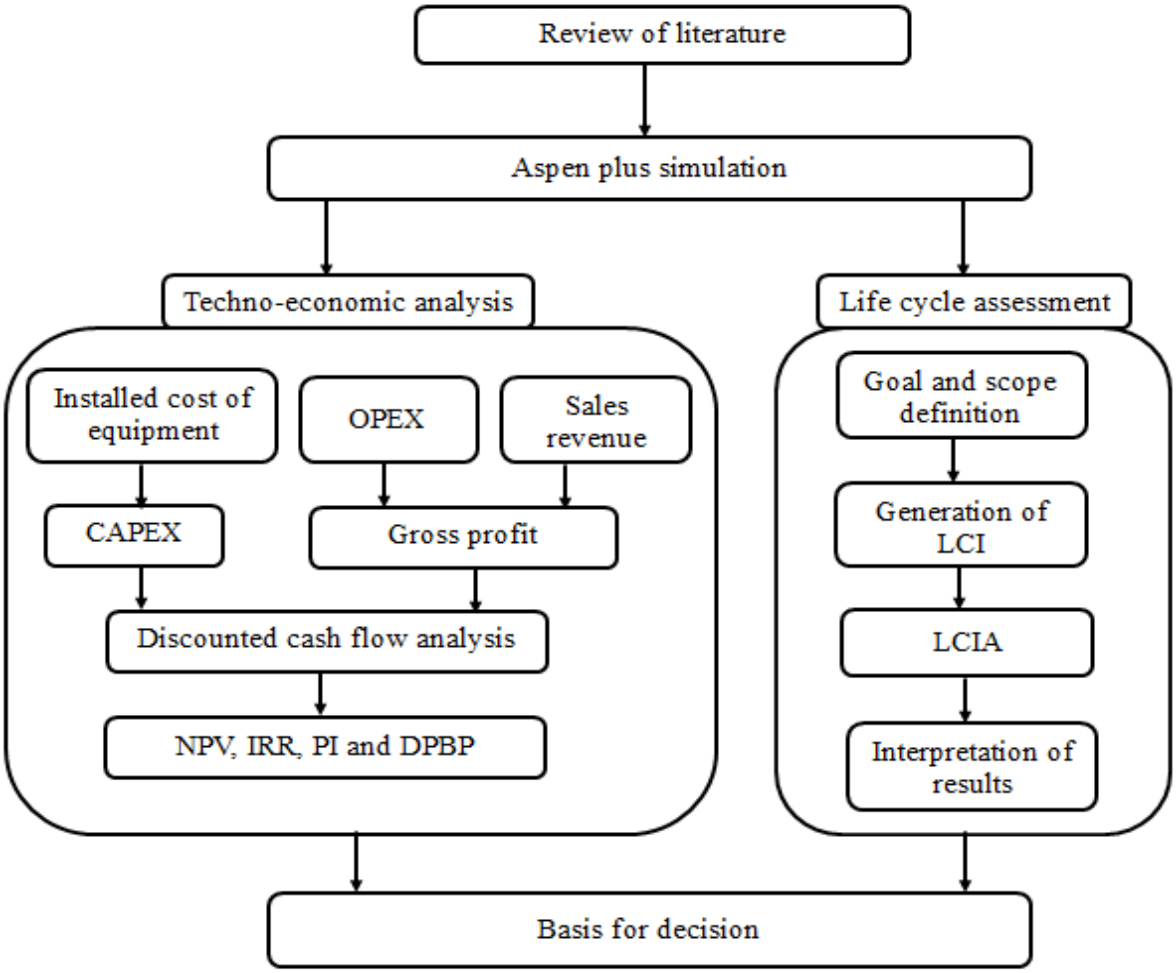

Figure 3. 1: Illustration of methodology used in the study

The chapter is divided into three sections. Section 3.2 covers all the procedures followed in Aspen plus simulation of six biomass to-biofuel conversion routes. The conversion routes are fast pyrolysis, Hydrothermal Liquefaction (HTL), Anaerobic Digestion (AD), fermentation, gasification and biodiesel production. It should be noted that the terms biogas production and bioethanol production, if used anywhere in this study, mean the same as anaerobic digestion and fermentation, respectively. The Process Flow Diagram (PFD) for each processing routes was prepared in Aspen plus and presented in this section. The screenshots of Aspen plus interface for each simulation are presented in Appendices B, C, D, E, F and G. The description and use of each of the equipment is also presented in this section. Process design, process modeling and equipment sizing were the main targets of this section.

Section 3.3 explains the methodology used in conducting the economic analysis of biofuels production from SCG. This section covers the estimation of Capital Expenditure (CAPEX) and Operating Expenses (OPEX), and the Discounted Cash Flow Analysis (DCFA). The data collected in section 3.2 served as input for this section. The main target of this section was to identify the most economically feasible processing route using the economic indicators, namely Net Present Value (NPV), Payback Period (PBP), Profitability Index (PI) and Internal Rate of Return (IRR). Microsoft Excel spreadsheets were used to conduct DCFA and these tables are presented in Appendix H.

Finally section 3.4 covers the procedure followed in conducting Life Cycle Assessment (LCA) of biofuels production from SCG. LCA was conducted using OpenLCA V1.11.0 software. The data collected in section 3.2 was input for this section. The mass and energy streams for each of the processing routes served as inputs and output flows during LCA study. The main aim of this section was to identify the most environmentally friendly processing route. The screenshots of the software interface are presented in Appendix I.

3.2. Aspen plus simulation

Six biomass-to-fuel processing routes, namely anaerobic digestion, fermentation, biodiesel production, fast pyrolysis, gasification and hydrothermal liquefaction were simulated in Aspen plus V11 purposely to obtain data (mass and energy balances) that was used to conduct both TEA and LCA of biofuels production from SCG. For purposes of fair comparison, all the biomass conversion technologies considered in this study processed the same amount of SCG, 2000 kg/h with moisture content of 50 wt.% (Afolabi, Sohail and Cheng 2020; Schmidt Rivera *et al.* 2020). The proximate and ultimate analysis and the biochemical composition of SCG were presented in Table 2.1, section 2.1. The methodology followed for each of the processing routes was explained, the process flow diagram prepared in Aspen plus and simulations were run to obtain mass and energy balances.

3.2.1. Fast pyrolysis

Aspen Plus process simulator was used to simulate the pyrolysis plant. The same method was employed in the studies conducted by (AlNouss *et al.* 2021; Goklani, Naga Prapurna and Srinath 2022; Hasan *et al.* 2022; Liu *et al.* 2022a).

3.2.1.1.Assumptions made

The following assumptions were made;

- Steady-state process (AlNouss *et al.* 2021; c; Jaroenkhasemmeesuk *et al.* 2022). This means that mass entering the process is equal to mass leaving the process.
- No pressure drop and isobaric in nature (Shahbaz *et al.* 2020; AlNouss *et al.* 2021; Goklani, Naga Prapurna and Srinath 2022). This means that pressure is constant throughout the process.
- There was no tar formation during pyrolysis (Shahbaz *et al.* 2020; AlNouss *et al.* 2021; Goklani, Naga Prapurna and Srinath 2022).
- Uniform particle distribution of biomass feedstock (Hasan *et al.* 2022; Jaroenkhasemmeesuk *et al.* 2022).
- Char only comprises of carbon, ash and high molecular weight lignin.
- Sulfur and nitrogen do not react. Nitrogen leaves pyrolysis reactor as vapor whereas sulfur leaves as a solid.

Whereas moisture content was defined as a conventional component, SCG and Ash were defined as non-conventional components and thus their enthalpy and density were calculated using empirical correlation methods; HCOALGEN and DCOALIGT correlations present in Aspen Plus software (AlNouss *et al.* 2021; Goklani, Naga Prapurna and Srinath 2022; Hasan *et al.* 2022). MIXCINC was used as the global flow for the simulation since both nonconventional and conventional components are present (Hasan *et al.* 2022; Liu *et al.* 2022a). Biomass was defined in Aspen plus by its ultimate, proximate and sulfanal analysis (Hasan *et al.* 2022). This data was obtained from the work of Mukherjee *et al.* (2022). The fluid package used was PENG-ROB since it can take into account the non-ideality (Shahbaz *et al.* 2020; Goklani, Naga Prapurna and Srinath 2022). Biomass components and pyrolysis intermediates (conventional solids) were entered in Aspen plus as user defined components outlined in Appendix A.

Figure 3.2 shows the process flow diagram for simulation of biomass fast pyrolysis and the descriptions of each equipment as used in Aspen plus software are outlined in Table 3.1. 2000 kg/h of wet SCG (50 wt.% moisture) was heated to 100 ^{0}C using an electric heater until all the moisture was vaporised. A separator was used to separate water vapor from SCG. Dried SCG then enters the RYield reactor where it is decomposed into its main building blocks (cellulose, hemicellulose and lignin), sulfur, nitrogen and ash by specifying their yields according to its ultimate analysis (Jaroenkhasemmeesuk *et al.* 2022). Cellulose and hemicellulose were represented by their monomers $C_6H_{10}O_5$ and $C_5H_8O_4$, respectively (Peters *et al.* 2017; Liu *et al.* 2022a), whereas lignin was represented as carbon-rich lignin, oxygen-rich linin and hydrogen-rich lignin with formulas $C_{15}H_{14}O_4$, $C_{20}H_{22}O_{10}$ and $C_{22}H_{28}O_9$, respectively (Peters *et al.* 2017; Gorensek, Shukre and Chen 2019). Decomposed biomass enters the stoichiometric reactor where primary decomposition of cellulose, hemicellulose and lignin occurred at 500 ^{0}C, 1 bar and 5 seconds residence time. The same process conditions were used by Jaroenkhasemmeesuk *et al.* (2022) for optimal bio-oil yield. The reactor is based on 7 stoichiometric reactions (equations 3.1 to 3.7) where cellulose is completely decomposed into final products whereas hemicellulose and lignin are converted into intermediates (HCE1, HCE2, LIGCC and LIGOH) and final pyrolysis products. The product stream from the first reactor enters the second reactor where hemicellulose and lignin intermediates are converted into final pyrolysis products using 5 stoichiometric reactions (equations 3.8 to 3.12). The pyrolysis products entered the cyclone to separate the solid residues from the product vapor. The pyrolysis vapor then passed through two condensers arranged in series to cool the vapor from

500 ^{0}C to 30 ^{0}C to separate Non-Condensable Gases (NCG) from bio-oil. Excess water was removed from bio-oil using Sep block available in Aspen plus model pallet.

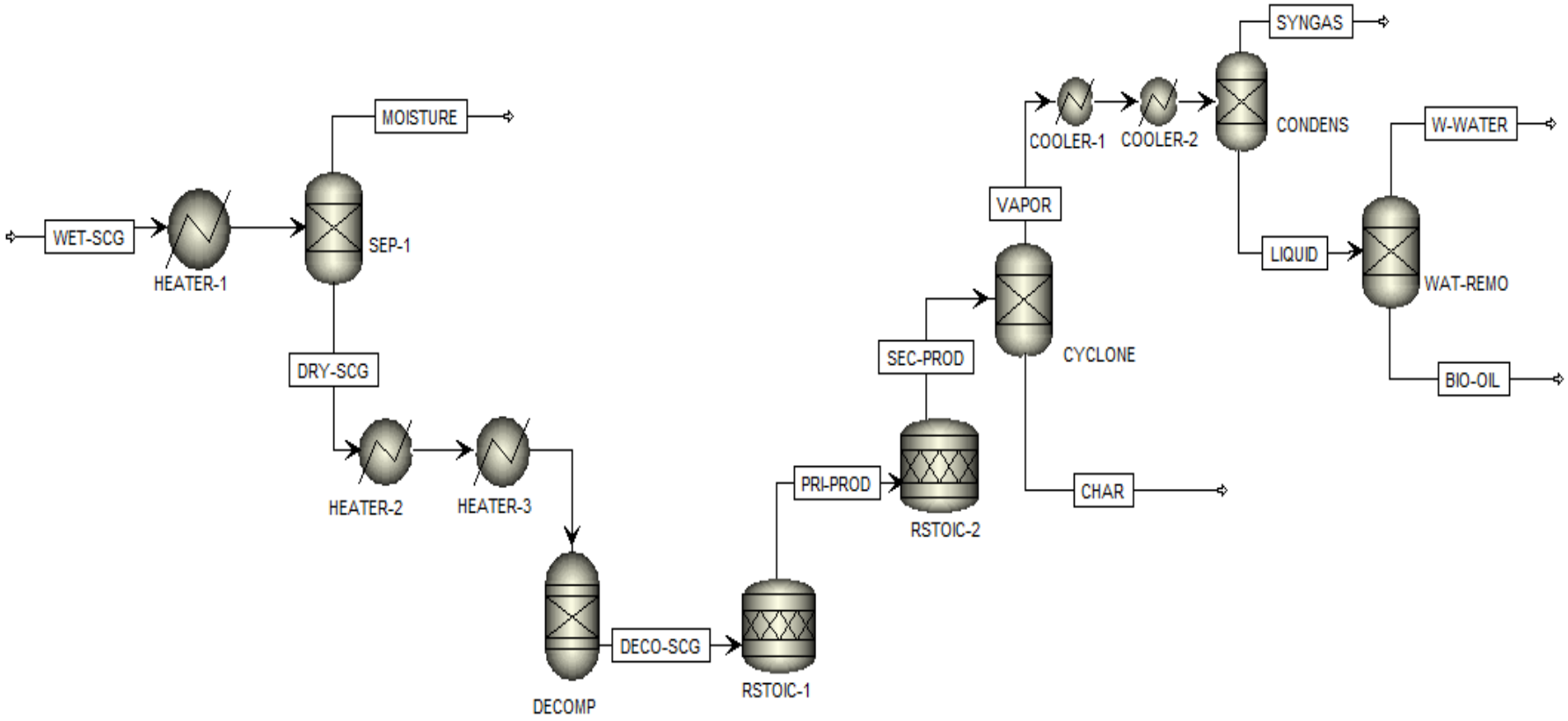

Figure 3. 2: Aspen plus PFD of biomass fast pyrolysis plant

Table 3. 1: Aspen plus operation blocks used in pyrolysis simulation

Block name in Aspen plus	Simulation name	Description
Heater	HEATER-1	Electric heater used to vaporize all the moisture from wet SCG
Sep	SEP-1	Separates moisture from the SCG
Heater	HEATER-2 HEATER-3	Electric heaters used to raise the temperature of dried biomass to 500 ^{0}C
RYield	DECOMP	Breaks down biomass into cellulose, hemicellulose and lignin, sulfur, nitrogen and ash
RStoic	RSTOIC-1	Simulates primary decomposition of cellulose, hemicellulose and lignin into pyrolysis products and intermediates
RStoic	RSTOIC-2	Simulates the decomposition of pyrolysis intermediates into final products
Sep	CYCLONE	Separates solids from pyrolysis vapor
Heater	COOLER-1 COOLER-2	Cools pyrolysis vapor to 30 ^{0}C
Sep	CONDENS	Condenses part of pyrolysis vapor to separate bio-oil from NCG (syngas)
Sep	WAT-REMO	Separates water from bio-oil

3.2.1.2.Reactions used in the model

The pyrolysis model was based on 12 stoichiometric reactions (equations 3.1 to 3.12) as outlined in Table 3.2. They are classified into two categories: primary and secondary biomass decomposition reactions. Primary biomass decomposition was modeled by 7 reactions (equations 3.1 to 3.7) whereas secondary biomass decomposition was modeled by 5 reactions (equations 3.8 to 3.12). The components participating in the reactions shown in Table 3.2 are represented by their component IDs as defined in Aspen plus process simulator. The full chemical names and chemical formulae of all components are listed in Appendix A (Tables A1, A2 and A3).

Table 3. 2: Equations used to model biomass fast pyrolysis (Peters *et al.* 2017; Gorensek, Shukre and Chen 2019; Jaroenkhasemmeesuk *et al.* 2022)

$CELL \rightarrow 0.4HAA + 0.05GLYOXAL + 0.15CH3CHO + 0.25HMFU + 0.35ALD3 + 0.15CH3OH + 0.3CH2O + 0.61CO + 0.36CO2 + 0.25H2 + 0.93H2O + 0.02HCOOH + 0.05C3H6O2 - N + 0.05CH4 + 0.61CHAR$	3.1
$CELL \rightarrow LVG$	3.2
$CELL \rightarrow 5H2O + 6CHAR$	3.3
$HCE \rightarrow 0.35HCE1 + 0.65HCE2$	3.4
$LIGC \rightarrow 0.35LIGCC + 0.1COUMARYL + 0.08PHENOL + 0.41C2H4 + H2O + 1.02CO + 0.7H2 + 0.3CH2O + 0.495CH4 + 5.735CHAR$	3.5
$LIGH \rightarrow LIGOH + 0.5ALD3 + 0.5C2H4 + 0.2HAA + 0.1CO + 0.1H2$	3.6
$LIGO \rightarrow LIGOH + CO2$	3.7
$HCE1 \rightarrow 0.6XYLAN + 0.2C3H6O2 - N + 0.12GLYOXAL + 0.2FURFURAL + 0.4H2O + 0.08H2 + 0.16CO$	3.8
$HCE1 \rightarrow 0.4H2O + 0.8CO2 + 0.05HCOOH + 1.6CO + 1.25H2 + 0.3CH2O + 0.625CH4 + 0.375C2H4 + 0.875CHAR$	3.9
$HCE2 \rightarrow 0.2H2O + CO + 0.575CO2 + 0.4CH2O + 0.1C2H5OH + 0.05HAA + 0.35ACAC + 0.025HCOOH + 0.25CH4 + 0.3CH3OH + 0.225C2H4 + 0.725H2 + CHAR$	3.10
$LIGCC \rightarrow 0.3COUMARYL + 0.2PHENOL + 0.35HAA + 0.7H2O + 0.65CH4 + 0.60C2H4 + 1.8CO + H2 + 6.75CHAR$	3.11
$LIGOH \rightarrow 0.21FE2MACR + 0.09ANISOLE + 0.09CH3CHO + 0.24CH2O + 1.36H2O + 0.96CH4 + 1.14CH3OH + 1.5H2 + 0.05CO2 + 3.84CO + 0.05HCOOH + 0.65C2H4 + 0.025HMWL + 0.1ACROL + 7.4CHAR$	3.12

3.2.2. Gasification

Feedstock properties including Moisture Content (MC), Ash Content (AC), volatile Matter (VM), Fixed Carbon (FC), elemental composition (C, H, O, N and S) were obtained from the work of Mukherjee *et al.* (2022) presented in Table 2.1 in section 2.1. Biomass and ash were modeled as non-conventional components and specified according to their ultimate and proximate analyses (Singh *et al.* 2022). DCOALIGT and HCOALGEN models in Aspen Plus were used to determine the density and enthalpy of non-conventional components (Singh *et al.* 2022).

3.2.2.1. Assumptions made

Several assumptions were made during biomass gasification Aspen plus modeling as follows;

- Since both conventional and non-conventional components are present, the model used MIXNC stream class (Yong and Abdul Rasid 2021).
- Redlich-Kwong-Soave-Boston-Mathias (RKS-BM) cubic equation (Yong and Abdul Rasid 2021) was the property method used.
- No pressure drop and all unit operations were at atmospheric pressure (Yong and Abdul Rasid 2021; Singh *et al.* 2022).
- Steady state operation (Yong and Abdul Rasid 2021; Singh *et al.* 2022).
- 25 ^{0}C was taken as ambient temperature (Yong and Abdul Rasid 2021).
- Tar formation is considered negligible (Singh *et al.* 2022).
- The decomposition of biomass is an instantaneous process (Singh *et al.* 2022).
- Temperature is uniformly distributed within the gasifier (Singh *et al.* 2022).
- Components in the volatile stream are majorly H_2, CH_4, CO, CO_2, N_2 and H_2O (Singh *et al.* 2022).
- Ash is taken as an inert component (Singh *et al.* 2022) .

Figure 3.3 shows the process flow diagram for simulation of biomass gasification and the descriptions of each equipment as used in Aspen plus software are outlined in Table 3.3. Wet SCG was first dried at 102 ^{0}C to remove moisture and this was modeled using RStoich reactor, RSTOICH (Yong and Abdul Rasid 2021; Singh *et al.* 2022). Then a flash separator, SEP-1 was used to separate moisture. Two electric heaters HEATER-1 and HEATER-2 were used to raise the temperature of dried biomass to 750 ^{0}C before it was sent to RYield reactor to model biomass

decomposition. The RYield reactor, RYIELD was used to decompose biomass at a temperature of 750 ^{0}C into its constituent elements (C, H, O, N, S and Ash) according to its ultimate and proximate analysis (Yong and Abdul Rasid 2021; Singh *et al.* 2022). A flash separator, SEP-2 was used to separate the volatiles stream from the char and ash (Singh *et al.* 2022). The volatile stream is not only composed of hydrogen, oxygen, nitrogen and sulfur but also carbon which is part of the volatile matter from the proximate analysis of biomass and was calculated as the difference between total elemental carbon content of biomass and its fixed carbon content (Singh *et al.* 2022). Char was taken as fixed carbon content of biomass. Ash was taken as inert and non-conventional component. The volatile stream from the flash separator was sent to RGibbs reactor, VOL-GASF at 750 ^{0}C and 1 bar pressure to model volatile gasification based on the Gibbs free energy minimisation principle (Singh *et al.* 2022). The exit stream from RGibbs reactor was mixed with char and the gasifying agent (steam) using mixer (M-100) and the combined stream sent to a second RGibbs reactor, CHA-GASF to model char gasification based on the Gibbs free energy minimisation principle. The flow rate of steam was adjusted until all the char (carbon) was volatilised. The gaseous product was sent to the cyclone, CYCLONE, to separate ash from producer gas. The gas was then cooled to a temperature below 100 ^{0}C by two coolers COOLER-1 and COOLER-2, connected in series. Syngas was cleaned by separator GAS-CLEA in order to remove water and other impurities.

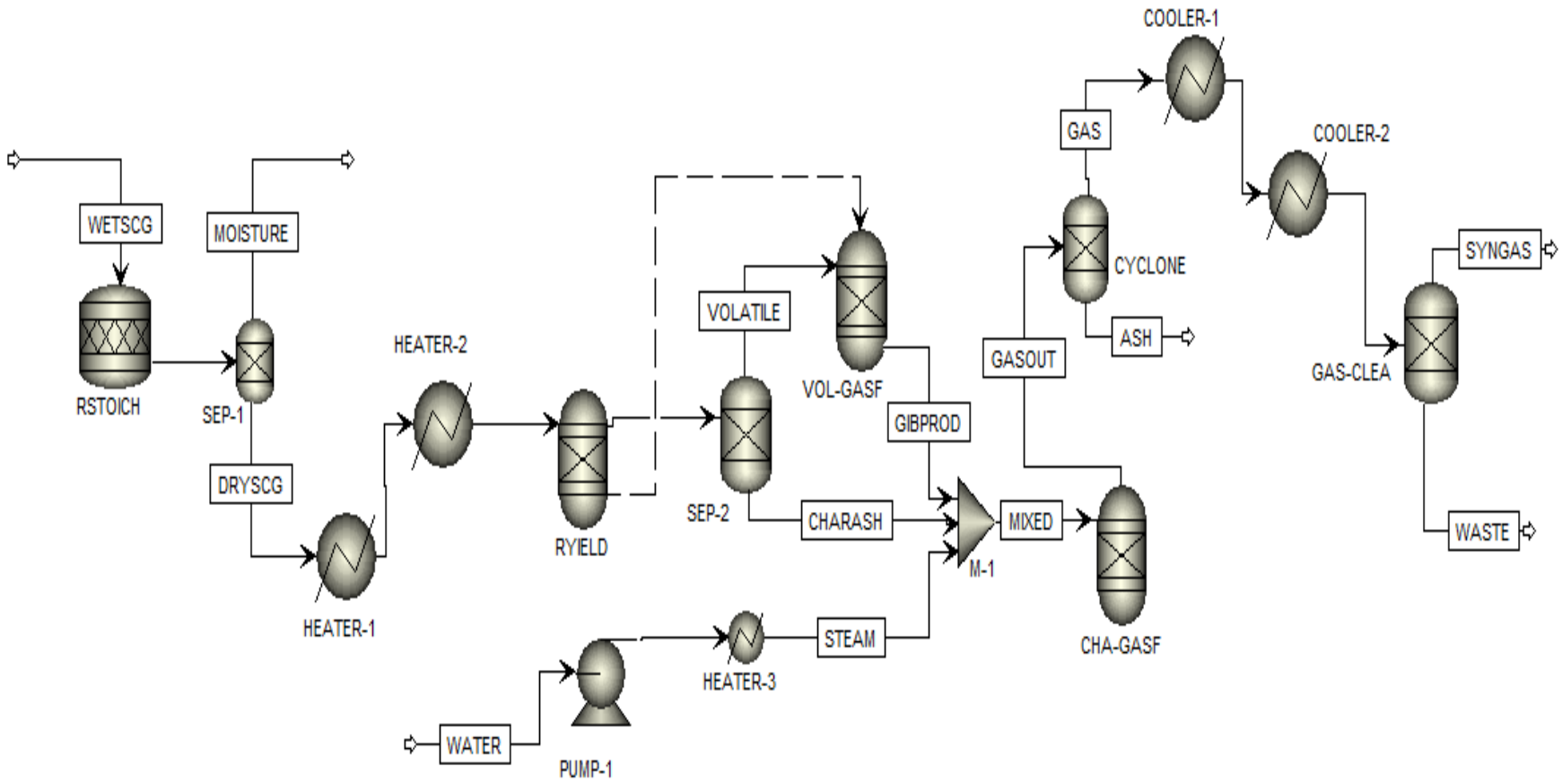

Figure 3. 3: Aspen plus PFD of biomass gasification

Table 3. 3: Aspen plus operation blocks used in gasification simulation

Block name in Aspen plus	Simulation name	Description
RStoich	RSTOICH	Models the removal moisture from SCG by the use of the stoichiometric reaction
Sep	SEP-1	Separates moisture from the SCG
Heater	HEATER-1 HEATER-2	Electric heaters to raise temperature of dried biomass to 750 ^{0}C
RYield	DECOMP	Breaks down biomass into its constituent elements according to its ultimate and proximate analysis
Sep	SEP-2	Separates volatiles from char and ash
RGibbs	VOL-GASF	Simulates volatiles gasification with the minimization of Gibbs free energy
Mixer	M-1	Mixes the gasifying agent (steam), char and volatiles before fed to CHA-GASF
RGibbs	CHA-GASF	Simulates char gasification with the minimization of Gibbs free energy
Sep	CYCLONE	Separates ash from syngas
Heater	COOLER-1 COOLER-2	Cools the producer gas to separate condensable gases
Sep	GAS-CLEA	Model syngas cleaning to remove impurities like water, hydrogen sulfide, ammonia and nitrogen

3.2.3. Hydrothermal liquefaction

HTL was modeled in a similar manner to pyrolysis. The model also relied on 12 stoichiometric reactions like in pyrolysis simulation (section 3.2.1). The remarkable difference between the two models was that pyrolysis needed biomass pre-drying and no process water was required. Conversely, HTL doesn't require moisture removal, however, process water was instead added to create slurry with solid content of less than 25% (Deuber *et al.* 2021).

Figure 3.4 shows the process flow diagram for simulation of HTL and the descriptions of each equipment as used in Aspen plus software are outlined in Table 3.4. The slurry was heated to a temperature of 300 ^{0}C (Aierzhati *et al.* 2021; Alherbawi *et al.* 2021; Zhang *et al.* 2021a) before being sent to RSTOIC-1 to model biomass primary decomposition based on 7 stoichiometric reactions (equations 3.1 to 3.7) presented in section 3.2.1. After the primary biomass decomposition, the slurry was sent to RSTOIC-2 to model biomass secondary decomposition relying on 5 stoichiometric reactions (equations 3.8 to 3.12). The products then entered the cyclone to separate char and ash from the vapor-liquid mixture. The vapor-liquid mixture was then condensed to ambient temperature to separate the NCG from bio-oil and water. Water was removed from bio-oil using Sep block, CONDENS as shown in Figure 3.4. Using a splitter, over 60% of the water was recycled and the rest of the water was discharged as wastewater.

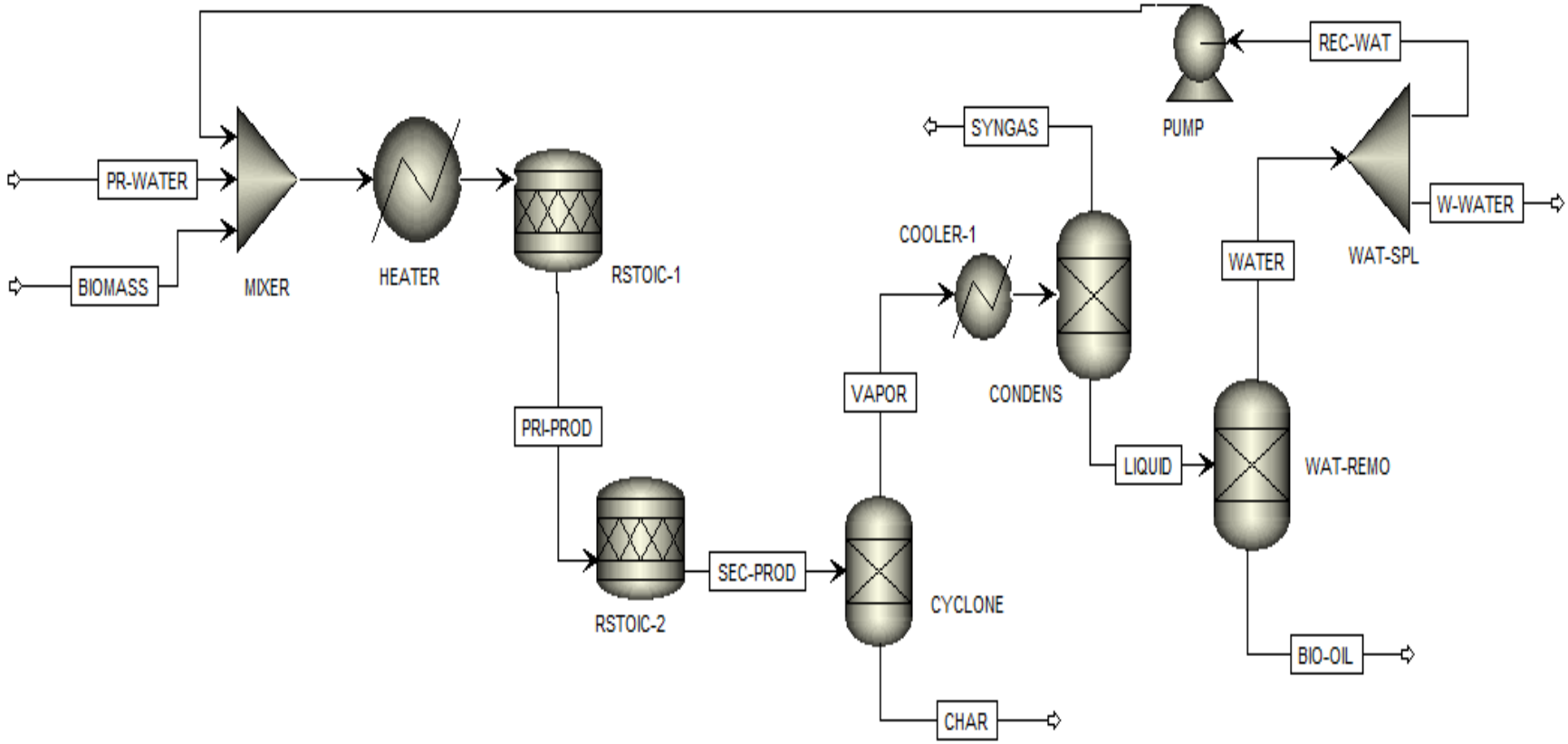

Figure 3. 4: Aspen plus PFD of hydrothermal liquefaction

Table 3. 4: Aspen plus operation blocks used in hydrothermal liquefaction simulation

Block name in Aspen plus	Simulation name	Description
Mixer	MIXER	Mixes wet biomass together with makeup and recycle water to form a slurry
Heater	HEATER	Electric heater used to raise the temperature of slurry to 300 ^{0}C
RStoic	RSTOIC-1	Simulates primary decomposition of cellulose, hemicellulose and lignin
RStoic	RSTOIC-2	Simulates the decomposition of biomass HTL intermediates into final products
Sep	CYCLONE	Separates char and ash from vapor-liquid mixture
Heater	COOLER-1	Cools pyrolysis vapor to 30 ^{0}C
Sep	CONDENS	Condenses part of pyrolysis vapor to separate bio-oil from NCG (syngas)
Sep	WAT-REMO	Separates water from bio-oil
FSplit	WAT-SPLIT	Used to split water into recycle and wastewater
Pump	PUMP	Pumps recycle water to MIXER

3.2.4. Biodiesel production

The description of the methodology used was divided into three sections, namely assumptions, coffee oil extraction, and fat hydrolysis and esterification.

3.2.4.1. Assumptions made

The following assumptions were made during Aspen plus simulation of biodiesel production process.

- SCG contains 18 wt.% coffee oil on a dry basis. Of the total oil content, 10% is free fatty acids and the rest triglycerides. The remaining solid mass of SCG is composed of cellulose, hemicellulose, lignin and ash.
- Triglycerides were modeled as triolein ($C_{57}H_{104}O_6$), free fatty acids as oleic acid ($C_{18}H_{34}O_2$) and biodiesel as methyl oleate ($C_{19}H_{36}O_2$). The same method was used by Feng *et al.* (2022).
- Drying stage leaves 3 wt.% moisture in dried SCG (Thoppil and Zein 2021).
- The ratio of solvent (hexane) to dried SCG is 5:1 (Thoppil and Zein 2021).
- The solvent extracts all the oil from dry SCG (Thoppil and Zein 2021).
- It was assumed that 97% of the residual water was extracted with the oil and only 3% remained in DSCG.
- Solvent loss of 7% was assumed and the rest was recycled to the mixer.
- Ambient temperature was 25 ^{0}C.

The fluid package used is non-random two liquid (NRTL) thermodynamic model (Gebremariam and Marchetti 2021), since polar compounds (ethanol and glycerol) are resent. Figure 3.5 shows the process flow diagram for the simulation of biodiesel production process and the descriptions of each equipment as used in Aspen plus software are outlined in Table 3.5.

3.2.4.2. Coffee oil extraction

Wet SCG was fed to the drier where 97% of the moisture was evaporated at 100 ^{0}C and 1 bar pressure. Dried SCG was conveyed to the extractor where it was contacted with hexane at ambient temperature for 45 minutes before the mixture was sent to the nozzle centrifugal decanter where solids were separated from the liquid mixture (Tian *et al.* 2021). The extract was pumped to the solvent recovery unit where hexane was completely evaporated at 70 ^{0}C leaving behind extracted

oil and part of residual water. The process of solvent recovery led to loss of some solvent and 7% of total solvent was lost. The remaining solvent was cooled to ambient temperature and recycled. The extracted coffee oil contained 6% of the residual water and the rest of residual water left the decanter with defatted SCG. Defatted SCG was conveyed to the dying unit where 90% of residual was removed using an electric heater. Then the dried SCG was sent to the pelletizing unit to produce coffee pellets. High quality biomass pellets should have utmost 12% moisture (Thoppil and Zein 2021).

3.2.4.3. Biodiesel production

Extracted oil and residual water (6 wt.%) mixture were mixed with process water before being heated by an electric heater to 250 ^{0}C. Process water flow rate was 45% of the total flow rate of wet coffee oil (Thoppil and Zein 2021). The heated mixture was sent to the fat splitter where triglycerides in the oil reacted with water at high temperatures to form free fatty acids and glycerol as shown by equation 3.13. 90% conversion of triglycerides was assumed.

$$C_{57}H_{104}O_6 + 3H_2O \rightarrow 3C_{18}H_{34}O_2 + C_3H_8O_3 \qquad 3.13$$

The reactor effluent was separated into two streams. Small traces of unreacted triglycerides and a mixture of glycerol and water was sent to the wet-glycerol storage tank. The stream of free fatty acids was cooled to 65 ^{0}C before being mixed with both makeup and recycle methanol in the molar ratio of 5:1 of methanol to free fatty acids (Tinoco-Caicedo *et al.* 2021). The resultant mixture was sent to the esterification reactor packed with SiO_2-HF beads (Thoppil and Zein 2021) which acted as catalyst for the reaction. All the free fatty acids reacted with excess methanol to form biodiesel and water according to equation 3.14.

$$C_{18}H_{34}O_2 + CH_3OH \rightarrow + C_{19}H_{36}O_2 + H_2O \qquad 3.14$$

The reactor effluent was sent to a distillation column operating at atmospheric pressure. With a reflux ratio of 2 and 12 equilibrium stages, 99% of methanol was recovered in the distillate and 99.9% of water and biodiesel in bottoms. 90% of the methanol was recycled back to the esterification unit and the rest was modeled as solvent lost. The bottoms were heated to 150 ^{0}C and sent to the flash column operating at 0.25 bar pressure, where 99.7% pure biodiesel was recovered with small traces of water and methanol.

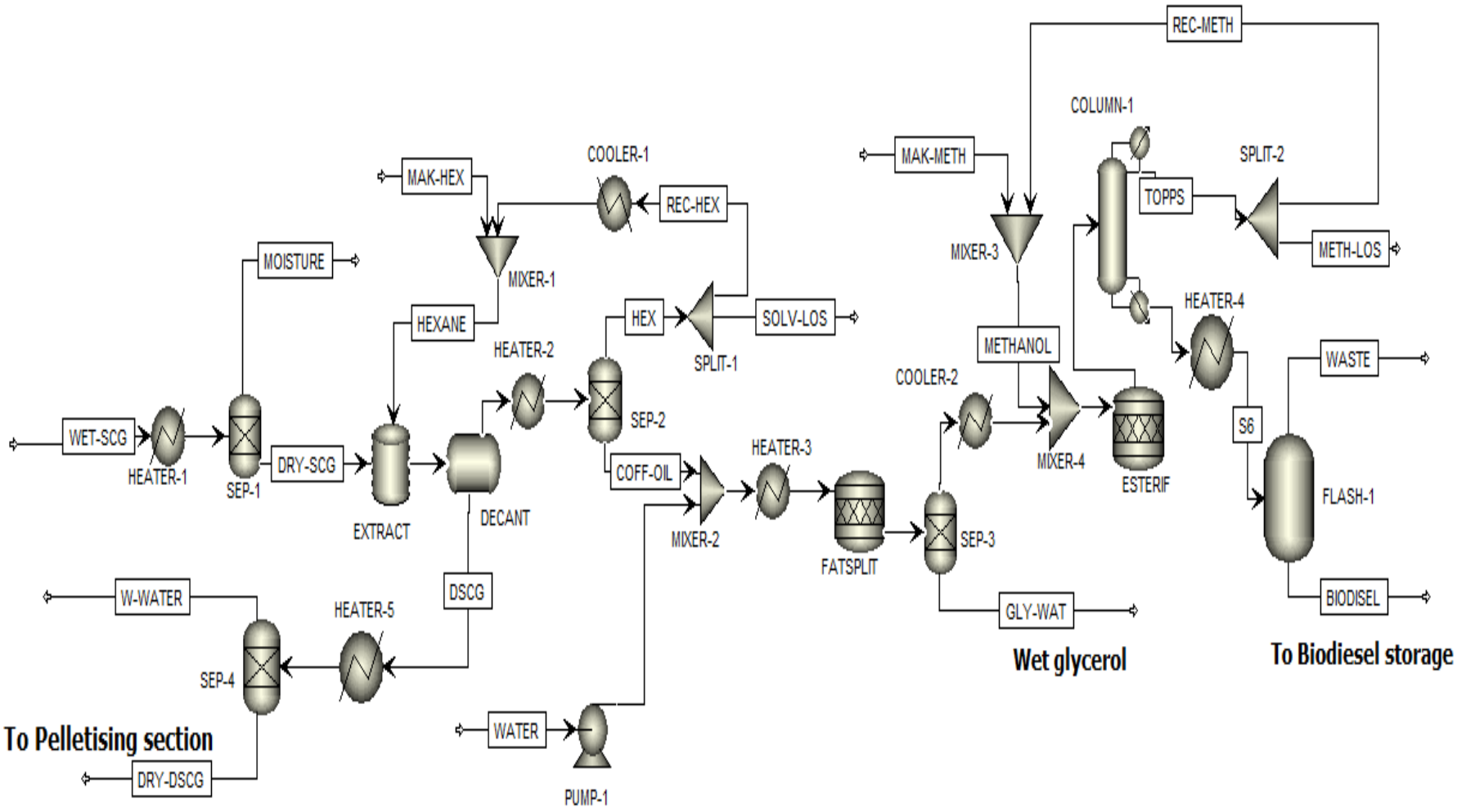

Figure 3. 5: Aspen plus PFD of biodiesel production

Table 3. 5: Aspen plus operation blocks used in biodiesel production simulation

Block name in Aspen plus	Simulation name	Description
Heater	HEATER-1	Electric heater that vaporizes all the moisture from SCG
Sep	SEP-1	Separates moisture from the SCG
Mixing Tank	EXTRACT	Allows for contact between solvent and SCG for maximum oil extraction
Decanter	DECANT	Separates DSCG from extracted oil and hexane
Heater	HEATER-2	Electric heater vaporizes all the hexane from coffee oil
Sep	SEP-2	Separates hexane from coffee oil
FSplit	SPLIT-1	Models solvent loss
Heater	COOLER-1	Shell and tube heat exchanger operating on cooling water. It cools recycle hexane to ambient temperature
Mixer	MIXER-1	Mixes recycle and makeup hexane before being fed to the extractor
Heater	HEATER-5	Electric heater that vaporizes all the moisture from DSCG
Sep	Sep-4	Separates moisture from the DSCG
Pump	PUMP-1	Pumps process water to mixer MIXER-2
Mixer	MIXER-2	Mixes coffee oil with process water
Heater	HEATER-3	Electric heater that raises the temperature of oil-water mixture to 250 ^{0}C required in the fat splitter
RStoic	FATSPLIT	Models hydrolysis of oil fat into glycerol and FFA based on reaction stoichiometry and conversion
Sep	SEP-3	Separates glycerol, water and traces of unreacted oil fat from formed FFA
Heater	COOLER-2	Shell and tube heat exchanger operating on cooling water. It cools the FFA stream from 250 ^{0}C to 65 ^{0}C before being with methanol
Mixer	MIXER-3	Mixes recycle and makeup methanol
Mixer	MIXER-4	Mixes methanol and FFA
RStoic	ESTERIF	Models esterification of FFA based on reaction stoichiometry and conversion
DSTWU	COLUMN-1	Distillation tower for methanol recovery from biodiesel and water
FSplit	SPLIT-2	Models methanol loss
Heater	HEATER-4	Electric heater that raises the temperature of biodiesel-water mixture to 150 ^{0}C
Flash2	FLASH-1	Separates biodiesel from water at low pressure

3.2.5. Bioethanol production

Biomass major components (cellulose, hemicellulose and lignin) were defined as conventional solids, ash was defined as nonconventional solid, whereas moisture content of biomass as a conventional component. Cellulose and hemicellulose were represented by their monomers $C_6H_{10}O_5$ and $C_5H_8O_4$, respectively, whereas lignin was defined as $C_{11}H_{12}O_4$. The estimated solid property model parameters of these solids, as outlined in Appendix A, were used to define them in Aspen plus software. Xylose and glucose were defined as D-xylose and Dextrose respectively, present in Aspen plus. MIXCINC was used as the global flow for the simulation since both nonconventional and conventional components were present. The fluid package used to calculate the thermodynamic properties was NRTL since both polar and non-polar components are present (Lyu *et al.* 2020).

Figure 3.6 shows the process flow diagram for the simulation of bioethanol production process and the descriptions of each equipment as used in Aspen plus software are outlined in Table 3.6. Process water together with recycle water was added to wet SCG to make slurry with solid content of about 25% (Liu *et al.* 2021). The slurry was sent to the steam explosion reactor (RSTOIC-1) where hemicellulose is hydrolyzed to form xylose at 180 ^{0}C, 2 bar pressure and 30 minutes residence time as shown by equation 3.15. The same conditions were used by (Lyu *et al.* 2020). This method was used because it is environmentally friendly as it does not use acids or chemicals and has low water consumption (Duarte *et al.* 2021). The reactor effluent was cooled to 32 ^{0}C by a shell and tube heat exchanger, COOLER-1, operating on cooling water. The cooled slurry was sent to the hydrolysis reactor, HYDROLY, where cellulose is hydrolyzed by enzyme cellulase to form glucose as shown by equation 3.16**.** A small fraction of hydrolysate after enzyme hydrolysis was used to cultivate fermenting yeast, *Saccharomyces cerevisiae* (Liu *et al.* 2021). Xylose and glucose were fermented in reactor, FERMENTA, by yeast to form ethanol and carbon dioxide as shown by equations 3.17 and 3.18. Hydrolysis and fermentation took place in a single reactor block, SSF, represented by two stoichiometric reactors HYDROLY and FERMENTA. Simultaneous saccharification and fermentation was used to avoid high accumulation of glucose which would otherwise inhibit the activity of enzyme cellulase. The same set up was used by Liu *et al.* (2021). The conversion rates of cellulose, hemicellulose, xylose and glucose were 0.88, 0.84, 0.68 and 0.90, respectively. The same assumptions were adopted by Lyu *et al.* (2020). The solid-liquid separator (plate and frame filter press), LIQ-SOLI, was used to separate unreacted biomass

from the product liquid mixture. The same method was used by (Duarte *et al.* 2021). The distillation column with 10 equilibrium stages, operating at atmospheric pressure was used to separate water from ethanol. Water exiting from the bottom of the column was split into the recycle stream and wastewater stream. About 47% of water was recycled back to MIXER-1. The distillate from the column is rich in ethanol, carbon dioxide and residual water. A flash column operating at 1.5 bars and 25 ^{0}C was used to expel carbon dioxide from ethanol. Molecular sieves adsorption (Lyu *et al.* 2020; Liu *et al.* 2021), DEHYDR, was used to remove any traces of residual water to obtain 99 wt.% pure bioethanol.

Reactions used in ethanol production

Pretreatment

$$C_5H_8O_4 + H_2O \rightarrow C_5H_{10}O_5 \quad 3.15$$

Hydrolysis

$$C_6H_{10}O_5 + H_2O \rightarrow C_6H_{12}O_6 \quad 3.16$$

Fermentation

$$3C_5H_{10}O_5 \rightarrow 5C_2H_5OH + 5CO_2 \quad 3.17$$

$$C_6H_{12}O_6 \rightarrow 2C_2H_5OH + 2CO_2 \quad 3.18$$

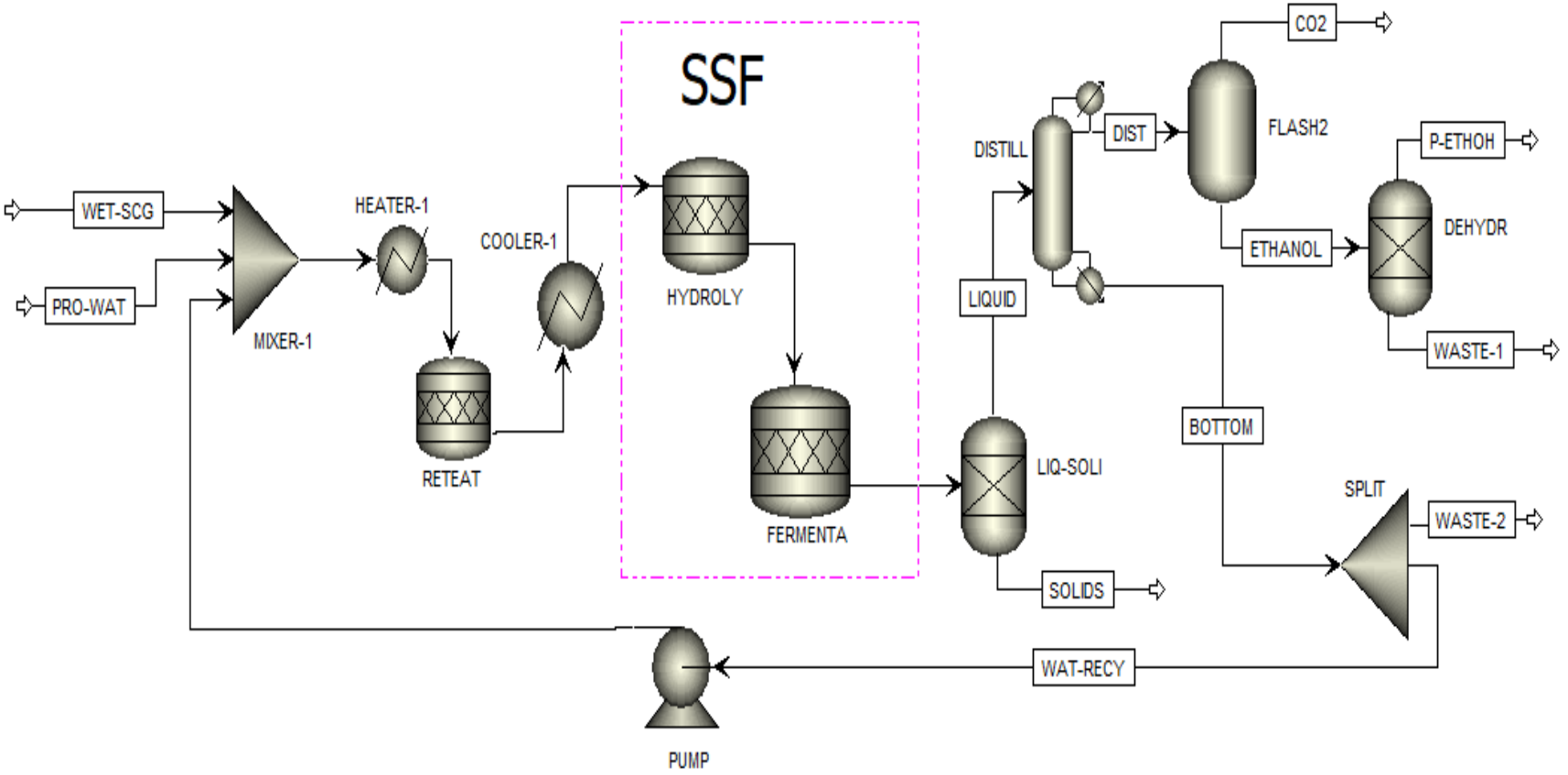

Figure 3. 6: Aspen plus PFD of bioethanol production

Table 3. 6: Aspen plus operation blocks used in bioethanol production simulation

Block name in Aspen plus	Simulation name	Description
Mixer	MIXER-1	Mixes recycle and makeup water with wet biomass to form a slurry
Heater	HEATER-1	Electric heater that raises the temperature of slurry to 180 ^{0}C
RStoic	PRETREAT	Models steam explosion of hemicellulose to form xylose at 2 bar pressure and 180 ^{0}C
Heater	COOLER-1	Cools the pretreatment reactor effluent from 180 ^{0}C to 30 ^{0}C
RStoic	HYDROLY	Models enzyme hydrolysis of cellulose to form glucose
RStoic	FERMENTA	Models the fermentation of xylose and glucose by yeast to form ethanol and CO_2
Sep	LIQ-SOLI	Solid-liquid separator used to remove unreacted biomass from the product mixture
DSTWU	DISTILL	Models a distillation column operating at atmospheric pressure, used to separate water from ethanol
Flash2	FLASH2	Flash column operating at 1.5 bar pressure and 25 ^{0}C used to separate CO_2 from ethanol
Sep	DEHYDR	Models the dehydration of ethanol to remove any traces of residual water
FSplit	SPLIT	Splits the bottom stream of the distillation column into recycle and waste streams
Pump	PUMP-1	Pumps recycle water to MIXER-1

3.2.6. Anaerobic digestion

Like in fermentation, biomass building blocks, cellulose, hemicellulose and lignin were defined as conventional solids, ash as nonconventional solid and moisture as a conventional component. The monomers $C_6H_{10}O_5$ and $C_5H_8O_4$ were used to represent cellulose and hemicellulose, respectively, whereas lignin was defined as $C_{11}H_{12}O_4$. The estimated solid property model parameters of these solids as outlined in Appendix A were used to define them in Aspen plus software. Xylose and glucose were defined as D-xylose and Dextrose, respectively, present in Aspen plus. MIXCINC was used as the global flow for the simulation since both nonconventional and conventional components were present. The fluid package used to calculate the thermodynamic properties was NRTL since liquids and gases are present (Naqi, Kuhn and Joseph 2019).

Figure 3.7 shows the process flow diagram for the simulation of biogas production process and the descriptions of each equipment as used in Aspen plus software are outlined in Table 3.8. Process water together with recycle water was added to wet SCG to make slurry with solid content less than 20% (Naqi, Kuhn and Joseph 2019). The slurry was heated by an electric heater, HEATER-1, to a temperature of 37 ^{0}C at 3 bars and then sent to the anaerobic digester modeled by four stoichiometric reactors in series. The same reaction conditions were used by Ravendran, Abdulrazik and Zailan (2019). The first reactor HYDROLY models hydrolysis of holocellulose to form xylose and glucose as shown by equations 3.19 and 3.20. The simple sugars are then converted into acetic acid and volatile fatty acids (propionic acid) in the second reactor, ACIDOG as shown by reaction equations 3.21 and 3.22. The volatile fatty acids are converted into acetic, carbon dioxide and hydrogen in the third reactor, ACETOG as shown by reaction equation 3.23. In the fourth reactor, METHANOG, acetic acid is converted into ethanol and carbon dioxide as hydrogen is being consumed as shown by equation 3.24. Feed hydrogen is added to ensure complete reaction of acetic acid. This helps to maximize the yield of biogas. Sulfur and nitrogen present in biomass according to its ultimate analysis reacted with hydrogen to form hydrogen sulfide and ammonia respectively, as shown in equations 3.25 and 3.26. The conversion rates of cellulose and hemicellulose were assumed to be 0.88 and 0.84, respectively. The same assumptions were adopted by Lyu *et al.* (2020). For all other reactions, conversions were set to one. The effluent from the bio-reactor was sent to the solid-liquid separator, SEP-1 to remove solids. The liquid mixture was heated to 53 ^{0}C (Ravendran, Abdulrazik and Zailan 2019) and then sent to the flash column, FLASH-1 operating at 53 ^{0}C and 1 bar pressure to separate water from biogas. Over 98%

of the biogas was recovered from the mixture, but together with hydrogen sulfide and ammonia as impurities. Over 74% of the water was recycled and mixed with makeup water using mixer, MIXER-2 and then mixed with biomass. Biogas was purified by adsorption on activated carbon (Naqi, Kuhn and Joseph 2019). Here, hydrogen sulfide and carbon dioxide were removed. This operation was modeled by a Sep block in Aspen plus represented as CO2-SEP in Figure 3.7.

3.2.6.1. Reactions used in anaerobic digestion

A set of stoichiometric reactions were used to model anaerobic digestion. There are four major reactions i.e. hydrolysis (equations 3.19 and 3.20), acidogenesis (equations 3.21 and 3.22), acetogenesis (equation 3.23) and methanogenesis (equation 3.24) as shown in Table 3.7. Equations 3.25 and 3.26 were used to model the formation of hydrogen sulfide and ammonia which are always co-produced with bio-methane during anaerobic digestion.

Table 3. 7: Set of equations used to model anaerobic digestion

Hydrolysis	
$C_5H_8O_4 + H_2O \rightarrow C_5H_{10}O_5$	3.19
$C_6H_{10}O_5 + H_2O \rightarrow C_6H_{12}O_6$	3.20
Acidogenesis	
$2C_5H_{10}O_5 \rightarrow C_3H_6O_2 + 3C_2H_4O_2 + CO_2 + H_2$	3.21
$C_6H_{12}O_6 \rightarrow C_3H_6O_2 + C_2H_4O_2 + CO_2 + H_2$	3.22
Acetogenesis	
$C_3H_6O_2 + 2H_2O \rightarrow C_2H_4O_2 + CO_2 + 3H_2$	3.23
Methanogenesis	
$C_2H_4O_2 + 4H_2 \rightarrow 2CH_4 + 2H_2O$	3.24
$S + H_2 \rightarrow H_2S$	3.25
$N_2 + 3H_2 \rightarrow 2NH_3$	3.26

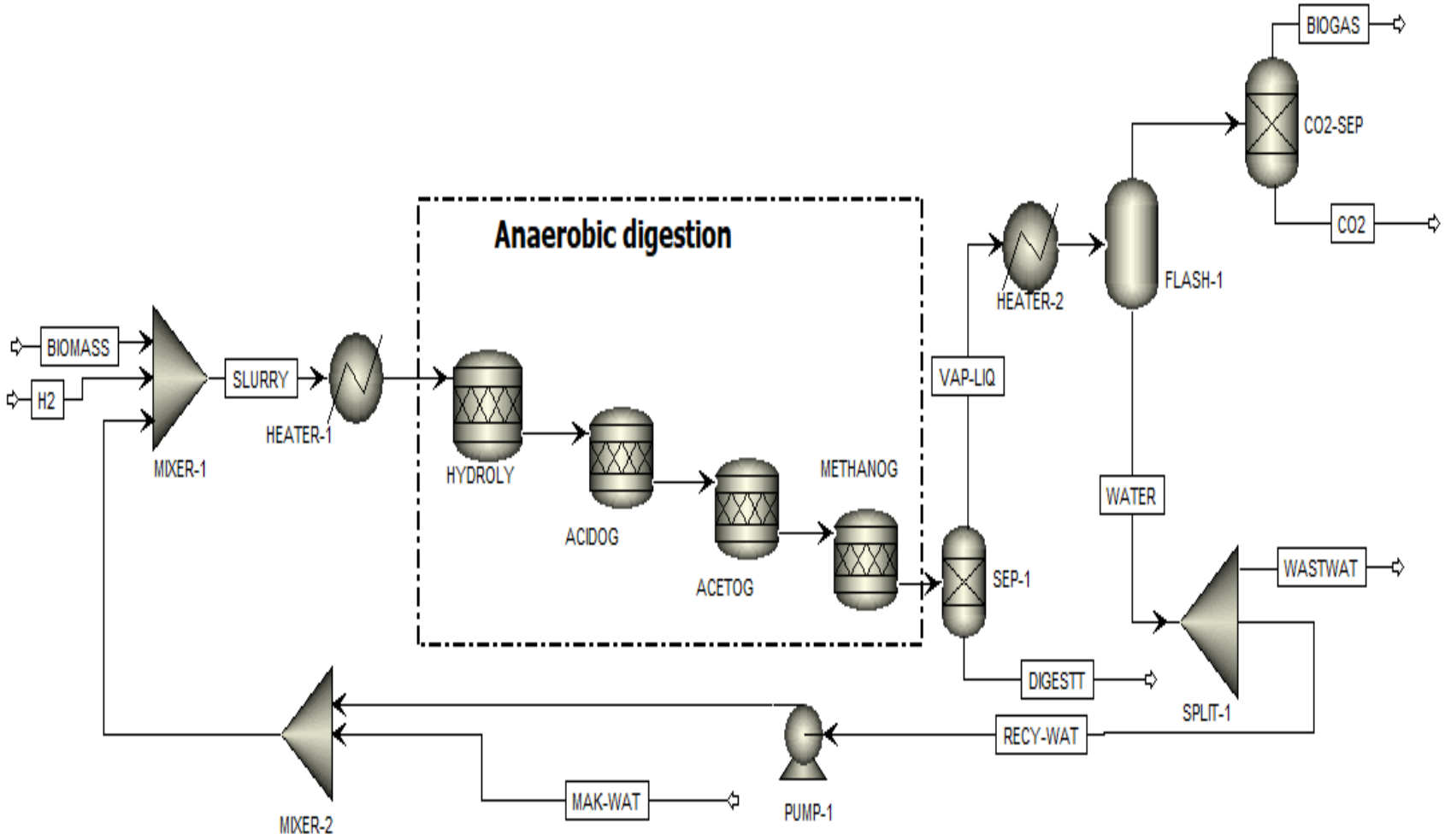

Figure 3. 7: Aspen plus PFD of anaerobic digestion

Table 3. 8: Aspen plus operation blocks used in anaerobic digestion simulation

Block name in Aspen plus	Simulation name	Description
Mixer	MIXER-1	Mixes biomass, hydrogen and water to form a slurry
Heater	HEATER-1	Electric heater that raises the temperature of slurry to 53 ^{0}C
RStoic	HYDROLY	Models hydrolysis of cellulose and hemicellulose to form glucose and xylose, respectively
RStoic	ACEDOG	Models acetogenesis reactions where large monomers are broken into volatile fatty acids
RStoic	ACETOG	Models acetogenesis reaction where volatile fatty acids are converted into acetic acid, CO_2 and hydrogen
RStoic	METHANOG	Models the conversion of acetic acid and hydrogen into methane and water
Sep	SEP-1	Solid-liquid separator used to remove unreacted biomass from the product mixture
Heater	HEATER-2	Electric heater that raises the temperature of the gas-liquid mixture to 53 ^{0}C before being sent to the flash column
Flash2	FLASH-1	Flash column operating at 1 bar pressure and 53 ^{0}C used to separate gases from water
FSplit	SPLIT-1	Splits the water stream into recycle and waste streams
Pump	PUMP-1	Pumps recycle water to MIXER-2
Mixer	MIXER-2	Mixes recycle water with make-up water
Sep	CO2-SEP	Separates carbon dioxide from bio-methane

3.3. Economic analysis

The economic analysis of biofuel production from SCG was conducted using the factorial method (Sinnott and Towler 2009). The method utilizes the total purchase of all major equipment as the basis for cost evaluation. In addition to equipment costs, there are other costs that are directly related to equipment installation. These include equipment elevation, piping, insulation materials and coatings, lighting, buildings, etc. Lang (1948) (Sinnott and Towler 2009) proposed factors to incorporate these costs into the cost of equipment to obtain what is commonly known as installed cost of equipment. The installed cost of equipment by definition is the Inside Battery Limit Investment (ISBL). All other costs are expressed as factors of ISBL investment. The major assumptions used in economic evaluation are summarized in Table 3.9.

Table 3. 9: General assumptions made in economic evaluation (Iglesias *et al.* 2021; Thoppil and Zein 2021)

Description	Value	Unit
Plant location	Umbogintwini, Kwazulu-Natal, South Africa	
Base year	2021	
Plant scale		Metric ton/year
Construction time	2	Years
Plant life	25	Years
Operating hours	7920	Hours/year
Plant capacity	100% normal throughput in year three (first year of production) until the last year of plant life	
Project financing	100	% own capital
Tax rate	28	%
Discount rate	12	%
Depreciation method	Straight-line	10% per year
Scrap value	0	USD
Exchange rate	17	ZAR/US$
Salary of an operator	529.41	USD/month
CEPCI for 2019 and 2021	607.5 and 708	respectively

3.3.1. Capital Expenditure

Capital Expenditure (CAPEX) is the sum of Fixed Capital Investment (FCI), Working Capital (WC) and Start-up Costs (SUC). Table 3.10 summarizes the calculation of CAPEX.

3.3.1.1. Fixed Capital Investment

Fixed Capital Investment (FCI) involves costs such as designing, constructing, erecting the plant and any modifications to be made. It is the sum of ISBL, the Off-site Plant Cost (OSBL), Engineering Costs (EC) and Contingency Costs (CC). ISBL plant costs were estimated using the factorial method (Sinnott and Towler 2009). The method estimates the ISBL plant cost as the total installed cost of major equipment.

The installed cost of equipment was determined using Aspen Process Economic Analyzer (APEA) embedded into Aspen plus software. The same method was used by Akbari, Oyedun and Kumar (2019). Aspen plus V11 software, launched in 2019 was used. The Chemical Engineering plant Cost Index (CEPCI) (Okolie *et al.* 2021) was used to update the results from the software to the base year (2021). The CEPCI for 2019 and 2021 is 607.5 and 708, respectively. The updated ISBL plant cost was calculated using equation 3.27.

$$\text{Updated ISBL} = \frac{\text{CEPCI}(2021)}{\text{CEPCI}(2019)} \times \text{Installed plant cost} \qquad 3.27$$

OSBL involves all costs related to site infrastructure to cater for plant modifications or expansion. It was estimated as 40% of ISBL (Sinnott and Towler 2009).

EC are the costs paid to contractors whose expertise is needed during project design, civil engineering works, equipment procurement and requisitions, supervision of construction process, etc. It was estimated as 10% of the sum of ISBL and OSBL (Sinnott and Towler 2009).

CC is costs included during project planning to cater for unforeseen circumstances like changes in prices adopted during the budgeting process. It was estimated as 10% of the sum of ISBL and OSBL (Sinnott and Towler 2009).

3.3.1.2. Working Capital

Working Capital (WC) is the amount of money spent from the first day of plant operation until a point in time when the revenue generated from sales of finished products can shoulder the day-to-day running of the project. WC was taken as 15% of the sum of ISBL and OSBL plant costs.

3.3.1.3. Startup Costs

Startup Costs (SUC) involves such costs needed for budget planning, research work, advertising, borrowing expenses if own capital is not available, license and insurance charges. SUC was taken as 10% of the sum of ISBL and OSBL plant costs.

Table 3. 10: Calculation of capital expenditure

Cost	Formula used
ISBL	Equation (3.3.1)
OSBL	40% of ISBL
EC	10% of (ISBL+OSBL)
CC	10% of (ISBL+OSBL)
FCI	ISBL+OSBL+EC+CC
WC	15% of (ISBL+OSBL)
SUC	10% of (ISBL+OSBL)
CAPEX	**FCI+WC+SUC**

3.3.2. Operating Expenses

Operating Expenses (OPEX) are costs required to run the day-to-day operations of the plant. It is calculated as the sum of Fixed Operating Costs (FOC) and Variable Operating Costs (VOC). FOC are fixed and do not depend on plant production rate. These include labor costs, supervision costs, rent, insurance and tax expenses, maintenance costs, costs to cover research and development, costs to pay fringe benefits of workers, their insurance and many others. Conversely, VOC vary with production rate, and these include raw material costs, utility costs and costs of consumables.

3.3.2.1. Variable operating costs

VOC were calculated as the sum of raw material costs, utility costs and cost of consumables. The cost of raw materials was uniform for all the six projects since a similar feed rate (2000 kg/h of wet SCG) was used.

The scenario used was that wet SCG was acquired for free from coffee brewing shops and other food processing industries around the Durban metropolitan area. It was assumed that wet SCG were collected from a radius of 50 km and was transported by trucks hired from cargo companies. Thus, the total cost of raw materials was the costs associated with transportation of wet SCG to the processing plant at Umbogintwini in Kwazulu-Natal, South Africa.

Umbogintwini was chosen as the ideal plant location because it is adjacent to Port of Durban which is South Africa's main port, thus making it easy to import the equipment and other chemicals. Also it will be easy to export finished products to the rest of the world. Cargo companies were consulted and on average, it costs 23.5 USD to transport one ton of wet SCG a distance of 50 km around Durban. Therefore, the total cost of raw materials per year was calculated as illustrated by equation 3.28.

$$\text{Cost of raw materials} = \left(\frac{2000 \times 7920}{1000}\right) \times 23.5294 = 372705 \text{ USD} \qquad 3.28$$

The cost of utilities depends on the project and it was calculated as the sum of electricity costs, cooling water and process water costs. It was assumed that all heaters were electric heaters powered by electricity from the national grid. Heat duty of heaters was converted to kilo watt hour (kWh) to determine the cost of electricity. Commercial or industrial electricity in South Africa stands at 0.073 USD per kWh according to GlobalPetrolPrices.com (2023a). The cost of cooling water was determined on assumption that all the coolers were Heat and Tube heat exchangers operating on cooling water. Equation 3.29 was used to calculate the flow rate of cooling water used to produce the required cooling.

$$\dot{m} = \frac{Q}{C \times \Delta T} \qquad 3.29$$

where;

$\dot{m} = \text{mass flow rate of cooling water in kg/s}$

$Q = \text{heat duty of a cooler in J/s}$

$C = \text{specific heat capacity of water in J/(kgK)}$

$\Delta T = \text{difference between temperature of water in and water out in Kelvin}$

It was assumed that cooling water is available at 25 ^{0}C and leaves the heat exchanger at 35 ^{0}C.

It was assumed that the flow rate of cooling water per month (kg/month) was enough for a whole year as it is continuously recycled. Big reservoirs of cooling water are available on site to enable reuse. Cooling water out of the heat exchanger was pumped to reservoirs and cooled by standing

in open air before being used again. No electricity was used to do this cooling. The quantity of cooling water in kilo liters was determined.

It was assumed that 1000 kg of water is equivalent to 1 kilo liter of water (since density of water is 1 kg/l). Commercial/industrial water in South Africa stands at 2.79 USD per kilo liter. The cost of process water was determined directly from the flow rate of input water according to mass balances.

The cost of consumables also varied from process to process, with the thermochemical process requiring almost no consumables whereas biological processes (fermentation and anaerobic digestion) and biodiesel production used consumables such as methanol, hexane, cellulose, catalysts, etc. During bioethanol production, the fermenting yeast *Saccharomyces cerevisiae* was produced on site. Actual prices of these items from online suppliers were used to calculate the cost of consumables for each process.

3.3.2.2. Fixed Operating Costs

FOC were calculated as the fraction of operating labor costs, ISBL and OSBL plant costs as shown in Table 3.11.

Table 3. 11: Calculation of fixed operating costs

Fixed Operating costs (FOC)	**Formula used**
Cost of operating labor per year (a)	Equation 3.30
supervision (b)	25% of (a)
Direct overhead (c)	40% of (a+b)
Maintenance (d)	4% of ISBL
Property taxes and insurance (e)	2% of ISBL
Rent of land (f)	2% of (ISBL +OSBL)
General plant overhead (g)	65% of (a+b+c+d)
Environmental charges (h)	1% of (ISBL+OSBL)
FOC	**a+b+c+d+e+f+g+h**

The Cost of Operating Labor (COL) was calculated based on the number of operators needed per shift. The plant operates 24 hours a day with 3 shifts of 8 hours each. The number of operators per shift (Naqi, Kuhn and Joseph 2019; Okolie *et al.* 2021; Feng *et al.* 2022; Mukherjee *et al.* 2022) was calculated using equation 3.30.

$$N_{OP} = (6.29 + 0.23N_{NP} + 31.7P^2)^{0.5} \quad 3.30$$

where;

$N_{OP} = \text{number of operators per shift}$

$N_{NP} = \text{number of non} - \text{particulate processing units in the process}$

$P = \text{number of particulate processing units in the process}$

It was assumed that only the biodiesel production plant had the particulate processing unit (pelletizing section). There was no particulate processing units for the rest of other projects.

The total number of operators needed for each plant was determined by multiplying the number of operators per shift by the three 8-hour shifts in a day.

It was assumed that each operator is paid 529.41 USD per month for a period of 12 months, which is the average minimum wage of an operator in South Africa (payscale 2023).

3.3.3. Total revenue

Revenues were calculated as the sum of sales of main products and by-products. The market prices of finished products were used when calculating product revenues.

3.3.4. Gross profit

Gross profit was determined by subtracting OPEX from total revenue.

3.3.5. Discounted Cash Flow Analysis

Microsoft Excel spreadsheets were used to do the Discounted Cash Flow Analysis (DCFA). Using DCFA, the Net Present Value (NPV), Discounted Payback Period (DPBP), Profitability Index (PI) and the Internal Rate of Return (IRR) were determined. The plant life was 25 years with 2021 as the base year. The first year (2021) was spent on conceptualization and process designing. The second year (2022) was spent on plant construction, equipment procurement and installation. Plant operations started in the third year (2023) and it was assumed that the plant operated at full capacity throughout the entire life of the project (until year 2045).

Depreciation expense was deducted from gross profit at a rate of 10% using the straight-line method. The scrap (salvage) value of the project was assumed to be zero. Taxable income was calculated by subtracting depreciation expense from gross profit. Tax paid was calculated by

multiplying taxable income by the tax rate. The South African corporate tax rate stands at 28%. The net profit (net cash flow) was calculated by subtracting tax paid from gross profit. The discount rate (12%) was used to calculate the discounted cash flow using equation 3.31.

$$DCF_n = \frac{CF_n}{(1+i)^n} \qquad 3.31$$

where;

$DCF_n =$ discounted cash flow in year n

$CF_n =$ net cash flow in year n

$i =$ discounting factor

The net cash flow in year one (2021) was zero as no money was spent or earned in this period. Time was spent on conceptualization and process design. The net cash flow in year two (2022) was negative as all the fixed capital was spent in this year but there was no plant operations, so no income was generated. The discount factor in this year was taken as one (Thoppil and Zein 2021).

The NPV was calculated as the summation of all the discounted cash flows throughout the entire life of the project. It was calculated as illustrated by equation 2.10. Microsoft Excel spreadsheets were used to calculate the NPV.

Profitability Index (PI) was calculated as illustrated by equation 2.12.

The IRR is the value of the discount factor for which NPV is zero. IRR was conveniently read from the figure when the NPV curve meets the discount rate axis.

A more realistic payback period was estimated when the cumulative Discounted Cash Flow (DCF) first becomes positive. Cumulative DCF gives a more realistic PBP because it is calculated after the project has paid tax and interest. This is called the discounted payback period (DPBP). DPBP was obtained from the graph when the curve of NPV meets the time axis.

3.4. Life Cycle Assessment

Life Cycle Assessment (LCA) was carried out in four steps, namely goal and scope definition, life cycle inventory, life cycle impact assessment and interpretation of results as outlined by the ISO 14040/44 methodology (Demichelis *et al.* 2020; Schmidt Rivera *et al.* 2020; Liu *et al.* 2021). OpenLCA V1.11.0 software, first developed in 2006 by GreenDelta, Berlin was used. The same software was used by Demichelis *et al.* (2020). The software was chosen because it is freely available and has free databases. It was downloaded from the OpenLCA nexus website.

3.4.1. Goal and scope definition

One of the main objectives of this study was to evaluate LCA comparing potential environmental impacts of biofuels production from SCG in order to define the production process with the lowest environmental impacts. The scope of this study was the basis for the decision on the most eco-friendly processing route for biofuels production from SCG. The functional unit was 2000 kg of wet SCG processed per hour. The same method was used by Liu *et al.* (2021) who considered the amount of biomass processed as a functional unit. A cradle-to-gate (Demichelis *et al.* 2020) system was selected and the system boundaries were transportation of wet SCG from source (coffee shops and coffee brewing industries) to the bio-refinery, biomass pretreatment and conversion of SCG to biofuels.

3.4.2. Life Cycle Inventory

The mass and energy flows between the system boundaries were used as inputs and outputs. Most of the flows were present in Agribalyse Version 3 database but others like lignin, biodiesel and hemicellulose were created as elementary flows since they were not present. Coffee residue, processed present in the database was selected as the raw material. Electricity, high voltage produced from hard coal was selected as electricity used for all the six studied processing plants. It was hypothesised that a total distance of 50 km travelled to collect wet SCG from source to plant gates was covered by a truck, EURO 5 of 16 – 32 tons. All other flows (inputs and outputs) were entered according to the mass balance results obtained from Aspen plus simulation of each processing route.

3.4.3. Life Cycle Impact Assessment

Agribalyse_v301_27052021 database downloaded from OpenLCA Nexus website (GreenDelta 2022) was used in this study. The ReCiPe 2016 Midpoint (H) was used as the impact assessment

method. The same method was used by Demichelis *et al.* (2020) and Schmidt Rivera *et al.* (2020). The selected impact categories were global warming, fossil resource scarcity, particulate matter formation, terrestrial acidification, freshwater eutrophication, marine eutrophication, mineral resource scarcity and water consumption. This study didn't consider normalisation and weighing steps. The same procedure was used by Lombardi and Francini (2020) in their study about the LCA of biogas main upgrading methods.

3.4.4. Interpretation of results

The main aim of conducting the LCA study was to choose the processing route with least environmental impacts. Six processing routes, namely pyrolysis, biodiesel production, hydrothermal liquefaction, gasification, anaerobic digestion and bioethanol production were comparatively analysed. For each impact category, 100% was assigned to the most impactful processing route as shown in section 4.4.2. These percentages were used to rank processing routes in ascending order of total percentages. The best processing route was one with the smallest total of percentages.

3.5. Summary

The overall methodology followed during Aspen plus simulation, economic analysis and life cycle assessment of biofuel production from SCG has been described in this chapter. Aspen plus V11 software was used to simulate six biomass-to-bioenergy conversion technologies and the Aspen process economic analyser was used to estimate the installed cost of all equipment for each project. The total cost of production and sales revenue were determined and used to evaluate the gross profit. Depreciation, a tax allowance, was computed using the straight-line method. The net profit was computed after deducting corporate tax and interest on capital from the gross profit. The discounted cash flow analysis was used to calculate the four economic indicators used in this study. The economic indicators were NPV, DPBP, PI and IRR. Life cycle assessment was conducted using OpenLCA V 1.11.0 software and the Agribalyse Version 3 database. Eight impact categories were used to assess the environmental impacts of producing biofuels from SCG. The impact categories were mineral resource scarcity, global warming, fossil fuels scarcity, terrestrial acidification, water consumption, particulate matter formation, marine eutrophication, and freshwater eutrophication.

4. RESULTS AND DISCUSSION

4.1. Introduction

This chapter presents all the findings of the present study. It has three major sections. Under section 4.2, all the results of Aspen plus simulation are presented. It encompasses the presentation of all mass and energy balances for each of the processing routes simulated. Section 4.3 covers the results of economic analysis including the installed cost of all equipment used, initial capital investment, operating expenditures and the results from the discounted cash flow analysis. Finally, the results of LCA are presented under section 4.4 including all the impact categories selected for the analysis and the interpretation of results. Also, the discussion of all the findings are presented in this chapter.

4.2. Aspen plus simulation

The mass and energy balances obtained from Aspen plus simulations are presented under this section. The mass balances are presented as input and output flow rates in kg/h, whereas energy balances as heating and cooling duties in kWh.

For purposes of fair comparison, all the six processing routes used the same flowrate of feedstock i.e. 2000 kg/h of wet SCG. The thermochemical conversion technologies (gasification and fast pyrolysis) required no consumables like catalysts and solvents. Gasification used 445 kg/h of process water since steam was used as the gasifying agent. However, HTL used a lot of water as a slurry of less than 25% solid content was fed to the process. Gasification and fast pyrolysis required a pre-dried biomass feedstock whereas HTL required no biomass pre-drying. The biochemical conversion technologies (AD and fermentation) required no biomass pre-drying, however, large amounts of water were used to prepare the required slurries of feedstock. On the other hand, biodiesel production required biomass drying prior to coffee oil extraction and large quantities of extraction solvent (hexane) were used to recover the oil from SCG.

Table 4.1 outlines the material flow in and out of the process during biodiesel production. Hexane was used as extraction solvent to recover coffee oil from dried SCG. Process water (70 kg/h) was used during fat hydrolysis to convert triglycerides into free fatty acids and glycerol. Methanol (52.41 kg/h) was used as a reactant in the esterification reaction to convert free fatty acids into biodiesel (159.28 kg/h) in the presence of SiO_2-HF beads as catalyst. After coffee oil extraction,

the defatted SCG was sent to the pelletizing section to produce coffee pellets at a production rate of 796.20 kg/h.

Table 4. 1: Mass balance for biodiesel production

Mass balance			
Input		**Output**	
Stream name	**Flow rate (kg/h)**	**Stream name**	**Flow rate (kg/h)**
Wet SCG	2000.00	Moisture	1002.01
Process water	70.00	Hexane loss	50.00
Makeup hexane	50.00	Methanol loss	31.94
Makeup methanol	52.41	Biodiesel	159.28
		Wet glycerol	93.79
		Wastewater	39.16
		Coffee pellets	796.20

Table 4.2 shows the mass balance for biomass gasification process. All the moisture (1033 kg/h) present in wet SCG was removed before the dried feedstock was sent to the gasifier. Process water (445 kg/h) was added to the gasifier after being vaporized since steam was used as the gasifying agent. Syngas (CO and H_2) was produced at the production rate of 1045.91 kg/h. Carbon dioxide produced during gasification and excess water were removed as waste stream at a flowrate of 330.17 kg/h. Ash present in SCG according to its proximate and ultimate analysis was considered as inert and left the process as a waste material.

Table 4. 2: Mass balance for biomass gasification

Mass balance			
Input		**Output**	
Stream name	**Flow rate (kg/h)**	**Stream name**	**Flow rate (kg/h)**
Wet SCG	2000.00	Moisture	1033.00
Process water	445	Hydrogen	97.05
		Carbon monoxide	948.86
		Methane	27.22
		Ash	9.00
		Waste	330.17

Table 4.3 shows the material flow in and out of the process during biomass fast pyrolysis. There was no any consumables added to the process. The process needed biomass pre-drying to remove the moisture in wet SCG. Bio-oil was the main product of the process whereas syngas and bio-char are also useful products formed during biomass fast pyrolysis.

Table 4. 3: Mass balance for biomass fast pyrolysis

Mass balance			
Input		**Output**	
Stream name	**Flow rate (kg/h)**	**Stream name**	**Flow rate (kg/h)**
Wet SCG	2000.00	Moisture	1000.00
		Bio-oil	417.00
		Syngas	349.00
		Water	93.00
		Bio-char	141.00

The yields of bio-oil, bio-char and syngas at optimal operating parameters (500 ^{0}C, 1 bar pressure and 5 seconds residence time) were 41.70%, 34.90% and 14.10%, respectively as shown in Table 4.3. The yields of pyrolysis products were calculated using the dry biomass feedstock. This is reasonably in agreement with observations made by Jaroenkhasemmeesuk *et al.* (2022) on fast pyrolysis of pine sawdust. At the same operating parameters, the observed product yields were 52.48%, 12.07% and 22.53% for bio-oil, bio-char and syngas, respectively. The variations between yields reported in their study and the current study is because different biomass types were used. Each of the biomass feedstocks had different proximate and ultimate analyses, hence the slight difference in product yields. The close similarity in product yields of both models can be used to validate the reliability of the model used in the present study. The highest bio-oil and syngas yield and lowest bio-char yield is attributed to the highest volatile matter (81.2 wt.%) and lowest fixed carbon (14.6 wt.%) content of SCG, respectively. Similar observations were made by AlNouss *et al.* (2021) on pyrolysis of five different biomass types, namely orange peel, banana peel, mango endocarp, apricot kernel shell, and date pits. They observed that the highest bio-char yield (50.9 wt.%) was obtained from date pits whereas mango endocarp gave the highest syngas yield (54.2 wt.%). Date pits had the highest carbon content whereas mango endocarp had the highest volatile matter content. It can therefore be inferred that high carbon content favors bio-char yield whereas high volatile matter content enhances bio-oil and syngas yield.

Table 4.4 shows mass balance for biomass HTL. There was no moisture removal but instead process water (100 kg/h) was required to create a slurry with solid content of not more than 25%. Product yields are exactly the same as those in biomass fast pyrolysis. This is because HTL and fast pyrolysis were modeled in a similar manner. The only remarkable difference between the two technologies is that unlike fast pyrolysis, HTL does not require biomass pre-drying.

Table 4. 4: Mass balance for hydrothermal liquefaction

Mass balance			
Input		**Output**	
Stream name	**Flow rate (kg/h)**	**Stream name**	**Flow rate (kg/h)**
SCG	2000.00	Bio-oil	417.00
Process water	100.00	Syngas	349.00
		Wastewater	1193.00
		Char	141.00

Table 4.5 shows material flow in and out of the process during bioethanol production process. There was no moisture removal but instead process water (100 kg/h) was required to create a slurry with solid content of not more than 25%. Bioethanol was produced at flowrate of 254.60 kg/h and collected at the bottom of the flash column whereas carbon dioxide left the process at the top of the column at a rate of 261.54 kg/h. The unreacted holocellulose and the recalcitrant lignin was recovered from the process at the bottom of the solid-liquid separator at a rate of 520.16 kg/h. Wastewater left the process at the bottom of the distillation column at a flowrate of 1063 kg/h.

Table 4. 5: Mass balance for bioethanol production

Mass balance			
Input		**Output**	
Stream name	**Flow rate (kg/h)**	**Stream name**	**Flow rate (kg/h)**
SCG	2000.00	Bioethanol	254.60
Process water	100.00	Digestate	520.16
		Wastewater	1063.00
		Carbon dioxide	261.54

Table 4.6 shows the mass and energy balance for anaerobic digestion. There was no moisture removal but instead process water (100 kg/h) was required to create a slurry with solid content of not more than 25%. Hydrogen (53 kg/h) was added to the bio-digester to maximize the production

of bio-methane. Biogas was produced at flowrate of 274.87 kg/h and collected at the top of the flash column. The unreacted holocellulose and the recalcitrant lignin was recovered from the process at a rate of 322 kg/h. The model produced a great amount of carbon dioxide at flowrate of 319 kg/h. Ammonia and hydrogen sulfide as the main impurities of biogas were produced from nitrogen and sulfur present in biomass according to its ultimate analysis.

Table 4. 6: Mass balance for anaerobic digestion

Mass balance			
Input		**Output**	
Stream name	**Flow rate (kg/h)**	**Stream name**	**Flow rate (kg/h)**
SCG	2000.00	Biogas	274.87
Process water	100.00	Digestate	322.00
Hydrogen	53.00	Wastewater	1210.00
		Carbon dioxide	319.00
		Ammonia	17.77
		Hydrogen sulfide	9.01

Table 4.7 outlines the cooling and heating duties for all the six processing routes. It can be seen that HTL required the highest heating duty, 2537.98 kWh followed by bioethanol production, gasification, biodiesel production, fast pyrolysis and lastly anaerobic digestion in descending order.

Table 4. 7: Cooling and heating duties for all the six processing routes

Conversion route	Energy balances	
	Heating duty (kWh)	**Cooling duty (kWh)**
Fast pyrolysis	414.77	294.86
HTL	2537.98	426.04
Gasification	1634.87	547.34
Biodiesel production	1110.93	394.59
Anaerobic digestion	136.00	0.00
Bioethanol production	2069.90	210.33

It can be critically noted that HTL consumed more heat energy compared to pyrolysis yet many researchers state that the advantage of HTL over pyrolysis is the use of wet biomass, hence no pre-drying is required. The optimal temperature for HTL is 300 ^{0}C (Aierzhati *et al.* 2021; Alherbawi

et al. 2021; Zhang *et al.* 2021a) which is way below that of pyrolysis, 500 ^{0}C (Jaroenkhasemmeesuk *et al.* 2022). This would mean that pyrolysis would require a higher heat duty than that of HTL which isn't the case in this study. This is because during HTL, biomass had to be mixed with water to obtain slurry of about 20% solid content (Deuber *et al.* 2021). A lot of heat was required to raise the temperature of the slurry to 300 ^{0}C compared to heat required for biomass drying and raising the temperature of dried biomass to 500 ^{0}C as in pyrolysis simulation. Thus, the ability of HTL to handle wet biomass was canceled by a lot of heating duty required to heat a large flow rate of the slurry.

During bioethanol production, no biomass drying was required but a great deal of heat (2069.90 kWh) was used compared to that of biodiesel production (1110.93 kWh) which required biomass drying prior to coffee oil extraction. Also, as it was the case for HTL, during fermentation, process water was added to wet biomass to obtain slurry of about 25% solid content (Liu *et al.* 2021). The pretreatment step employed steam explosion (Duarte *et al.* 2021) which required the slurry to be raised to a temperature of 250 ^{0}C. Also, a great deal of heat energy was consumed during ethanol distillation as a high flow rate of crude ethanol was handled due to a large amount of process water being used in the process. Conversely, for biodiesel production, a smaller flow rate of crude biodiesel was handled in the distillation column since dry coffee oil was used in the esterification process. The only water present was that co-produced with biodiesel in the esterification reaction as shown by equation 3.14 in section 3.2.4.

As expected, anaerobic digestion required the smallest heating duty of all the six processing routes simulated because the biological reactions occurred at mesosphilic conditions (temperature of 37 ^{0}C). The reactions are being catalysed by microorganisms and no heating is required during down processing, making AD the most energy saving processing route. This study did not consider production of energy onsite like the Combined Heat and Power (CHP) or heat recovery as it was beyond the scope of the study. The main aim of the study is to quantify all the energy requirements for each processing route as a basis to estimate electricity requirements since it was assumed that all the heat was supplied by electric heaters.

The cooling duty shows the cooling requirements for each of the processing routes. It was assumed that all the cooling duty was removed by shell and tube heat exchangers operating on cooling water. It was observed that gasification had the highest cooling duty, 547.34 kWh because the

product gas mixture had to be condensed from 750 ^{0}C to a temperature below 100 ^{0}C in order to remove moisture and other condensable gases. This is a bigger temperature difference and yet the amount of heat removed is proportional to the temperature gradient.

The cooling duty in biodiesel production (394.59 kWh) is almost twice that in bioethanol production (210.33 kWh) although for heating duty, the reverse is true. This is because a lot of cooling is required to recover hexane during coffee oil extraction. A large flow rate of hexane is used to maximize coffee oil yield. The solvent is separated from coffee oil through evaporation and condensation before it is returned to the extractor. Also, a reasonable amount of heat must be removed, in order to lower the temperature of FFAs from the fat splitter to a temperature of 65 ^{0}C, before being sent to the esterification unit to produce biodiesel.

During HTL, the vapor-liquid mixture from the cyclone had to be cooled from 300 ^{0}C to 25 ^{0}C in order to separate syngas from bio-oil-water mixture. A similar process unit exists during pyrolysis where the vapor from the cyclone was cooled from 500 ^{0}C to 25 ^{0}C in order to separate syngas from bio-oil. However, the total cooling duty for HTL (426.04 kWh) is much bigger than that of pyrolysis (294.86 kWh). This is attributed to a large flow rate of water used in HTL as heat removed is proportional to the mass of substance through which heat transfer occurs.

Just like for the heating requirement, biogas production (AD) requires almost no cooling because anaerobic digestion occurs at mesosphilic conditions. The disadvantage with AD is longer residence time, usually days, and difficulty of separating biogas from other gaseous impurities co-produced with it.

4.3. Economic analysis

This section presents results from the economic analysis of biofuels production from SCG. It includes the equipment cost and installed cost of equipment, ISBL plant cost, CAPEX, OPEX, sales revenue, gross profit and the discounted cash flow analysis for all the six processing routes considered in the present study.

4.3.1. Equipment costing

Upon successful running of the simulation, Aspen Process Economic Analyzer (APEA) embedded into Aspen plus was used to estimate the installed cost of all equipment. The software does this in three steps: equipment mapping, sizing and cost evaluation (Akbari, Oyedun and Kumar 2019). Mapping is necessary because some blocks used during a simulation don't always represent real equipment and needs to be removed or different equipment in the model pallet was selected to represent real equipment. For example, during biomass drying, moisture removal was modeled as a stoichiometric reaction with the help of the RStoich reactor block, yet in actual sense, it is an electric heater doing the job. All coolers were mapped as shell and tube heat exchangers operating on cooling water. The software does the sizing of mapped equipment according to mass and energy balances. The APEA provided estimates of unit costs and installed costs of all equipment presented in this section. With the help of Chemical Engineering Plant Cost Index (CEPCI), the installed cost of all equipment was updated to the base year (2021) to estimate the ISBL investment as illustrated by equation 3.27. The CEPCI for 2019 was used as the base since the version of the software used (Aspen plus v.11) was launched in 2019.

The total installed cost of all equipment corresponds to the ISBL plant cost (Sinnott and Towler 2009). It was assumed that for all the equipment, carbon steel was the material of construction. The installed cost of equipment is much bigger than the unit cost of equipment because it includes additional costs as equipment erection, piping, instrumentation and control, civil engineering, structures and building, lagging and painting, etc. Because APEA was used to estimate the cost of equipment, all these correlations are automatically calculated by the software and there was no need of using correlations proposed by Lang (1948) and Hand (1958) as outlined in Table 2.6.

Table 4.8 depicts the unit costs and installed costs of all the major equipment used during fermentation simulation. The updated ISBL cost for fermentation was 1,272,768 USD and this is largely contributed by the fermentation reactor, ethanol distillation column, the pretreatment reactor and the cyclone (LIQ-SOLI) used to separate the solids from the liquid mixture. As expected, the water recycle pump had the smallest installed cost of equipment (30,600 USD).

Table 4. 8: Cost of all equipment used in fermentation

Name of Equipment used in simulation	Equipment Cost [USD]	Installed Cost [USD]
COOLER-1	24,700	110,400
DISTILL	33,900	169,000
HEATER-1	73,500	104,300
FLASH2	16,400	103,600
DEHYDR	16,400	103,600
FERMENTA	49,100	196,200
PUMP	4,800	30,600
LIQ-SOLI	16,900	118,100
PRETEAT	29,200	156,300
ISBL plant cost		1,092,100
Updated ISBL plant cost		**1,272,768**

Table 4.9 outlines the unit costs and installed costs of all major equipment used in biogas production. The updated ISBL plant cost was 1,026,046 USD. As shown in Figure 3.7, the AD was modeled using for stoichiometric reactors but in practical sense its biomass hydrolysis and all other three reactors represent one real reactor. The hydrolysis reactor, HYDROLY had the highest installed cost, followed by the acetogenesis reactor ACETOG. Both these reactors can be added to represent a single bio-digester. Also, the recycle water pump was the least contributor to the total installed cost of all equipment during AD.

Table 4. 9: Cost of all equipment used during anaerobic digestion

Name of Equipment used in simulation	Equipment Cost [USD]	Installed Cost [USD]
HEATER-2	8,400	56,100
PUMP-1	4,300	33,800
FLASH-1-flash vessel	18,900	107,300
CO2-SEP	16,900	118,100
HYDROLY	68,000	216,800
ACETOG	58,600	162,300
HEATER-1	41,600	64,100
Sep-1	19,500	121,900
ISBL plant cost		880,400
Updated ISBL plant cost		**1,026,046**

Table 4.10 shows the unit cost and installed cost of equipment used during biodiesel production. The updated ISBL plant cost was 2,242,408 USD. The distillation column, COLUMN-1, was the biggest contributor to the ISBL cost, followed by fat splitter, coffee oil extractor, the esterification reactor and the flash column, FLASH-1 in descending order.

Table 4. 10: Cost of all equipment used during biodiesel production

Name of equipment used in simulation	Equipment Cost [USD]	Installed Cost [USD]
COOLER-2	8,400	54,900
PUMP-1	4,800	29,400
HEATER-4	8,400	57,100
COOLER-1	36,000	136,200
Sep-2	16,900	124,500
FLASH-1	16,900	127,200
HEATER-2	10,600	74,700
ESTERIF	34,600	172,000
Sep-3	16,900	141,400
DECANT	19,500	121,900
FATSPLIT	34,200	176,100
HEATER-3	8,900	75,600
HEATER-5	8,400	57,100
COLUMN-1	38,800	180,900
Sep-4	16,900	125,700
EXTRACT	69,700	175,400
HEATER-1	65,400	94,000
ISBL plant cost		1,924,100
Updated ISBL plant cost		**2,242,408**

Table 4.11 shows the equipment cost and installed cost of equipment used during HTL. The updated ISBL was 1,142,823 USD which is largely contributed by the HTL reactor. Since biomass primary and secondary decomposition were modeled as two separate stoichiometric reactors, it was imperative to size these two reactors separately in order to cater for the total cost of a single real reactor. It should be noted from Table 4.11 that both reactors (RSTOIC-1 and RSTOIC-2) have almost the same installed cost. The actual cost of the HTL is the total cost of these two reactors.

Table 4. 11: Cost of all equipment used during hydrothermal liquefaction

Name of equipment used in simulation	Equipment Cost [USD]	Installed Cost [USD]
PUMP	4,900	30,800
RSTOIC-2	23,100	164,500
RSTOIC-1	22,800	164,200
WAT-REMO	19,500	129,800
COOLER-1	10,200	72,400
CYCLONE	19,500	146,300
HEATER	30,400	146,900
CONDENS	16,900	125,700
ISBL plant cost		980,600
Updated ISBL plant cost		**1,142,823**

Table 4.12 shows the installed cost of all equipment used during biomass fast pyrolysis. The two stoichiometric reactors, RSTOIC-1 and RSTOIC-2 modeled biomass primary and secondary decomposition. They were sized separately even though in practice pyrolysis occurs in a single reactor. The sum of the installed costs of these two reactors gives an estimate of the pyrolysis reactor needed. Therefore, the pyrolysis reactor is the biggest contributor of the total installed cost of all equipment, followed by the cyclone, CYCLONE. Sep-1, as used in the simulation, was used to model biomass moisture removal and it was mapped as an electric dryer.

Table 4. 12: Cost of all equipment used during biomass fast pyrolysis

Name of equipment used in simulation	Equipment Cost [USD]	Installed Cost [USD]
Sep-1	16,900	125,700
RSTOIC-2	25,500	206,700
RSTOIC-1	69,900	253,200
HEATER-2	11,200	81,000
HEATER-3	11,200	81,000
COOLER-1	11,900	100,400
HEATER-1	8,900	64,800
COOLER-2	10,300	72,400
CYCLONE	45,200	223,300
WAT-REMO	16,900	118,100
CONDENS	16,900	118,100
ISBL plant cost		1,444,700
Updated ISBL plant cost		**1,683,700**

Table 4.13 shows the installed cost of equipment used during biomass gasification. The updated ISBL plant cost was 1,799,893 USD. The model used steam as the gasifying agent and the installed cost of a fluidized bed gasifier was hypothesized to be the sum of the installed cost of these two reactors, CHA-GASF and VOL-GASF. This means that the gasifier is the largest contributor to the total installed cost of all equipment in biomass gasification. Biomass pre-drying was modeled by RStoic reactor, RTOICH with the aid of a separator, Sep-1, representing an electric dryer. The installed cost of the dryer was assumed to be the summation of installed costs of RTOICH and Sep-1.

Table 4. 13: Cost of all equipment used during biomass gasification

Name of equipment used in simulation	Equipment Cost [USD]	Installed Cost [USD]
PUMP-1	4,800	29,400
COOLER-2	8,400	54,900
CHA-GASF	34,300	232,000
HEATER-1	8,900	65,400
RSTOICH	48,000	186,100
COOLER-1	8,400	54,900
CYCLONE	16,900	141,900
Sep-1	16,900	125,700
HEATER-2	11,200	81,000
Sep-2	16,900	141,900
HEATER-3	9,200	73,500
VOL-GASF	34,300	232,000
GAS-CLEA	16,900	125,700
ISBL plant cost		1,544,400
Updated ISBL plant cost		**1,799,893**

4.3.2. Cost categories

The capital costs required for setting up the bioprocessing plant and the costs required to run their day-to-activities are outlined in Table 4.14.

Table 4. 14: Cost categories

Cost category (USD)	Biodiesel	Gasification	Pyrolysis	HTL	Bioethanol	Biogas
ISBL plant cost	2,242,408	1,799,893	1,683,700	1,142,823	1,272,768	1,026,046
OSBL investment	896,963	719,957	673,480	457,129	509,107	410,419
EC	313,937	251,985	235,718	159,995	178,188	143,647
CC	313,937	251,985	235,718	159,995	178,188	143,647
FCI	3,767,245	3,023,821	2,828,616	1,919,942	2,138,251	1,723,758
WC	470,906	377,978	353,577	239,993	267,281	215,470
SUC	313,937	251,985	235,712	159,995	178,188	143,647
CAPEX	4,552,088	3,653,784	3,417,911	2,319,930	2,583,720	2,082,874
Cost of labor	114,353	57,177	57,177	571,77	57,177	57,177
FOC	617,222	395,483	380,611	311,378	328,011	296,431
Cost of raw materials	372,706	372,706	372,706	372,706	372,706	372,706
Cost of electricity	642,298	945,216	239,806	1,467,356	1,196,736	78,777
Cost of cooling water	63,668	88,315	47,577	68,742	324,528	0
Cost of process water	1,547	9,835	0	2,210	2,210	2,210
Total cost of water	65,216	98,150	47,577	70,952	326,738	2,210
Cost of utilities	707,513	1,043,367	287,383	1,538,308	1,523,473	80,988
Cost of consumables	688,035	0	0	0	0	1,049,400
VOC	1,768,254	1,416,072	660,088	1,911,014	1,896,179	1,503,093
OPEX	2,385,476	1,811,556	1,040,699	2,222,392	2,224,191	1,799,524

4.3.2.1. Installed cost of equipment

Figure 4.1 shows the installed cost of all equipment for all the six processing routes. It can be seen that biodiesel production had the highest installed cost of equipment, followed by gasification, pyrolysis, bioethanol production and lastly biogas production. The installed costs of all equipment are outlined in Table 4.14. Biodiesel production has the highest installed cost of all equipment compared to all other processing routes because of many processing units involved which include biomass pre-drying, coffee oil extraction, defatted SCG removal, hexane recovery, fat splitting, esterification, methanol recovery, biodiesel purification and the pelletizing section, as shown in Figure 3.5. Gasification is the second processing route with the highest installed cost of equipment even though it is not the second biggest in terms of processing units. Gasification has six major processing steps, namely biomass drying, biomass heating to 750 ^{0}C, gasification in the fluidized bed gasifier, gas-solid separation, syngas cooling and gas cleaning (Figure 3.3) whereas pyrolysis has seven processing steps which includes biomass drying, biomass heating to 500 ^{0}C, pyrolysis, vapor-solid separation, vapor cooling, gas-liquid separation and bio-oil drying as shown in Figure 3.2. Based on the number of processing units, pyrolysis would be expected to have the higher installed cost of equipment that is needed for gasification, however, the reverse is also true. This is because gasification takes place at higher temperatures (750 ^{0}C) than pyrolysis (500 ^{0}C), hence it requires stronger materials of construction that are resistant to high temperatures. These materials are expensive, making the installed cost of equipment in gasification higher than that for pyrolysis.

In this study, HTL was simulated in a similar manner like pyrolysis, however, the installed cost of equipment in HTL is much lower than that in pyrolysis. This is because HTL contains fewer processing units as it does not involve bio-mass drying and vapor condensation as in pyrolysis as shown in Figure 3.4. This is the major advantage of HTL over pyrolysis.

The installed cost of equipment for bioethanol production is higher than that of HTL biogas production because bioethanol production has more processing units than both HTL and biogas production. Bioethanol involves six major processing units that include biomass pretreatment, simultaneous saccharification and fermentation, solid-liquid separation, ethanol distillation, carbon dioxide removal and ethanol dehydration. On the other hand, biogas production involves

four processing units including, anaerobic digestion, solid-liquid separation, vapor liquid separation and biogas cleaning as shown in Figure 3.7.

Of all processing routes, biogas had the smallest installed cost of equipment because it had the least number of processing steps and biological reactions and downstream processing took place at mesosphilic conditions. It can therefore be concluded that the installed cost of equipment required for any biorefinery depends upon the number of processing units involved and the conditions (temperature and pressure) involved. The more the number of processing steps, the more are the equipment needed and hence higher installed equipment costs. Similarly, the higher the temperature and pressure involved, the higher is the installed cost of equipment because special materials like alloys which are pressure and temperature resistant are needed. The special materials are always expensive.

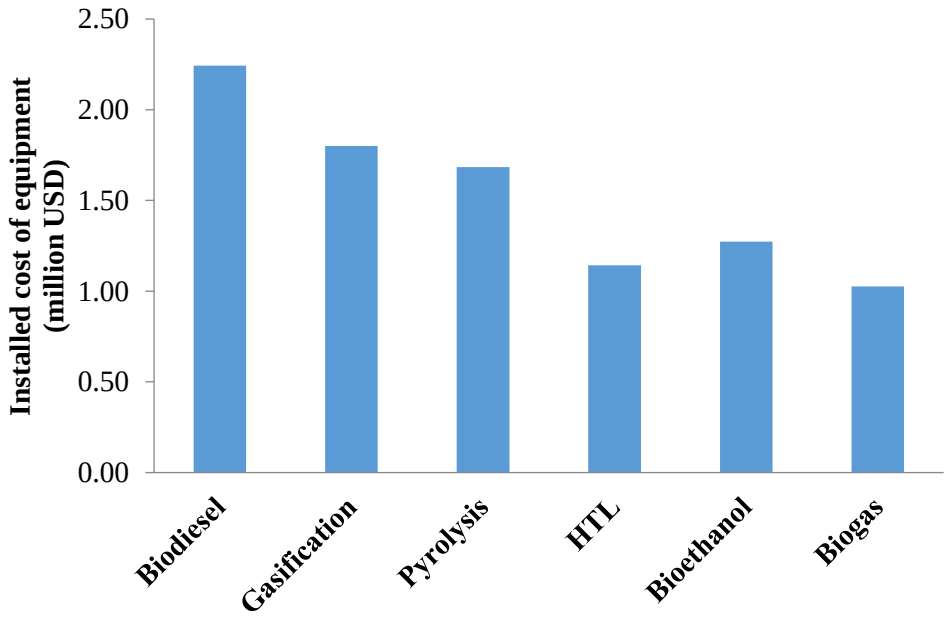

Figure 4. 1: Installed cost of all equipment used in biomass-to-fuel conversion

4.3.2.2. Capital expenditure

Figure 4.2 depicts the capital expenditure required to purchase and install equipment, build and erect the biorefineries. It follows exactly the same trend as installed cost of equipment, with biodiesel production having the highest CAPEX, followed by gasification, pyrolysis, bioethanol

production and lastly biogas production. This is because, as shown in Table 3.10, CAPEX was calculated as the function of installed cost of equipment also known as the ISBL plant cost.

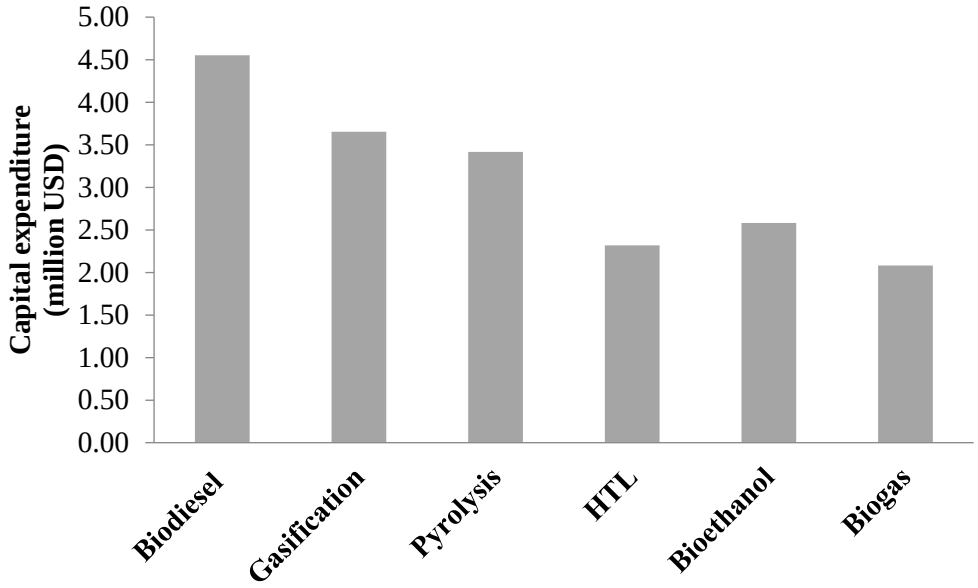

Figure 4. 2: Capital expenditure needed for each of the biomass-to-fuel conversion routes

4.3.2.3. Operating expenses

Figure 4.3 shows the fixed operating expenses required to run the biorefineries per annum. Again the FOC show the same variation as installed cost of equipment or the ISBL plant cost, with biodiesel production requiring the highest FOC, followed by gasification, pyrolysis, bioethanol production and lastly biogas production. This is because FOC was calculated as a function of the number of operators per shift and ISBL plant cost as shown in Table 3.11. According to equation 3.30, the number of operators per shift depends on the number of particulate and non-particulate processing units in the process. It was assumed that all processing routes except biodiesel production did not have particulate processing units. It was assumed otherwise for biodiesel production to cater for the pelletizing section and the many processing units involved in the process. As a result, all other processing routes needed the same number of workers (three operators per shift) whereas biodiesel production needed six operators per shift. Since the day is made up of three 8-hour shifts, the total number of operators needed for biodiesel production was eighteen whereas nine operators were needed for all other processing routes. It was assumed that

each operator was to receive a consolidated salary of 529.41 USD per month for a period of 12 months, which is the average minimum wage of an operator in South Africa (payscale 2023). For this reason, the cost of operating expenses for biodiesel production is much higher than that for other processing routes since it needs more operators than any other processing route. Additionally, the ISBL plant cost for biodiesel production is higher than that of other processing routes.

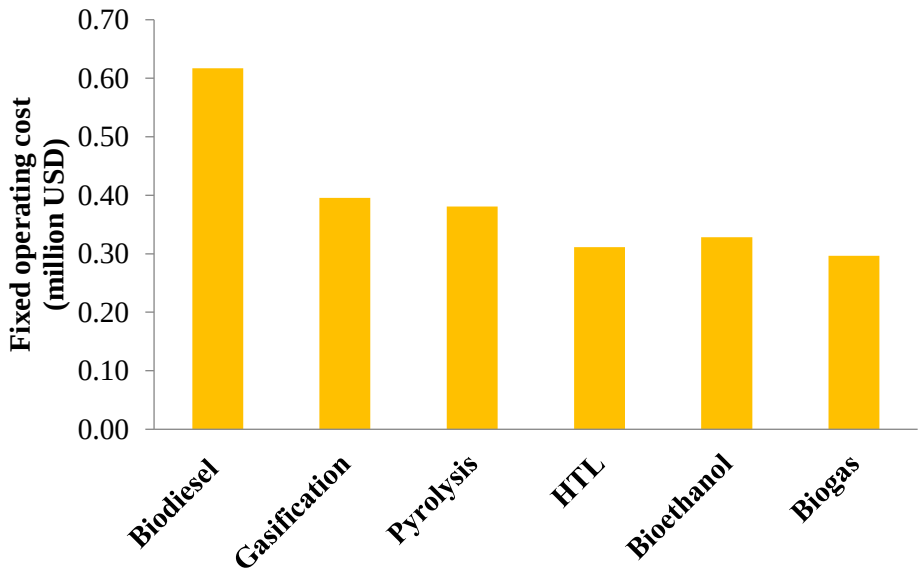

Figure 4. 3: Fixed operating expenses

4.3.2.4. Cost of electricity

The cost of electricity for each of the six processing routes is shown by Figure 4.4. HTL had the highest cost of electricity (1,467,356 USD) followed by bioethanol production (1,196,735 USD), gasification (945,216 USD), biodiesel production (642,298 USD), pyrolysis (239,806 USD) and biogas (78,777 USD) had the least power consumption.

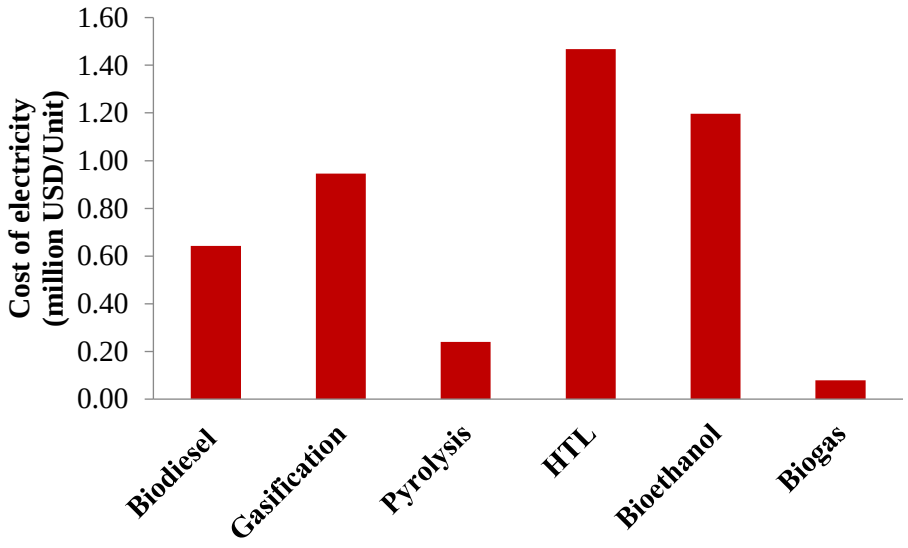

Figure 4. 4: Cost of electricity

The cost of electricity is highest for HTL because of a big flow rate of slurry that had to be heated from 25 ^{0}C to 300 ^{0}C which was used as the optimal temperature for the reaction. Of all the processing routes, HTL had the highest flow rate of the feed since a slurry of about 20% solids is required for optimal bio-crude yield. Pyrolysis unexpectedly had the second lowest cost of electricity and much lower compared to HTL yet many researchers state that the advantage of HTL over pyrolysis is the ability to handle wet biomass, eliminating the need for the biomass pre-drying step which consumes a lot of heat energy. This means that for HTL to be cost effective in terms of energy consumption, feedstock conditions like slurry content and optimal reaction temperature must be investigated. Higher solid content of slurry and lower reaction temperature can help to reduce the energy consumption of the process.

Bioethanol production consumed the second largest amount of electricity because of biomass pretreatment and bioethanol distillation units. The pretreatment reaction used steam explosion at 180 ^{0}C and yet the slurry of about 25% solids was used for optimal hemicellulose hydrolysis. A great deal of heat was required to raise the temperature of the large flow rate of the slurry to 180 ^{0}C, hence consuming a lot of electricity. Secondly, a lot of heat was consumed in the reboiler during bioethanol distillation to the large flow rate of ethanol-water mixture that was fed to the distillation column.

Gasification consumed more electricity than pyrolysis although both processing routes require biomass pre-drying. This is because of very high gasification temperature (750 ^{0}C) compared to 500 ^{0}C used during biomass fast pyrolysis. The cost of electricity for biodiesel production is higher than that for pyrolysis because a great deal of heat was consumed during hexane recovery, fat hydrolysis and methanol recovery in the distillation column. Of all processing routes, biogas production had the least cost of electricity because anaerobic digestion took place at mesophilic conditions. A small amount of heat was required to raise the temperature of the slurry from 25 ^{0}C to 37 ^{0}C needed for biological reactions. Another process unit that needed heating was during the separation of water from biogas. The vapor liquid mixture was heated to a temperature of 53 ^{0}C before being sent to the flash column where 98% of biogas was recovered from the mixture.

Therefore, it can be stated that electricity consumption depends upon the flow rate of substances, temperature difference caused by heating and downstream processes like distillation. This is the reason why HTL and bioethanol production which did not require biomass pre-drying had the higher electricity consumption.

4.3.2.5. Cost of water

Figure 4.5 shows the cost of water for each of the biomass-to-biofuels conversion routes. Bioethanol production had the highest water consumption cost (326,738 USD), followed by gasification (98,150 UD), HTL (70,952 USD), biodiesel production (65,216 USD), pyrolysis (47,577 USD) and lastly biogas production (2,210 USD).

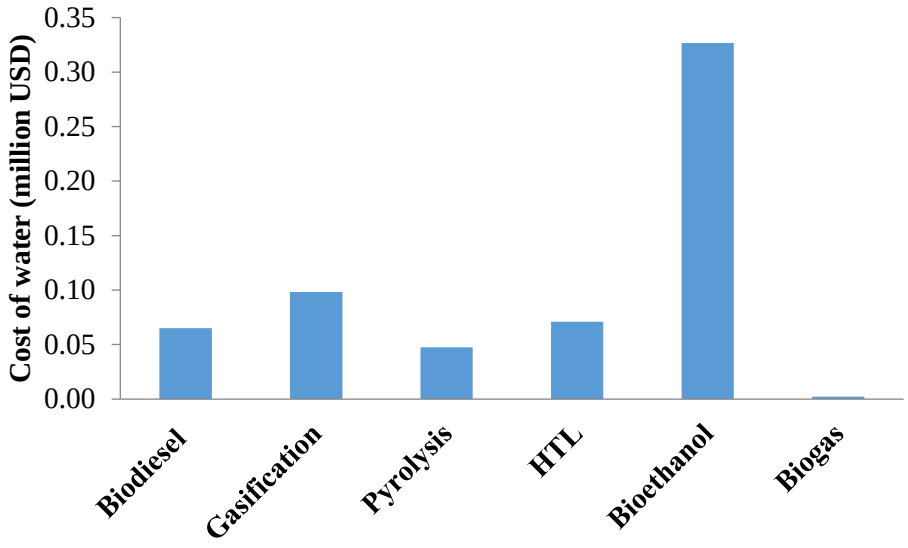

Figure 4. 5: Cost of water

The cost of water is the summation of process water and cooling water costs. Processing water is the amount of water that was added to the process. 100 kg/h of water was added to wet biomass during biogas production, HTL and bioethanol production to create slurry with the required solid content. 445 kg/h of water was used in gasification as the gasifying agent whereas 70 kg/h of water was used in biodiesel production during fat hydrolysis. It was assumed that all the necessary cooling for all the conversion routes was achieved by shell and tube heat exchangers operating on cooling water. The flow rate of cooling water was calculated by equation 3.29. It was assumed that cooling water had to be recycled 11 times a year implying that water needed in one month was enough to do the cooling for the whole year. Larger water reservoirs are present on site to store this water before being reused. There was no money assigned for construction of cooling water reservoirs because all costs associated with plant modifications or addition of some facilities were included in the OSBL plant cost as shown in Table 4.14.

Bioethanol production had the highest water consumption because a lot of cooling water was used in the condenser during ethanol distillation and for cooling of the pretreated slurry from 180 ^{0}C to 32 ^{0}C before being sent to the SSF unit. Gasification is the second highest water consuming processing route because a large amount of water was used to condense the vapor coming from the cyclone from 750 ^{0}C to 25 ^{0}C in order to remove water from syngas. HTL had higher water costs than pyrolysis even though pyrolysis vapor was cooled from 500 ^{0}C to 25 ^{0}C whereas the

vapor-liquid mixture during HTL was cooled from 300 ^{0}C to 25 ^{0}C in order to separate NCG (syngas) from bio-oil and bio-crude, respectively. This is because, although the temperature difference for pyrolysis is higher than that for HTL, a large flow rate of vapor-liquid mixture required a lot of cooling water compared to a smaller flow rate of pyrolysis vapor. During biodiesel production, cooling water was used during hexane recovery, cooling of the fat from the fat splitter and methanol recovery in the distillation column. Biogas production did not require any cooling because anaerobic digestion took place at mesophilic conditions.

4.3.2.6. Cost of raw materials

All processing routes used the same quantity of raw materials (2000 kg/h of wet SCG). It was assumed that wet SCG were collected around Durban metropolitan with a hypothetical distance of 50 km from source to plant gates. Wet SCG were acquired for free of charge from coffee brewing companies, cafeterias and cafes, and the cost of transportation is the only cost associated with feedstock acquisition. On consultation with small size private cargo companies around Durban, an average of 23.5 USD was required to transport 1 ton of raw materials a distance of 50 km. Using equation 3.28, the cost of raw materials was estimated to be 372,706 USD per year, as reported in Table 4.14.

4.3.2.7.Cost of utilities

Figure 4.6 depicts the cost of utilities for all the six biorefineries, also outlined in Table 4.14. The cost of utilities was estimated as the sum of electricity costs, cooling water and process water costs. Bioethanol production and HTL had the highest total cost of utilities, 1,523,473 USD and 1,538,308 USD, respectively. Bioethanol production had the highest water costs whereas HTL had the highest electricity costs. The cost of utilities for gasification, biodiesel production, and pyrolysis and biogas production were 1,043,367 USD, 707,513 USD, 287,383 USD and 80,988 USD, respectively.

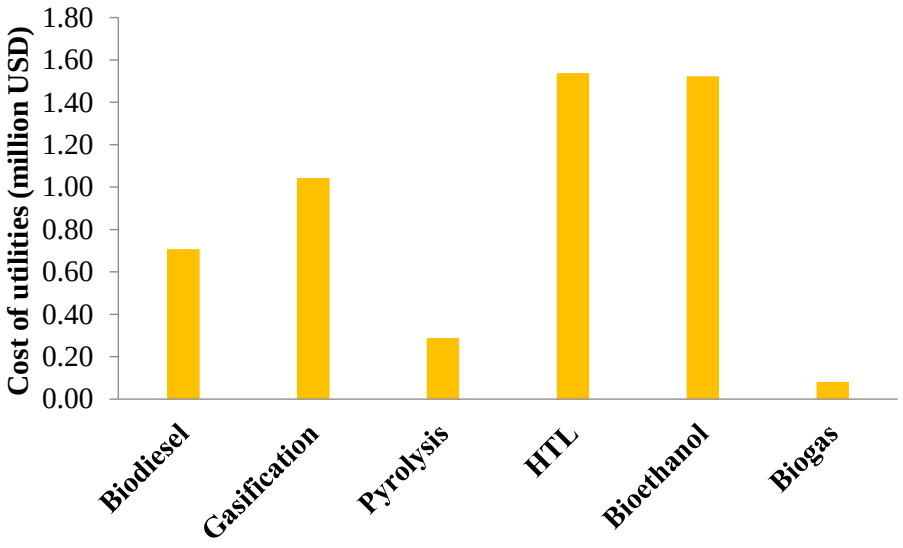

Figure 4. 6: Cost of utilities

4.3.3. Economic indicators

Table 4.15 shows all the economic feasibility indices that were used in this study as the basis for choosing the best processing route economic wise. The decision relied on four economic indicators, namely NPV, IRR, DPBP and PI. The best processing route is one with the biggest NPV, highest IRR, shortest DPBP and biggest PI. Figure 4.7 and Figure 4.8 show plots of NPV against interest rate and plant life, respectively. From 4.7, the IRR of a project can be determined whereas DPBP can be obtained from Figure 4.8.

Of all the six processing routes compared, only bioethanol production was not economically feasible. This is because the operating expenditure for bioethanol production is bigger than the revenue generated from sales of finished products. This implies that no profit is generated from its operations. For such a project, there is no chance of recovering the capital invested regardless of length of its life. At the end of 25 years, bioethanol production generated a net loss of 3,148,744 USD (negative NPV). No other economic index can be calculated for such a project, however, the remaining projects were compared and ranked in descending order with the most economically feasible project in position one.

Table 4. 15: Economic indictors

Indicator	Biodiesel	Gasification	Pyrolysis	HTL	Bioethanol	Biogas
Total revenue (USD)	3,865,856	3,399,264	2,747,686	2,747,686	2,125,332	2,766,614
Gross profit (USD)	1,480,380	1,587,708	1,706,987	525,294	-98,856	967,090
NPV (USD)	3,908,992	5,420,729	6,338,335	682,375	-3,148,744	3,444,508
IRR (%)	24	32	37	16		34
DPBP (years)	8.0	6.0	5.4	13.0		5.7
MFSP (USD/kg)	0.26	0.29	0.12	0.41		0.92
PI	0.86	1.48	1.85	0.29		1.65

4.3.3.1. Sales revenue

Sales revenue is the sum of all cash inflows realized from sales of finished products produced. To maximize profit, all products, both main and co-products were hypothesized to have been sold. The prices of all the finished products are summarised in Table 4.16. All of the prices were estimated from different websites whose references are also presented in Table 4.16. For biodiesel production, biodiesel was the main product but also wet glycerol and coffee pellets were sold. For pyrolysis and HTL, the main products were bio-oil and bio-crude, respectively, whereas bio-char and syngas were co-products for both processing routes. The price of bio-crude was assumed to be the same as that of crude petroleum whereas the price of bio-char was assumed to be the same as that of fossil coal. The price of syngas was estimated by combining the fractional prices of green hydrogen and carbon monoxide since they are the main components of syngas. The digestate and solid residues left during anaerobic digestion and fermentation, respectively, were sold as compost manure. The total revenues obtained from each of the processing route were reported in Table 4.15.

Table 4. 16: Selling prices of finished products

Finished products	Actual selling price (USD/kg)	Reference
Bioethanol	0.93	GlobalPetrolPrices.com (2023b)
Biodiesel	0.82	Greenthermoenergy (2023)
Biogas	1.20	Nelissen *et al.* (2020)
Bio-oil	0.45	SAshares (2023)
Bio-crude	0.45	SAshares (2023)
Bio-char	0.16	Theglobaleconomy.com (2023)
Syngas	0.40	S&Pglobal (2021) and Chemicalbook (2023)
Coffee pellets	0.41	Thefirewoodcompany (2023)
Digestate	0.06	Essentialcompost (2023)
Glycerol	0.50	Selinawamucii (2023)

4.3.3.2. Net present value

NPV indicates the net cash flows accumulated at the end of project life. Positive NPV means that the sales of finished product are high enough to cover operating expenses, pay tax to the government, interest on capital invested, recovers the initial investment and leaves a net income (profit) to the investor. Negative NPV does not necessarily mean that the sales of finished product are less than the operating expenses like in bioethanol production; it may be as a result of small profit which cannot surpass the deductions of tax, interest rate and initial capital investment. NPV alone cannot be relied on to make an informed decision on alternatives with different capital expenditure (CAPEX). This is because NPV is dependent on capital invested. An example is gasification and biodiesel production with NPV of 5,420,729 USD and 3,908,992 USD, respectively. The NPV of these projects is higher than that of biogas production (3,444,508 USD) yet biogas production is better than them economic wise. This is because NPV of bigger projects is always higher than that of smaller projects. As shown in Table 4.14, the CAPEX of biodiesel production (4,552,088 USD) and gasification (3,653,784 USD) are higher than that of biogas production (2,082,874 USD).

4.3.3.3. Internal rate of return

A more meaningful economic index is the internal rate of return (IRR). It does not depend on the amount of capital invested or the plant life of the project, thus, can be used to compare projects of different sizes (Sinnott and Towler 2009). IRR is the measure of how much interest on capital

invested a project can be able to pay and still recovers the capital invested at the end of its life. As in a common saying that a dollar today is better than a dollar in future, lenders are only persuaded by the interest paid to them. This means that the most economically feasible project is the one with the highest IRR. Figure 4.7 depicts the plot of NPV against interest rate for all the projects except bioethanol production which gave a negative NPV at minimum interest rate of 12%. The results of Figure 4.7 are also included in Table 4.15. Pyrolysis had the highest IRR (37%) and HTL had the lowest (16%). This means that even if the interest rate is raised from 12 to 37% and 12 to 16% for pyrolysis and HTL, respectively, the projects can be able to pay tax, interest on capital borrowed and still recover the capital invested at the end of project life. However, no investor would desire to invest capital borrowed at high interest because it reduces the net profit generated.

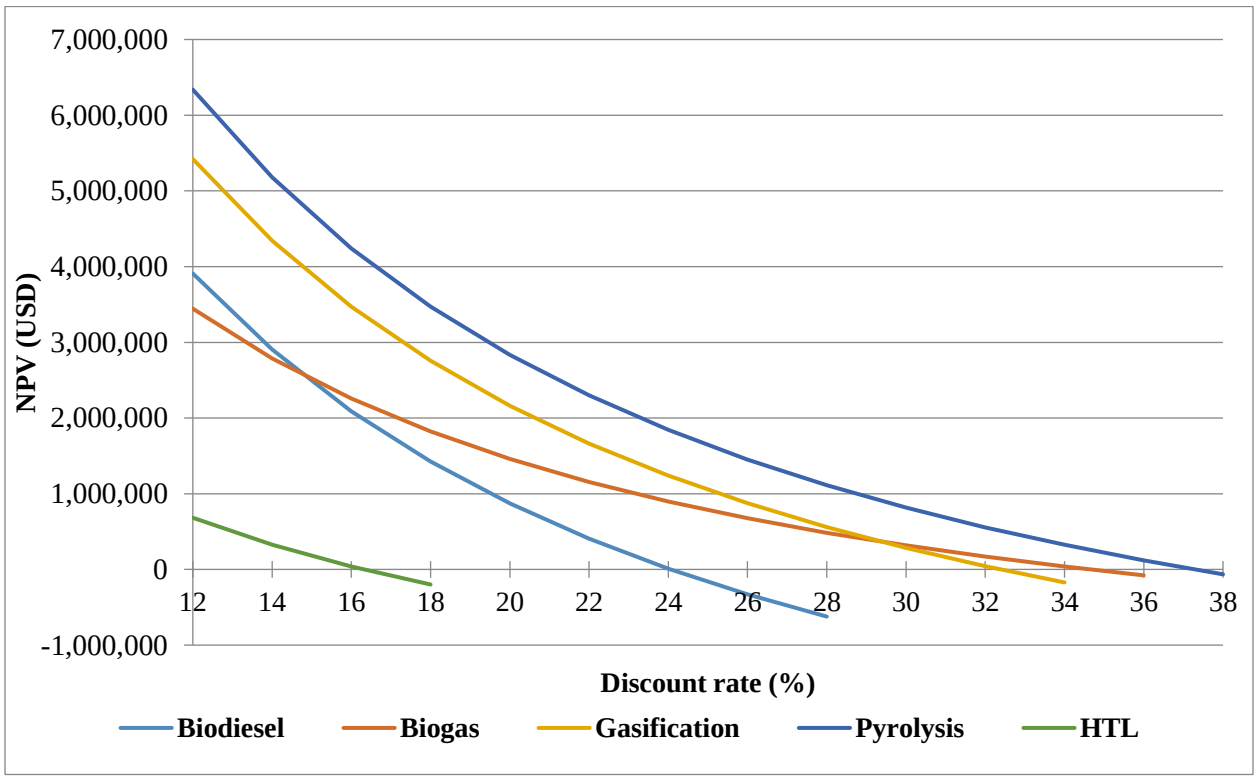

Figure 4. 7: Graph of NPV against discount rate

4.3.3.4.Discounted payback time

Another useful economic indicator is the discounted payback period (DPBP). It is the amount of time in years it takes the net cash flows to be equal to the initial capital invested. This means that the shorter the DPBP, the more economically feasible the project is. This is because any investor would desire to recover their money invested in as short a time as possible. Projects with longer DPBP are susceptible to unforeseen circumstances which may affect their profitability. For example, during the COVID-19 pandemic, almost all countries instituted total lockdown on their economics which led to companies making a lot of losses. So investing one's money in any project means taking a risk and the sooner that money is recovered, the better is the investment. DPBP was obtained from the plot of NPV against plant life as shown in Figure 4.8. The point at which the NPV curve meets the time axis is the DPBP. Fast pyrolysis had the shortest payback time (5.40 years), followed by biogas production (5.70 years), gasification (6.0 years), biodiesel production (8.0 years) and HTL (13.0 years). This means that fast pyrolysis and biogas production with the shortest PBP were the most economically profitable processing routes. It was not possible to estimate PBP for bioethanol production as the revenues were smaller than operating expenses, implying that the project was not profitable at all.

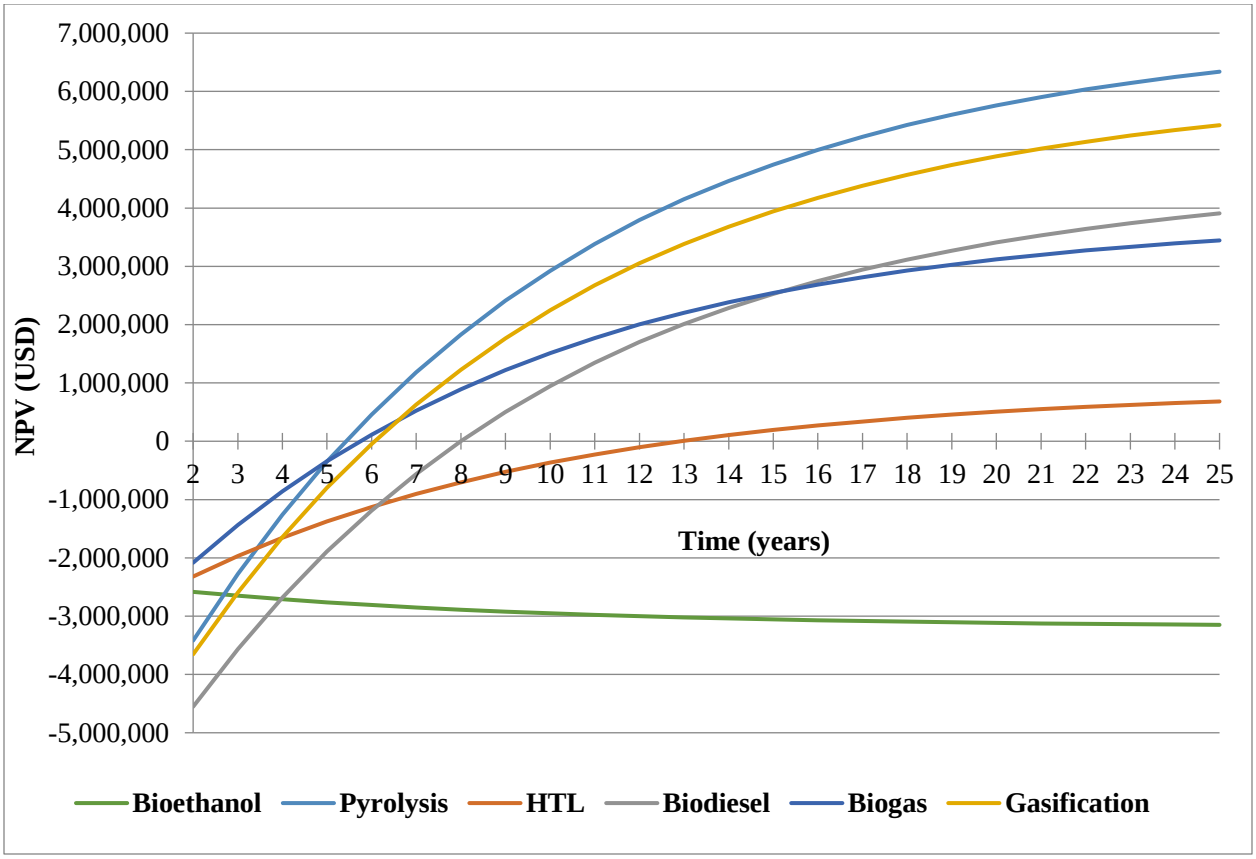

Figure 4. 8: Graph of NPV against time

4.3.3.5. Profitability index

Profitability index (PI) is yet another useful economic indicator which is simply the ratio of NPV to CAPEX. It is an indicator of how much NPV exceeds the capital expenditure. A more profitable project is one with the highest profitability index. As shown in Table 4.15, pyrolysis had the highest PI (1.85) followed by biogas production (1.65), gasification (1.48), biodiesel production (0.86) and lastly HTL (0.29). This means that pyrolysis is the most economically feasible processing route because its NPV is 1.85 times bigger than the capital invested.

4.4. Life cycle assessment

A comparative LCA was conducted for all six processing routes with the aim of selecting one with least environmental impacts. The following section presents the results from the LCA study.

4.4.1. Impact assessment results

Eight impact categories were used to evaluate the environmental impacts of biofuels production from SCG. Table 4.17 shows the LCA impact indicators in their respective units. The interpretation of LCA results is presented in section 4.4.2.

Table 4. 17: Impact assessment results for the six compared processing routes

LCA impact indicator	Unit	Pyrolysis	HTL	Biogas	Bioethanol	Biodiesel	Gasification
Fine particulate matter formation	kg $PM_{2.5}$ eq	1.10	6.62	0.38	5.40	2.91	4.28
Fossil resource scarcity	kg oil eq	111.86	637.01	42.98	521.24	284.05	413.64
Freshwater eutrophication	kg P eq	0.31	1.91	0.10	1.56	0.84	1.23
Global warming	kg CO_2 eq	462.33	2694.20	9558.10	2202.20	1194.10	1744.90
Marine eutrophication	kg N eq	0.02	0.12	7.42	0.10	0.05	0.08
Mineral resource scarcity	kg Cu eq	0.13	0.56	0.08	0.46	0.27	0.38
Terrestrial acidification	kg SO_2 eq	3.18	19.21	1.08	15.67	8.44	12.45
Water consumption	m^3	1.13	5.13	0.71	4.27	2.41	3.82

4.4.2. Interpretation of results

As presented in Table 4.17, each impact indicator was reported in their respective units. It was assumed that all the impact indicators had the same weight and the best processing route was the one with the least total of percentages of all the impact categories added. The percentages of impact categories were plotted as shown in Figure 4.17, with 100% assigned to the most impactful processing route.

4.4.2.1. Water consumption

Figure 4.9 shows the impact of each processing route on water consumption. HTL had the highest impact (5.13 m^3) followed by bioethanol production (4.27 m^3), gasification (3.82 m^3), biodiesel production (2.41 m^3), pyrolysis (1.13 m^3) and lastly biogas production with a water consumption of 0.71 m^3. This is explained by the amount of electricity consumed by each processing route which is also in the same order as shown in Figure 4.4 in section 4.3. It was assumed that all the heating was provided by electric heaters powered by electricity from the national grid. In South Africa, the major source of electricity is generated from coal. The process of electricity generation from coal includes different stages that involve coal mining, coal transportation and coal combustion. Coal combustion produces heat energy which is used to vaporize water in order to generate steam that drives turbines and generate electricity. Since water is used in electricity generation, a process with high electricity consumption is expected to have a higher impact on water consumption. This is the reason why HTL with the highest electricity consumption had the highest impact on water consumption, whereas biogas production with the lowest electricity consumption had the least impact on water consumption.

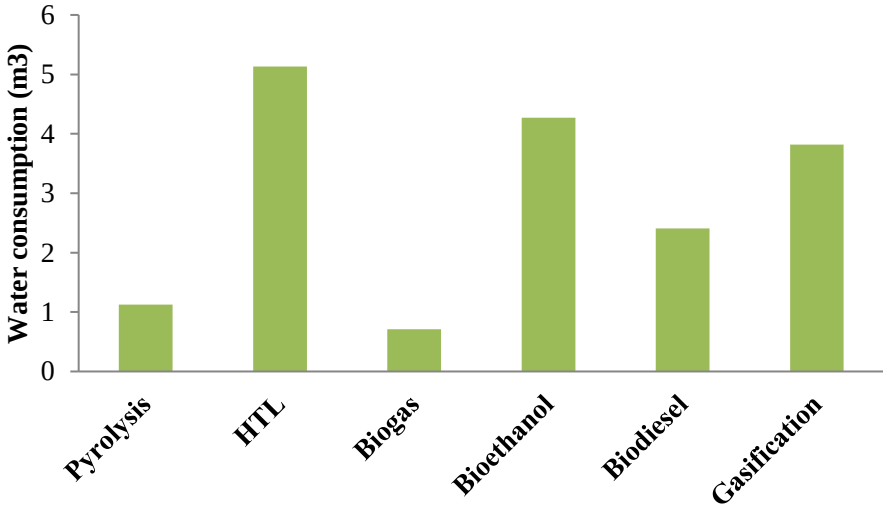

Figure 4. 9: Impacts of processing routes on water consumption

4.4.2.2. Terrestrial acidification

Terrestrial acidification explains the acid content of the soil due to the deposition of acidic gases mainly nitrogen and sulfur oxides (NO_x and SO_2). Soil acid levels have a direct impact on plant growth as soil pH is one of the import soil qualities. Figure 4.10 shows the impacts of the processing routes on terrestrial acidification. HTL had the highest impact (19.21 kg SO_2 eq) followed by bioethanol production (15.67 kg SO_2 eq), gasification (12.45 kg SO_2 eq), biodiesel production (8.44 kg SO_2 eq), fast pyrolysis (3.18 kg SO_2 eq) and lastly biogas production (1.08 kg SO_2 eq). This trend is exactly the same as that for electricity consumption as shown in Figure 4.4 in section 4.3. Appreciable quantities of sulfur and carbon naturally exist with coal and so the process of coal combustion results in production of sulfur and nitrogen oxides. Thus, a processing route with high electricity consumption produces a higher impact on terrestrial acidification, whereas a processing route with the lowest electricity consumption poses the least impact on terrestrial acidification. This is the reason why HTL had the highest impact on terrestrial acidification and biogas production has the smallest.

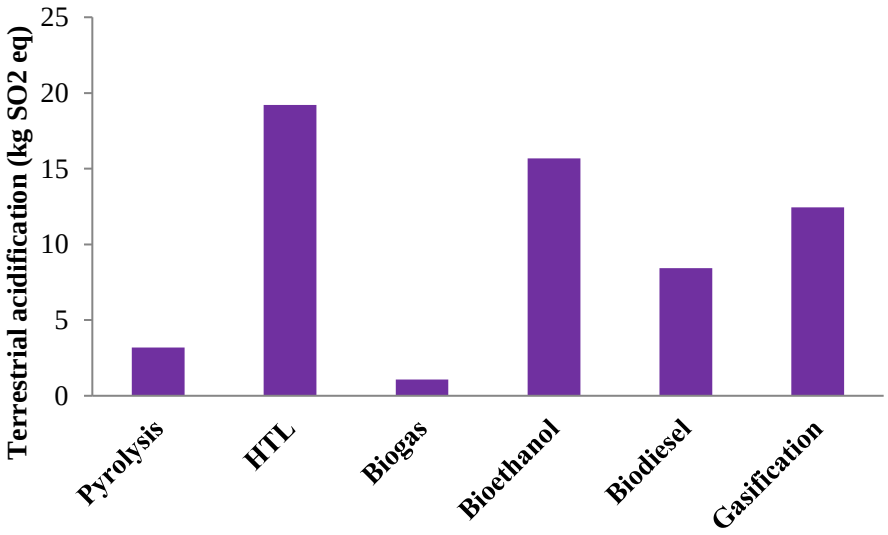

Figure 4. 10: Impacts of processing routes on terrestrial acidification

4.4.2.3. Mineral resource scarcity

Figure 4.11 shows the impacts of the processing routes on mineral resource scarcity. HTL had the highest impact (0.56 kg Cu eq) followed by bioethanol production (0.46 kg Cu eq), gasification (0.38 kg Cu eq), biodiesel production (0.27 kg Cu eq), fast pyrolysis (0.13 kg Cu eq) and lastly AD with 0.08 kg of Cu equivalent. This trend is exactly the same as that for electricity consumption as shown in Figure 4.4 in section 4.3. Since electricity generation was from coal combustion, a processing route with the highest electricity consumption had to have the biggest impact on mineral resource scarcity and vice versa. The process of coal mining and coal transportation involves the consumption of minerals including coal itself and fossil fuels used in vehicles to transport coal from coal mines to plant gates.

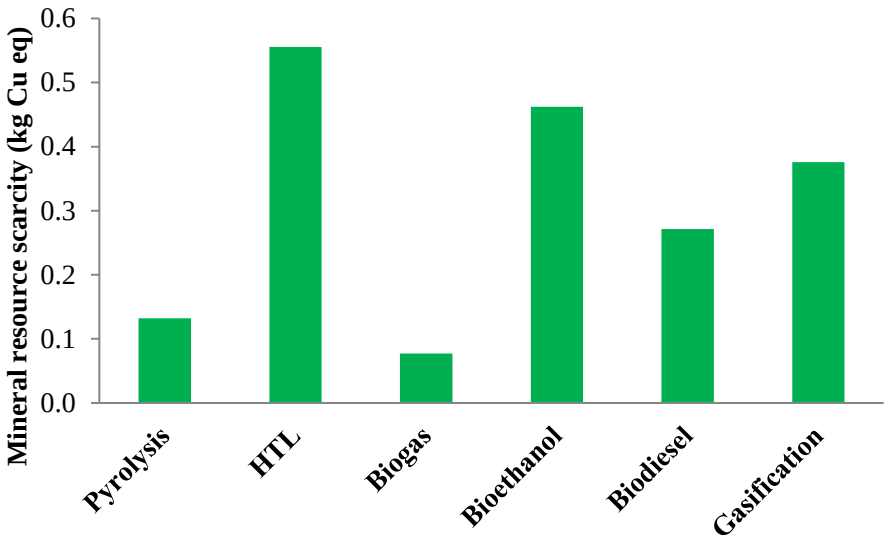

Figure 4. 11: Impacts of processing routes on mineral resource scarcity

4.4.2.4. Freshwater eutrophication

Freshwater eutrophication is a phenomenon where freshwater bodies (lakes and rivers) are excessively rich in nutrients, mainly nitrogen and phosphorous leading to plant and algal growth. The biomass decomposes and produces a lot of carbon dioxide which lowers the pH of water. The lowered water pH slows the growth of fish and other organisms. As shown in Figure 4.12, HTL had the highest impact on freshwater eutrophication (1.91 kg P eq) followed by bioethanol production (1.56 kg P eq), gasification (1.23 kg P eq), biodiesel production (0.84 kg P eq), fast

pyrolysis (0.31 kg P eq) and finally biogas production (0.10 kg P eq). This trend is explained by the trend in electricity consumption of these processing routes which is decreasing in the same order as the impact on freshwater eutrophication. This is because nitrogen and phosphorous are naturally existing with coal and a process with high electricity consumption means large quantities of coal have been combusted. The process coal combustion releases nitrogen and phosphorous into the environment which find their way in water bodies causing eutrophication.

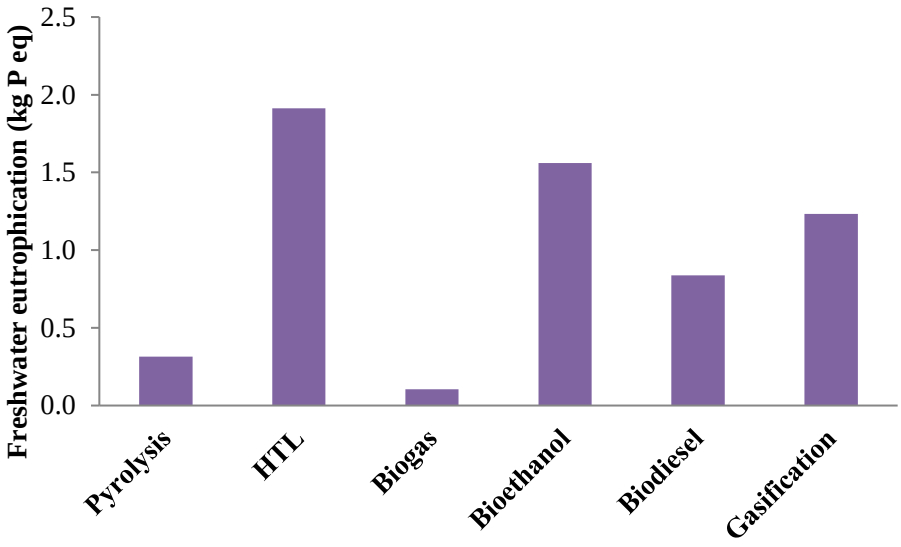

Figure 4. 12: Impacts of processing routes on freshwater eutrophication

4.4.2.5. Marine eutrophication

Marine eutrophication refers to a phenomenon when ocean or sea water is excessively rich in nutrients enhancing the rapid growth of plants and algal biomass. Figure 4.13 shows the impacts of all the processing routes on marine eutrophication. Biogas production had abnormally the highest impact on marine eutrophication (7.42 kg N eq) compared to all other processing routes. HTL had the second highest impact on marine eutrophication (0.12 kg N eq) followed by bioethanol production (0.08 kg N eq), biodiesel production (0.05 kg N eq), and lastly pyrolysis with 0.02 kg N eq. This trend is explained by both methane production and electricity consumption of each process with methane production being the highest contributor. Of all the processing routes, anaerobic digestion produced the largest quantities of methane (274.87 kg/h) as shown in

Table 4.6. Other processing routes like gasification, pyrolysis and HTL produced insignificant quantities of methane in relation to that produced from AD, making biogas production having abnormally the highest impact on marine eutrophication. For the rest of the processing routes, the trend in marine eutrophication is because of the similar trend in electricity consumption. Electricity generation from coal involves coal combustion which emits nitrogen oxides in the atmosphere. These nitrogen compounds find their way into the oceans causing marine eutrophication.

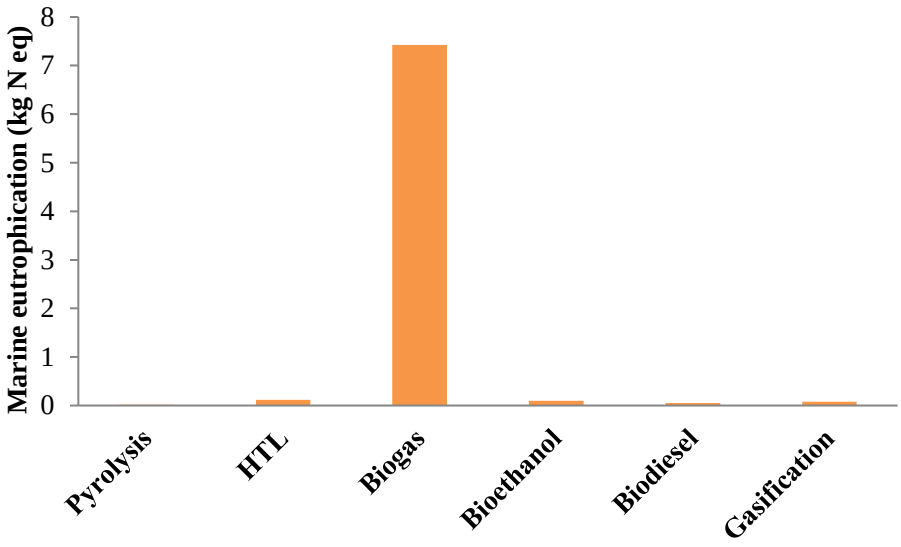

Figure 4. 13: Impacts of processing routes on marine eutrophication

4.4.2.6. Global warming

Global warming is the long-term raise in earth's temperatures due to accumulation of greenhouse gases (GHGs) around the earth. These gases, which are mainly carbon dioxide and methane, form a blanket around the earth's atmosphere and absorb heat from the sun resulting in high temperatures. Global warming or climate change is as a result of both natural calamities like volcanic eruptions and human activities but by far human activities are the main cause of global warming. Burning of fossil fuels like coal and petroleum derived fuels is the main perpetrator of global warming due to excessive emissions of GHGs. As shown in Figure 4.14, biogas production had the highest impact on global warming (9558.10 kg CO_2 eq) followed by HTL (2694.20 kg CO_2 eq), bioethanol production (2202.20 kg CO_2 eq), gasification (1744.90 kg CO_2 eq), biodiesel

production (1194.10 kg CO_2 eq) and lastly fast pyrolysis with a global warming potential of 462.33 kg CO_2 eq. Biogas production had the highest global warming potential because, of all the processing routes, it is the highest producer of methane and carbon dioxide which are responsible for global warming. As shown in Table 4.6, AD produced 274.87 kg/h and 319.00 kg/h of methane and carbon dioxide, respectively. The trend in global warming potential for HTL, bioethanol production, gasification, biodiesel production to fast pyrolysis is explained by the trend in electricity consumption which also decreased in the same order as shown in Figure 4.4 in section 4.3. Since electricity consumed during bioconversion was generated from coal combustion, HTL with the highest electricity consumption had the second highest global warming potential, whereas pyrolysis with the least electricity had the lowest impact on global warming. The processing of electricity generation including coal mining, coal transportation and coal combustion emit a lot of GHGs.

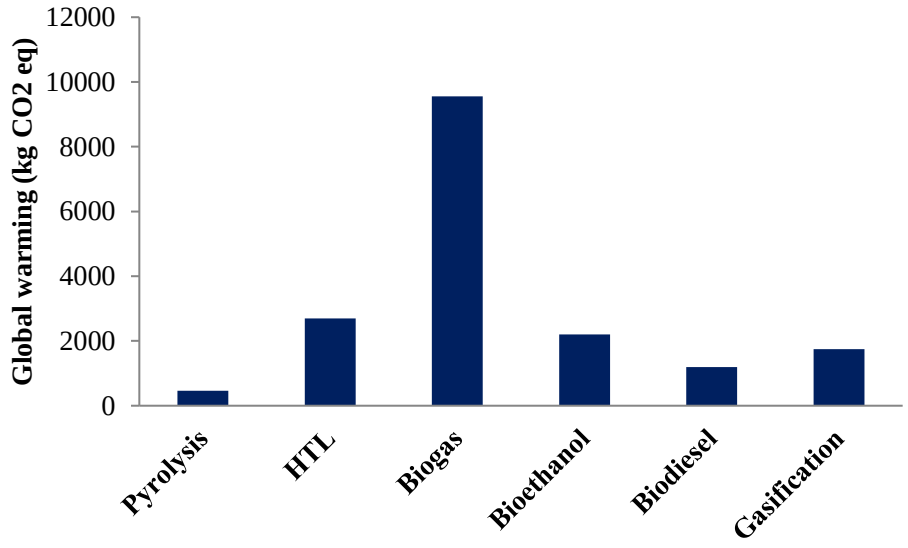

Figure 4. 14: Impacts of processing routes on global warming

4.4.2.7. Fossil resource scarcity

Figure 4.15 shows the impacts of the processing routes on fossil resource depletion. HTL had the highest impact (637.01 kg oil eq) followed by bioethanol production (521.24 kg oil eq), gasification (413.64 kg oil eq), biodiesel production (284.05 kg oil eq), fast pyrolysis (111.86 kg

oil eq) and lastly AD with 42.98 kg of oil equivalent. This trend is exactly the same as that for electricity consumption as shown in Figure 4.4 in section 4.3. Since electricity generation was from coal combustion, a processing route with the highest electricity consumption had the biggest impact on fossil resource scarcity whereas a processing route with the lowest energy consumption had the least impact on fossil fuel depletion. During electricity generation, coal mining and coal transportation consume fossil fuels used in excavators and vehicles that transport coal from coal mines to plant gates.

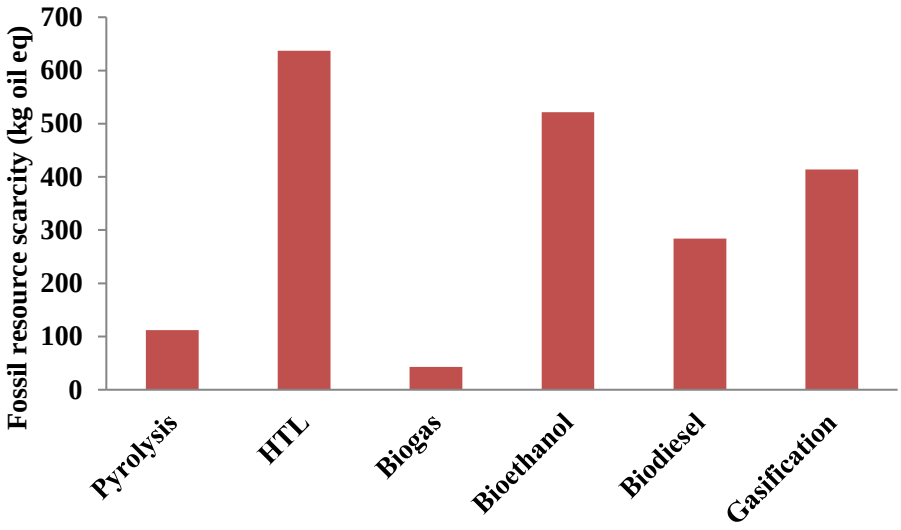

Figure 4. 15: Impacts of processing routes on fossil resource scarcity

4.4.2.8. Fine particulate matter

Fine particulates ($P_{2.5}$) are minute particles in the air that have diameters less than or equal to 2.5 microns. $P_{2.5}$ is a result of both outdoor and indoor activities. Outdoor activities include natural calamities like world fires and volcanic eruptions, and human activities like combustion of wood fuels, coal and petroleum derived fuels in combustion engines. On the other hand indoor activities include smoking of tobacco, cooking, burning of candles, fuel lamps, fuel burning heaters and many others. Short and long-term exposure to fine particulates has severe effects on human health. Short-term exposure can cause health complications like irritations of eyes, nose or throat, coughing, sneezing, running nose or breathing difficulties, whereas chronic exposure can result in

adverse health problems like asthma or death if $P_{2.5}$ finds their way to lungs through the respiratory tract. As shown in Figure 4.16, HTL had the highest impact on particulate matter formation (6.62 kg $PM_{2.5}$ eq) followed by bioethanol production (5.40 kg $PM_{2.5}$ eq), gasification (4.28 kg $PM_{2.5}$ eq), biodiesel production (2.91 kg $PM_{2.5}$ eq), fast pyrolysis (1.10 kg $PM_{2.5}$ eq) and finally biogas production (0.38 kg $PM_{2.5}$ eq). This trend is explained by the trend in electricity consumption of these processing routes which is decreasing in the same order as the impact on particulate matter formation. This is because electricity generation from coal involves coal mining, coal transportation and coal combustion which produce a lot of particulates. Thus HTL with the highest electricity consumption had the biggest impact on particulate matter formation, whereas biogas production with the lowest electricity consumption had the least impact on fine particulate matter formation.

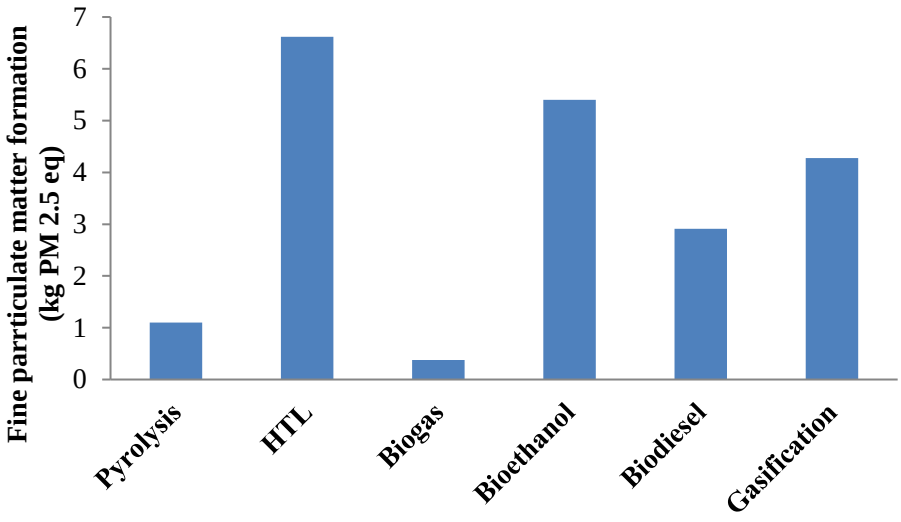

Figure 4. 16: Impacts of processing routes on fine particulate matter formation

4.4.2.9. Ranking of processing routes

This section presents the rankings of processing routes according to the overall environmental impacts. Figure 4.17 shows the comparison of impact categories for all the processing technologies, with 100% assigned to the most impactful technology and the rest are expressed relative to it. For purposes of fair comparison, it was assumed that all the impact categories had the same strength. The total score for each processing route was the sum of impact percentages.

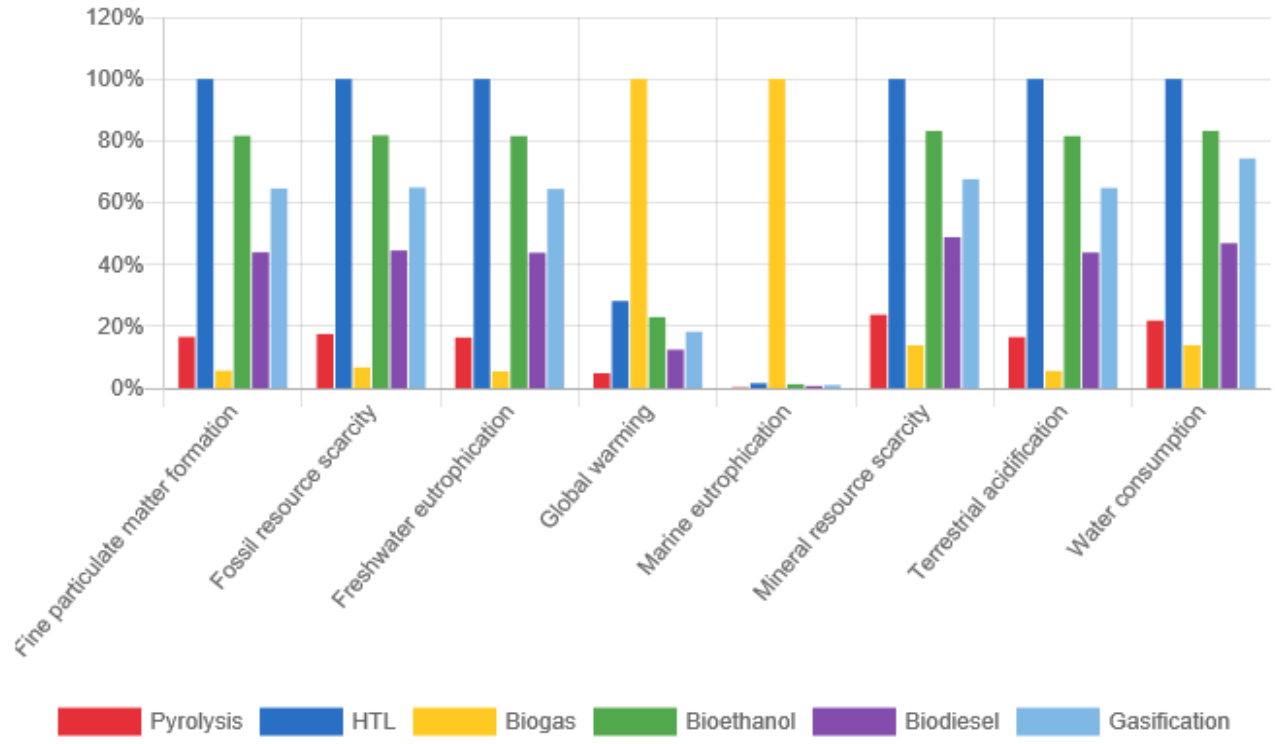

Figure 4. 17: Comparison of impact categories for all six processing routes

For each impact category, 100% corresponds to the most impactful processing route.

Table 4. 18: Impact categories percentage score of processing routes

LCA impact indicator (%)	Pyrolysis	HTL	Biogas	Bioethanol	Biodiesel	Gasification
Fine particulate matter formation	18	100	06	82	43	64
Fossil resource scarcity	18	100	06	82	43	64
Freshwater eutrophication	17	100	05	82	43	64
Global warming	06	28	100	28	12	18
Marine eutrophication	01	02	100	02	02	02
Mineral resource scarcity	22	100	16	83	50	68
Terrestrial acidification	18	100	06	82	44	66
Water consumption	21	100	16	83	48	76
Total score	**121**	**630**	**255**	**524**	**285**	**422**

The data presented in Table 4.18 was extracted from Figure 4.17. A processing route with the smallest total score (percentage) is the most environmentally friendly processing route, whereas the one with the biggest total score is the worst environmentally friendly processing route. This

implies that fast pyrolysis with the smallest total score (121) is the most environmentally friendly processing route, followed by biogas production (255), biodiesel production (285), gasification (422), bioethanol production (524) and lastly HTL with a total score of 630. Since electricity production was the major contributor to environmental impacts, fast pyrolysis and biogas production with least electricity consumption were the most environmentally friendly processing routes. However, fast pyrolysis is better than biogas production even though biogas production was the least electricity consuming processing route. This is due to a large production of methane (biogas) and carbon dioxide during AD and yet the two gases were the biggest contributors of global warming. HTL was the worst environmentally processing route overall because it was the most electricity consuming technology.

4.5. Summary

The results of Aspen plus simulation (mass and energy balances), economic analysis and life cycle assessment have been presented and discussed in this chapter. Of all the six processing routes considered in the study, HTL was the highest electricity consuming process with a heating duty of 2538 kWh where biogas production was the least electricity consuming processing with a heating duty of 136 kWh. The discounted cash flow analysis was employed to assess the economic feasibility of producing biofuels from SCG. The economic indicators calculated were NPV, IRR, DPBP and PI. Fast pyrolysis was the best processing route economically with the biggest NPV of 6,338,335 USD, highest IRR of 37%, shortest DPBP of 5.4 years, and the biggest PI of 1.85. Conversely, bioethanol production from SCG was not economically feasible under the set of assumptions made in this study. The project was not able to recover the initial capital invested at the end of the plant life. The results of environmental impact assessment showed that the highest electricity consuming processing route was the worst project environmentally. Consequently, HTL, the highest electricity consuming project had the biggest negative impacts on the environment. However, biogas production with least electricity consumption requirements was not the best processing route environmentally and this is due to large production of carbon dioxide and methane during anaerobic digestion. These gases were the largest contributors of global warming. This left fast pyrolysis in position one among the best environmentally friendly processing routes.

5. CONCLUSION AND RECOMMENDATIONS

5.1. Conclusion

The study aimed at conducting TEA and LCA of biofuels conversion technologies from wet SCG. Six processing routes, namely fast pyrolysis, biogas production, biodiesel production, gasification, hydrothermal liquefaction and bioethanol production were simulated in Aspen plus V11 to obtain the mass and energy balances. Aspen process economic analyzer was used to estimate the installed cost of all major equipment for each processing route. All other plant costs were estimated as factors of installed cost of all major equipment. The discounted cash flow analysis was employed to assess the economic profitability of the simulated processing routes using economic indicators like NPV, PI, BPBP and IRR. Lastly, LCA was evaluated using the ISO 14040/44 methodology. OpenLCA V1.11.0 software was used as a tool for LCA study.

The following conclusions were drawn from this study:

- Aspen plus process simulator is a complete tool that can always be used to evaluate the economic analysis of projects before execution in order to void pursuing dead ends. A real biorefinery can be mimicked by the software without necessarily running a pilot plant. This helps to minimise the costs spent during research and development.

- SCG is a potential feedstock for biorefineries. Multiple value added products and biofuels can be obtained from a single feedstock. For example, during pyrolysis, bio-oil, syngas and biochar can be obtained from the same feedstock. During HTL, bio-crude, syngas and hydro-char were recovered from the single feedstock. This helps to maximise the profitability of the biorefineries.

- Electricity consumption was the biggest contributor of environmental impacts. This is because electricity was generated from coal. The process of coal mining, coal transportation and coal combustion involve a lot of emissions of gases, particulates, depletion of mineral and fossil fuel resources.

- Fast pyrolysis is the most economically feasible and environmentally friendly processing route. This is attributed to its moderate operating costs since it doesn't consume a lot of

electricity and requires almost no consumables like catalysts and drying agents as it is the case for biochemical conversion technologies. Low electricity consumption helps to reduce its contribution to environmental impacts.

- Bioethanol production was not an economically feasible processing route because of very high operating costs and low ethanol yields. The operating costs were raised by large electricity and water consumption levels making it difficult for revenues obtained from the sales of finished products being equal to or exceeding the operating expenses. Also, bioethanol production was not a good processing route environmentally because of large electricity consumption, yet electricity consumption was the biggest contributor of environmental impacts.

- The economic profitability of the biorefineries was highly dependent on operating expenses, product yield and prices at which final products were sold.

- Anaerobic digestion (biogas production) had the biggest impacts on global warming and marine eutrophication due to high production of methane and carbon dioxide which are the highest perpetrators of climate change.

- Although hydrothermal liquefaction did not require biomass pre-drying and occurs at relatively lower temperatures compared to fast pyrolysis, it was the most electricity consuming processing route. This is because a large heat duty was required to raise the temperature of the big flow rate of the slurry to the optimal temperature needed for HTL reactions.

5.2. Recommendations

The following recommendations can help to guide in future research on valorisation of waste biomass:

- Future studies should consider the use of pinch technology to reduce on heating and cooling requirements during bioconversion. This will reduce the operating expenses which are otherwise raised by high electricity and water consumption. The reduced electricity consumption will also help to reduce on the environmental footprints of the biorefineries, hence making bioconversion more environmentally friendly processes.

- Optimal operating conditions for hydrothermal liquefaction need to be further investigated if the technology is to be fully commercialized. Focus needs to be put on the operating temperature and solid content of the slurry. Currently, the technology needs a slurry of a very low solid content which requires a lot of water to be added hence rising the flow rate of the feed. Consequently, a lot of heat is consumed to raise the temperature of the slurry to an optimal temperature (300 ^{0}C) required for HTL reactions.

- The optimal plant location should be investigated in order to reduce the costs associated with feedstock collection and transportation.

- Water consumption can be reduced by investigating the possibility of reusing cooling water more than 11 times a year that was estimated in this study.

- There is a need to venture into the study assessing the economic feasibility of combining more processing routes on the same feedstock. For example, during biodiesel production, the defatted SCG could be used as feedstock for gasification or pyrolysis to produce more valuable products other than just low value coffee pellets.

- Commercialisation of carbon dioxide produced during anaerobic digestion should be investigated. It can be used during supercritical carbon dioxide of lipids from SCG during biodiesel production. This will increase the profitability of the biogas production process and reduce its impacts on global warming.

- Future studies should also focus on the social-economic impacts of biofuels production from waste biomass. Social-economic factors like income levels, employment patterns and education levels within the community where the biorefineries are proposed to be located need to be investigated.

- Future studies should focus on using kinetic reaction models other than the stoichiometric reaction and equilibrium models that were used in this study during Aspen plus simulations. Kinetic models are superior because they are more accurate and can be used for optimization, however, they are more complex and require a lot of

information like reaction kinetics. Some technologies like HTL are still under investigation and limited information is available about its kinetics.

REFERENCES

Afolabi, O. O. D., Sohail, M. and Cheng, Y.-L. 2020. Optimisation and characterisation of hydrochar production from spent coffee grounds by hydrothermal carbonisation. *Renewable Energy*, 147: 1380-1391.

Aierzhati, A., Watson, J., Si, B., Stablein, M., Wang, T. and Zhang, Y. 2021. Development of a mobile, pilot scale hydrothermal liquefaction reactor: Food waste conversion product analysis and techno-economic assessment. *Energy Conversion and Management: X*, 10.

Akbari, M., Oyedun, A. O. and Kumar, A. 2019. Comparative energy and techno-economic analyses of two different configurations for hydrothermal carbonization of yard waste. *Bioresource Technology Reports*, 7.

Akbari, M., Oyedun, A. O. and Kumar, A. 2020. Techno-economic assessment of wet and dry torrefaction of biomass feedstock. *Energy*, 207.

Alherbawi, M., Parthasarathy, P., Al-Ansari, T., Mackey, H. R. and McKay, G. 2021. Potential of drop-in biofuel production from camel manure by hydrothermal liquefaction and biocrude upgrading: A Qatar case study. *Energy*, 232.

AlNouss, A., Parthasarathy, P., Mackey, H. R., Al-Ansari, T. and McKay, G. 2021. Pyrolysis Study of Different Fruit Wastes Using an Aspen Plus Model. *Frontiers in Sustainable Food Systems*, 5.

Alper, K., Wang, Y.-Y., Meng, X., Tekin, K., Karagoz, S. and Ragauskas, A. J. 2021. Use of a Lewis acid, a Brønsted acid, and their binary mixtures for the hydrothermal liquefaction of lignocellulose. *Fuel*, 304.

Anaya Menacho, W., Mazid, A. M. and Das, N. 2022. Modelling and analysis for biogas production process simulation of food waste using Aspen Plus. *Fuel*, 309.

Araujo, M. N., dos Santos, K. C., do Carmo Diniz, N., de Carvalho, J. C. and Corazza, M. L. 2022. A biorefinery approach for spent coffee grounds valorization using pressurized fluid extraction to produce oil and bioproducts: A systematic review. *Bioresource Technology Reports*, 18.

Atabani, A., Ala'a, H., Kumar, G., Saratale, G. D., Aslam, M., Khan, H. A., Said, Z. and Mahmoud, E. 2019. Valorization of spent coffee grounds into biofuels and value-added products: Pathway towards integrated bio-refinery. *Fuel*, 254: 115640.

Barbera, E., Menegon, S., Banzato, D., D'Alpaos, C. and Bertucco, A. 2019. From biogas to biomethane: A process simulation-based techno-economic comparison of different upgrading technologies in the Italian context. *Renewable Energy*, 135: 663-673.

Biswas, B., Sahoo, D., Sukumaran, R. K., Krishna, B. B., Kumar, J., Reddy, Y. S., Adarsh, V. P., Puthiyamadam, A., Mallapureddy, K. K., Ummalyma, S. B. and Bhaskar, T. 2022. Co-

hydrothermal liquefaction of phumdi and paragrass an aquatic biomass: Characterization of bio-oil, aqueous fraction and solid residue. *Journal of the Energy Institute*, 102: 247-255.

Bot, B. V., Axaopoulos, P. J., Sakellariou, E. I., Sosso, O. T. and Tamba, J. G. 2022. Energetic and economic analysis of biomass briquettes production from agricultural residues. *Applied Energy*, 321.

Brachi, P., Santes, V. and Torres-Garcia, E. 2021. Pyrolytic degradation of spent coffee ground: A thermokinetic analysis through the dependence of activation energy on conversion and temperature. *Fuel*, 302.

Brigagãoa, G. V., Araújoa, O. d. Q. F., de Medeirosa, J. L., Mikulcicb, H. and Duicb, N. 2019. A techno-economic analysis of thermochemical pathways for corncob-to-energy: Fast pyrolysis to bio-oil, gasification to methanol and combustion to electricity. *Fuel Processing Technology*, 193: 12.

Chemicalbook. 2023. *Carbon monoxide*. Available: https://www.chemicalbook.com/Price/CARBON-MONOXIDE.htm (Accessed 05/03/2023).

Chen, G., Guo, X., Liu, F., Ma, Z., Cheng, Z., Yan, B. and Ma, W. 2019. Gasification of lignocellulosic biomass pretreated by anaerobic digestion (AD) process: An experimental study. *Fuel*, 247: 324-333.

Chen, T., Zhang, J., Wang, Z., Zhao, R., He, J., Wu, J. and Qin, J. 2020. Oxygen-enriched gasification of lignocellulosic biomass: Syngas analysis, physicochemical characteristics of the carbon-rich material and its utilization as an anode in lithium ion battery. *Energy*, 212.

Dattatraya Saratale, G., Bhosale, R., Shobana, S., Banu, J. R., Pugazhendhi, A., Mahmoud, E., Sirohi, R., Kant Bhatia, S., Atabani, A. E., Mulone, V., Yoon, J. J., Seung Shin, H. and Kumar, G. 2020. A review on valorization of spent coffee grounds (SCG) towards biopolymers and biocatalysts production. *Bioresour Technol*, 314: 123800.

Daylan, B. and Ciliz, N. 2016. Life cycle assessment and environmental life cycle costing analysis of lignocellulosic bioethanol as an alternative transportation fuel. *Renewable Energy*, 89: 578-587.

de Caprariis, B., De Filippis, P., Petrullo, A. and Scarsella, M. 2017. Hydrothermal liquefaction of biomass: Influence of temperature and biomass composition on the bio-oil production. *Fuel*, 208: 618-625.

Demichelis, F., Laghezza, M., Chiappero, M. and Fiore, S. 2020. Technical, economic and environmental assessement of bioethanol biorefinery from waste biomass. *Journal of Cleaner Production*, 277.

Deuber, R. d. S., Fernandes, D. S., Bressanin, J. M., Watson, J., Chagas, M. F., Bonomi, A., Fregolente, L. V. and Watanabe, M. D. B. 2021. Techno-economic assessment of HTL integration to the Brazilian sugarcane industry: An evaluation of different scenarios. *Industrial Crops and Products*, 173.

Duarte, A., Uribe, J. C., Sarache, W. and Calderón, A. 2021. Economic, environmental, and social assessment of bioethanol production using multiple coffee crop residues. *Energy*, 216.

Elias Bamaca Saquic, B., Irmak, S., Wilkins, M. and Smith, T. 2021. Effect of precursors on graphene supported platinum monometalic catalysts for hydrothermal gasification of biomass compounds to hydrogen. *Fuel*, 290.

Essentialcompost. 2023. *Organic compost*. Available: https://www.ecompost.co.za/ (Accessed 18/02/2023).

Feng, L., Liu, J., Lu, H., Liu, B. and Chen, Y. 2022. Techno-economic and profitability analysis of plant for producing biodiesel from fresh vegetable oil and waste frying oil on large-scale. *Fuel*, 323.

Ferronato, N., Calle Mendoza, I. J., Ruiz Mayta, J. G., Gorritty Portillo, M. A., Conti, F. and Torretta, V. 2022. Biomass and cardboard waste-based briquettes for heating and cooking: Thermal efficiency and emissions analysis. *Journal of Cleaner Production*, 375.

Forero, J. A. J., Tran, T. H. T., Tana, T., Baker, A., Beltramini, J., Doherty, W. O. S. and Moghaddam, L. 2022. Hydrothermal liquefaction of sugarcane bagasse to bio-oils: Effect of liquefaction solvents on bio-oil stability. *Fuel*, 312.

Fu, J., Wu, X., Liu, J., Evrendilek, F., Chen, T., Xie, W., Xu, W. and He, Y. 2023. Co-circularity of spent coffee grounds and polyethylene via co-pyrolysis: Characteristics, kinetics, and products. *Fuel*, 337.

Gebremariam, S. N. and Marchetti, J. M. 2021. Process simulation and techno-economic performance evaluation of alternative technologies for biodiesel production from low value non-edible oil. *Biomass and Bioenergy*, 149.

GlobalPetrolPrices.com. 2023a. *South Africa electricity prices*. Available: https://www.globalpetrolprices.com/South-Africa/electricity_prices/ (Accessed 22/02/2023).

GlobalPetrolPrices.com. 2023b. *South Africa ethanol prices*. Available: https://www.globalpetrolprices.com/South-Africa/ethanol_prices/ (Accessed 17/04/2023).

Glushkov, D. O., Nyashina, G. S., Anand, R. and Strizhak, P. A. 2021. Composition of gas produced from the direct combustion and pyrolysis of biomass. *Process Safety and Environmental Protection*, 156: 43-56.

Goklani, B., Naga Prapurna, P. V. and Srinath, S. 2022. Simulation of pyrolytic conversion of Walnut shell waste to value added products. *Materials Today: Proceedings*, Article ID.

Gonzalez-Arias, J., Baena-Moreno, F. M., Sanchez, M. E. and Cara-Jimenez, J. 2021. Optimizing hydrothermal carbonization of olive tree pruning: A techno-economic analysis based on experimental results. *Sci Total Environ*, 784: 147169.

Gonzalez-Arias, J., Sanchez, M. E. and Cara-Jimenez, J. 2022. Profitability analysis of thermochemical processes for biomass-waste valorization: a comparison of dry vs wet treatments. *Sci Total Environ*, 811: 152240.

Gorensek, M. B., Shukre, R. and Chen, C.-C. 2019. Development of a thermophysical properties model for flowsheet simulation of biomass pyrolysis processes *ACS Sustainable Chemistry & Engineering* 7:9017-9027.

GreenDelta. 2022. *OpenLCA nexus: Your source for LCA and sustainability data*. Available: https://nexus.openlca.org/databases (Accessed August 2022).

Greenthermoenergy. 2023. *Pricing*. Available: http://www.greenthermo.co.za/pricing/ (Accessed 22/02/2023).

Hasan, M. M., Rasul, M. G., Jahirul, M. I. and Khan, M. M. K. 2022. Modeling and process simulation of waste macadamia nutshell pyrolysis using Aspen Plus software. *Energy Reports*, 8: 429-437.

Hoang, A. T., Huang, Z., Nižetić, S., Pandey, A., Nguyen, X. P., Luque, R., Ong, H. C., Said, Z., Le, T. H. and Pham, V. V. 2022. Characteristics of hydrogen production from steam gasification of plant-originated lignocellulosic biomass and its prospects in Vietnam. *International Journal of Hydrogen Energy*, 47 (7): 4394-4425.

Iglesias, S. P., Miyazaki, M. R., Mariano, A. P. and Franco, T. T. 2021. Techno-economic assessment of bio-oil produced from Eucalyptus forestry residues. *Industrial Crops & Products*, 171: 113936.

Jaroenkhasemmeesuk, C., Tippayawong, N., Shimpalee, S., Ingham, D. B. and Pourkashanian, M. 2022. Improved simulation of lignocellulosic biomass pyrolysis plant using chemical kinetics in Aspen Plus® and comparison with experiments. *Alexandria Engineering Journal*, Article ID.

Karmee, S. K. 2018. A spent coffee grounds based biorefinery for the production of biofuels, biopolymers, antioxidants and biocomposites. *Waste management*, 72: 240-254.

Khan, M. S. A., Grioui, N., Halouani, K. and Benelmir, R. 2022. Techno-economic analysis of production of bio-oil from catalytic pyrolysis of olive mill wastewater sludge with two different cooling mechanisms. *Energy Conversion and Management*, 13: 100170.

Khounani, Z., Nazemi, F., Shafiei, M., Aghbashlo, M. and Tabatabaei, M. 2019. Techno-economic aspects of a safflower-based biorefinery plant co-producing bioethanol and biodiesel. *Energy Conversion and Management*, 201.

Kibret, H. A., Kuo, Y.-L., Ke, T.-Y. and Tseng, Y.-H. 2021. Gasification of spent coffee grounds in a semi-fluidized bed reactor using steam and CO2 gasification medium. *Journal of the Taiwan Institute of Chemical Engineers*, 119: 115-127.

Kumar, P., Subbarao, P. M. V., Kala, L. D. and Vijay, V. K. 2022. Real-time performance assessment of open-top downdraft biomass gasifier system. *Cleaner Engineering and Technology*, 7: 100448.

Kushwah, A., Reina, T. R. and Short, M. 2022. Modelling approaches for biomass gasifiers: A comprehensive overview. *Science of the Total Environment*, 834: 155243.

Lachos-Perez, D., Cesar Torres-Mayanga, P., Abaide, E. R., Zabot, G. L. and De Castilhos, F. 2022. Hydrothermal carbonization and Liquefaction: differences, progress, challenges, and opportunities. *Bioresour Technol*, 343: 126084.

Leow, Y., Yew, P. Y. M., Chee, P. L., Loh, X. J. and Kai, D. 2021. Recycling of spent coffee grounds for useful extracts and green composites. *RSC Adv*, 11 (5): 2682-2692.

Li, Q., Yuan, X., Hu, X., Meers, E., Ong, H. C., Chen, W.-H., Duan, P., Zhang, S., Lee, K. B. and Ok, Y. S. 2022. Co-liquefaction of mixed biomass feedstocks for bio-oil production: A critical review. *Renewable and Sustainable Energy Reviews*, 154.

Liu, F., Guo, X., Wang, Y., Chen, G. and Hou, L. a. 2021. Process simulation and economic and environmental evaluation of a corncob-based biorefinery system. *Journal of Cleaner Production*, 329.

Liu, Y., Yang, X., Zhang, J. and Zhu, Z. 2022a. Process Simulation of Preparing Biochar by Biomass Pyrolysis Via Aspen Plus and Its Economic Evaluation. *Waste and Biomass Valorization*, 13 (5): 2609-2622.

Liu, Z., Zhao, C., Cai, L. and Long, X. 2022b. Steady state modelling of steam-gasification of biomass for H2-rich syngas production. *Energy*, 238.

Lombardi, L. and Francini, G. 2020. Techno-economic and environmental assessment of the main biogas upgrading technologies. *Renewable Energy*, 156: 440-458.

Ly, H. V., Lee, B., Sim, J. W., Tran, Q. K., Kim, S.-S., Kim, J., Brigljevi, B., Hwang, H. T. and Lim, H. 2022. Catalytic pyrolysis of spent coffee waste for upgrading sustainable bio-oil in a bubbling fluidized-bed reactor: Experimental and techno-economic analysis. *Chemical Engineering Journal*, 247: 130956.

Lyu, H., Zhang, J., Zhai, Z., Feng, Y. and Geng, Z. 2020. Life cycle assessment for bioethanol production from whole plant cassava by integrated process. *Journal of Cleaner Production*, 269.

Mahapatra, S., Kumar, D., Singh, B. and Sachan, P. K. 2021. Biofuels and their sources of production: A review on cleaner sustainable alternative against conventional fuel, in the framework of the food and energy nexus. *Energy Nexus*, 4.

Martinovic, F. L., Kiss, F. E., Micic, R. D., Simikić, M. Đ. and Tomić, M. D. 2018. Comparative techno-economic analysis of single-step and two-step biodiesel production with supercritical methanol based on process simulation. *Chemical Engineering Research and Design*, 132: 751-765.

Mayer, F., Bhandari, R. and Gath, S. 2019. Critical review on life cycle assessment of conventional and innovative waste-to-energy technologies. *Sci Total Environ*, 672: 708-721.

Medina-Martos, E., Istrate, I.-R., Villamil, J. A., Gálvez-Martos, J.-L., Dufour, J. and Mohedano, Á. F. 2020. Techno-economic and life cycle assessment of an integrated hydrothermal carbonization system for sewage sludge. *Journal of Cleaner Production*, 277.

Mishra, R. K., kumar, V., Kumar, P. and Mohanty, K. 2022. Hydrothermal liquefaction of biomass for bio-crude production: A review on feedstocks, chemical compositions, operating parameters, reaction kinetics, techno-economic study, and life cycle assessment. *Fuel*, 316.

Moreira, L. C., Borges, P. O., Cavalcante, R. M. and Young, A. F. 2022. Simulation and economic evaluation of process alternatives for biogas production and purification from sugarcane vinasse. *Renewable and Sustainable Energy Reviews*, 163.

Mukherjee, A., Okolie, J. A., Niu, C. and Dalai, A. K. 2022. Techno – Economic analysis of activated carbon production from spent coffee grounds: Comparative evaluation of different production routes. *Energy Conversion and Management: X*, 14.

Mumtaz, M., Baqar, Z., Hussain, N., Afifa, Bilal, M., Azam, H. M. H., Baqir, Q.-u.-a. and Iqbal, H. M. N. 2022. Application of nanomaterials for enhanced production of biodiesel, biooil, biogas, bioethanol, and biohydrogen via lignocellulosic biomass transformation. *Fuel*, 315.

Mupondwa, E., Li, X., Tabil, L., Sokhansanj, S. and Adapa, P. 2017. Status of Canada's lignocellulosic ethanol: Part I: Pretreatment technologies. *Renewable and Sustainable Energy Reviews*, 72: 178-190.

Nagappan, S., Bhosale, R. R., Nguyen, D. D., Chi, N. T. L., Ponnusamy, V. K., Woong, C. S. and Kumar, G. 2021. Catalytic hydrothermal liquefaction of biomass into bio-oils and other value-added products – A review. *Fuel*, 285.

Naqi, A., Kuhn, J. N. and Joseph, B. 2019. Techno-economic analysis of producing liquid fuels from biomass via anaerobic digestion and thermochemical conversion. *Biomass and Bioenergy*, 130.

NETL. 2024. *Fluidised bed gasifiers*. Available: https://netl.doe.gov/research/coal/energy-systems/gasification/gasifipedia/fluidizedbed#:~:text=Fluidized%2Dbed%20gasifiers%20suspend%20feedstock,coal%20particles%20already%20undergoing%20gasification. (Accessed 12/02/2024).

Nelissen, D., Faber, J., Veen, R. v. d., Grinsven, A. v., Shanthi, H. and Toorn, E. v. d. 2020. *Availability and costs of liquefied bio- and synthetic methane*. CE Delt. Available: www.cedelft.eu (Accessed 04/03/2023).

Okolie, J. A., Tabat, M. E., Gunes, B., Epelle, E. I., Mukherjee, A., Nanda, S. and Dalai, A. K. 2021. A techno-economic assessment of biomethane and bioethanol production from crude glycerol through integrated hydrothermal gasification, syngas fermentation and biomethanation. *Energy Conversion and Management: X*, 12.

Pacheco, J. R., Villardi, H. G. D., Cavalcante, R. M. and Young, A. F. 2022. Biodiesel production through non-conventional supercritical routes: Process simulation and technical evaluation. *Energy Conversion and Management*, 251.

Patel, M., Zhang, X. and Kumar, A. 2016. Techno-economic and life cycle assessment on lignocellulosic biomass thermochemical conversion technologies: A review. *Renewable and Sustainable Energy Reviews*, 53: 1486-1499.

payscale. 2023. *Average production operator hourly pay in South Africa*. Available: https://www.payscale.com/research/ZA/Job=Production_Operator/Hourly_Rate (Accessed 20/04/2023).

Pereira, Woodman, Brahmbhatt and Chuck. 2019. The Optimized Production of 5-(Hydroxymethyl)furfural and Related Products from Spent Coffee Grounds. *Applied Sciences*, 9 (16).

Peters, J. F., Banks, S. W., Bridgwater, A. V. and Dufour, J. 2017. A kinetic reaction model for biomass pyrolysis processes in Aspen Plus. *Applied Energy*, 188: 595–603.

Rajesh Banu, J., Kavitha, S., Yukesh Kannah, R., Dinesh Kumar, M., Preethi, Atabani, A. E. and Kumar, G. 2020. Biorefinery of spent coffee grounds waste: Viable pathway towards circular bioeconomy. *Bioresour Technol*, 302: 122821.

Ravendran, R. R., Abdulrazik, A. and Zailan, R. 2019. Aspen plus simulation of optimal biogas production in anaerobic digestion process. Paper presented at the *Materials Science and Engineering*. IOP Publishing, 012001.

Rijo, B., Dias, A. P. S., Ramos, M. and Ameixa, M. 2022. Valorization of forest waste biomass by catalyzed pyrolysis. *Energy*, 243: 122766.

Rijo, B., Soares Dias, A. P., Ramos, M., de Jesus, N. and Puna, J. 2021. Catalyzed pyrolysis of coffee and tea wastes. *Energy*, 235.

Rodionova, M. V., Bozieva, A. M., Zharmukhamedov, S. K., Leong, Y. K., Chi-Wei Lan, J., Veziroglu, A., Veziroglu, T. N., Tomo, T., Chang, J.-S. and Allakhverdiev, S. I. 2022. A comprehensive review on lignocellulosic biomass biorefinery for sustainable biofuel production. *International Journal of Hydrogen Energy*, 47 (3): 1481-1498.

S&Pglobal. 2021. *Experts explain why green hydrogen costs have fallen and will keep falling*. Available: https://www.spglobal.com/marketintelligence/en/news-insights/latest-news-headlines/experts-explain-why-green-hydrogen-costs-have-fallen-and-will-keep-falling-63037203 (Accessed 05/03/2023).

Sadhukhan, J., Martinez-Hernandez, E., Amezcua-Allieri, M. A., Aburto, J. and Honorato S, J. A. 2019. Economic and environmental impact evaluation of various biomass feedstock for bioethanol production and correlations to lignocellulosic composition. *Bioresource Technology Reports*, 7.

Sahoo, A., Saini, K., Jindal, M., Bhaskar, T. and Pant, K. K. 2021. Co-Hydrothermal Liquefaction of algal and lignocellulosic biomass: Status and perspectives. *Bioresour Technol*, 342: 125948.

SAshares. 2023. *Oil price*. Available: https://sashares.co.za/crude-oil-price/#gs.vnwszs (Accessed 04/03/2023).

Scarsella, M., de Caprariis, B., Damizia, M. and De Filippis, P. 2020. Heterogeneous catalysts for hydrothermal liquefaction of lignocellulosic biomass: A review. *Biomass and Bioenergy*, 140.

Schmidt Rivera, X. C., Gallego-Schmid, A., Najdanovic-Visak, V. and Azapagic, A. 2020. Life cycle environmental sustainability of valorisation routes for spent coffee grounds: From waste to resources. *Resources, Conservation and Recycling*, 157.

Selinawamucii. 2023. *US glycerol prices*. Available: https://www.selinawamucii.com/insights/prices/united-states-of-america/glycerol.com/ (Accessed 20/02/2023).

Shahbaz, M., AlNouss, A., Parthasarathy, P., Abdelaal, A. H., Mackey, H., McKay, G. and Al-Ansari, T. 2020. Investigation of biomass components on the slow pyrolysis products yield using Aspen Plus for techno-economic analysis. *Biomass Conversion and Biorefinery*, 12 (3): 669-681.

Shahbeik, H., Peng, W., Kazemi Shariat Panahi, H., Dehhaghi, M., Guillemin, G. J., Fallahi, A., Amiri, H., Rehan, M., Raikwar, D., Latine, H., Pandalone, B., Khoshnevisan, B., Sonne, C., Vaccaro, L., Nizami, A.-S., Gupta, V. K., Lam, S. S., Pan, J., Luque, R., Sels, B., Tabatabaei, M. and Aghbashlo, M. 2022. Synthesis of liquid biofuels from biomass by hydrothermal gasification: A critical review. *Renewable and Sustainable Energy Reviews*, 167.

Sharma, A., Singh, G. and Arya, S. K. 2020. Biofuel from rice straw. *Journal of Cleaner Production*, 277.

Singh, M., Salaudeen, S. A., Gilroyed, B. H. and Dutta, A. 2022. Simulation of biomass-plastic co-gasification in a fluidized bed reactor using Aspen plus. *Fuel*, 319.

Sinnott, R. and Towler, G. 2009. *Chemical engineering design*. fifth ed. UK: Elsevier.

Taleb, F., Ammar, M., Mosbah, M. B., Salem, R. B. and Moussaoui, Y. 2020. Chemical modification of lignin derived from spent coffee grounds for methylene blue adsorption. *Sci Rep*, 10 (1): 11048.

Tezer, O., Karabag, N., Ongen, A. and Colpan, C. O. 2022. Biomass gasification for sustainable energy production: A review. *International Journal of Hydrogen Energy*, Article ID: 15419-15433.

Thefirewoodcompany. 2023. *Wood pellets 15 kg*. Available: https://tfwc.co.za/product/wood-pellets/ (Accessed 23/02/2023).

Theglobaleconomy.com. 2023. *World economic indicators*. Available: https://www.theglobaleconomy.com/World/ (Accessed 05/03/2023).

Thoppil, Y. and Zein, S. H. 2021. Techno-economic analysis and feasibility of industrial-scale biodiesel production from spent coffee grounds. *Journal of Cleaner Production*, 307.

Tian, H., Zhou, T., Huang, Z., Wang, J., Cheng, H. and Yang, Y. 2021. Integration of spent coffee grounds valorization for co-production of biodiesel and activated carbon: An energy and techno-economic case assessment in China. *Journal of Cleaner Production*, 324.

Tinoco-Caicedo, D. L., Mero-Benavides, M., Santos-Torres, M., Lozano-Medina, A. and Blanco-Marigorta, A. M. 2021. Simulation and exergoeconomic analysis of the syngas and biodiesel production process from spent coffee grounds. *Case Studies in Thermal Engineering*, 28.

Vilen, A., Laurell, P. and Vahala, R. 2022. Comparative life cycle assessment of activated carbon production from various raw materials. *J Environ Manage*, 324: 116356.

Yong, Y. S. and Abdul Rasid, R. 2021. Process simulation of hydrogen production through biomass gasification: Introduction of torrefaction pre-treatment. *International Journal of Hydrogen Energy*, Article ID.

Zabaniotou, A. and Kamaterou, P. 2019. Food waste valorization advocating Circular Bioeconomy - A critical review of potentialities and perspectives of spent coffee grounds biorefinery. *Journal of Cleaner Production*, 211: 1553-1566.

Zhang, C., Han, L., Yan, M., Xia, J., Rong, N., Baloch, H. A., Guo, H., Wu, P., Xu, G. and Ma, K. 2021a. Hydrothermal co-liquefaction of rice straw and waste cooking-oil model compound for bio-crude production. *Journal of Analytical and Applied Pyrolysis*, 160.

Zhang, S., Yang, J., Wang, S., Rupasinghe, H. P. V. and He, Q. 2021b. Experimental exploration of processes for deriving multiple products from spent coffee grounds. *Food and Bioproducts Processing*, 128: 21-29.

Zhang, Z., Delcroix, B., Rezazgui, O. and Mangin, P. 2021c. Simulation and techno-economic assessment of bio-methanol production from pine biomass, biochar and pyrolysis oil. *Sustainable Energy Technologies and Assessments*, 44.

Zhou, X., Zhao, J., Chen, M., Zhao, G. and Wu, S. 2022. Influence of catalyst and solvent on the hydrothermal liquefaction of woody biomass. *Bioresour Technol*, 346: 126354.

Zhu, Y., Jones, S. B., Schmidt, A. J., Billing, J. M., Santosa, D. M. and Anderson, D. B. 2020. Economic impacts of feeding microalgae/wood blends to hydrothermal liquefaction and upgrading systems. *Algal Research*, 51.

APPENDICES

APPENDIX A: Aspen plus user-defined components

Table A 1: Biomass input components (Gorensek, Shukre and Chen 2019)

Component name	Component ID	Class in Aspen Plus	Chemical formula
C-rich lignin	LIGC	Solid	$C_{15}H_{14}O_4$
O-rich lignin	LIGO	Solid	$C_{20}H_{22}O_{10}$
H-rich lignin	LIGH	Solid	$C_{22}H_{28}O_9$
Hemicellulose	HCE	Solid	$C_5H_8O_4$
Cellulose	CELL	solid	$C_6H_{10}O_5$

Table A 2: Biomass fast pyrolysis intermediates (Gorensek, Shukre and Chen 2019)

Component name	Component ID	Class in Aspen Plus	Chemical formula
Secondary lignin intermediate	LIG	Solid	$C_{11}H_{12}O_4$
C-rich lignin intermediate	LIGCC	Solid	$C_{15}H_{14}O_4$
H/O-rich lignin intermediate	LIGOH	Solid	$C_{19}H_{22}O_8$
Activated hemicellulose 1	HCE1	Solid	$C_5H_8O_4$
Activated hemicellulose 2	HCE2	solid	$C_5H_8O_4$

Table A 3: Biomass fast pyrolysis end products (Gorensek, Shukre and Chen 2019)

Component name	Component ID	Class in Aspen Plus	Chemical formula
Char (carbon-graphite)	CHAR	Solid	C
Sinapyl aldehyde	FE2MACR	Conventional	$C_{11}H_{12}O_4$
Glyoxal	GLYOXAL	Conventional	$C_2H_2O_2$
Ethylene	C2H4	Conventional	C_2H_4
Acetaldehyde	CH3CHO	Conventional	C_2H_4O
Acetic acid	ACAC	Conventional	$C_2H_4O_2$
Glycol aldehyde	HAA	Conventional	$C_2H_4O_2$
Ethanol	C2H5OH	Conventional	C_2H_6O
Acrolein	ACROL		C_3H_4O
n-propionaldehyde	ALD3	Conventional	C_3H_6O
3-hydroxypropanal	C3H6O2-N	Conventional	$C_3H_6O_2$
Furfural	FURF	Conventional	$C_5H_4O_2$
xylosan	XYLAN	conventional	$C_5H_8O_4$
Levoglucosan	LVG	Conventional	$C_6H_{10}O_5$
Phenol	PHENOL	Conventional	C_6H_6O
5-hydroxymethyl-furfural	HMFU	Conventional	$C_6H_6O_3$
Anisole	ANISOLE	Conventional	C_7H_8O
p-coumaryl alcohol	COUMARYL	Conventional	$C_9H_{10}O_2$
Formaldehyde	CH2O	Conventional	CH_2O
Formic acid	HCOOH	conventional	CH_2O_2
Methane	CH4	conventional	CH_4
Methanol	CH3OH	Conventional	CH_4O
Carbon monoxide	CO	conventional	CO
Carbon dioxide	CO2	Conventional	CO_2
hydrogen	H2	Conventional	H_2
Water	H2O	Conventional	H_2O
High-molecular weight lignin	HMWL	solid	$C_{24}H_{28}O_4$

Table A 4: Estimated solid properties used in this model (Gorensek, Shukre and Chen 2019)

Component ID	Molecular weight (kg/kmol)	Enthalpy of formation (kJ/gmol)	Heat capacity coefficients (J/(gmolK))		Solid density ($kmol/m^3$)
			C_1	C_2	
LIG	208.21388	-729.31	13.2251	0.82834	7.3002
LIGC	258.27376	-759.39	16.4048	1.02749	5.8852
LIGCC	258.27376	-759.39	16.4048	1.02749	5.8852
LIGH	436.45892	-1722.7	27.7226	1.73636	3.4826
LIGO	422.38868	-1847.5	26.8289	1.68039	3.5986
LIGOH	378.37888	-1429.2	24.0335	1.50530	4.0171
CELL	162.1424	-1019.0	-1.5328	0.67527	9.3745
HCE	132.11612	-759.2	-1.2489	0.55022	11.5050
HCE1	132.11612	-759.2	-1.2489	0.55022	11.5050
HCE2	132.11612	-759.2	-1.2489	0.55022	11.5050
HMWL	380.48392	-958.26	24.1672	1.51368	3.9949

Table A 5: Estimated fluid properties model parameters for conventional fluids (Gorensek, Shukre and Chen 2019)

	C3H6O2-N	COUMARYL	FE2MACR	XYLAN
Molecular weight (kg/kmol)	74.07944	150.1772	208.21388	132.11612
Enthalpy of formation (kJ/gmol)	-345.3	-193.5	-483.8	-642.3
Critical temperature (K)	605.0	791.4	837.9	744.3
Critical pressure (bar)	56.36	56.90	29.25	2.134
Acentric factor	1.133	1.198	0.981	0.292
Ideal gas heat capacity estimates (J/gmol-K)				
Cp (298K)	91.46	177.30	240.85	142.76
Cp (400K)	109.33	225.11	302.37	179.06
Cp (500K)	126.37	264.73	357.37	215.39
Cp (600K)	141.02	296.16	402.54	240.55
Cp (800K)	164.75	342.81	471.36	281.03
Cp (1000K)	182.00	374.75	520.31	307.48
Aly-Lee heat capacity equation coefficients (J/kmol-K)				
C_{CP1}	77793.84	128972.6	190226.6	115298.4
C_{CP2}	106997.7	342667.4	491979.1	224458.5
C_{CP3}	814.165	1575.222	1728.691	824.2086
C_{CP4}	66750.56	266861.9	371592.6	59411.96
C_{CP5}	2048.402	728.2816	797.2112	2302.592
C_{CP6}	298	298	298	298
C_{CP7}	1000	1000	1000	1000
Extended Antoine equation coefficients (K/Pa)				
C_{PL1}	136.9781	286.7075	286.6149	135.2637
C_{PL2}	-13924.84	-25124.63	-25391.53	-14336.53
C_{PL3}	-15.46495	-37.26739	-37.28766	-15.74501
C_{PL4}	$1.3038x10^{-17}$	$1.48627x10^{-5}$	$1.36118x10^{-5}$	$2.2459x10^{-18}$
C_{PL5}	6	2	2	6
C_{PL6}	261.15	406.15	406.15	455.4
C_{PL7}	605	791.4	837.9	744.3

APPENDIX B: Biodiesel production simulation

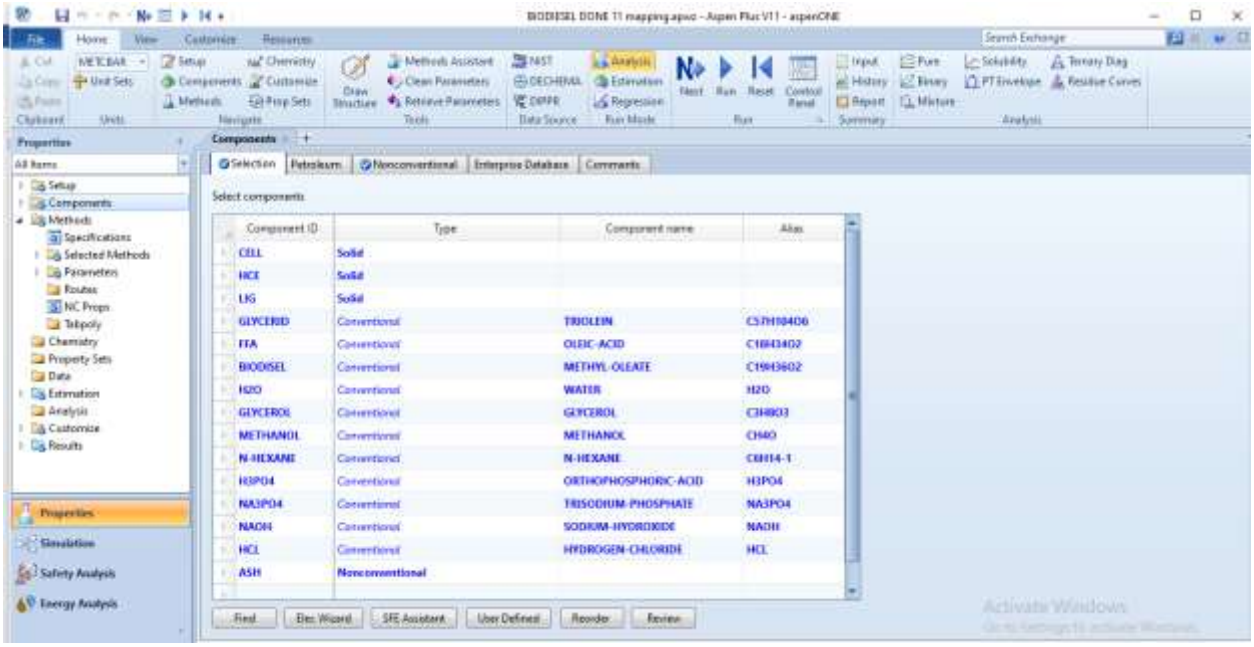

Figure B 1: Defined components in biodiesel simulation

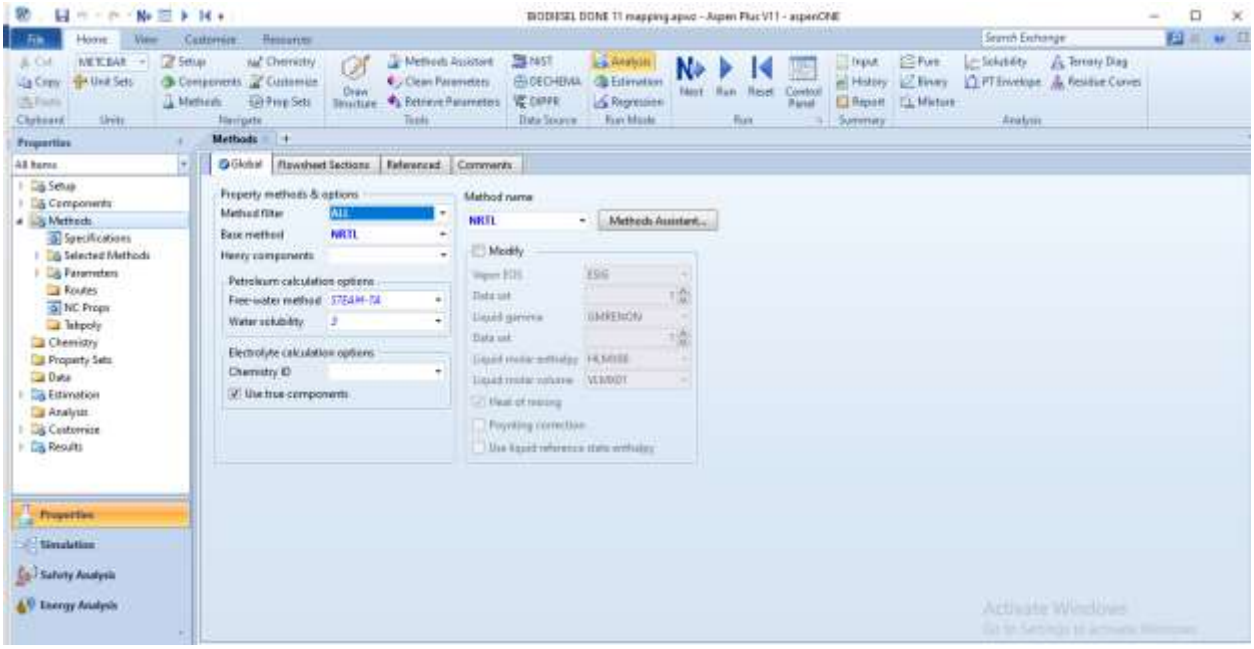

Figure B 2: Fluid package used in biodiesel simulation

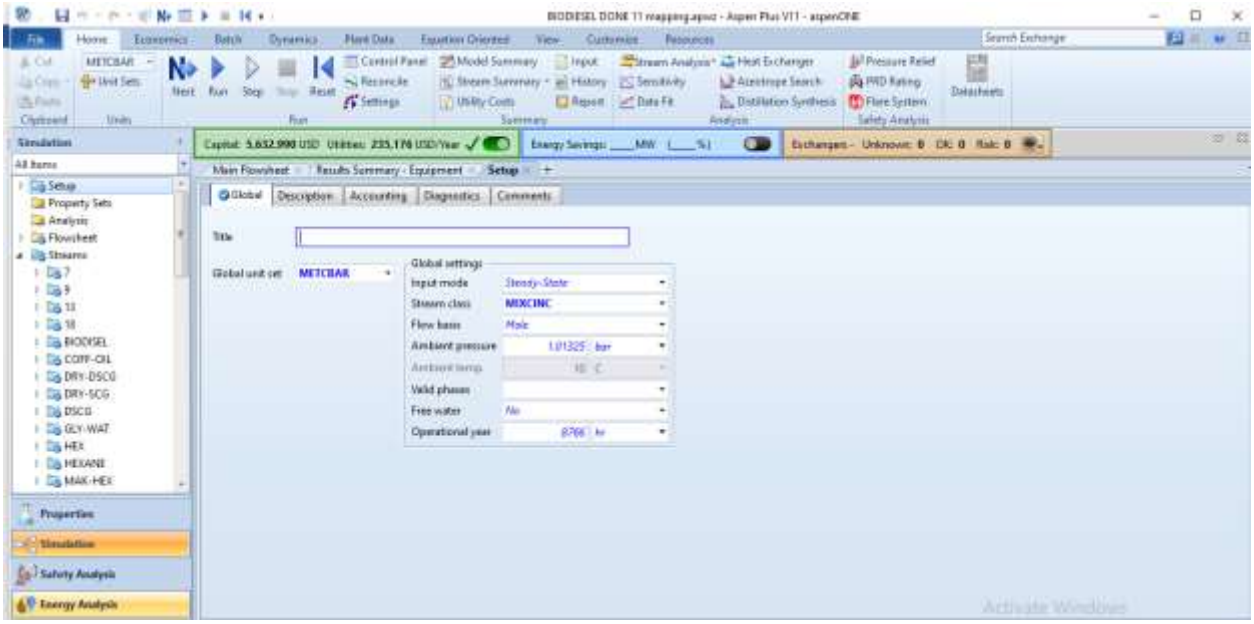

Figure B 3: Global flow used in biodiesel simulation

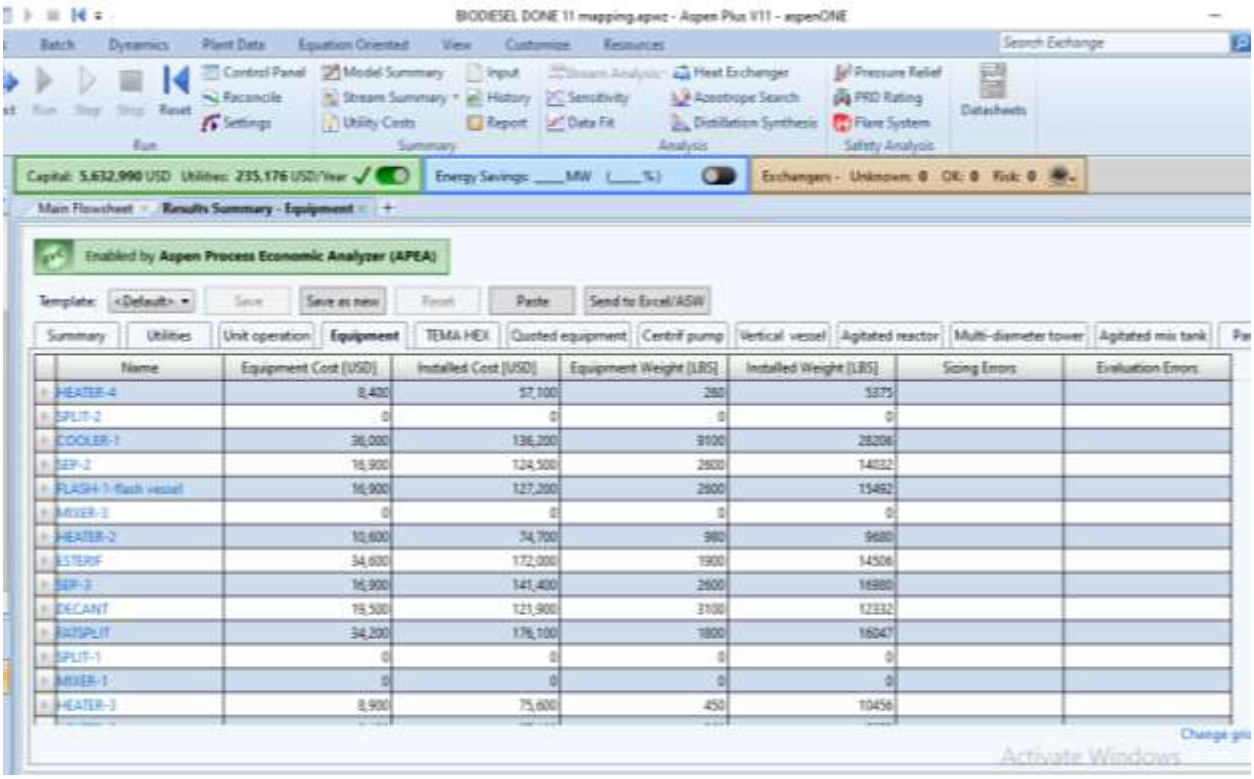

Figure B 4: Equipment costing in biodiesel simulation

APPENDIX C: Bioethanol production simulation

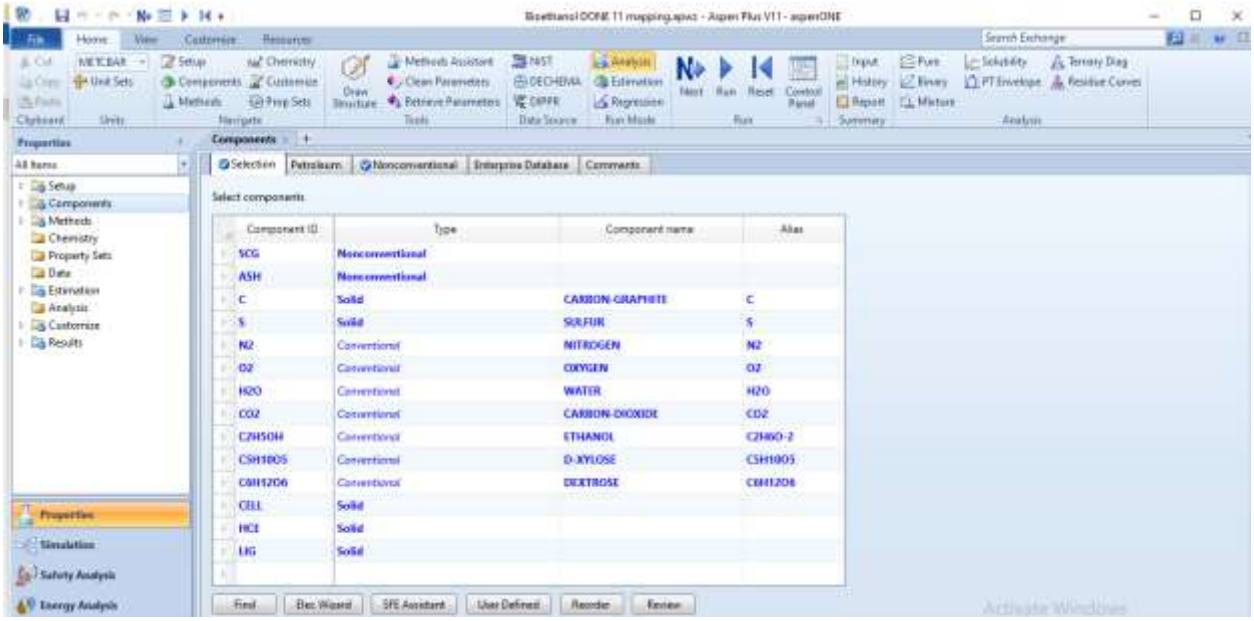

Figure C 1: Defined components in bioethanol simulation

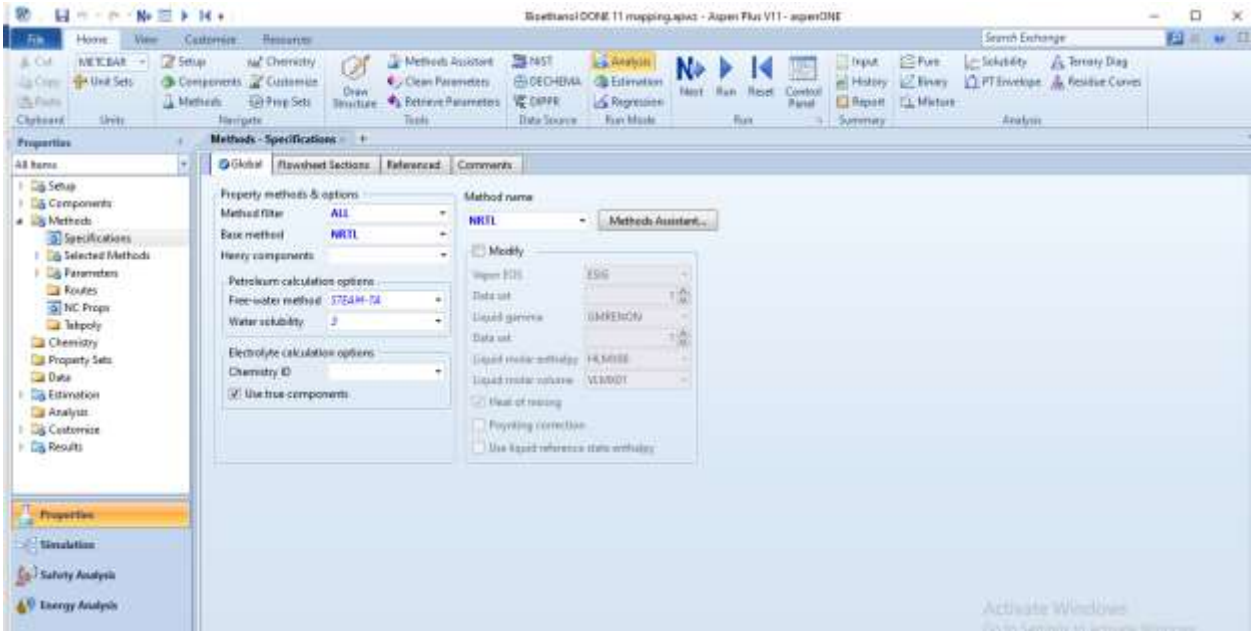

Figure C 2: Fluid package used in bioethanol simulation

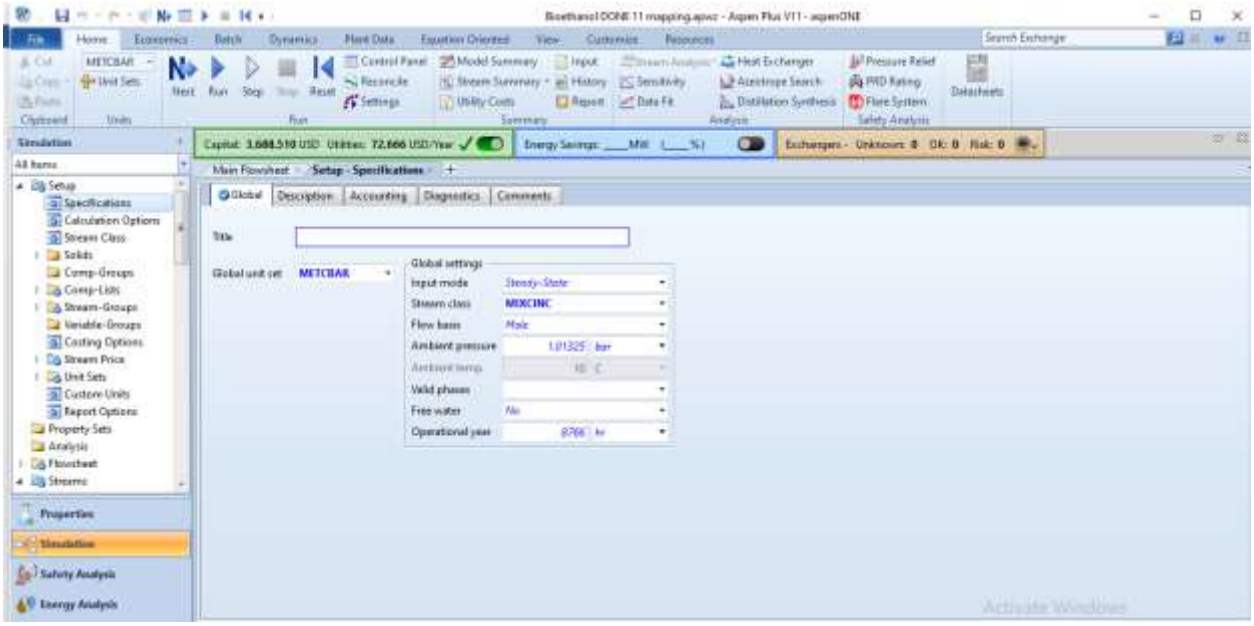

Figure C 3: Global flow used in bioethanol simulation

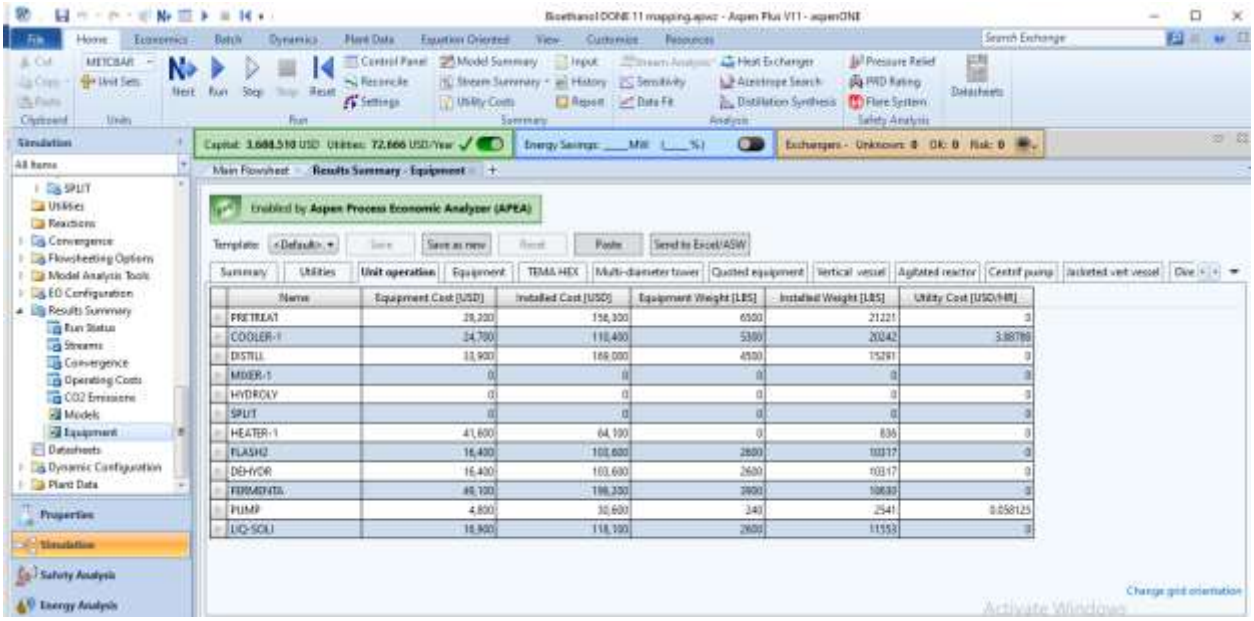

Figure C 4: Equipment costing in bioethanol simulation

APPENDIX D: Biogas production simulation

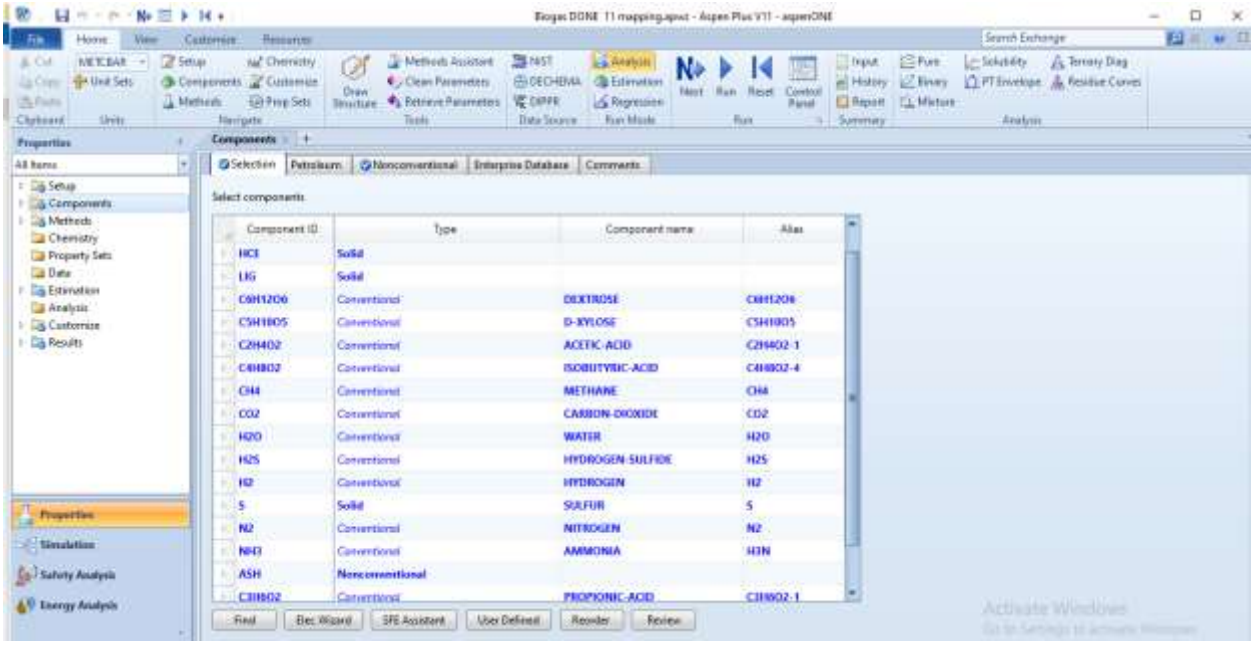

Figure D 1: Defined components in biogas simulation

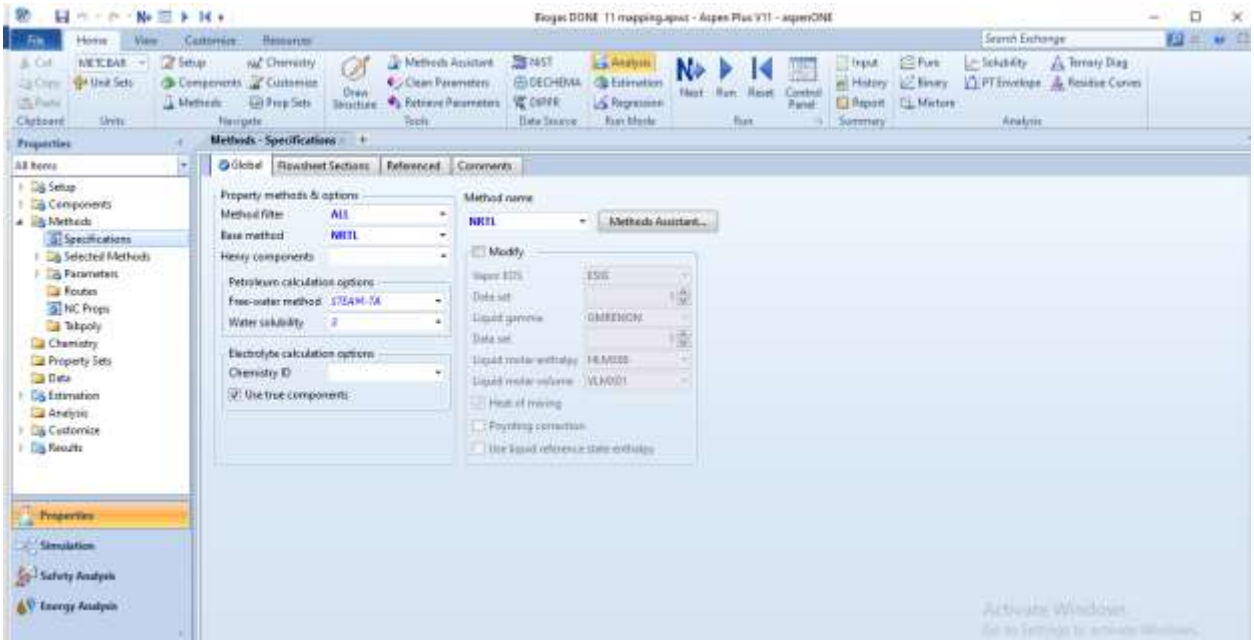

Figure D 2: Fluid package used in biogas simulation

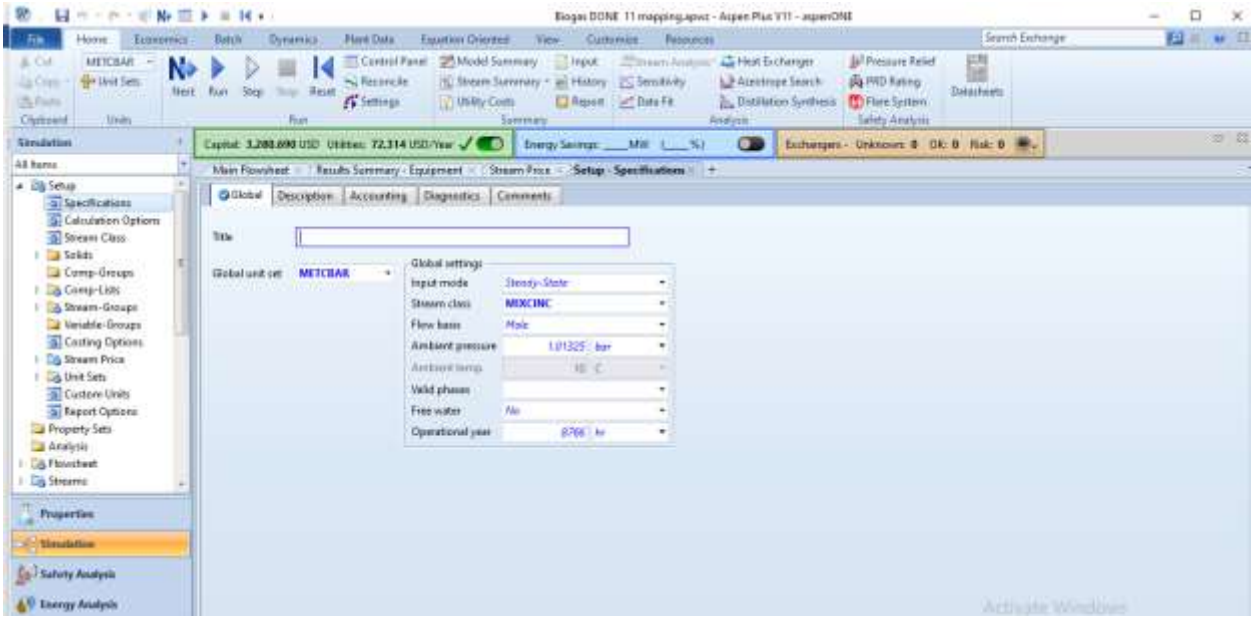

Figure D 3: Global flow used in biogas simulation

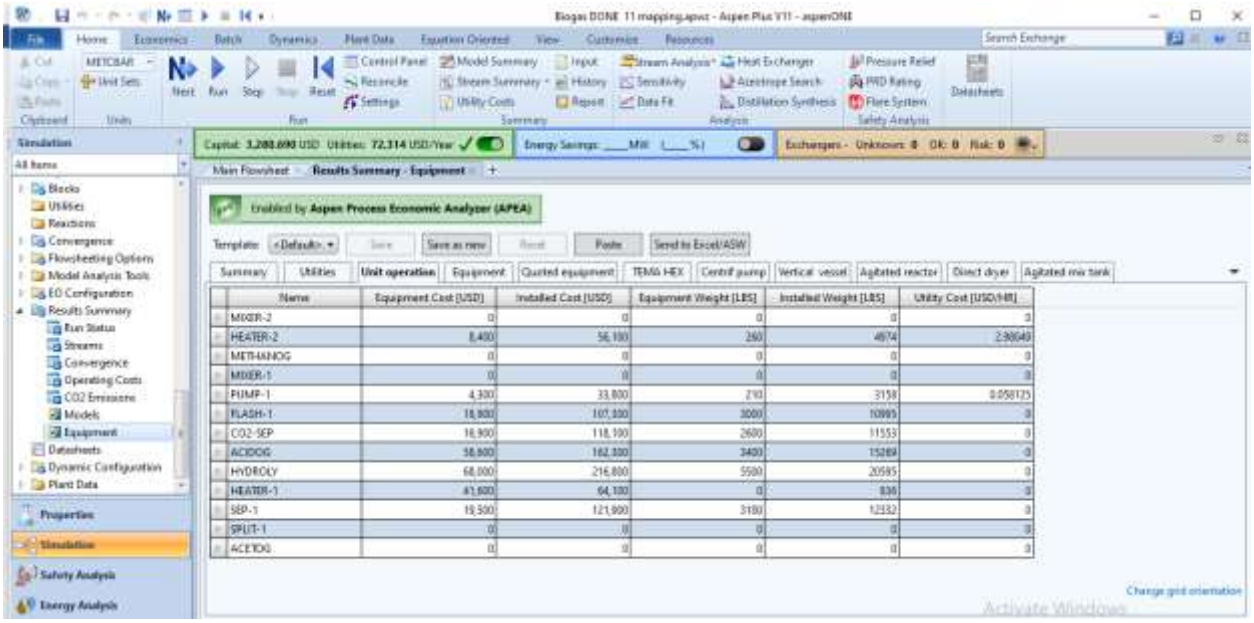

Figure D 4: Equipment costing in biogas simulation

APPENDIX E: Fast pyrolysis simulation

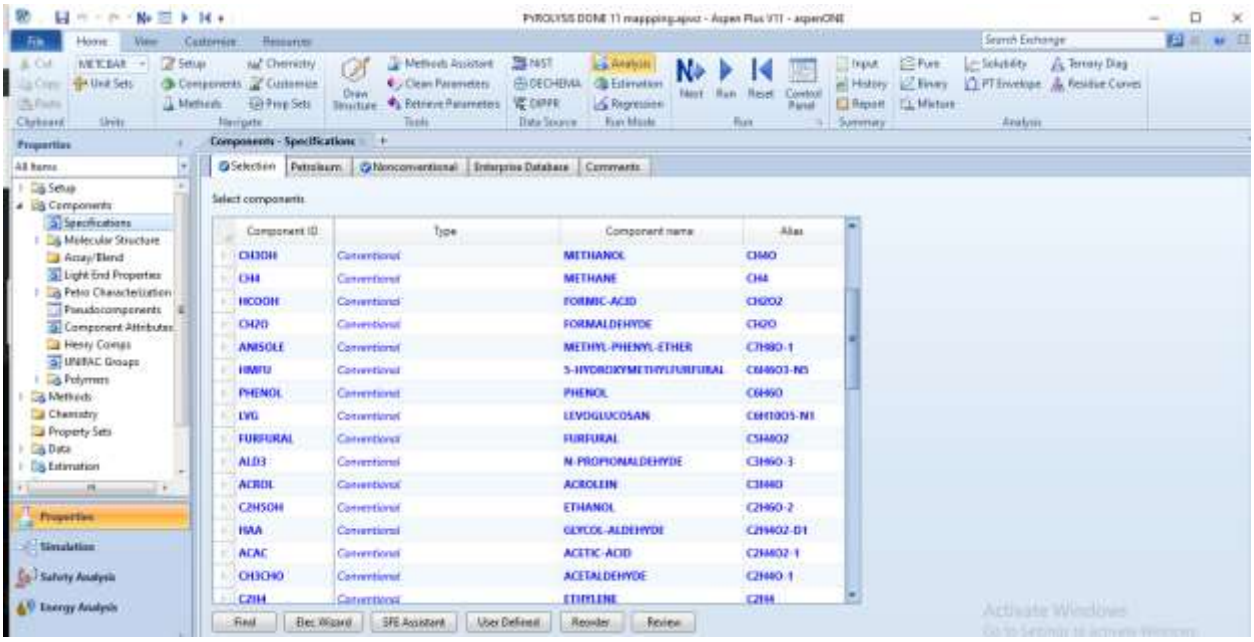

Figure E 1: Defined components in fast pyrolysis simulation

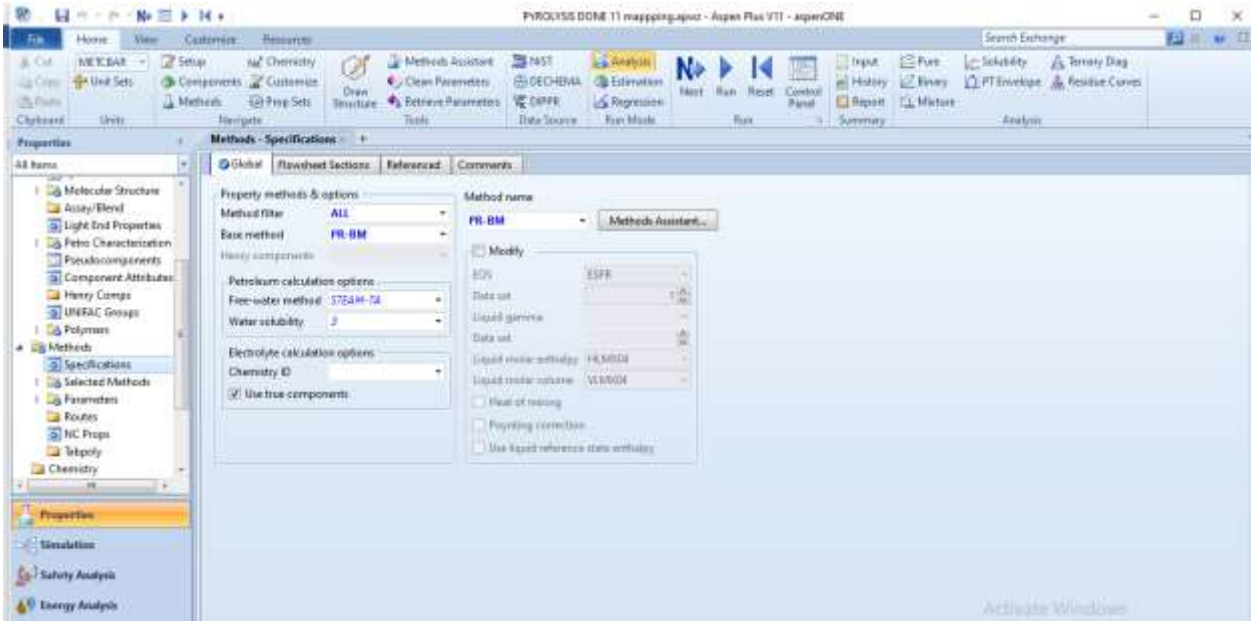

Figure E 2: Fluid package used in fast pyrolysis simulation

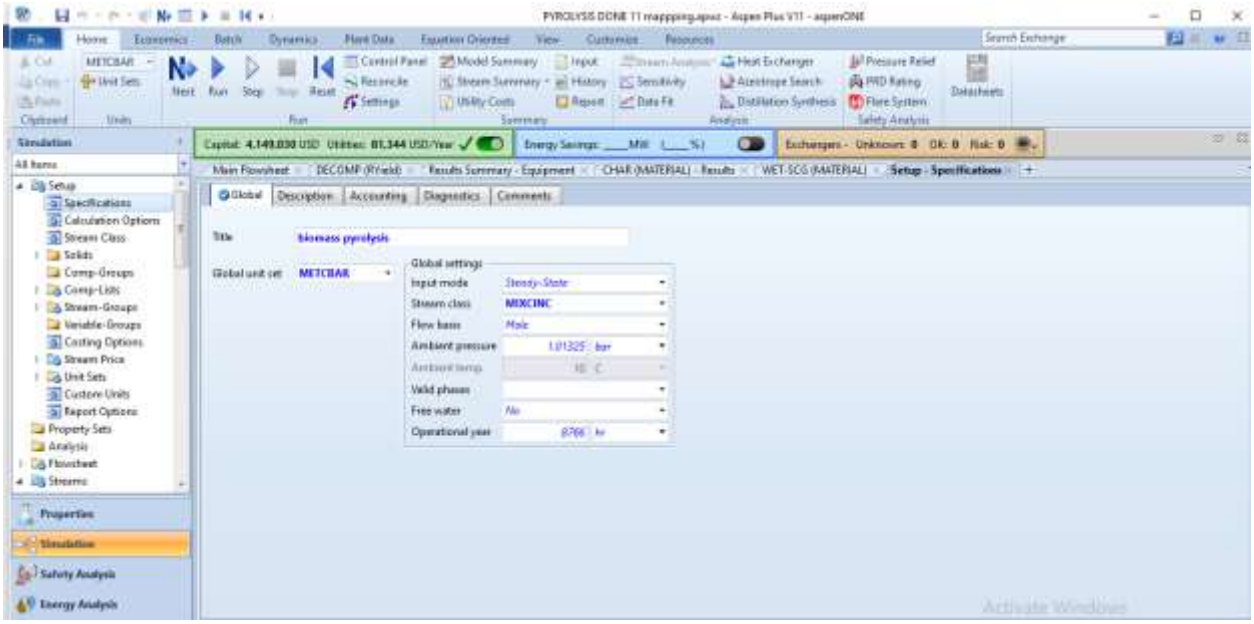

Figure E 3: Global flow used in fast pyrolysis simulation

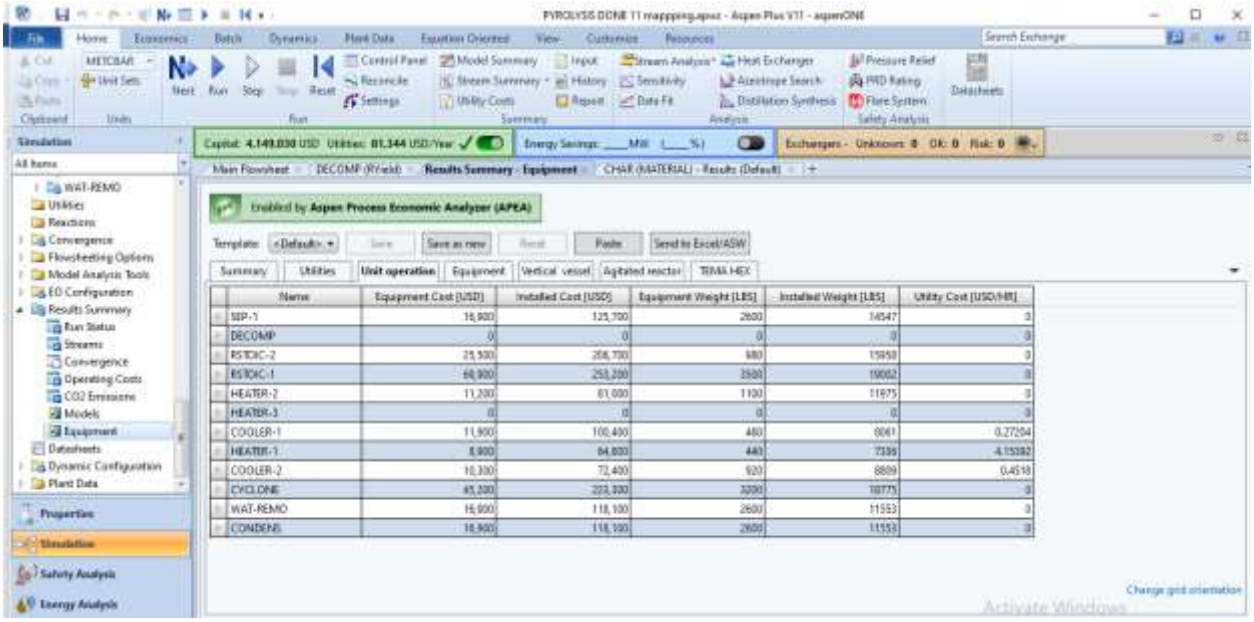

Figure E 4: Equipment costing in fast pyrolysis simulation

APPENDIX F: HTL simulation

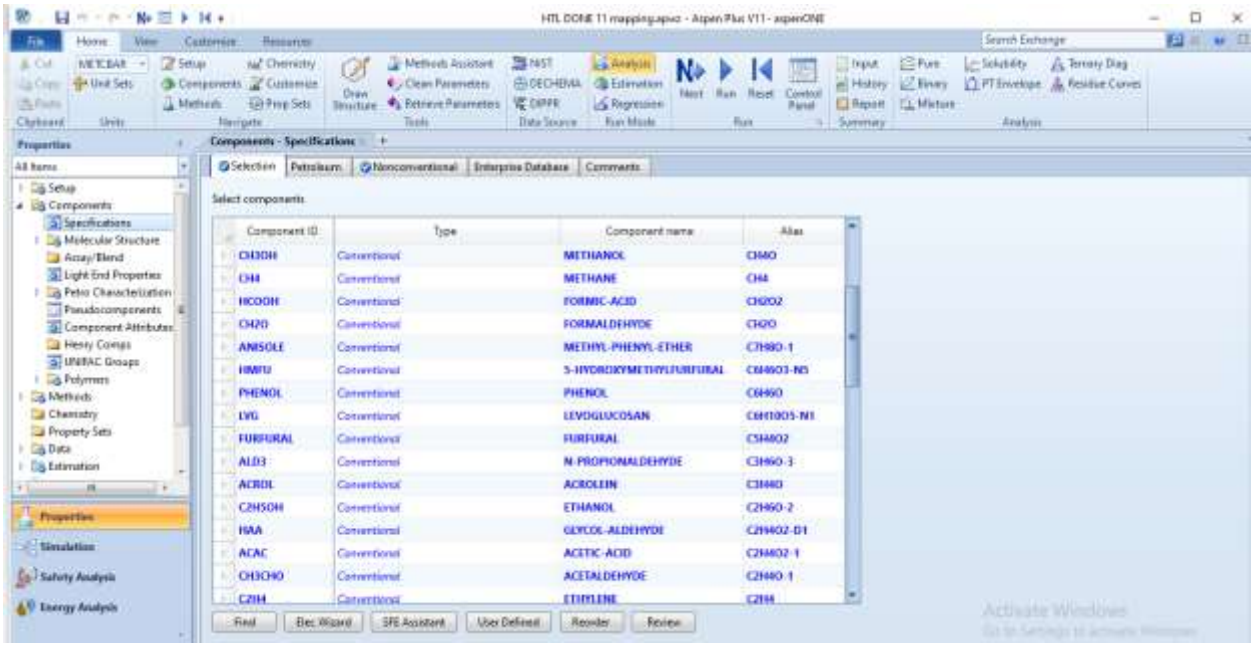

Figure F 1: Defined components in HTL simulation

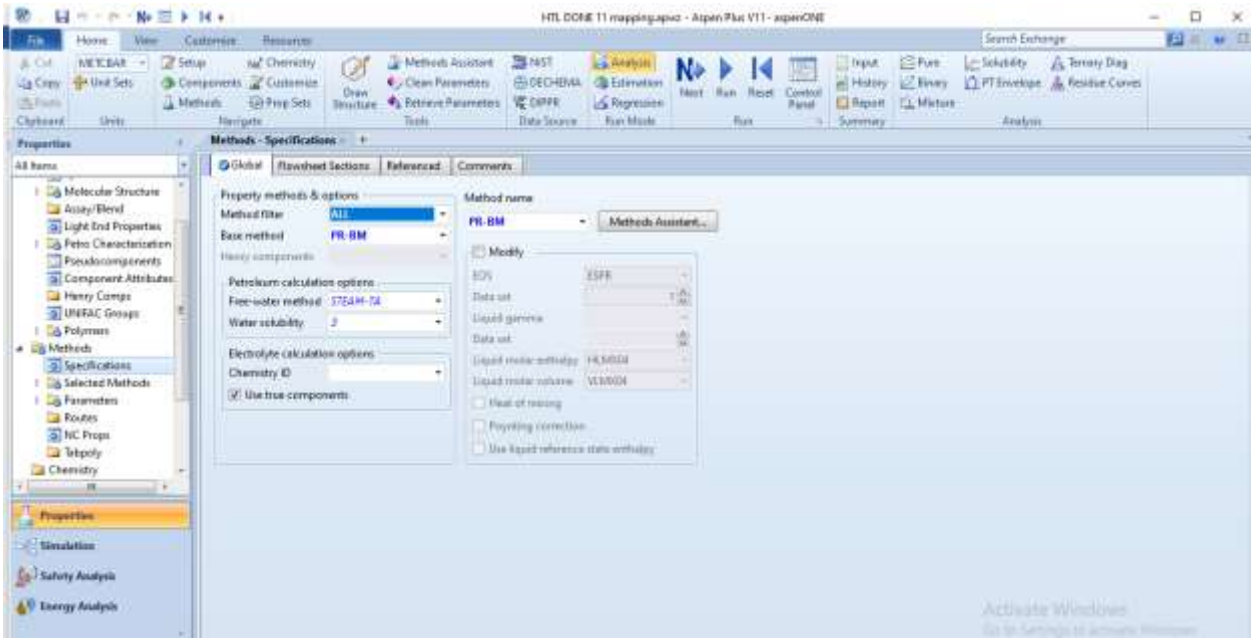

Figure F 2: Fluid package used in HTL simulation

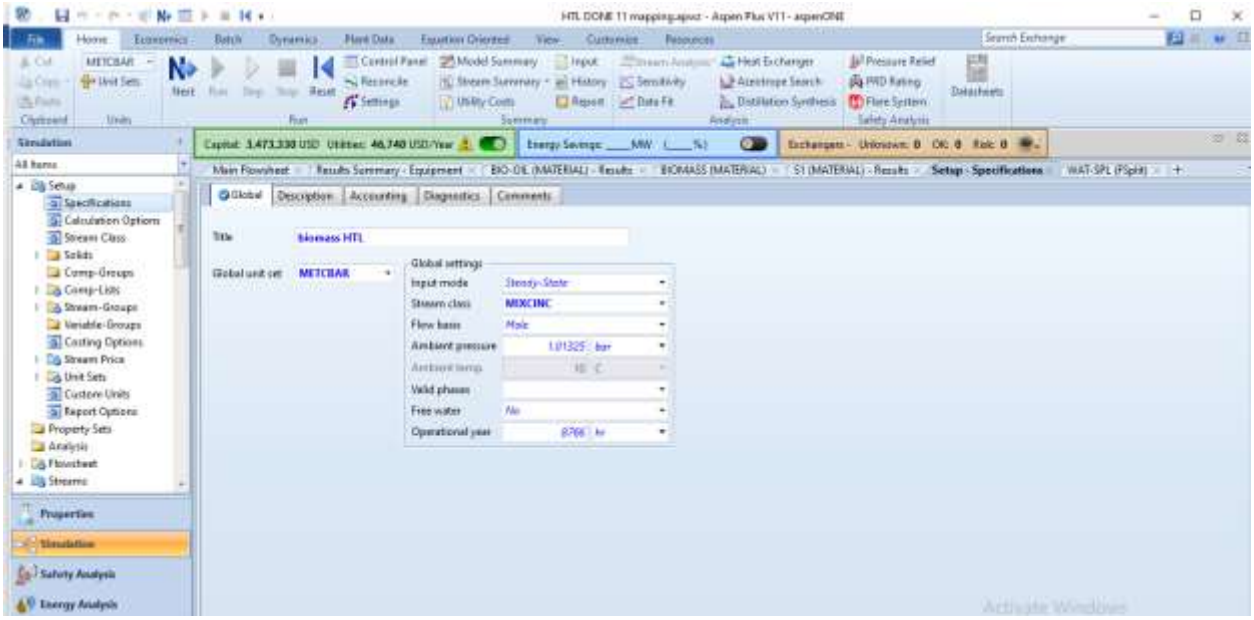

Figure F 3: Global flow used in HTL simulation

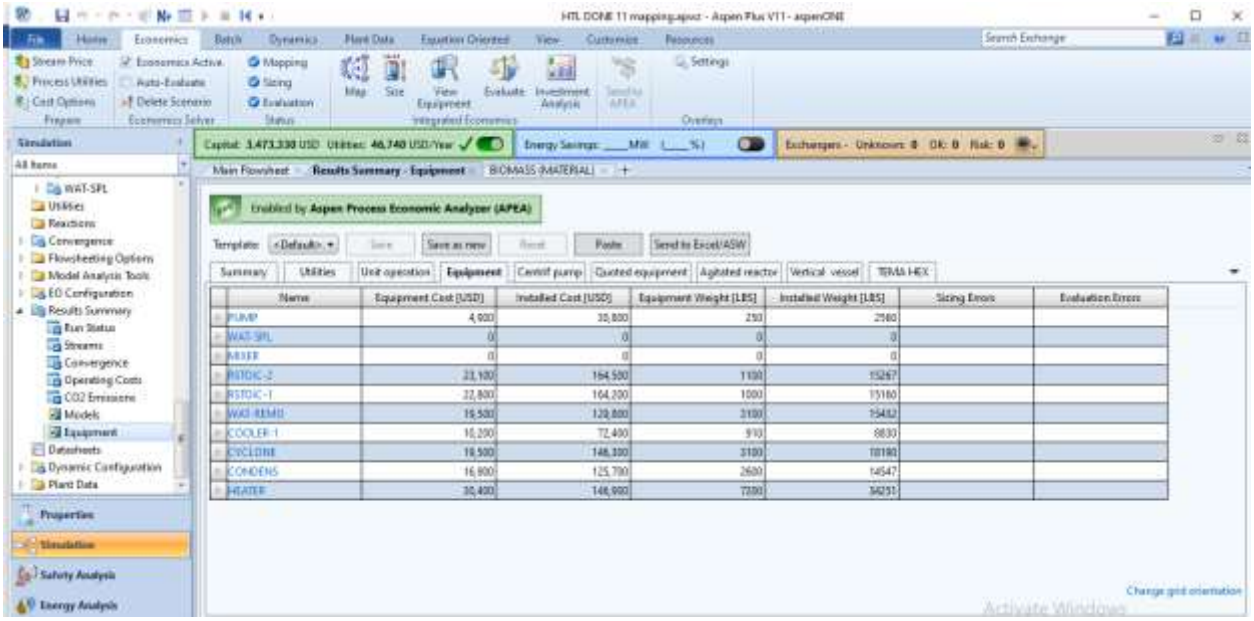

Figure F 4: Equipment costing in HTL simulation

APPENDIX G: Gasification simulations

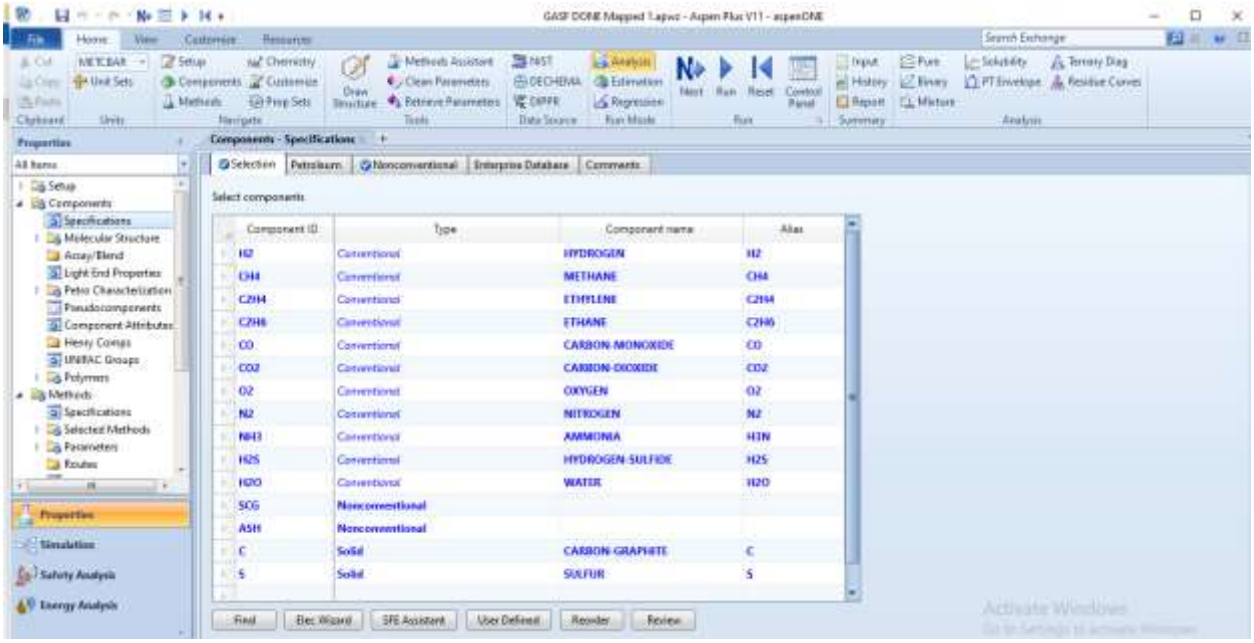

Figure G 1: Defined components in gasification simulation

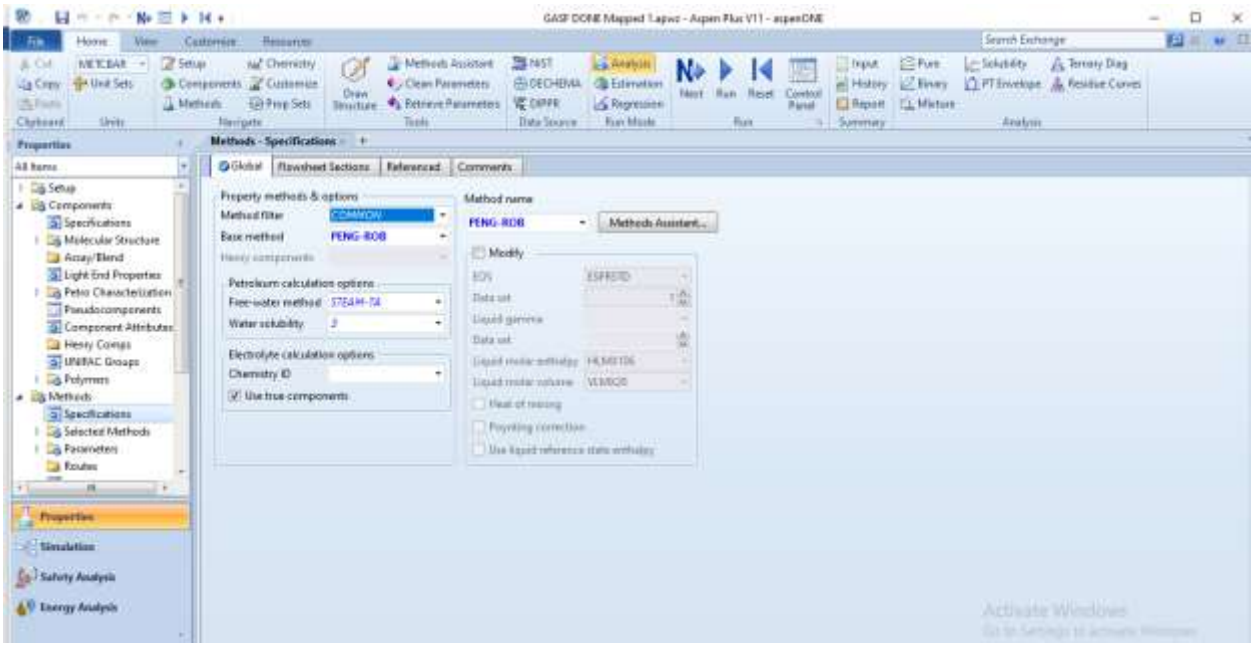

Figure G 2: Fluid package used in gasification simulation

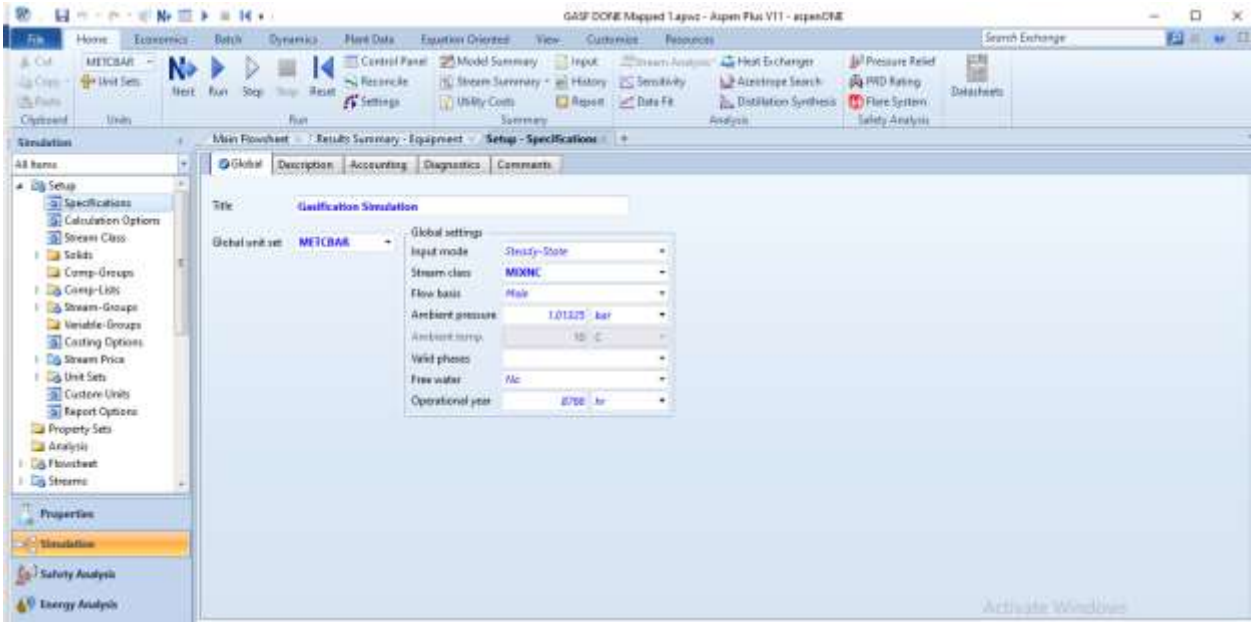

Figure G 3: Global flow used in gasification simulation

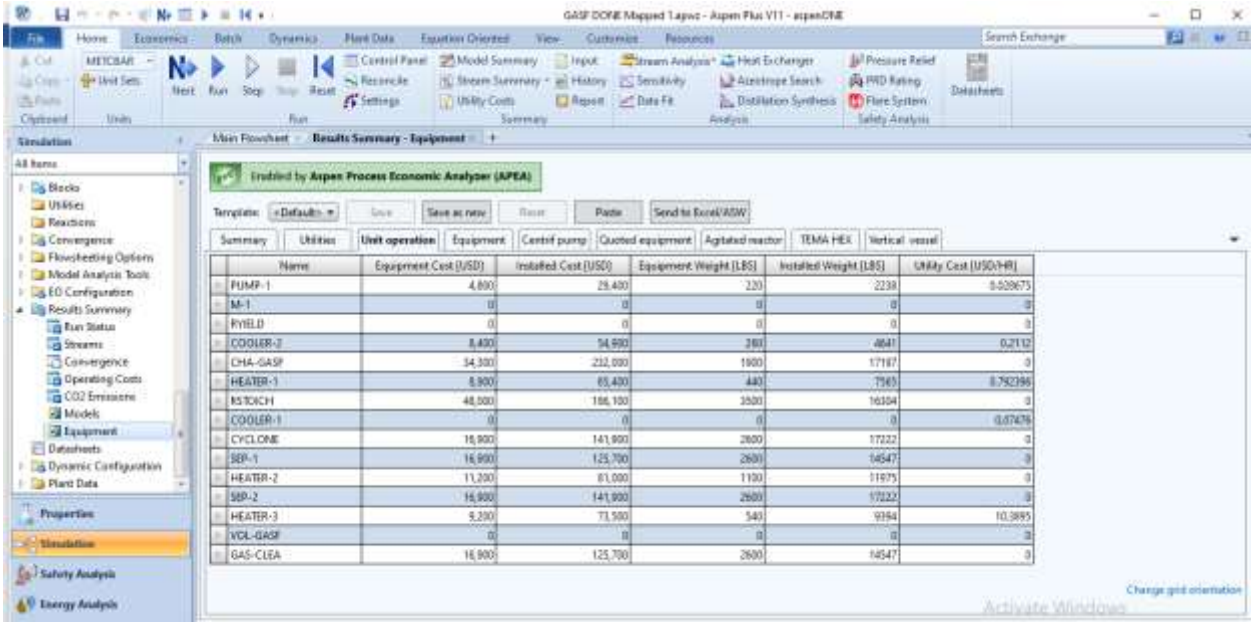

Figure G 4Equipment costing in gasification simulation

APPENDIX H: Discounted cash flow analysis

Table H 1: Discounted cash flow analysis biodiesel production

Year	Investment	Gross Profit	Depreciation	Taxable income	Tax paid	Cah flows	Discount factor	DCF	CDCF
2021	0	0	0	0	0	0	0	0	0
2022	4552088.04	0	0	0	0	-4552088.04	1	-4552088.04	-4552088.04
2023	0	1480379.964	148037.9964	1332341.967	373055.7509	1107324.213	0.892857143	988682.333	-3563405.707
2024	0	1480379.964	148037.9964	1332341.967	373055.7509	1107324.213	0.797193878	882752.083	-2680653.624
2025	0	1480379.964	148037.9964	1332341.967	373055.7509	1107324.213	0.711780248	788171.5027	-1892482.121
2026	0	1480379.964	148037.9964	1332341.967	373055.7509	1107324.213	0.635518078	703724.556	-1188757.565
2027	0	1480379.964	148037.9964	1332341.967	373055.7509	1107324.213	0.567426856	628325.4964	-560432.0684
2028	0	1480379.964	148037.9964	1332341.967	373055.7509	1107324.213	0.506631121	561004.9075	572.8390634
2029	0	1480379.964	148037.9964	1332341.967	373055.7509	1107324.213	0.452349215	500897.2388	501470.0779
2030	0	1480379.964	148037.9964	1332341.967	373055.7509	1107324.213	0.403883228	447229.6775	948699.7554
2031	0	1480379.964	148037.9964	1332341.967	373055.7509	1107324.213	0.360610025	399312.2121	1348011.968
2032	0	1480379.964	148037.9964	1332341.967	373055.7509	1107324.213	0.321973237	356528.7608	1704540.728
2033	0	1480379.964	0	1480379.964	414506.3899	1065873.574	0.287476104	306413.1825	2010953.911
2034	0	1480379.964	0	1480379.964	414506.3899	1065873.574	0.256675093	273583.1987	2284537.109
2035	0	1480379.964	0	1480379.964	414506.3899	1065873.574	0.22917419	244270.7131	2528807.823

2036	0	1480379.964	0	1480379.964	414506.3899	1065873.574	0.204619813	218098.851	2746906.674
2037	0	1480379.964	0	1480379.964	414506.3899	1065873.574	0.182696261	194731.1169	2941637.79
2038	0	1480379.964	0	1480379.964	414506.3899	1065873.574	0.163121662	173867.0687	3115504.859
2039	0	1480379.964	0	1480379.964	414506.3899	1065873.574	0.145644341	155238.4542	3270743.313
2040	0	1480379.964	0	1480379.964	414506.3899	1065873.574	0.13003959	138605.7627	3409349.076
2041	0	1480379.964	0	1480379.964	414506.3899	1065873.574	0.116106777	123755.1452	3533104.221
2042	0	1480379.964	0	1480379.964	414506.3899	1065873.574	0.103666765	110495.6654	3643599.887
2043	0	1480379.964	0	1480379.964	414506.3899	1065873.574	0.092559612	98656.8441	3742256.731
2044	0	1480379.964	0	1480379.964	414506.3899	1065873.574	0.08264251	88086.46795	3830343.199
2045	0	1480379.964	0	1480379.964	414506.3899	1065873.574	0.073787956	78648.6321	**3908991.83**

Table H 2: Discounted cash flow analysis bioethanol production

Year	Investment	Gross Profit	Depreciation	Taxable income	Tax paid	Cash flows	Discount factor	DCF	CDCF
2021	0.00	0.00	0	0.00	0.00	0	0.00	0.00	0.00
2022	2583719.84	0.00	0	0.00	0.00	-2583719.84	1.00	-2583719.84	-2583719.84
2023	0.00	-98858.60	-9885.8597	-88972.74	-24912.37	-73946.23	0.89	-66023.42	-2649743.26
2024	0.00	-98858.60	-9885.8597	-88972.74	-24912.37	-73946.23	0.80	-58949.48	-2708692.74
2025	0.00	-98858.60	-9885.8597	-88972.74	-24912.37	-73946.23	0.71	-52633.47	-2761326.21
2026	0.00	-98858.60	-9885.8597	-88972.74	-24912.37	-73946.23	0.64	-46994.17	-2808320.38
2027	0.00	-98858.60	-9885.8597	-88972.74	-24912.37	-73946.23	0.57	-41959.08	-2850279.45
2028	0.00	-98858.60	-9885.8597	-88972.74	-24912.37	-73946.23	0.51	-37463.46	-2887742.92
2029	0.00	-98858.60	-9885.8597	-88972.74	-24912.37	-73946.23	0.45	-33449.52	-2921192.44
2030	0.00	-98858.60	-9885.8597	-88972.74	-24912.37	-73946.23	0.40	-29865.64	-2951058.08

2031	0.00	-98858.60	-9885.8597	-88972.74	-24912.37	-73946.23	0.36	-26665.75	-2977723.83
2032	0.00	-98858.60	-9885.8597	-88972.74	-24912.37	-73946.23	0.32	-23808.71	-3001532.54
2033	0.00	-98858.60	0	-98858.60	-27680.41	-71178.19	0.29	-20462.03	-3021994.57
2034	0.00	-98858.60	0	-98858.60	-27680.41	-71178.19	0.26	-18269.67	-3040264.23
2035	0.00	-98858.60	0	-98858.60	-27680.41	-71178.19	0.23	-16312.20	-3056576.44
2036	0.00	-98858.60	0	-98858.60	-27680.41	-71178.19	0.20	-14564.47	-3071140.91
2037	0.00	-98858.60	0	-98858.60	-27680.41	-71178.19	0.18	-13003.99	-3084144.90
2038	0.00	-98858.60	0	-98858.60	-27680.41	-71178.19	0.16	-11610.70	-3095755.60
2039	0.00	-98858.60	0	-98858.60	-27680.41	-71178.19	0.15	-10366.70	-3106122.30
2040	0.00	-98858.60	0	-98858.60	-27680.41	-71178.19	0.13	-9255.98	-3115378.28
2041	0.00	-98858.60	0	-98858.60	-27680.41	-71178.19	0.12	-8264.27	-3123642.55
2042	0.00	-98858.60	0	-98858.60	-27680.41	-71178.19	0.10	-7378.81	-3131021.37
2043	0.00	-98858.60	0	-98858.60	-27680.41	-71178.19	0.09	-6588.23	-3137609.59
2044	0.00	-98858.60	0	-98858.60	-27680.41	-71178.19	0.08	-5882.34	-3143491.94
2045	0.00	-98858.60	0	-98858.60	-27680.41	-71178.19	0.07	-5252.09	-3148744.03

Table H 3: Discounted cash flow analysis biogas production

Year	**Investment**	**Gross Profit**	**Depreciation**	**Taxable income**	**Tax paid**	**Cah flows**	**Discount factor**	**DCF**	
2021	0	0	0	0	0	0	0	0	
2022	2082874.232	0	0	0	0	-2082874.232	1	-2082874.232	
2023	0	1402690.054	140269.0054	1262421.048	353477.8935	1049212.16	0.892857143	936796.5716	
2024	0	1402690.054	140269.0054	1262421.048	353477.8935	1049212.16	0.797193878	836425.5103	
2025	0	1402690.054	140269.0054	1262421.048	353477.8935	1049212.16	0.711780248	746808.4914	

2026	0	1402690.054	140269.0054	1262421.048	353477.8935	1049212.16	0.635518078	666793.2959	
2027	0	1402690.054	140269.0054	1262421.048	353477.8935	1049212.16	0.567426856	595351.157	
2028	0	1402690.054	140269.0054	1262421.048	353477.8935	1049212.16	0.506631121	531563.5331	
2029	0	1402690.054	140269.0054	1262421.048	353477.8935	1049212.16	0.452349215	474610.2974	
2030	0	1402690.054	140269.0054	1262421.048	353477.8935	1049212.16	0.403883228	423759.1941	
2031	0	1402690.054	140269.0054	1262421.048	353477.8935	1049212.16	0.360610025	378356.4233	
2032	0	1402690.054	140269.0054	1262421.048	353477.8935	1049212.16	0.321973237	337818.2351	
2033	0	1402690.054	0	1402690.054	392753.215	1009936.839	0.287476104	290332.7078	
2034	0	1402690.054	0	1402690.054	392753.215	1009936.839	0.256675093	259225.6319	
2035	0	1402690.054	0	1402690.054	392753.215	1009936.839	0.22917419	231451.4571	
2036	0	1402690.054	0	1402690.054	392753.215	1009936.839	0.204619813	206653.0867	
2037	0	1402690.054	0	1402690.054	392753.215	1009936.839	0.182696261	184511.6845	
2038	0	1402690.054	0	1402690.054	392753.215	1009936.839	0.163121662	164742.5755	
2039	0	1402690.054	0	1402690.054	392753.215	1009936.839	0.145644341	147091.5852	
2040	0	1402690.054	0	1402690.054	392753.215	1009936.839	0.13003959	131331.7725	
2041	0	1402690.054	0	1402690.054	392753.215	1009936.839	0.116106777	117260.5112	
2042	0	1402690.054	0	1402690.054	392753.215	1009936.839	0.103666765	104696.885	
2043	0	1402690.054	0	1402690.054	392753.215	1009936.839	0.092559612	93479.36161	

2044	0	1402690.054	0	1402690.054	392753.215	1009936.839	0.08264251	83463.71572	
2045	0	1402690.054	0	1402690.054	392753.215	1009936.839	0.073787956	74521.17475	

Year	Investment	Gross Profit	Depreciation	Taxable income	Tax paid	Cah flows	Discount factor	DCF
2021	0	0	0	0	0	0	0	0
2022	2583719.842	0	0	0	0	-2583719.842	1	-2583719.
2023	0	477717.4029	47771.74029	429945.6626	120384.7855	357332.6174	0.892857143	319046.9
2024	0	477717.4029	47771.74029	429945.6626	120384.7855	357332.6174	0.797193878	284863.3
2025	0	477717.4029	47771.74029	429945.6626	120384.7855	357332.6174	0.711780248	254342.2
2026	0	477717.4029	47771.74029	429945.6626	120384.7855	357332.6174	0.635518078	227091.3
2027	0	477717.4029	47771.74029	429945.6626	120384.7855	357332.6174	0.567426856	202760.1
2028	0	477717.4029	47771.74029	429945.6626	120384.7855	357332.6174	0.506631121	181035.8
2029	0	477717.4029	47771.74029	429945.6626	120384.7855	357332.6174	0.452349215	161639.1
2030	0	477717.4029	47771.74029	429945.6626	120384.7855	357332.6174	0.403883228	144320.6
2031	0	477717.4029	47771.74029	429945.6626	120384.7855	357332.6174	0.360610025	128857.7

2032	0	477717.4029	47771.74029	429945.6626	120384.7855	357332.6174	0.321973237	115051.5
2033	0	477717.4029	0	477717.4029	133760.8728	343956.5301	0.287476104	98879.28
2034	0	477717.4029	0	477717.4029	133760.8728	343956.5301	0.256675093	88285.07
2035	0	477717.4029	0	477717.4029	133760.8728	343956.5301	0.22917419	78825.95
2036	0	477717.4029	0	477717.4029	133760.8728	343956.5301	0.204619813	70380.32
2037	0	477717.4029	0	477717.4029	133760.8728	343956.5301	0.182696261	62839.57
2038	0	477717.4029	0	477717.4029	133760.8728	343956.5301	0.163121662	56106.76
2039	0	477717.4029	0	477717.4029	133760.8728	343956.5301	0.145644341	50095.32
2040	0	477717.4029	0	477717.4029	133760.8728	343956.5301	0.13003959	44727.96
2041	0	477717.4029	0	477717.4029	133760.8728	343956.5301	0.116106777	39935.68
2042	0	477717.4029	0	477717.4029	133760.8728	343956.5301	0.103666765	35656.86
2043	0	477717.4029	0	477717.4029	133760.8728	343956.5301	0.092559612	31836.48
2044	0	477717.4029	0	477717.4029	133760.8728	343956.5301	0.08264251	28425.43
2045	0	477717.4029	0	477717.4029	133760.8728	343956.5301	0.073787956	25379.84

Table H 4: Discounted cash flow analysis fast pyrolysis

Year	**Investment**	**Gross Profit**	**Depreciation**	**Taxable income**	**Tax paid**	**Cah flows**	**Discount factor**	**DCF**	
2021	0	0	0	0	0	0	0	0	0

2022	3417910.499	0	0	0	0	-3417910.499	1	-3417910.499	-3417910.499
2023	0	1706986.616	170698.6616	1536287.955	430160.63	1276825.989	0.892857143	1140023.205	-2277887.294
2024	0	1706986.616	170698.6616	1536287.955	430160.63	1276825.989	0.797193878	1017877.861	-1260009.433
2025	0	1706986.616	170698.6616	1536287.955	430160.63	1276825.989	0.711780248	908819.5189	-351189.9141
2026	0	1706986.616	170698.6616	1536287.955	430160.63	1276825.989	0.635518078	811445.999	460256.0849
2027	0	1706986.616	170698.6616	1536287.955	430160.63	1276825.989	0.567426856	724505.3563	1184761.441
2028	0	1706986.616	170698.6616	1536287.955	430160.63	1276825.989	0.506631121	646879.7824	1831641.224
2029	0	1706986.616	170698.6616	1536287.955	430160.63	1276825.989	0.452349215	577571.2343	2409212.458
2030	0	1706986.616	170698.6616	1536287.955	430160.63	1276825.989	0.403883228	515688.602	2924901.06
2031	0	1706986.616	170698.6616	1536287.955	430160.63	1276825.989	0.360610025	460436.2518	3385337.312
2032	0	1706986.616	170698.6616	1536287.955	430160.63	1276825.989	0.321973237	411103.7963	3796441.108
2033	0	1706986.616	0	1706986.616	477956.25	1229030.364	0.287476104	353316.8608	4149757.969
2034	0	1706986.616	0	1706986.616	477956.25	1229030.364	0.256675093	315461.4829	4465219.452
2035	0	1706986.616	0	1706986.616	477956.25	1229030.364	0.22917419	281662.0383	4746881.49
2036	0	1706986.616	0	1706986.616	477956.25	1229030.364	0.204619813	251483.9627	4998365.453
2037	0	1706986.616	0	1706986.616	477956.25	1229030.364	0.182696261	224539.2524	5222904.705
2038	0	1706986.616	0	1706986.616	477956.25	1229030.364	0.163121662	200481.4754	5423386.18
2039	0	1706986.616	0	1706986.616	477956.25	1229030.364	0.145644341	179001.3173	5602387.498

2040	0	1706986.616	0	1706986.616	477956.25	1229030.364	0.13003959	159822.6048	5762210.103
2041	0	1706986.616	0	1706986.616	477956.25	1229030.364	0.116106777	142698.7542	5904908.857
2042	0	1706986.616	0	1706986.616	477956.25	1229030.364	0.103666765	127409.602	6032318.459
2043	0	1706986.616	0	1706986.616	477956.25	1229030.364	0.092559612	113758.5732	6146077.032
2044	0	1706986.616	0	1706986.616	477956.25	1229030.364	0.08264251	101570.1547	6247647.187
2045	0	1706986.616	0	1706986.616	477956.25	1229030.364	0.073787956	90687.63809	**6338334.825**

Table H 5: Discounted cash flow analysis HTL

Year	**Investment**	**Gross Profit**	**Depreciation**	**Taxable income**	**Tax paid**	**Cah flows**	**Discount factor**	**DCF**	
2021	0	0	0	0	0	0	0	0	0
2022	2319930.114	0	0	0	0	-2319930.114	1	-2319930.114	-2319930.11
2023	0	525293.7419	52529.37419	472764.3677	132374.023	392919.719	0.892857143	350821.1776	-1969108.94
2024	0	525293.7419	52529.37419	472764.3677	132374.023	392919.719	0.797193878	313233.1943	-1655875.74
2025	0	525293.7419	52529.37419	472764.3677	132374.023	392919.719	0.711780248	279672.4949	-1376203.25
2026	0	525293.7419	52529.37419	472764.3677	132374.023	392919.719	0.635518078	249707.5848	-1126495.66
2027	0	525293.7419	52529.37419	472764.3677	132374.023	392919.719	0.567426856	222953.2007	-903542.461
2028	0	525293.7419	52529.37419	472764.3677	132374.023	392919.719	0.506631121	199065.3577	-704477.104

2029	0	525293.7419	52529.37419	472764.3677	132374.023	392919.719	0.452349215	177736.9266	-526740.177
2030	0	525293.7419	52529.37419	472764.3677	132374.023	392919.719	0.403883228	158693.6844	-368046.493
2031	0	525293.7419	52529.37419	472764.3677	132374.023	392919.719	0.360610025	141690.7897	-226355.703
2032	0	525293.7419	52529.37419	472764.3677	132374.023	392919.719	0.321973237	126509.6336	-99846.0692
2033	0	525293.7419	0	525293.7419	147082.2477	378211.4942	0.287476104	108726.7669	8880.697622
2034	0	525293.7419	0	525293.7419	147082.2477	378211.4942	0.256675093	97077.47042	105958.168
2035	0	525293.7419	0	525293.7419	147082.2477	378211.4942	0.22917419	86676.31288	192634.4809
2036	0	525293.7419	0	525293.7419	147082.2477	378211.4942	0.204619813	77389.56507	270024.046
2037	0	525293.7419	0	525293.7419	147082.2477	378211.4942	0.182696261	69097.82595	339121.8719
2038	0	525293.7419	0	525293.7419	147082.2477	378211.4942	0.163121662	61694.48746	400816.3594
2039	0	525293.7419	0	525293.7419	147082.2477	378211.4942	0.145644341	55084.3638	455900.7232
2040	0	525293.7419	0	525293.7419	147082.2477	378211.4942	0.13003959	49182.46768	505083.1909
2041	0	525293.7419	0	525293.7419	147082.2477	378211.4942	0.116106777	43912.91757	548996.1085
2042	0	525293.7419	0	525293.7419	147082.2477	378211.4942	0.103666765	39207.96212	588204.0706
2043	0	525293.7419	0	525293.7419	147082.2477	378211.4942	0.092559612	35007.10903	623211.1796
2044	0	525293.7419	0	525293.7419	147082.2477	378211.4942	0.08264251	31256.34735	654467.527
2045	0	525293.7419	0	525293.7419	147082.2477	378211.4942	0.073787956	27907.45299	**682374.98**

Table H 6: Discounted cash flow analysis Gasification

Year	Investment	Gross Profit	Depreciation	Taxable Income	Tax Paid	Cash Flows	Discount factor	DCF	
2021	0	0	0	0	0	0	0	0	0
2022	3653783.467	0	0	0	0	-3653783.467	1	-3653783.467	-3653783.467
2023	0	1587708.253	158770.8253	1428937.428	400102.48	1187605.773	0.892857143	1060362.297	-2593421.169
2024	0	1587708.253	158770.8253	1428937.428	400102.48	1187605.773	0.797193878	946752.0513	-1646669.118
2025	0	1587708.253	158770.8253	1428937.428	400102.48	1187605.773	0.711780248	845314.3315	-801354.7863
2026	0	1587708.253	158770.8253	1428937.428	400102.48	1187605.773	0.635518078	754744.9389	-46609.84745
2027	0	1587708.253	158770.8253	1428937.428	400102.48	1187605.773	0.567426856	673879.4097	627269.5623
2028	0	1587708.253	158770.8253	1428937.428	400102.48	1187605.773	0.506631121	601678.0444	1228947.607
2029	0	1587708.253	158770.8253	1428937.428	400102.48	1187605.773	0.452349215	537212.5396	1766160.146
2030	0	1587708.253	158770.8253	1428937.428	400102.48	1187605.773	0.403883228	479654.0532	2245814.2
2031	0	1587708.253	158770.8253	1428937.428	400102.48	1187605.773	0.360610025	428262.5475	2674076.747
2032	0	1587708.253	158770.8253	1428937.428	400102.48	1187605.773	0.321973237	382377.2746	3056454.022
2033	0	1587708.253	0	1587708.253	444558.311	1143149.942	0.287476104	328628.2918	3385082.313
2034	0	1587708.253	0	1587708.253	444558.311	1143149.942	0.256675093	293418.1176	3678500.431
2035	0	1587708.253	0	1587708.253	444558.311	1143149.942	0.22917419	261980.4622	3940480.893
2036	0	1587708.253	0	1587708.253	444558.311	1143149.942	0.204619813	233911.1269	4174392.02

2037	0	1587708.253	0	1587708.253	444558.311	1143149.942	0.182696261	208849.2205	4383241.241
2038	0	1587708.253	0	1587708.253	444558.311	1143149.942	0.163121662	186472.5183	4569713.759
2039	0	1587708.253	0	1587708.253	444558.311	1143149.942	0.145644341	166493.3199	4736207.079
2040	0	1587708.253	0	1587708.253	444558.311	1143149.942	0.13003959	148654.7499	4884861.829
2041	0	1587708.253	0	1587708.253	444558.311	1143149.942	0.116106777	132727.4553	5017589.284
2042	0	1587708.253	0	1587708.253	444558.311	1143149.942	0.103666765	118506.6565	5136095.941
2043	0	1587708.253	0	1587708.253	444558.311	1143149.942	0.092559612	105809.5147	5241905.455
2044	0	1587708.253	0	1587708.253	444558.311	1143149.942	0.08264251	94472.78101	5336378.236
2045	0	1587708.253	0	1587708.253	444558.311	1143149.942	0.073787956	84350.69733	**5420728.93**

APPENDIX I: Life cycle assessment

Figure I 1: OpenLCA V1.11.0 software interface

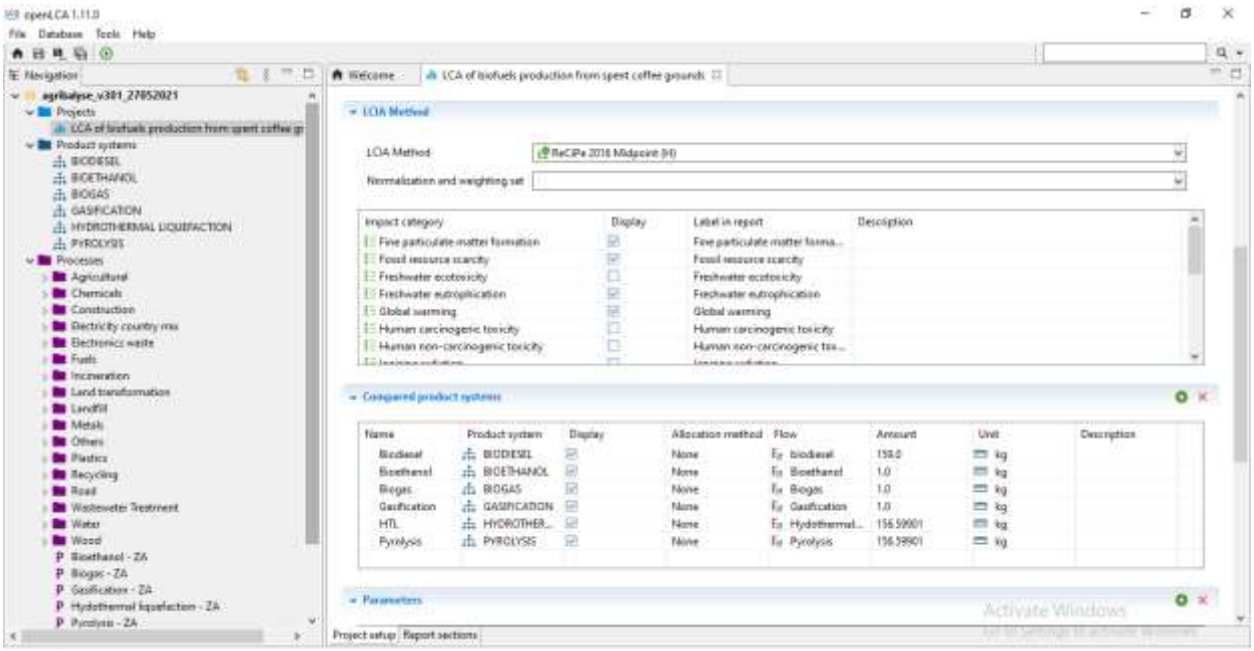

Figure I 2: Compared product systems and selected impact categories

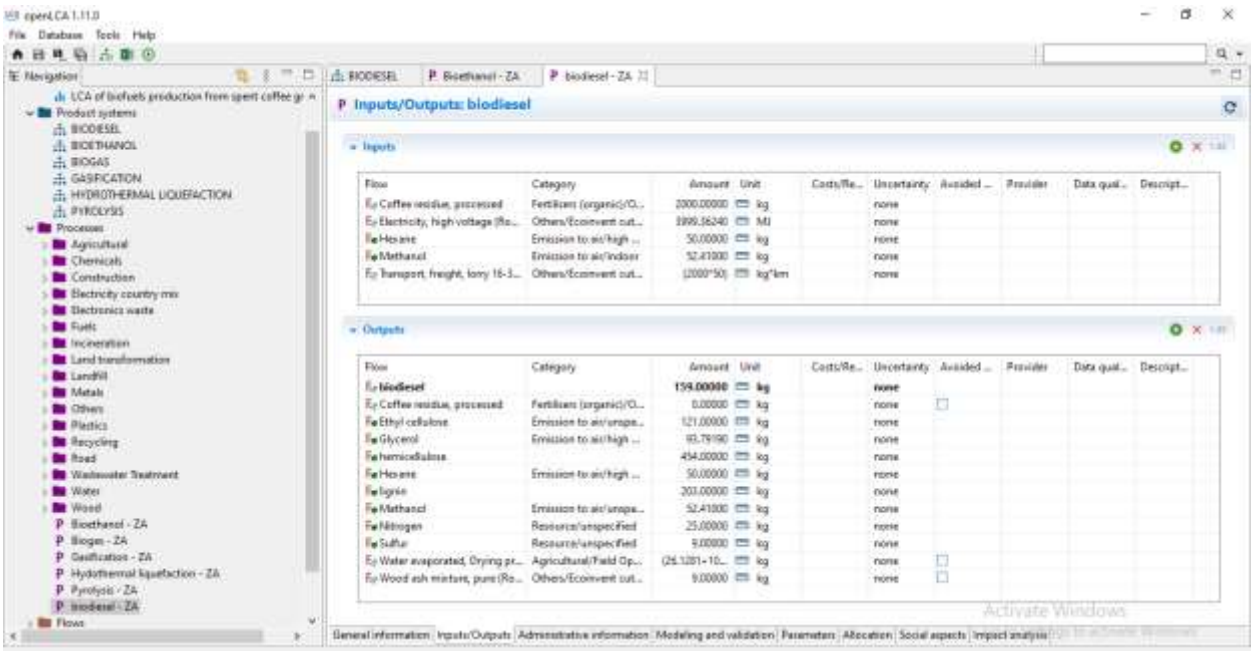

Figure I 3: Life cycle inventory for biodiesel production

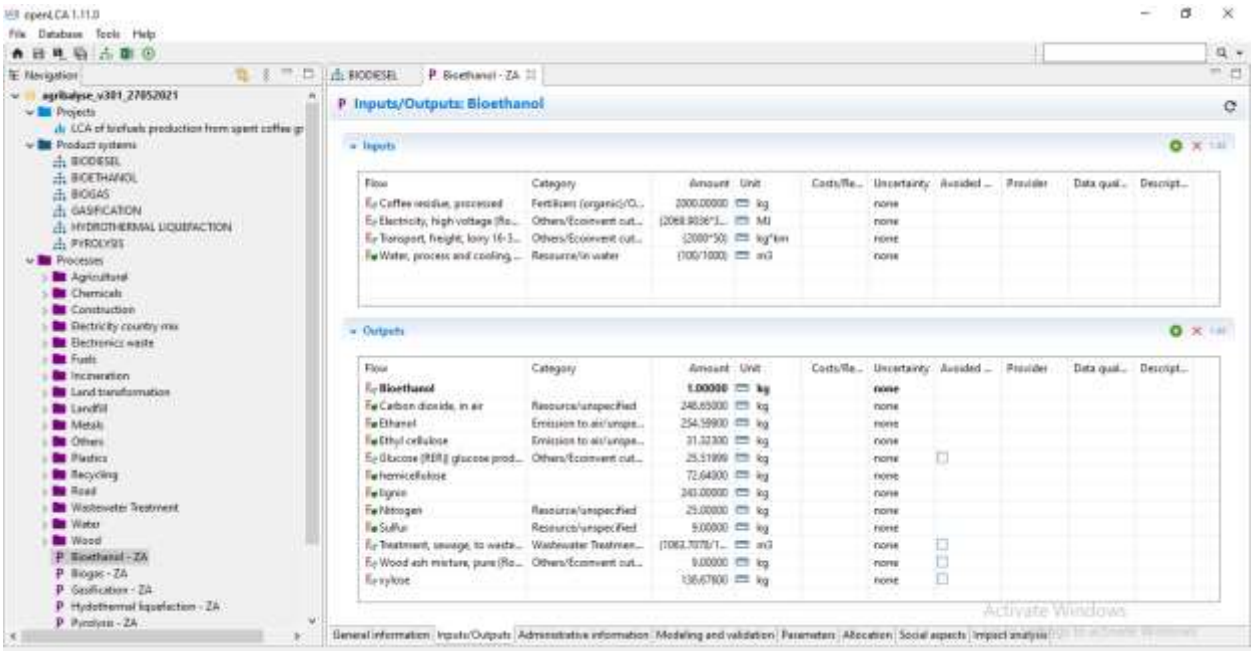

Figure I 4: Life cycle inventory for bioethanol production

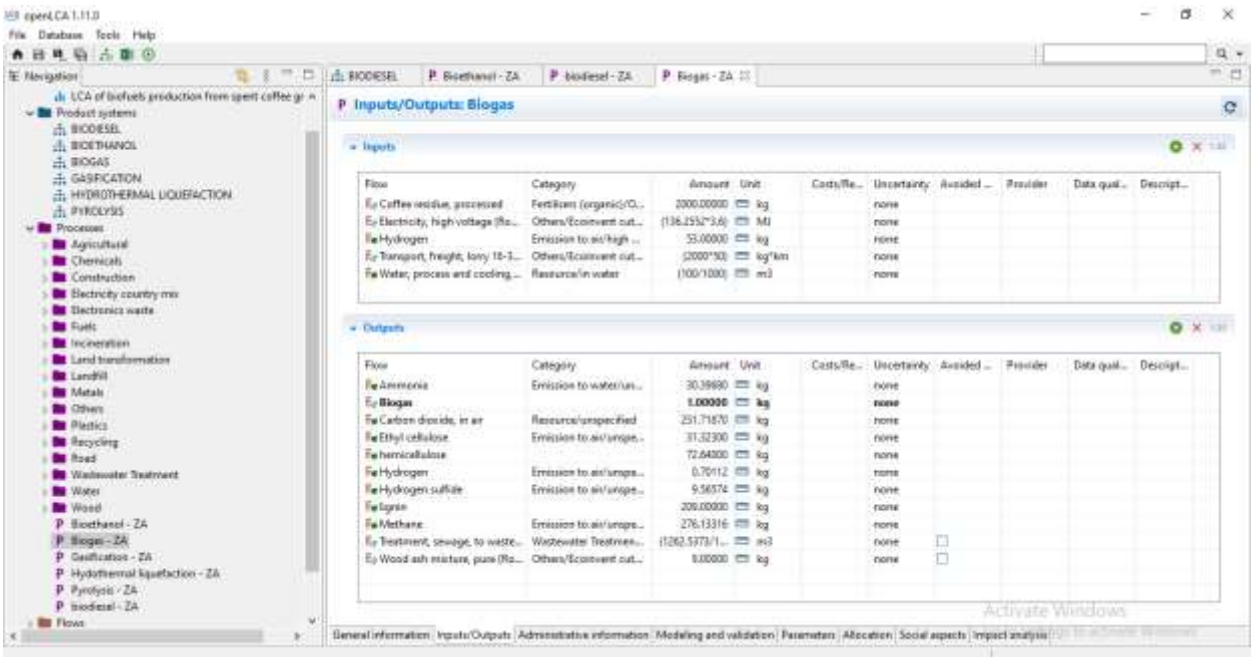

Figure I 5: Life cycle inventory for biogas production

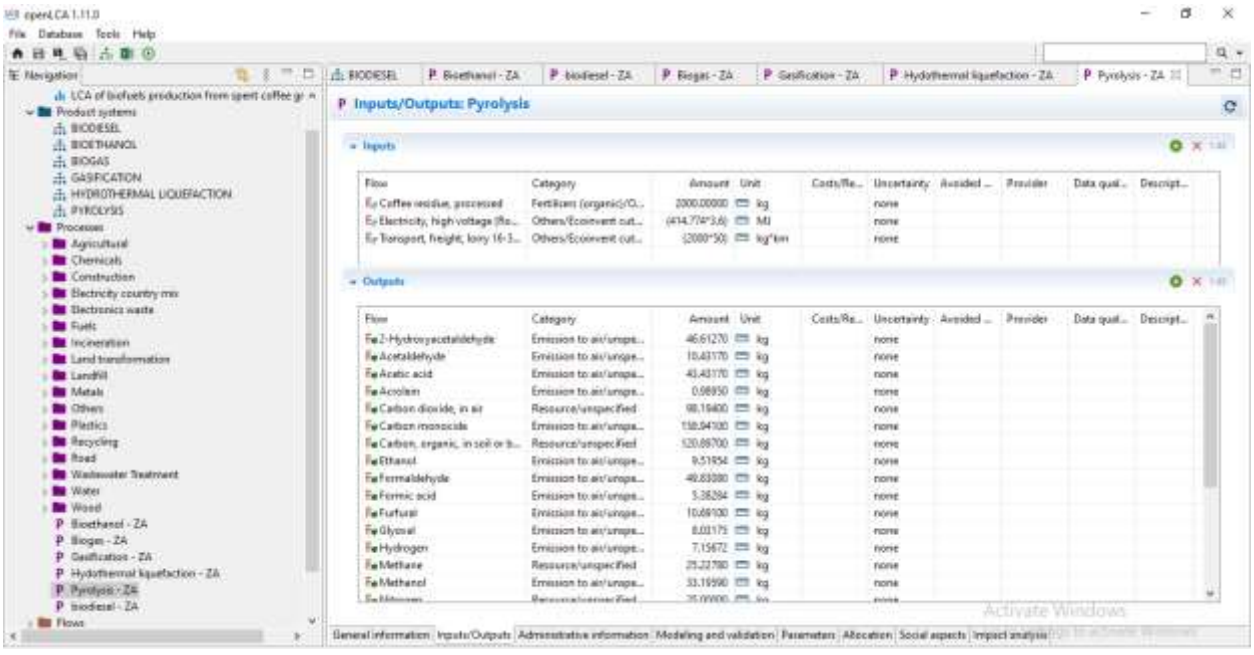

Figure I 6: Life cycle inventory for fast pyrolysis

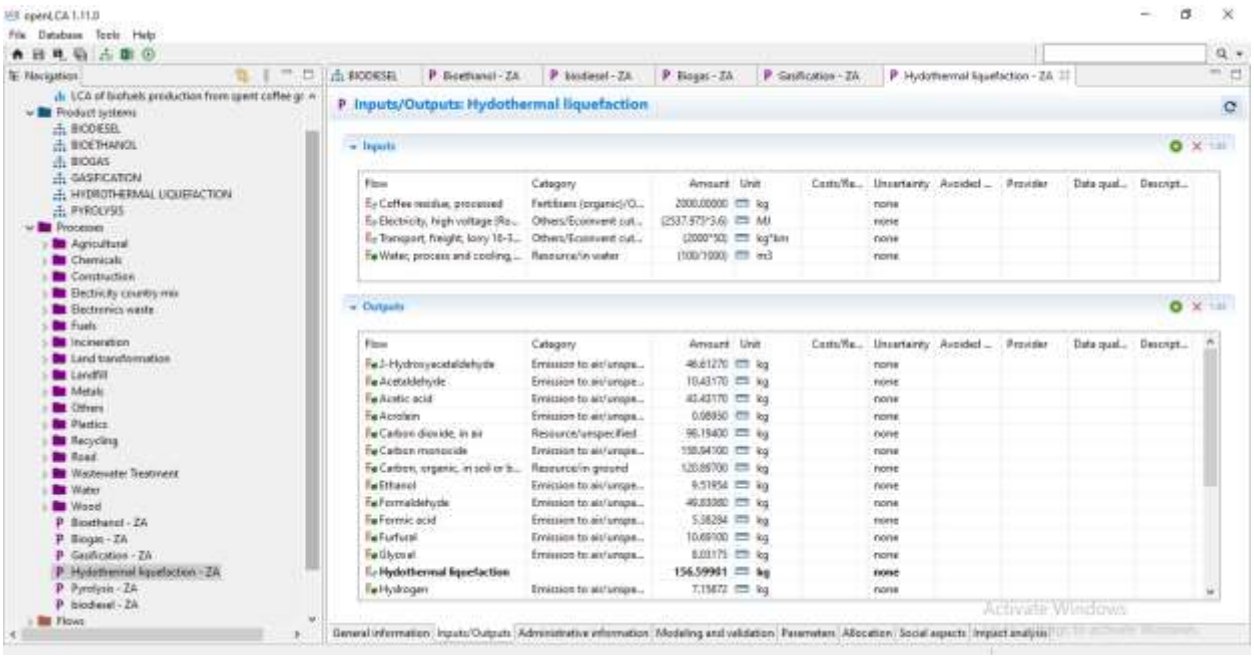

Figure I 7: Life cycle inventory for HTL

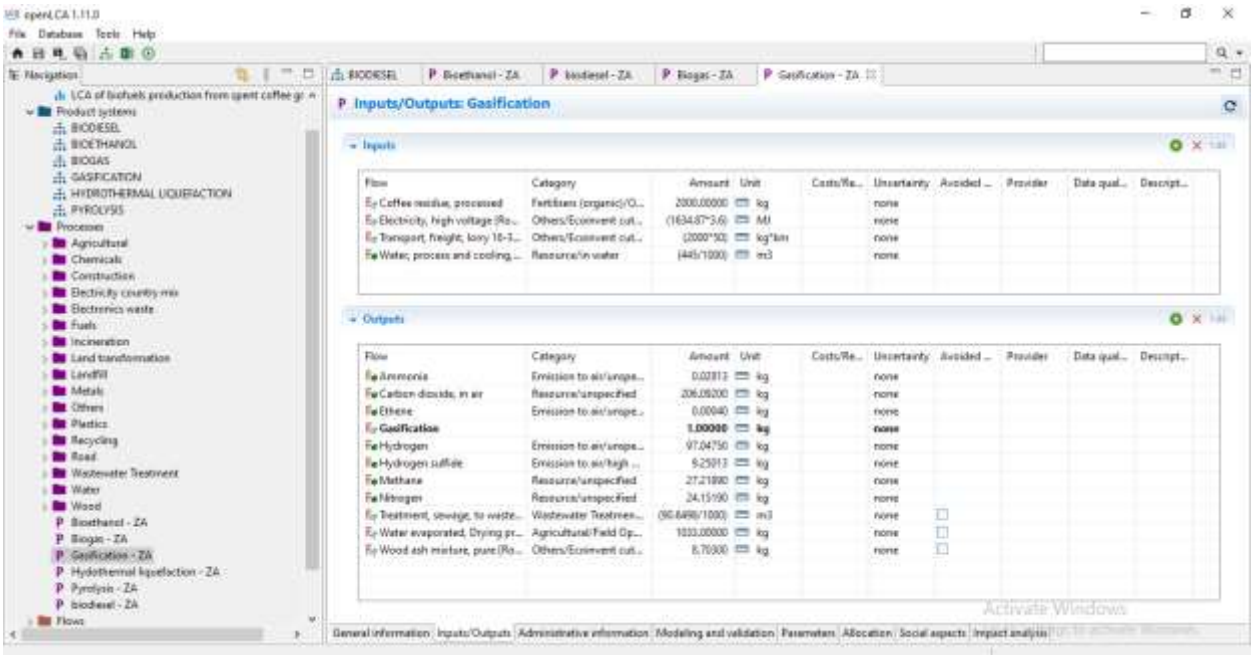

Figure I 8: Life cycle inventory for gasification